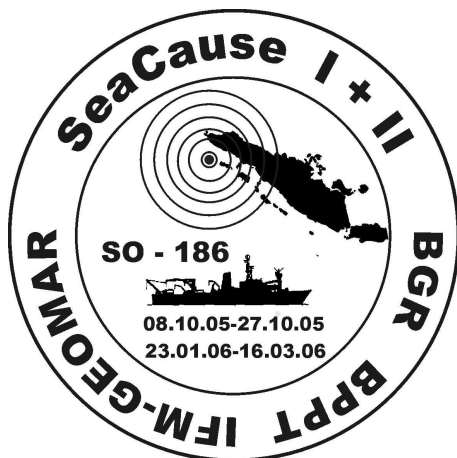


Abschlussbericht

SO186 SeaCause

Der Tsunami von Sumatra 2004

-
Georisikopotenzial entlang der
aktiven Konvergenzzone der
eurasischen und
indo-australischen Platten,
Sumatra (Indonesien)



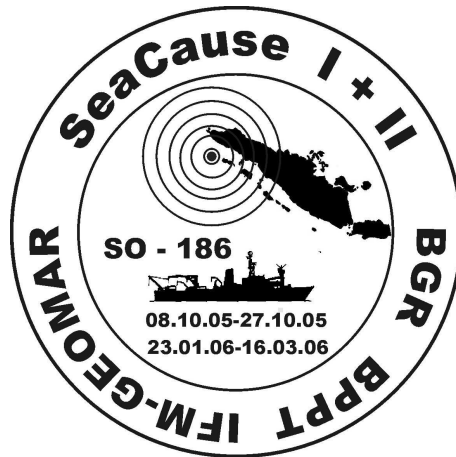
BUNDESANSTALT FÜR GEOWISSENSCHAFTEN UND ROHSTOFFE (BGR), HANNOVER
und
LEIBNIZ-INSTITUT FÜR MEERESWISSENSCHAFTEN (IFM-GEOMAR), KIEL

Abschlussbericht
Sonne-Fahrt SO-186 SeaCause I & II

DER TSUNAMI VON SUMATRA 2004

-

**GEORISIKOPOTENZIAL ENTLANG DER AKTIVEN KONVERGENZZONE DER
EURASISCHEN UND INDO-AUSTRALISCHEN PLATTEN, SUMATRA (INDONESIEN)**



-
1. Wissenschaftliche Leiter: Christoph Gaedicke (BGR) & Heidrun Kopp (IFM-GEOMAR)
2. Wissenschaftliche Beiträge: U. Barckhausen, K. Berglar, G. Delisle, D. Franke, S. Glaubitz, I. Heyde, S. Ladage, R. Lutz, Chr. Müller, M. Schauer, M. Schnabel (BGR)
E. Flüh, I. Grevemeyer, D. Klaeschen, A. Krabbenhöft, C. Papenberg, W. Weinrebe, M. Zillmer (IFM-GEOMAR)
3. Auftraggeber: Bundesministerium für Bildung und Forschung (BMBF)
4. Förderkennzeichen: 03G0186A und 03G0186B
5. Ort, Datum: Hannover/Kiel, 30. März 2009

Abschlussbericht des Vorhabens 03G0186A und 03G0186B „SeaCause I & II“

Zuwendungsempfänger: Bundesanstalt für Geowissenschaften und Rohstoffe (BGR)
Postfach 51 01 53
30631 Hannover

und IFM-Geomar
Wischhofstr. 1-3
24148 Kiel

Förderkennzeichen: 03G0186A (BGR)
03G0186B (IFM-GEOMAR)

Projektleiter: Dr. Christoph Gaedicke (BGR, Koordinator)
Prof. Dr. Heidrun Kopp (IFM-GEOMAR)

Vorhabenbezeichnung: SO 186 SeaCause I & II

Laufzeit des Vorhabens: 01.09.2005 – 30.09.2008

Berichtszeitraum: 01.09.2005 bis 28.02.2009

Inhalt

Vorbemerkung

1. Wissenschaftliche Ergebnisse

- 1.1 Bathymetrie
- 1.2 Magnetik
- 1.3 Gravimetrie
- 1.4 Seismologische Untersuchungen zur räumlichen Verteilung der Nachbeben
- 1.5 Ursache der Segmentierung der Erdbebenbruchflächen
- 1.6 Massentransfer und Seismotektonik entlang der Sumatra Subduktionszone
- 1.7 Seismostratigraphie und Tektonik der Vorderbogenbecken
- 1.8 Das Kohlenwasserstoffsystem des Simeulue Beckens
- 1.9 Literaturverzeichnis

2 Änderungen der Ziele des Vorhabens

3 Ergebnisse von dritter Seite mit Relevanz zum laufenden Projekt

4 Fortschreibung des Verwertungsplans

Anhang I. Liste der Publikationen (peer-review Verfahren)

Anhang II. . Liste der Diplomarbeiten

Anhang III. Liste der öffentlichen Präsentation von Ergebnissen seit Projektbeginn bis Februar 2009 (Kurzfassungen für Poster und Vorträge)

Anhang IV. Publikationen

Vorbemerkung

An der BGR sind zwei durch das BMBF geförderte Projekte in der Auswertung: SO186 SeaCause (Förderkennzeichen: 03G0186A) und SO189 SUMATRA (03G0189A). Beide Projekte wurden mit FS Sonne im Fore-Arc Bereich Sumatras durchgeführt. Dabei wurden sehr umfangreiche geophysikalische Datensätze akquiriert. Die Auswertung erfolgt für beide Projekte durch dieselben Wissenschaftler. Es ergeben sich vorher nicht abschätzbare Synergien, die von enormem Vorteil für die Themenkomplexe beider Projekte sind. So wurden im Projekt SeaCause Hinweise auf das Vorkommen von Kohlenwasserstoffen im Simeulue Becken gefunden, die auch im Zentrum der Untersuchungen des SUMATRA-Projektes stehen. Das Simeulue Becken war jedoch nicht ursprünglich Zielgebiet und Gegenstand des SUMATRA Projektes. Auf der anderen Seite profitiert das SeaCause-Projekt vom SUMATRA-Projekt durch die Datensätze vor Zentral- und Südsumatra. Eine klare Trennung der Datensätze ist aus diesem Grund weder möglich noch von Seiten der Projektleitung gewünscht. Viele Ergebnisse und daraus resultierende Publikationen oder Tagungsbeiträge basieren daher auf beiden Datensätzen - und zum Teil zusätzlich auf externen Daten (vor allem Bathymetrie) oder älteren Daten von SO137 GINCO. Daraus ergibt sich, dass Teile des Arbeitsprogramms der beiden Projekte Überschneidungen aufweisen und dass Hinweise auf Tagungsbeiträge und Publikationen in den Zwischenberichten beider Projekte erscheinen. Publikationen, die beiden Projekten zugeordnet werden müssen, sind mit Stern * gekennzeichnet.

Die Fahrten des FS SONNE im Rahmen des Projektes SeaCause waren darüber hinaus eng verknüpft mit der Einrichtung eines Tsunami-Frühwarnsystems vor Indonesien (GITEWS-Projekt). Im Zuge der Ausfahrten wurde dem SIMRAD-System auf FS SONNE eine Kartierung des Meeresbodens vor Nord-Sumatra durchgeführt, unter anderem um geeignete Lokationen für die Frühwarn-Bojen zu erkunden.

1. Wissenschaftliche Ergebnisse

Am 26. Dezember 2004 wurden Nord Sumatra und weite Regionen von Südostasien von einem katastrophalen $M_w=9.3$ Erdbeben und Tsunami verwüstet. Nur knapp drei Monate später wurde am 28 März 2005 die Region südlich des ersten Schüttergebiets von einem weiteren $M_w=8.6$ Erdbeben getroffen. Die mit der Subduktion der Indo-Australischen Platte unter den kontinentalen Sunda-Block verbundenen Prozesse waren Auslöser für die verheerenden Erdbeben und stehen somit im Mittelpunkt der wissenschaftlichen Arbeiten am Kontinentrand vor Sumatra im Rahmen des SeaCause-Projektes.

1.1 Bathymetrie

Die bathymetrischen Daten, die im Rahmen des SeaCause Projektes aufgezeichnet worden sind, wurden mit den Daten vorhergehender und nachfolgender FS SONNE Fahrten in der Region verknüpft. Darüber hinaus wurden auch weitere Datensätze englischer, französischer, japanischer und US-amerikanischer Forschungsexpeditionen integriert. Es existiert nun eine Kompilation dieser zur Verfügung stehenden Datensätze, die den größten Teil des Sumatra Tiefseegrabens und Kontinentthanges abdeckt. Die Vorderbogenbecken (Aceh, Simeulue und Nias) weisen auch bereits eine erhebliche Überdeckung auf. Grosse Lücken dagegen existieren noch im Bereich des Siberut Beckens und in den flacheren Bereichen des Kontinentthanges. Abbildung 1 zeigt eine Karte der Überdeckung der zur Verfügung stehenden Fächerecholot Datensätze, Abbildung 2 den letzten Stand der Kompilation der Meeresbodenkarte.

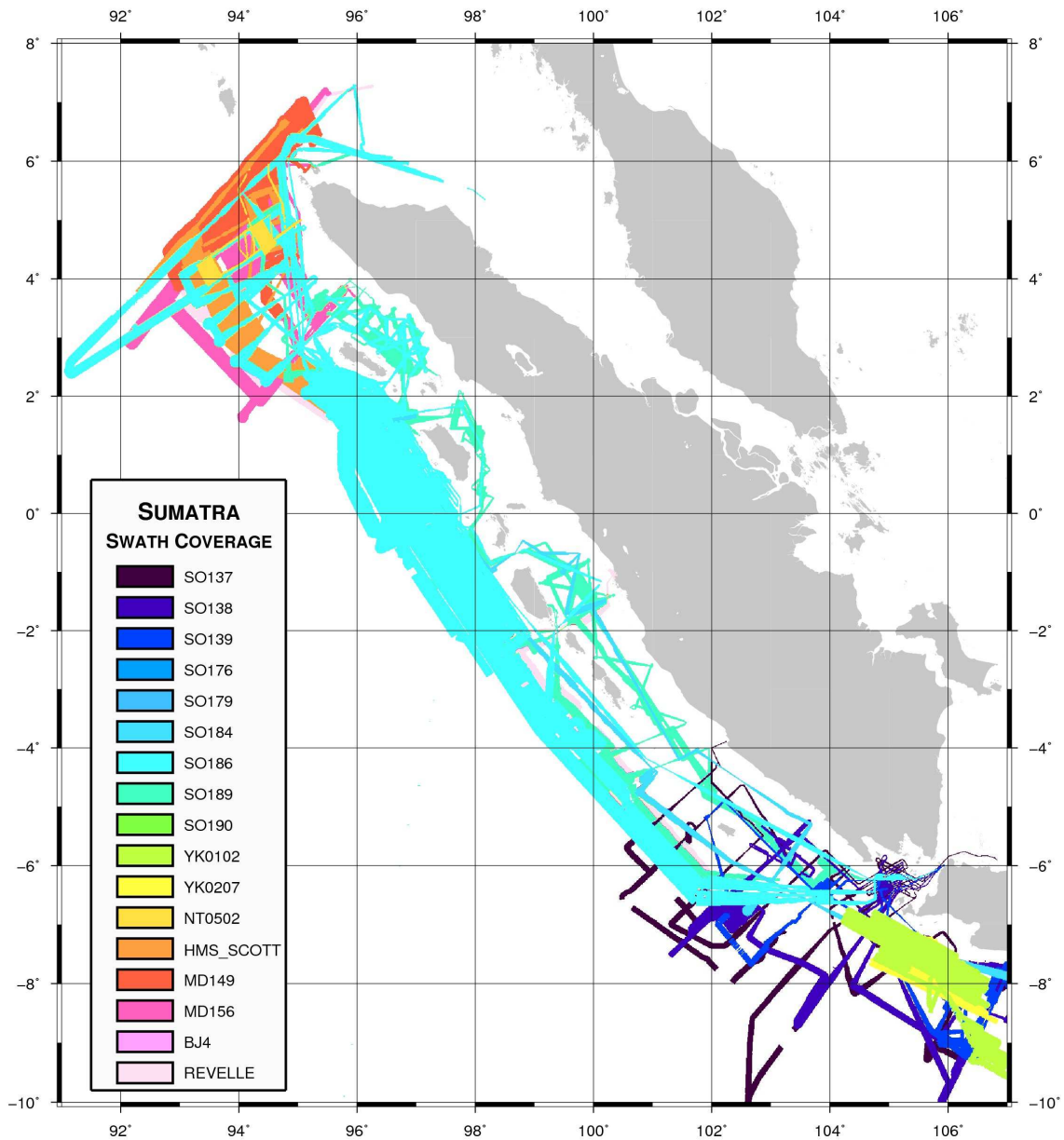


Abbildung 1 Karte der Überdeckung mit Fächerecholotdaten des Meeresbodens vor Sumatra. SO – FS SONNE (Deutschland); YK – R/V Yokosuka (Japan); R/V Natsushima (Japan); MD – R/V Marion Dufresne (Frankreich); BJ4 – R/V Baruna Jaja 4 ; Revelle – R/V Roger Revelle (US)

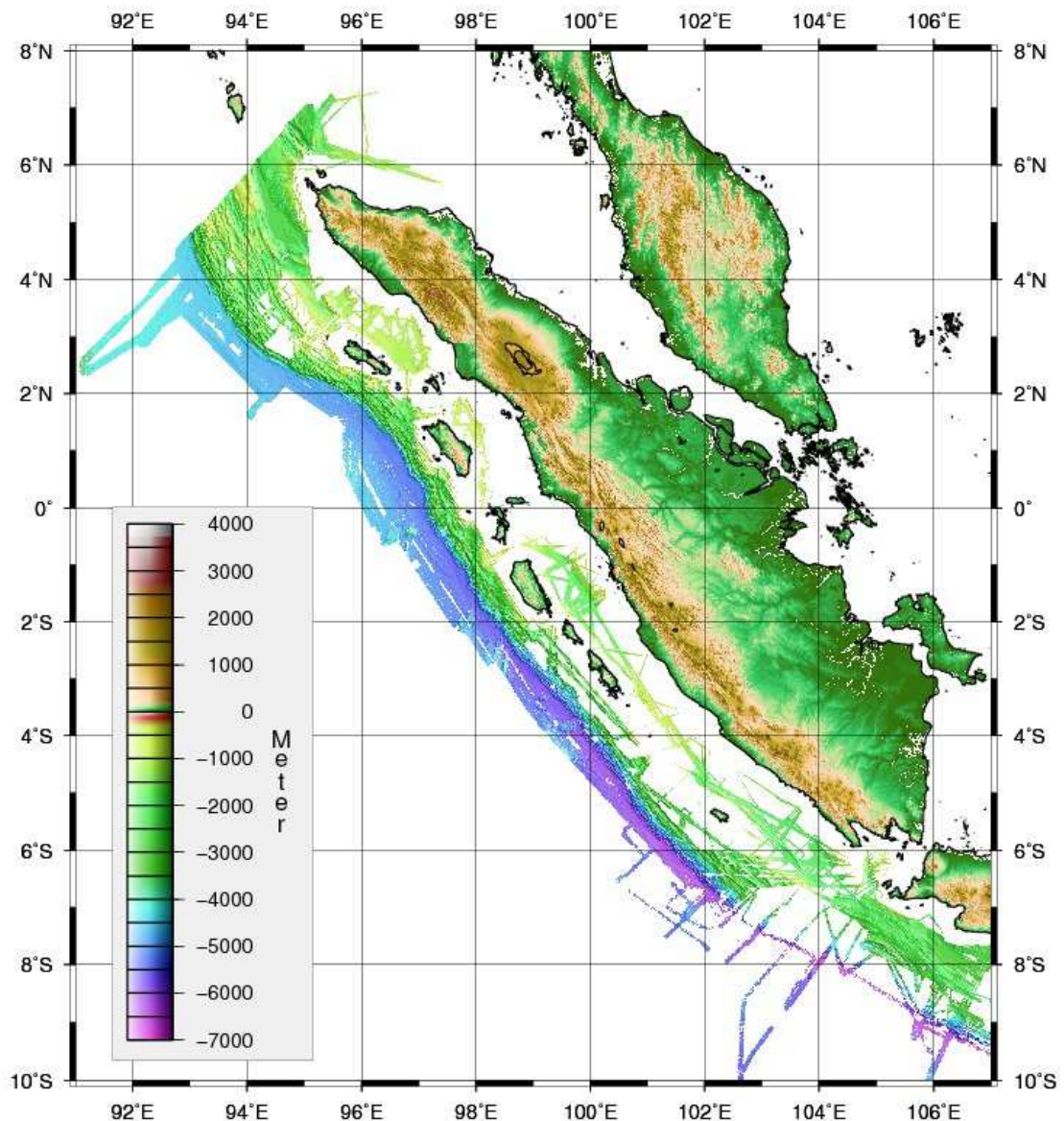


Abb. 2: Bathymetrische Karte des Meeresbodens vor Sumatra.

1.2 Magnetik

Die modernen reflexionsseismischen Methoden, die im SeaCause-Projekt angewendet wurden, können sehr detailreich die oberen Schichten der Erdkruste unter dem Meeresboden abbilden. An der Subduktionszone vor Sumatra ergeben die seismischen Sektionen jedoch bereits wenige Kilometer landwärts der Subduktionsfront nur noch wenige Informationen über die abtauchende Platte. Es steht außer Frage, dass die wesentlichen tektonischen Strukturen der subduzierenden Platte auch die überfahrende Platte und die Subduktionszone als Ganzes beeinflussen. Deshalb ist es notwendig, prominente Strukturen der ozeanischen Platte wie z.B. Bruchzonen, inaktive Spreizungsrücken und Seamount-Ketten in ihrem noch nicht subduzierten Teil seewärts der Subduktionsfront zu kartieren und in die Subduktionszone hinein zu extrapolieren. Teilweise können diese Strukturen in

hochauflösender Bathymetrie und in gravimetrischen Daten erkannt werden, am zuverlässigsten lassen sie sich jedoch aus der Beobachtung von magnetischen Seafloor Spreading Anomalien ableiten. Deshalb liegen die wichtigsten magnetischen Messungen westlich des Sundagrabens, wo Teile der ozeanischen Kruste während der Fahrten SO186-I und SO186-II geophysikalisch vermessen wurden. Diese Daten wurden mit weiteren Messdaten der Fahrten SO137, SO138 und SO189 zu einem Datensatz zusammengeführt, der große Teile der Subduktionszone vor Sumatra und der angrenzenden Ozeangebiete überdeckt. (Abb. 3).

Fast der gesamte Magnetik-Datensatz wurde mit einem longitudinalen Gradientenmagnetometer gemessen, bei dem zwei Totfeldsensoren im Abstand von 700 m und 850 m hinter dem Schiff geschleppt werden. Die Daten wurden nach einem Verfahren prozessiert, das bei Engels et al. (2008) beschrieben ist. Durch das Prozessing konnten zeitlich veränderliche magnetische Variationen aus dem äußeren Anteil des Erdmagnetfeldes, die in der Größenordnung von ± 50 nT lagen, weitgehend aus den Daten bereinigt werden.

Um die Überdeckung der magnetischen Kartierung auszuweiten, wurden versuchsweise Daten der GEODAS-Datenbank (NGDC, 2007) aus den an das Messgebiet der SONNE-Fahrten angrenzenden Gebieten mit einbezogen (Abb. 4). Die relativ wenigen magnetischen Profile stammen überwiegend aus den Jahren zwischen 1955 und 1975 und haben nicht die gleiche Qualität wie die neuen Daten, obwohl sie mit dem CM4 Feldmodell von Sabaka et al. (2004) korrigiert wurden. Die erweiterte Karte (Abb. 4) enthält nicht entscheidend mehr Information als die SONNE-Kartierung alleine.

Im Seegebiet vor Nord-Sumatra verdecken besonders mächtige Sedimente des Bengal-Fächers fast alle morphologischen Strukturen der basaltischen ozeanischen Kruste in der bathymetrischen Kartierung. Dort, wo während des SeaCause-Projektes magnetische Daten gemessen wurden, kann die Interpretation von Liu et al. (1982) bestätigt werden (Abb. 3 und 4). Die Krustenstruktur der Indo-Australischen Platte östlich des Ninetyeast-Ridges wird von einer Serie von N-S streichenden Bruchzonen mit Abständen zwischen 80 km und 200 km dominiert, an denen Alterssprünge der Kruste von bis zu 15 Millionen Jahren auftreten. Die Krustenalter an der Subduktionszone bewegen sich im Bereich zwischen 45 und 68 Millionen Jahren. In den detaillierten magnetischen Karten finden sich Hinweise für weitere, bisher unbekannte Bruchzonen (Abb. 4). Diese werden auch von den auf den SONNE-Fahrten durchgeführten Gravimetrie-Messungen unterstützt.

Die „Rupture Areas“ der beiden katastrophalen Erdbeben vom 26.12.2004 und dem 28.03.2005 werden durch eine scharfe Grenze getrennt, die unter der Insel Simeulu hindurch verläuft. Dieses ist nahe dem Bereich, in dem eine der Bruchzonen der ozeanischen Platte nach der Interpretation von Liu et al. (1982) in die Subduktionszone eintritt. Eine Detaildarstellung der Magnetik um Simeulu mit Daten aus allen verfügbaren Quellen (Abb. 5) zeigt, dass die Verlängerung der Bruchzone nicht unter dem Nordende der Insel, sondern unter ihrer Mitte vermutet werden muss und damit möglicherweise exakt mit der Trennlinie zwischen den beiden Rupture Areas zusammenfällt. Die Rupture Area des Erdbebens vom März 2005 ist nach Süden hin von einer weiteren prominenten Bruchzone, dem Investigator-Rücken begrenzt und liefert damit einen weiteren Hinweis darauf, dass die tektonischen Vorgänge in der Subduktionszone zu einem erheblichen Teil von den Strukturen der subduzierenden Platte kontrolliert werden.

Im Bereich des äußeren Hochs und der Beckenstrukturen des Forearcs zeigen die magnetischen Daten nur eine geringe Variabilität. Dieses ist ein Hinweis darauf, dass der Akkretionskeil vollständig aus weitgehend unmagnetischen Sedimenten aufgebaut ist und auch im Basement der Beckenstrukturen mächtige Abfolgen von Sedimentgesteinen vermutet werden müssen.

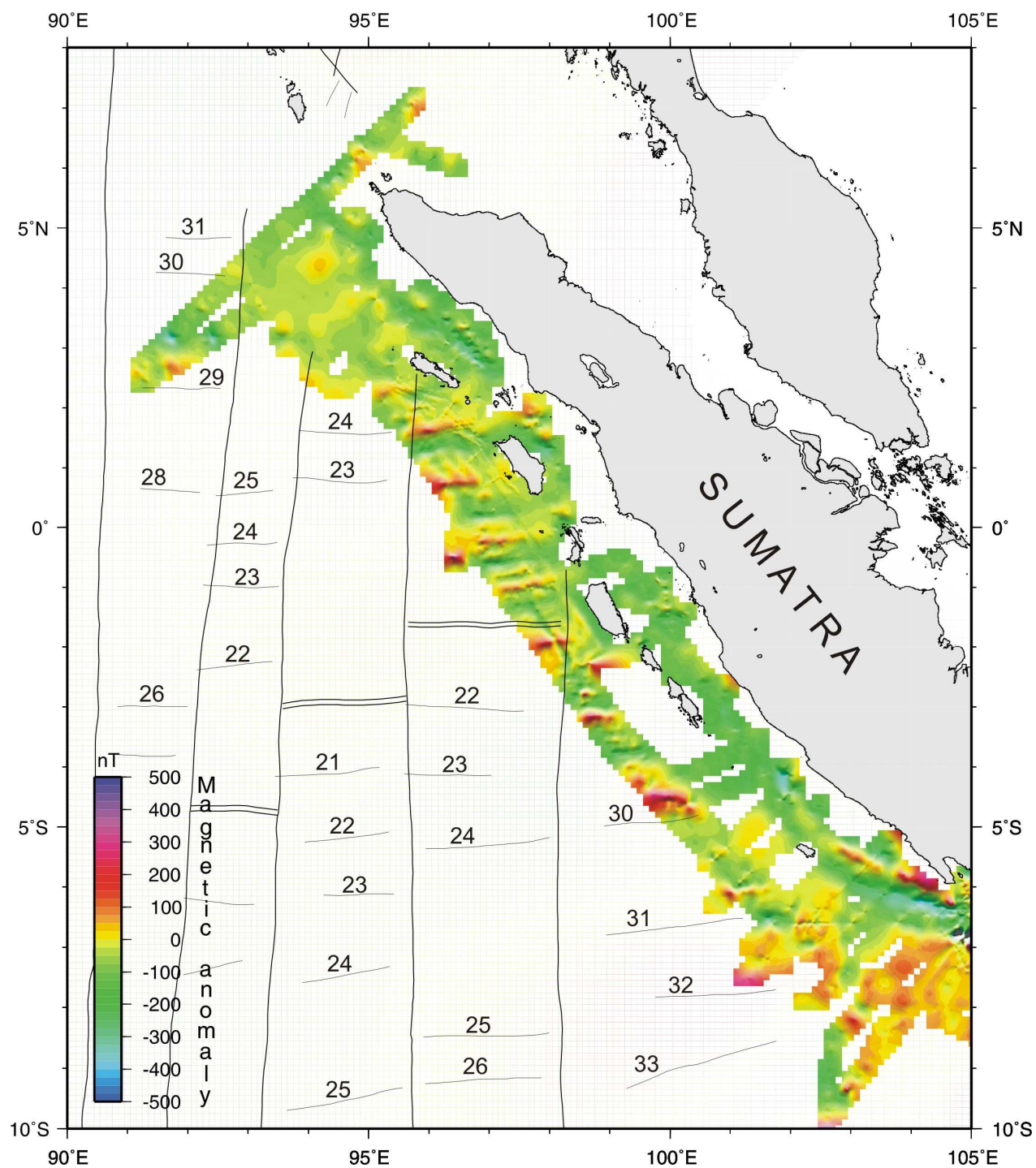


Abb. 3: Karte der magnetischen Anomalien vor Sumatra aus Daten der Forschungsfahrten SO137, SO138, SO186-I, SO186-II und SO189. Schwarze Striche und Zahlen geben Seafloor Spreading Anomalien und Bruchzonen nach Liu et al. (1982) an.

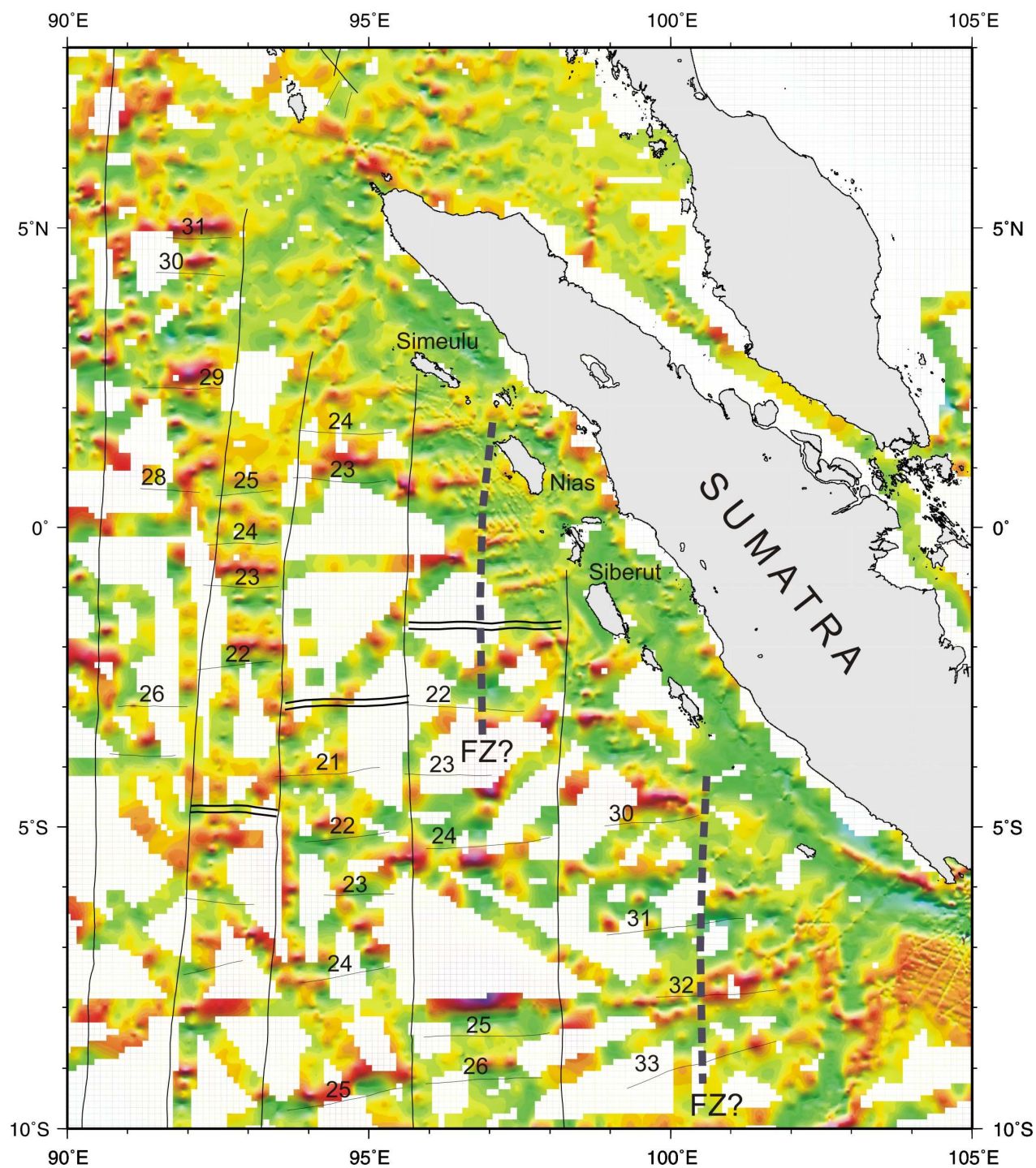


Abb. 4: Karte der magnetischen Anomalien im nordöstlichen Indischen Ozean vor Sumatra aus Daten verschiedener SONNE-Fahrten (vgl. Abb. 3) und Daten der GEODAS-Datenbank (NGDC, 2007). Gestrichelte Linien geben vermutete Bruchzonen an, die in der Interpretation von Liu et al. (1982) (durchgezogene Linien) nicht enthalten sind.

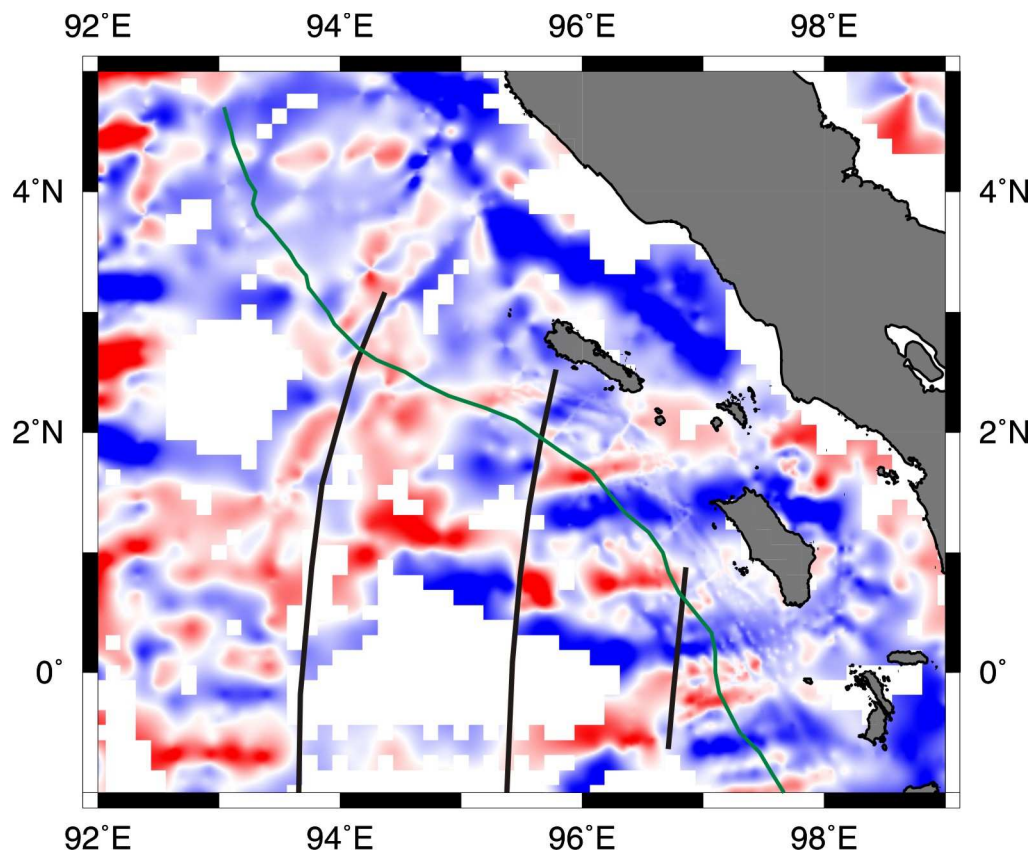


Abb. 5: Detailkarte der magnetischen Anomalien vor den Inseln Simeulu und Nias. Die Bruchzonen verlaufen etwas gekrümmter als in der Interpretation von Liu et al. (1982) und stimmen dadurch noch besser mit der beobachteten tektonischen Segmentierung der Subduktionszone überein.

1.3 Gravimetrie

Während beider SO-186 SeaCause Fahrten wurden marine Schweremessungen mit dem KSS31M Seegravimeter der BGR durchgeführt. Gemessen wurden Daten entlang von Profilen mit einer Gesamtlänge von etwa 19500 km. Die Analyse der Differenzen der gemessenen Schweredaten an Kreuzungspunkten zeigt, dass die Genauigkeit der Schweremessungen besser als 0,6 mGal ist. Für die weiteren Betrachtungen wurden die Schweredaten der SUMATRA Fahrt (SO-189) sowie die Daten, die 1998/99 während der SONNE Fahrten SO-137 und SO-138 (GINCO) gewonnen wurden, mit einbezogen. Insgesamt liegen nun Schweredaten vor Sumatra entlang einer Gesamtprofillänge von ca. 35000 km von Aceh im Norden bis zur Sundastrasse im Süden vor (Abb. 6).

Die Freiluftschwereanomalien der Schiffsmessungen wurden mit Anomaliendatensätzen verglichen, die aus der Satellitenaltimetrie gewonnen wurden. Es handelt sich um die Daten

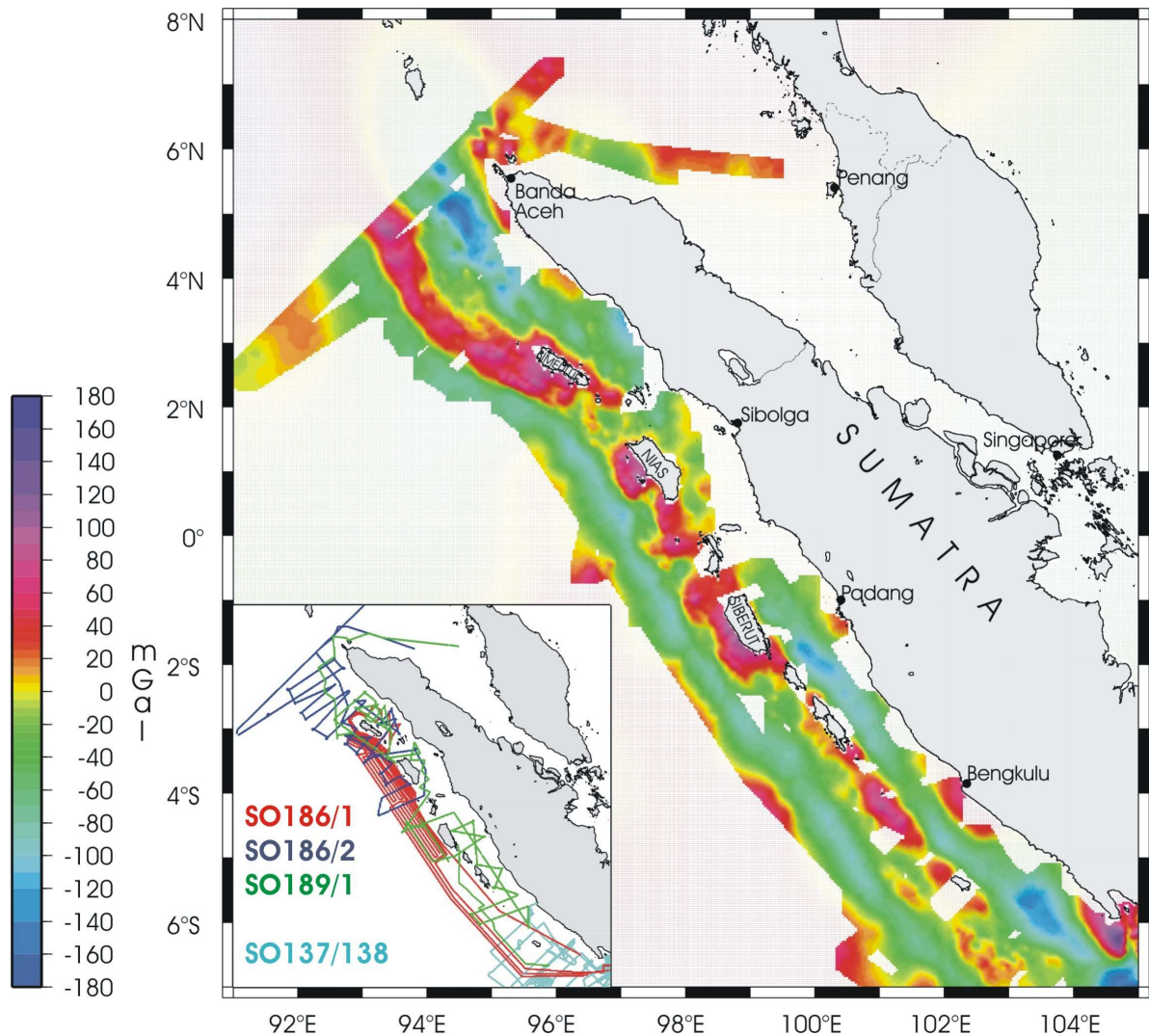


Abb. 6: Karte der Freiluftschwereanomalien. Die Karte ist bis zu einem Abstand von 15 Bogenminuten von den Schiffprofilen dargestellt.

von Sandwell and Smith (1997) (SDW15.1) und von Andersen and Knudsen (2001) vom KMS in Kopenhagen (KMS02). Die deutlich geringeren Differenzen führten Einbeziehung der KMS02 Daten für Gebiete in denen keine Schiffsmessungen durchgeführt wurden. Die Karte der Freiluftschwereanomalien zeigt Abb. 7.

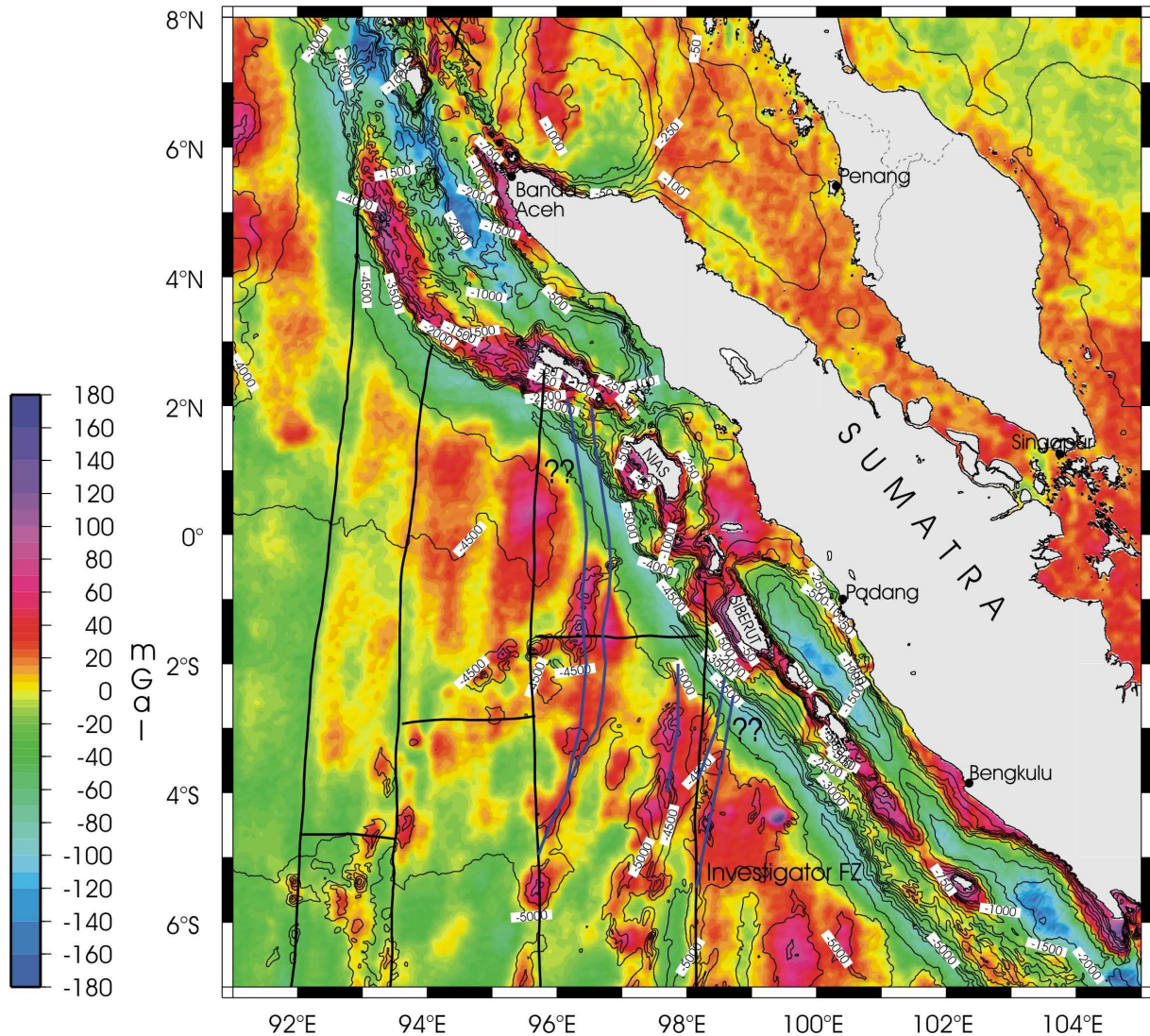


Abb. 7: Karte der Freiluftschwereanomalien. Das zugrundeliegende Schwereraster wurde nach Zusammenfügung der Schiffsdaten und der KMS02 Satellitenschweredaten erstellt. Dargestellt sind die Störungszonen nach Cande et al. (1989) und vermutete zusätzliche. Der Karte ist die GEBCO Bathymetrie (IOC, IHO, and BODC, 2003) unterlegt.

Die ozeanische Kruste im SW ist charakterisiert durch Freiluftschwereanomalien zwischen -30 und 80 mGal. Die positiven Anomalien resultieren in weiten Bereichen aus dem Einfluss der Aufwölbung der Indo-Australischen Platte vor dem Abtauchen. Darüber hinaus finden sich N-S streichende Anomalien. Diese können mit einer Reihe von Störungszonen, wie der Investigator FZ bei 98°E korreliert werden. Durch die neuen Schweredaten zeigen sich bei einigen deutliche Auffächerungen. Landwärts verläuft eine etwa 50 km breite negative Anomalie, wobei die Werte von NW nach SW bis etwa -160 mGal abfallen. Diese spiegelt den Sundagraben mit zunehmenden Wassertiefen wider. Die Füllung mit Grabensedimenten nimmt somit von Süden nach Norden beträchtlich zu. Zur Küste hin steigen die Schwerewerte an und erreichen eine Zone relativer Maxima von +60 bis +160 mGal im Bereich des Outer Arc Hochs. Diese Zone ist etwa 120 km breit, wobei das Hoch im Süden weniger ausgeprägt als im Norden ist. Nördlich von 2°N liegt das Schwerehoch sehr dicht am Graben und erreicht seine höchsten Werte bereits im Hangbereich. Dieses weist auf die Akkretion von großen Sedimentvolumina in jüngster Zeit hin. Weiter nach NE folgen lang gestreckte negative Anomalien. Sie korrelieren mit Forearc Becken, die Sedimentfüllungen von bis zu 7 km Mächtigkeit aufweisen. Im Bereich des Äquators ist kein Becken ausgebildet. Das EW streichende Schwerehoch in diesem Gebiet zeigt eine deutliche geographische Korrelation mit dem Schwerehoch der Investigator Störungszone auf der sich

anschließenden ozeanischen Kruste im Süden. Ein Zusammenhang zwischen Beiden ist wahrscheinlich. Die Subduktion der Störungsszone ist ein möglicher Grund für den Wechsel der Streichrichtung sowohl des Grabens als auch des Outer Arcs und Forearcs nördlich von Nias.

Des Weiteren wurden die Anomalien der Bouguerschwere sowie isostatische Residualanomalien unter verschiedenen Annahmen berechnet. Die Anomalien der Bouguerschwere im Bereich der ozeanischen Kruste sind stark positiv (bis zu +460 mGal), wobei die Werte von Norden nach Süden deutlich ansteigen. Dieses spiegelt neben der abnehmenden Sedimentbedeckung auch das zunehmende Alter der ozeanischen Kruste wider. Die N-S streichenden Störungszonen unterteilen die ozeanische Kruste in Bereiche unterschiedlicher gravimetrischer Signatur. Durch die Subtraktion des Schwereeffektes der isostatischen Kompensationswurzel von den Bouguerschwerewerten erhält man die isostatischen Residualanomalien. Diese sind im Bereich des Grabens und des Outer Arc Hochs deutlich und zeigen die gleiche Polarität der Freiluftschwereanomalien. Dieses resultiert aus dem dynamischen Gleichgewicht durch die Kompression des Subduktionssystems. Der Graben wird im Vergleich zum isostatischen Gleichgewicht nach unten gedrückt und der Outer Arc oben gehalten. Die isostatischen Residualanomalien zeigen jedoch vor allem im Bereich des Outer Arc Hochs neue Details. Insgesamt ist die Interpretation isostatischer Anomalien in diesem tektonischen Rahmen schwierig.

Zur weiteren Interpretation der Schweredaten wurde mit Hilfe des Softwarepaketes IGMAS (Schmidt and Götze, 1998) ein 3D Dichtemodell erstellt. MCS Reflexions- und Refraktionsseismikdaten wurden bei der Modellgeometrie berücksichtigt. Der tiefere Verlauf der subduzierenden ozeanischen Kruste wurde mit Hilfe seismologischer Daten bestimmt. Das Dichtemodell besteht aus 33 parallelen Ebenen. Die Morphologie der ozeanischen Kruste ist weitgehend flach. Sie hat eine Mächtigkeit von 7-8 km. Die Subduktionssituation ändert sich im Bereich von Simeulue recht abrupt. S von Simeulue beträgt der Abtauchwinkel an der Subduktionsfront 4 bis 5°, nimmt jedoch auf etwa 15° unter den Forearc Becken zu. Der Akkretionskeil mit steilem Hang an der Deformationsfront hat eine Breite von etwa 100 km. Er ist aus Einheiten variierender Dichte aufgebaut, die das schuppenförmige Aufstapeln widerspiegeln. N von Simeulue wandert die Subduktion bis zu 100 km landwärts und wir beobachten eine Deckenstapelung von bis zu 5 km Mächtigkeit über einer quasi horizontalen ozeanischen Kruste. Diese Decken haben eine einheitliche geringe Dichte von 2,2 g/cm³, die in der Dichte der ankommenden Grabensedimente entspricht. Weiter landwärts finden sich Forearc Becken mit bis zu 5 km Sedimenten. Der Aufbau der Becken ist asymmetrisch mit einem tieferen Teil im SW. Unterhalb der Becken findet sich kontinentale Kruste relativ hoher Dichte (2,9 g/cm³). Abb. 8 zeigt die perspektivische Ansicht des Dichtemodells von NNW bzw. S.

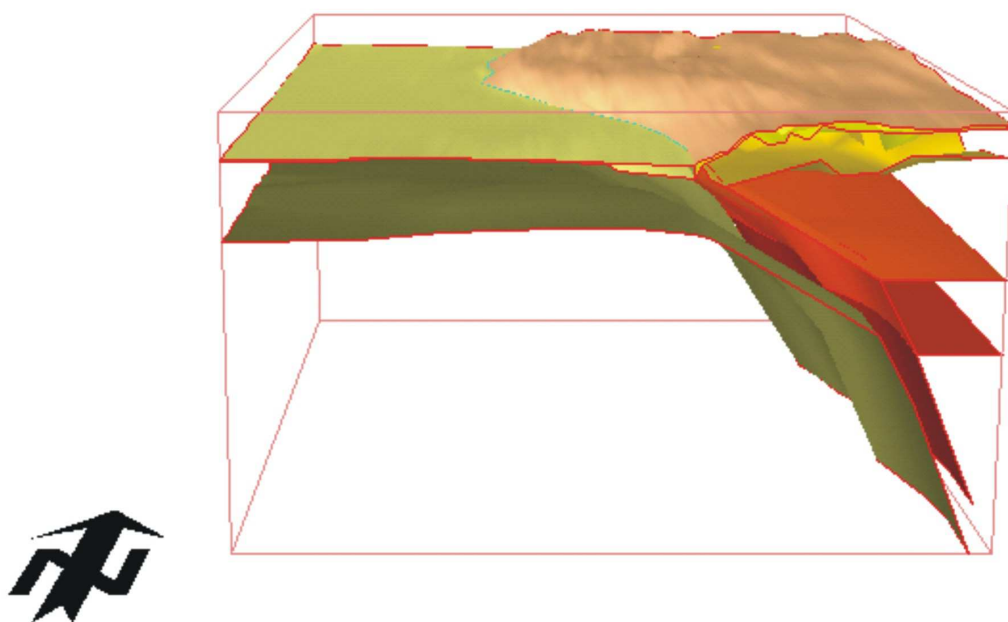
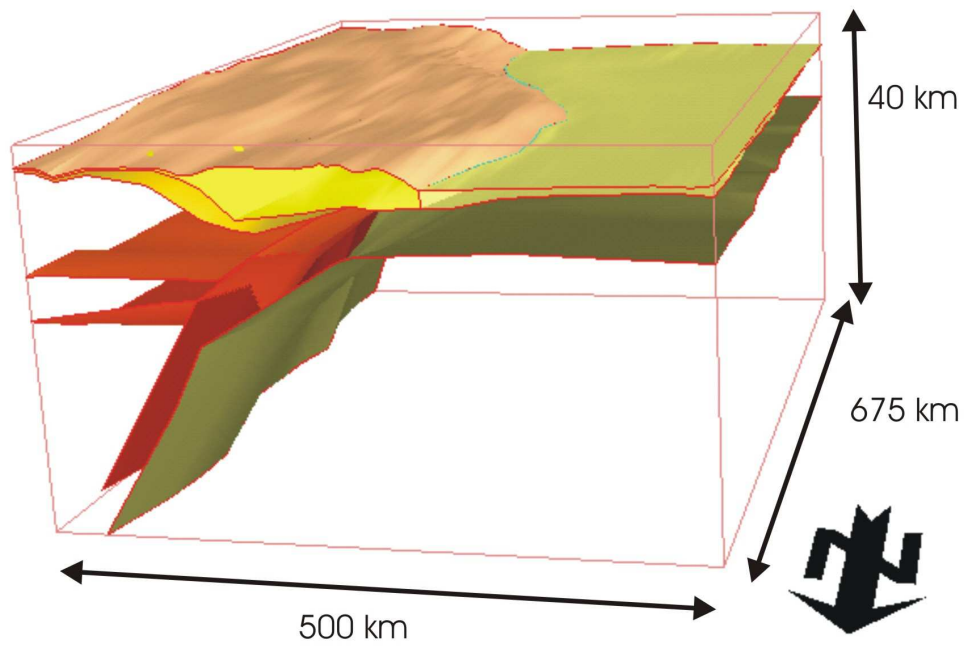


Abb. 8: Perspektivische Ansicht des nördlichen Teils des Dichtemodells von S (oben) und von NNW (unten).

1.4 Seismologische Untersuchungen zur räumlichen Verteilung der Nachbeben

Ein Ziel der seismologischen Arbeiten der Forschungsfahrt SO186 des Forschungsschiffs *SONNE* war die Registrierung der Nachbeben an der Segmentgrenze beider Schüttergebiete in der Region um die Insel Simeulue. Während der Projekte SeaCause und GITEWS wurden insgesamt 53 seismologische Stationen auf den Meeresboden ausgelegt (Abb. 9). Das seismische Netz aus Ozeanbodenseismometern (OBS) und Ozeanbodenhydrophonen (OBH) zeichnete in der Zeit zwischen dem 12. Oktober 2005 und dem 2. März 2006 eine Vielzahl von Nachbeben auf. Die Standzeit der Instrumente lag zwischen zwei Wochen und fünf Monaten. Im Mittel operierten über den Einsatzzeitraum jedoch mindestens 15 bis 20 Stationen. Bislang wurden rund 1200 Ereignisse in den Daten identifiziert (im Durchschnitt 8-9 Ereignisse pro Tag) und vorläufig lokalisiert, wobei als Selektionskriterium mindestens 5 Stationen ein individuelles Beben registrieren mussten, um in den Katalog aufgenommen zu werden. Weitere Daten liegen von sieben Landstationen vor, welche die Universität von Cambridge, England, auf der Inseln Simeulue zwischen Dezember 2005 und März 2006 betrieb.

Die Verteilung der Erdbeben zeigt eine klare räumliche Verteilung der Ereignisse. In der Zone zwischen dem Tiefseeegraben und ca. 50 km landwärts liegen (nahezu) keine Nachbeben. Die meisten Beben liegen nahe der seismischen Front (ca. 50-70 km landwärts des Tiefseeegrabens). Die Lage der seismischen Front korreliert mit einer Temperatur von rund 100°C in der Kopplungszone. Darüber hinaus ist anzumerken, dass alle größeren Ereignisse ($M > 4$), welche auch teleseismisch registriert wurden, in dieser Zone liegen. Darüber hinaus tritt seismische Aktivität in der Kopplungszone nur in einer Zone von ~50 km bis 150 km landwärts des Tiefseeegrabens auf. Das Fehlen von Erdbeben weiter landwärts könnte durch einen serpentinisierten Mantelkeil bedingt sein (Grevemeyer & Tiwari, 2006). Sollte der Mantel entlang der Kontaktzone zwischen Oberplatte und abtauchender Platte in der Tat durch Serpentinminerale charakterisiert sein, so würden die Reibungseigenschaften der Serpentine ein seismogenes Reibungsgleiten verhindern.

Im Weiteren nutzen wir die mit dem lokalen Netzwerk registrierten Ereignisse (Magnitude von $M > 4$), um die Genauigkeit einer regionalen bzw. teleseismischen Lagebestimmung der Epizentren zu untersuchen. Im Mittel lag die Abweichung zwischen den Epizentren des Amerikanischen *National Earthquake Information Center's* (NEIC – PDE Katalog) und den Epizentren des SO186-Netzwerks bei ~17 km, wobei die maximale Abweichung bei 81 km und die minimale Abweichung bei 2.4 km lag. Diese Ungenauigkeit in der teleseismischen Lagebestimmung ist für die bislang untersuchten Erdbeben aus den Monaten Oktober und November unabhängig von der Magnitude.

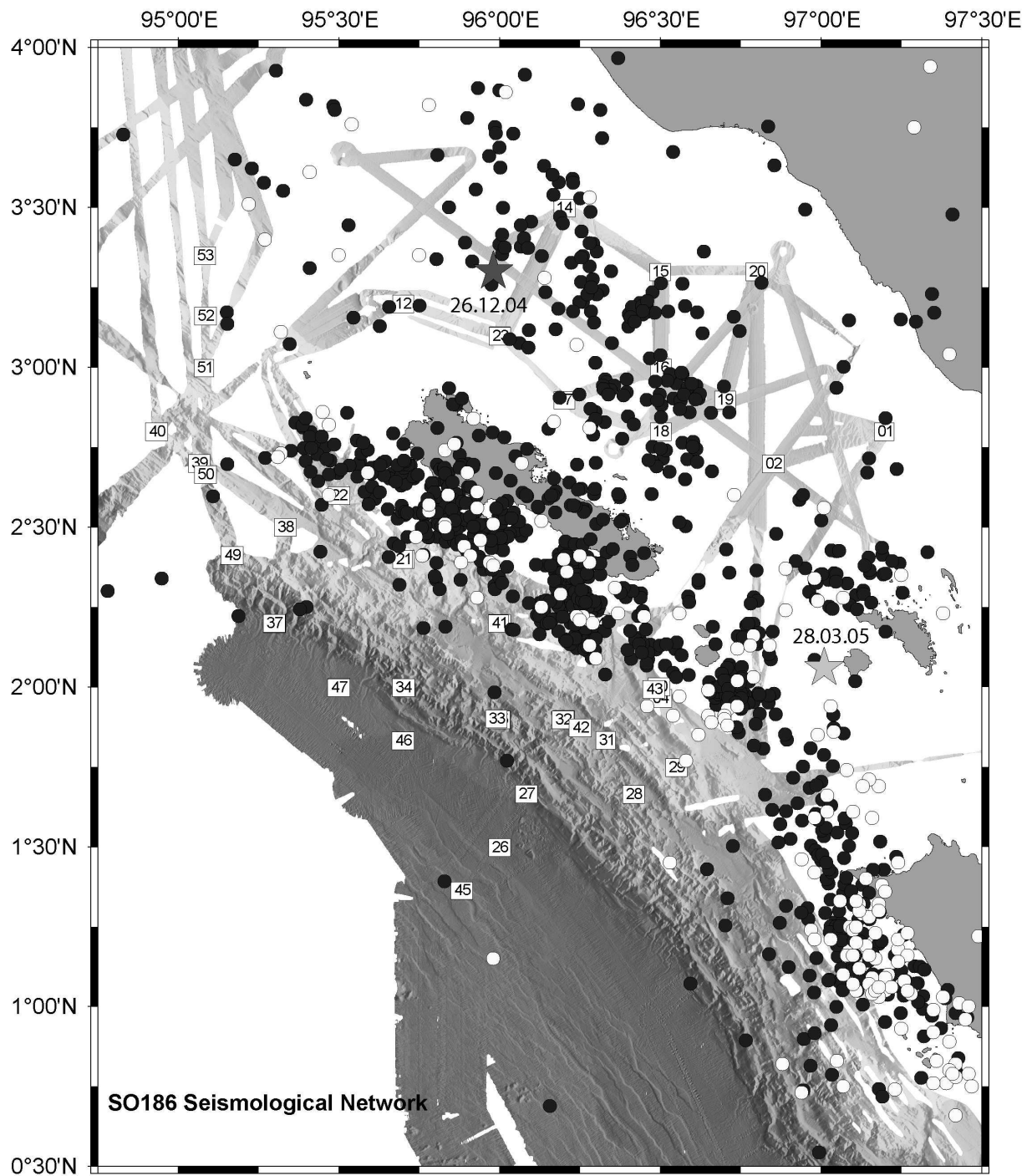


Abb. 9: Lagekarte des seismologischen Netzwerks der SO186-Expeditionen. Schwarze Punkte markieren Erdbeben, welche mit dem Netzwerk lokalisiert wurden. Weiße Punkte sind teleseismisch registrierte Erdbeben des NEIC-PDE Katalogs ($M > 4$).

1.5 Ursache der Segmentierung der Erdbebenbruchflächen

Die Bruchflächen der großen Erdbeben von 2004 und 2005 vor der Nordküste Sumatras zeigen eine abrupte südliche bzw. nördliche Begrenzung. Bis zu dieser Grenze reichte sowohl jeweils die Bruchfläche während der Erdbeben als auch die Epizentren der Nachbeben (Ammon et al., 2005). Das verdeutlicht die Bedeutung der Kenntnis von Segmentgrenzen für eine bessere Risikovorhersage. Wesentliches Ziel der Projekte SeaCause (SO186) und SUMATRA (SO189) war, die Struktur der abtauchenden Unterplatte zu erfassen, um deren Einfluss auf die Deformation im Akkretionskeil und auf die Entwicklung der Fore-Arc Becken abzuschätzen.

Auf Basis von insgesamt mehr als 9700 km Mehrkanalreflexionsseismik in Kombination mit Bathymetrie, Magnetik und Gravimetrie und weitwinkelseismischen Profilen können wir die Struktur der subduzierenden Platte, des Akkretionskeils und der Fore-Arc Becken abbilden. Im Bereich der Segmentgrenze westlich der Insel Simeulue identifizieren wir ein etwa 60 bis 80 km breites, topographisches Hoch auf der ozeanischen Kruste (Franke et al., 2008), das weitgehend durch Sedimente des Bengalfächers bedeckt ist. Diese Hochlage hat wahrscheinlich ihren Ursprung in einer inaktiven Bruchzone der ozeanischen Kruste. Mit der Konvergenz der Platte in nordnordöstlicher Richtung kollidiert der Rücken und kommt zur Subduktion bei etwa $2^{\circ}\text{N}/95,5^{\circ}\text{E}$. Östlich der Hochlage identifizieren wir unter dem Akkretionskeil einen Sprung oder Riss in der subduzierenden Platte. Die Nachbebenaktivität der Beben vom 26.12.2004 und 28.03.2005 endet jeweils in Höhe dieses Risses (Abb.10). In den weitwinkelseismischen Daten zeichnet sich der Riss über eine Breite von ca. 40 km und einer Sprunghöhe von etwa 3 km aus. Die Änderung der Tiefenlage der abtauchenden Platte korrespondiert mit einer Änderung der Reflektivität der Oberkante der ozeanischen Kruste.

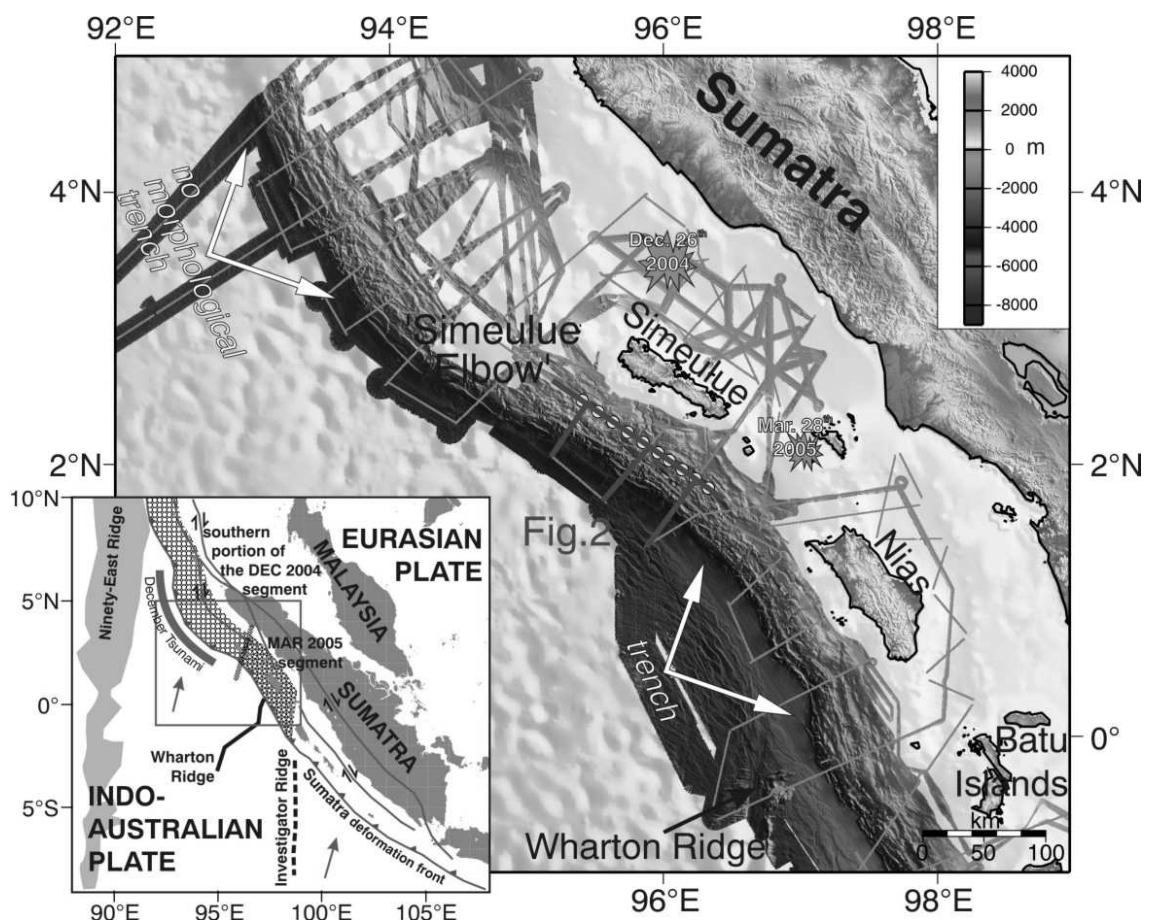


Abb. 10: Lage der seismischen Profile im Arbeitsgebiet. Die kleine Karte zeigt die Segmente aus der Nachbebenaktivität der Erdbeben 2004 und 2005 (aus: Franke et al. 2008).

Die Kombination der reflexionsseismischen und weitwinkelseismischen Daten belegt ein nordnordöstliches Streichen in Verlängerung der oben genannten Bruchzone.

Unsere Untersuchungen legen nahe, dass die subduzierende Platte entlang der Segmentgrenze gerissen ist und sich der Abtauchwinkel unter dem vorderen Akkretionskeil signifikant von Nord nach Süd versteilt (Abb. 11). Die ererbte Bruchzone scheint damit wesentlichen Einfluss auf die Ausdehnung von Erdbebenbruchflächen zu haben. Aber auch Erdbeben auf der ozeanischen Platte westlich der Subduktionszone zeigen Blattverschiebungskomponenten parallel zu den ozeanischen Bruchzonen. Damit zeichnen diese sich als Schwächezonen aus, die auch bei der Subduktion Einfluss auf die Bruchflächen von Erdbeben haben. Der Sprung in der ozeanischen Kruste unter dem Akkretionskeil wiederum verhinderte das Brechen des südlichen Segments während des 2004 Bebens.

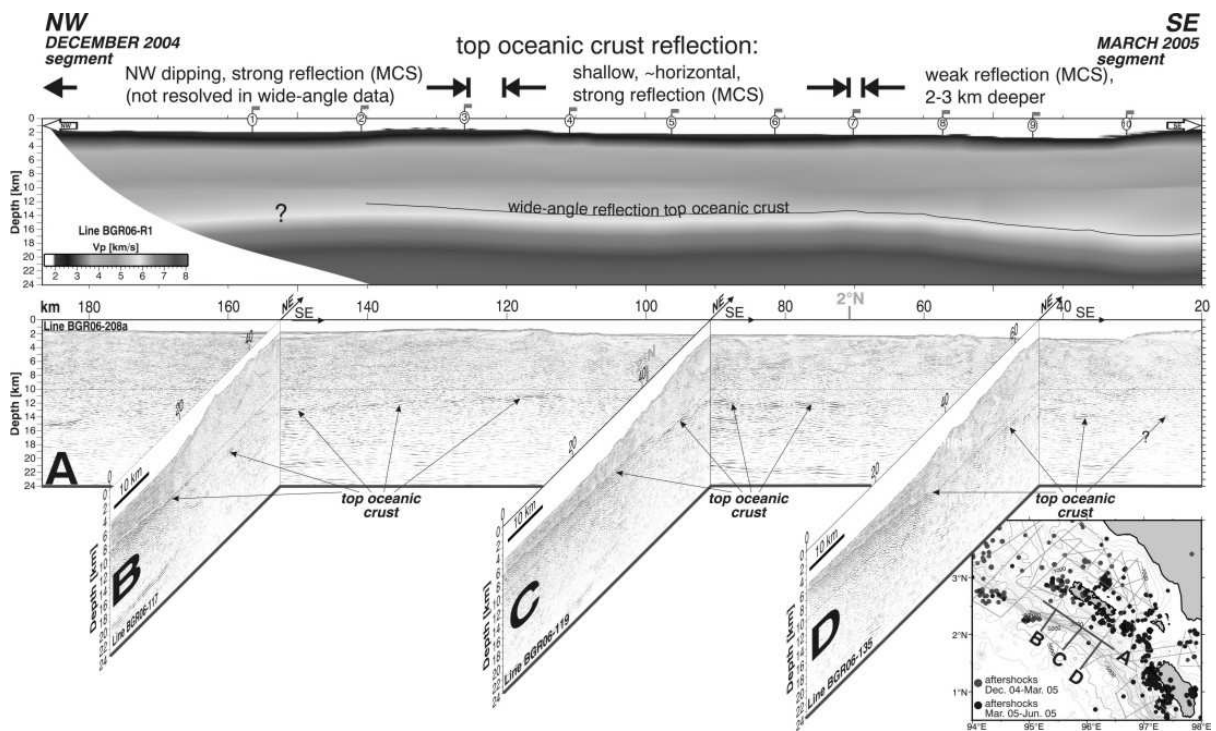


Abb. 11: Oben ist das Geschwindigkeitsmodell aus dem weitwinkelseismischen Profil (A auf der kleinen Karte) dargestellt, unten sind reflexionsseismische Profile parallel und senkrecht zur Deformationsfront abgebildet (aus: Franke et al. 2008).

1.6 Massentransfer und Seismotektonik entlang der Sumatra Subduktionszone

Die ozeanische Platte, die im Bereich von Sumatra subduziert wird, wird in ihrer seewärtigen Ausdehnung durch das Wharton Becken dominiert, das eine nach Norden hin zunehmende Sedimentbedeckung aufweist. Nach Westen ist das Becken durch den Ninetyeast Rücken, eine aseismische, ca. Nord-Süd verlaufende bathymetrische Struktur, begrenzt. Der Meeresboden im Wharton Becken wurde vor 85 Mio Jahren bis vor 45 Mio Jahren am Wharton Rücken gebildet. Der Wharton Rücken stellt ein fossiles Spreizungszentrum dar, das heute in versetzten Segmenten, die in ost-westlicher Richtung verlaufen, in die Subduktionszone eintritt (Liu et al., 1983; Royer and Sandwell, 1989). Die Mehrzahl der bathymetrischen Strukturen des Wharton Beckens verläuft allerdings in nord-südlicher Richtung. Hierbei handelt es sich meist um reaktivierte Störungszonen (Deplus et al., 1998; Abercrombie et al., 2003), die z.B. bei 93°, 94° und 96° Ost auftreten und im nördlichen Bereich von Sedimenten verdeckt sind (Sandwell and Smith, 1997; Hébert, 1996). Die markanteste Ausnahme bildet die Investigator Störungszone, die bei 98.25° Ost in den Tiefseegraben eintritt und aus mehreren parallelen Rückenstrukturen besteht. Diese Störungszone bildet auf der ozeanischen Platte eine Segmentgrenze in Bezug auf das Plattenalter und damit einhergehend auf die thermische Ausbildung, da hier ein Alterssprung von über 10 Mio Jahren stattfindet (Liu et al., 1983).

In den bathymetrischen Daten lässt sich eine Segmentierung der Oberplatte erkennen, die mit variierendem Materialtransfer einhergeht. Die Bereiche des Kontinentrandes, die sich nordwestlich der Investigator Störungszone befinden und als Nias- und Siberut-Segment bezeichnet werden (Ladage et al., 2006), liegen innerhalb der seismischen Aktivitätszone in Bezug auf die Mega-Beben der Jahre 2004/2005. Diese Segmente unterliegen einer frontalen Erosion des Subduktionskomplexes, was sich in einer Übersteilung des unteren Kontinenthangs aufgrund von Porenüberdrücken und der Subduktions bathymetrischer Erhebungen auf der ozeanischen Platte äußert. Damit einhergehend sind Materialbewegungen von der Oberplatte in den Tiefseegraben nachzuverfolgen.

Die Bereiche des Kontinentrandes südlich der Investigator Störungszone hingegen unterliegen der neotektonischen Bildung junger Akkretionsrücken. Diese sind Ausdruck der Wiederherstellung des Kontinenthangs durch frontale Akkretion nach der Migration des Wharton Rückens und der Investigator Störungszone. Dieses 600 km lange ‚Enggano-Segment‘ weist insgesamt ruhigere und glattere Meeresbodenstrukturen auf, ohne Anzeichen für extensive Erosionsprozesse.

Dieser unterschiedlichen, scharf begrenzten Segmente sind morphologisch durch eine unterschiedliche Struktur des unteren Kontinenthangs gekennzeichnet. Das Enggano-Segment weist einen flachen unteren Hang auf mit Akkretionsrücken, die als jünger einzustufen sind als die Akkretionsstrukturen im Norden (Ladage et al., 2006). Lokal scharf begrenzte frontale Erosion in diesem Segment ist lediglich in einem Bereich auszumachen, wo ein einzelner untermeerischer Vulkan von unregelmäßiger Ausdehnung und Struktur in die Subduktionszone eintritt (99.6°E/3.8°S). Ansonsten findet frontale Akkretion der Sedimente im Tiefseegraben statt und führt zur Ausbildung von kohärenten Akkretionsrücken mit Längen zwischen 20 km – 70 km.

Das Siberut-Segment, was nach Süden durch den Eintrittspunkt der Investigator Störungszone in den Tiefseegraben begrenzt wird sowie nach Norden durch den Wharton Rücken, unterlag hingegen einer erheblichen tektonischen Beanspruchung durch die Kollision des Wharton Rückens. Dies äußert sich in einem unteren Hang, der erheblich geologisch und tektonisch restrukturiert wurde und typische Anzeichen zeigt, die von der rezenten Subduktion bathymetrischer Strukturen stammen. Der aktive Akkretionskeil wurde erodiert, während sich eine Anzahl von kleineren Becken in mittlerer Hanglage ausgebildet haben, alternierend

mit lokalen morphologischen Hochs. Diese Topographie ist typisch für einen Kontinenthang, der rezent durch die Subduktion von z. B. Rückenstrukturen oder untermeerischen Vulkanen überprägt wurde (Collot and Fisher, 1989; Dominguez et al., 1998; Laursen et al., 2002, Hampel et al., 2004).

Das Nias-Segment wiederum, das sich nördlich des Wharton-Rückens erstreckt, ist charakterisiert durch einen steil ansteigenden unteren Hang, der extensive geomorphologische Anzeichen für Oberflächenerosion zeigt. Obwohl das frontale Akkretionsprisma in diesem Segment noch intakt ist, so ist doch die gesamte Oberflächenstruktur erheblich rauher und ungleichmäßiger als im südlichen Enggano-Segment, was auch auf ein gut ausgebildetes System von Materialkanälen in den Tiefseeegraben zurückzuführen ist, die den unteren Hang durchschneiden. Zahlreiche Hangrutschungen transportieren Material teilweise bis zu mehreren Kilometern seewärts der Deformationsfront (Henstock et al., 2006). Anzeichen für Erosion finden sich ebenfalls in den seismischen Daten, die hier präsentiert werden.

Der Wechsel im Mechanismus des Materialtransfers von Süden nach Norden geht einher mit einer Aufsteilung des unteren Hanges und einem sich vergrößerendem vorderen Öffnungswinkel. Diese Änderung in der Hanggeometrie ist vermutlich auf Porenüberdrücke zurückzuführen, die als vernachlässigbar vor Süd-Sumatra anzusehen sind (Kopp und Kukowski, 2003), während ein hoher Fluiddruck vor Nord-Sumatra zu erwarten ist (Prawirodirdjo et al., 1997; Briggs et al., 2006). Eine Übersteilung des unteren Kontinentanges findet ebenfalls in Bereichen statt, wo es zu einer Kollision bathymetrischer Strukturen auf der Unterplatte mit der Deformationsfront kommt (Ballance et al., 1989).

Die großskalige morphotektonische Segmentierung der Sumatra Subduktionszone ist somit hauptsächlich auf die Subduktion reaktiver Störungszonen und aseismischer Rücken des Wharton Beckens zurückzuführen und spiegelt sich auch in ihrer seismotektonischen Segmentierung wider. Ausdruck hierfür sind vor allem die scharf begrenzten Nachbebenregionen der Beben von 2004/2005. Ein weiterer Faktor stellt der Wechsel in der Interplattenbewegung dar, der aus dem geographischen Verlauf der Subduktionszone vor Nord-Sumatra resultiert (Kennett und Cummins, 2005; DeShon et al., 2006). Variationen in der Geometrie der Subduktionszone sind ebenfalls eng verknüpft mit einem Wechsel in den physikalischen Eigenschaften, die u.a. durch die hohe Variabilität im Plattenalter der ozeanischen Lithosphäre hervorgerufen wird (Lay et al., 2005). Das Plattenalter vor Sumatra deckt eine Zeitspanne von 40 Mio Jahren ab, mit Alterssprüngen von bis zu 10 Mio Jahren, was auf eine Variation in der Lithosphärenmächtigkeit bzw. des Auftriebs und vorallem auch auf einen Wechsel in den thermischen Eigenschaften der einzelnen Segmente hinweist.

Die Ausdehnung der seismischen Aktivität der Beben aus den Jahren 1861, 2004 und 2005 zeigt eine ausgeprägte geographische Übereinstimmung mit den Segmentgrenzen. Diese Begrenzung in den Nachbebenzonen deutet darauf hin, dass sich die Erdbeben nicht über Plattensegmentgrenzen, die mit einem ausgeprägten Wechsel in der Geometrie, Materialstärke, Fluidgehalt oder Spannungen verbunden sind, hinweg fortpflanzen (Hilley et al., 2001; Krüger und Ohrnberger, 2005).

1.7 Seismostratigraphie und Tektonik der Vorderbogenbecken

Die Vorderbogenbecken vor Sumatra liegen zwischen dem Festland und dem seewärtig vorgelagerten äußeren Hoch. Das Untersuchungsgebiet umfasst drei Vorderbogenbecken – das Aceh Becken im Norden, das Simeulue Becken in der Mitte und das Nias Becken im Süden (Abb. 12). Die Wassertiefe der Becken nimmt nach Norden hin zu. Die variierenden Beckenfüllungen zeigen unterschiedliche Beckenentwicklung an, die insbesondere durch Blattverschiebungssysteme beeinflusst sind.

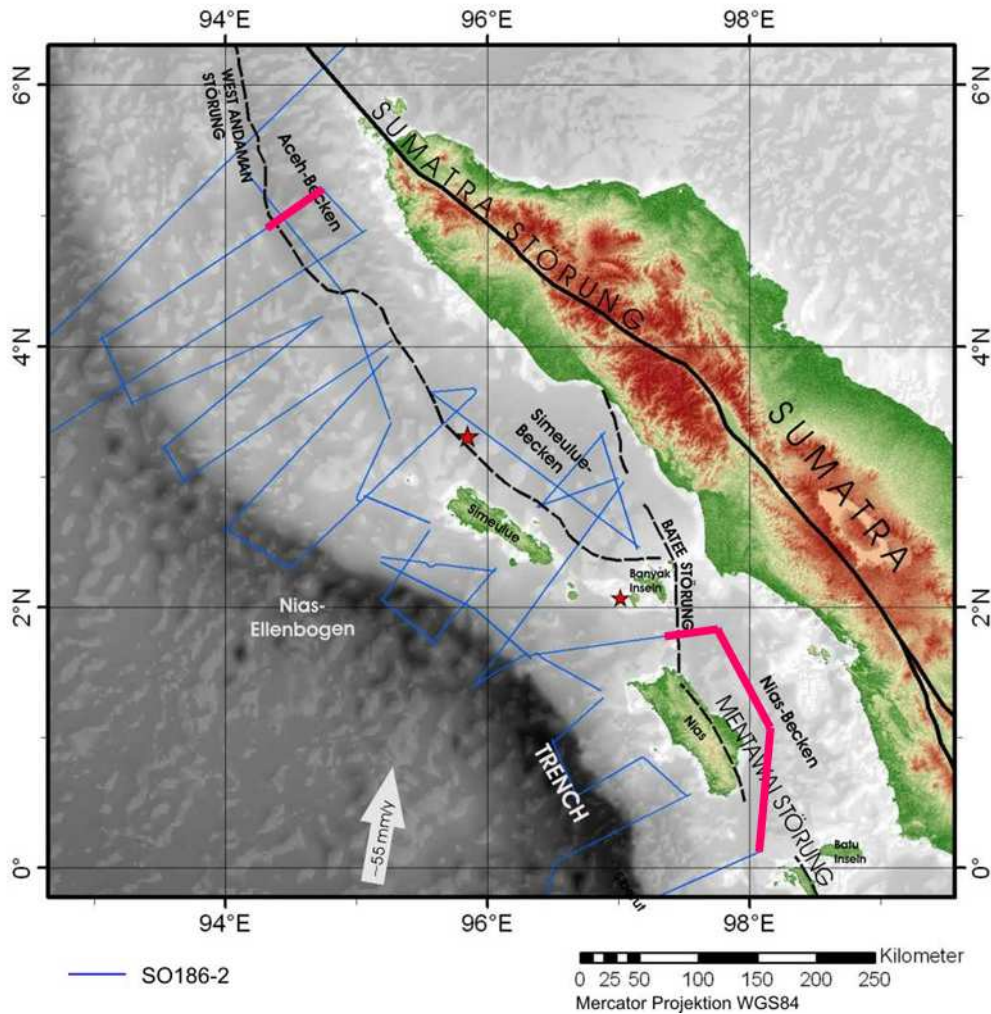


Abb. 12: Lage der Vorderbogenbecken vor Sumatra. Mit blauer Farbe sind die MCS Profile im Arbeitsgebiet gekennzeichnet. In roter Farbe die Ausschnitte für Abb. 13 und 15.

Aceh-Becken

Das Aceh-Becken ist das nördlichste Vorderbogenbecken Sumatras und liegt zwischen der West-Andaman-Störung und der Sumatra-Störung. Die maximale Wassertiefe beträgt 2800 m. Neogene Sedimente weisen eine gute Stratifizierung auf und zeigen durchschnittliche Mächtigkeiten von 2 s (Zweiweglaufzeit; TWT), mit einem Maximum im Süden. Dort ist eine regelmäßige Beckenarchitektur zu finden, wogegen im Norden des Beckens starker Einfluss von Blattverschiebungen seit dem oberen Miozän zu einem komplexeren Aufbau geführt hat.

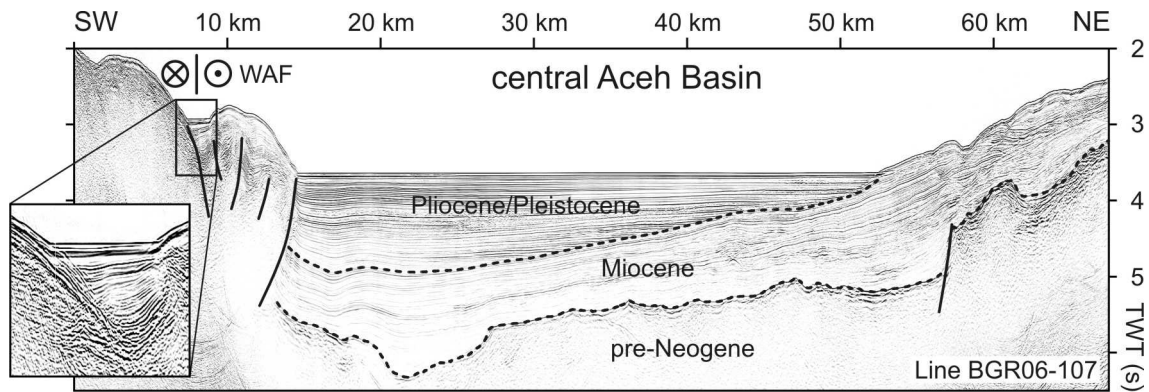


Abb. 13: Mehrkanalseismisches Profil über den zentralen Bereich des Aceh-Beckens. Die miozänen Sedimente sind in Richtung Tiefsee-graben verkippt. Die Vergrößerung zeigt die typische Ausprägung der WAF am Westrand des Aceh-Beckens, eine syntektonisch verfüllte Depression eingefasst von etwa 6 km breiten Antiklinalen.

Simeulue-Becken

Das Simeulue-Becken weist eine maximale Wassertiefe von 1300 m auf und zeigt Neogene Sedimentmächtigkeiten von bis zu 5 s (TWT). Wir haben drei Phasen der Subsidenzentwicklung im Neogen identifiziert: Eine früh- bis mittelmiozäne Phase ist charakterisiert durch initiale Subsidenz in mehreren Halbgräben entlang des westlichen Beckenrandes. Im späten Miozän und Pliozän vereinen sich diese zu einem einheitlichen tiefsee-grabenparallelen Subsidenzzentrum, welches sich am Ende diese Phase ostwärts ausweitert und eine dort entwickelte Karbonatplattform versinken lässt. In der letzten, bis heute andauernden Phase zeigt das zentrale Simeulue-Becken Anzeichen von Inversion.

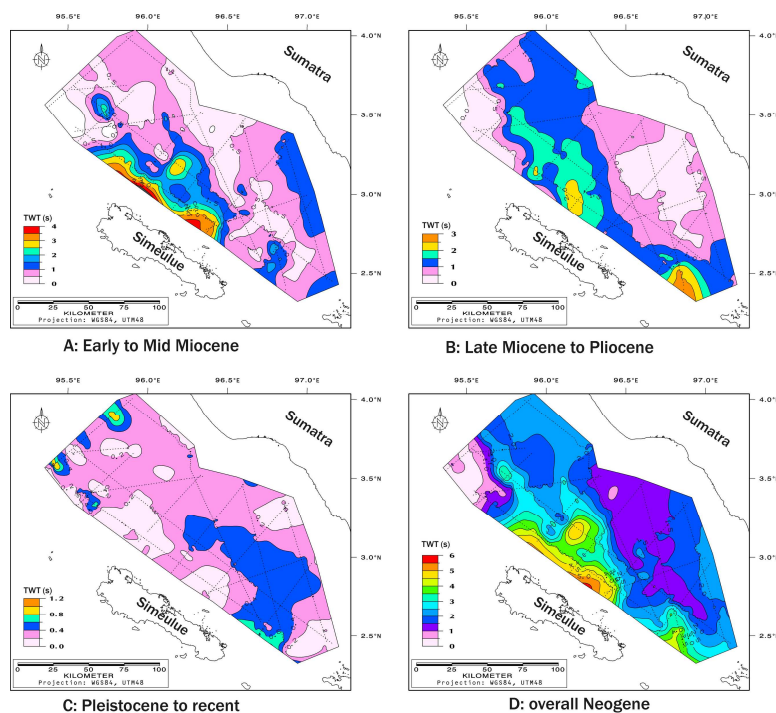


Abb. 14: TWT-Isochoren-Karte der Neogenen Sedimente im Simeulue-Becken. Die gepunkteten Linien zeigen das basierende seismische Profilnetz. A: Die früh- bis mittelmiozäne Abfolge zeigt mehrere Maxima entlang des westlichen Beckenrandes. B: Das späte Miozän und Pliozän ist durch eine gleichmäßigere Sedimentmächtigkeit gekennzeichnet. C: Im Plio/Pleistozän liegt das Maximum der Sedimentmächtigkeit im Südosten. D: Die höchste Mächtigkeit der neogenen Sedimente liegt nordöstlich der Insel Simeulue.

Nias-Becken

Das Nias-Becken ist maximal 900 m tief und weist eine durchschnittliche Neogene Sedimentmächtigkeit von 2.5 s (TWT) auf. Die Beckensubsidenz zeigt vier Hauptphasen: (1) Vom frühen bis späten Miozän liegt das Depozentrum im südlichen Teilbecken. Dort erreichen die Sedimente Mächtigkeiten bis 2 s (TWT). (2) Das späte Miozän ist durch ein nordwärts progradierendes System charakterisiert. Im südlichen Teilbecken weist eine Erosionsdiskordanz auf Hebung hin. (3) Im Pliozän hat sich das Depozentrum in das nördliche Teilbecken verlagert. (4) Pleistozäne Sedimentation findet relativ gleichmäßig im gesamten Becken statt, der nordwestliche Beckenbereich wird durch die Batee-Störung gehoben.

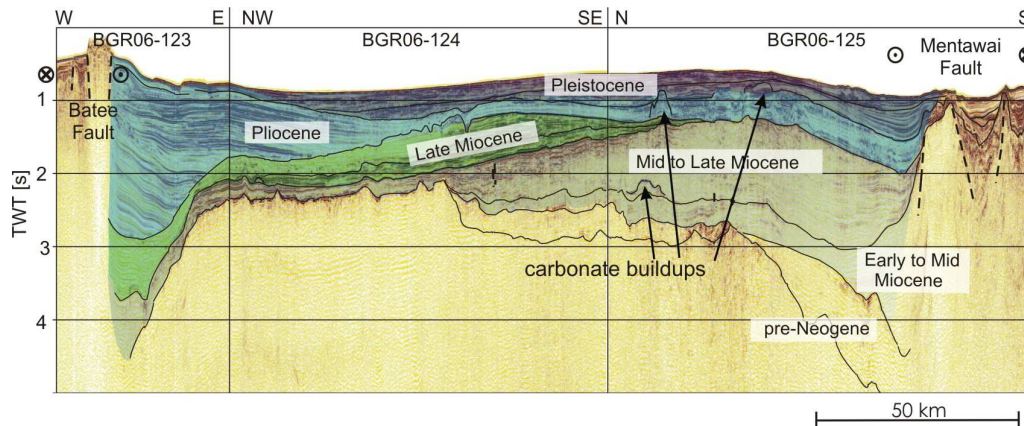


Abb. 15: Zusammengesetztes Mehrkanalseismikprofil entlang der Beckenachse des Nias-Beckens. Das Depozentrum verlagert sich im oberen Miozän vom südlichen in das nördliche Teilbecken.

Blattverschiebungssysteme

Eine Untersuchung der seismischen Sequenzen und der Ozeanbodentopographie der Simeulue- und Aceh-Becken und des angrenzenden Bereiches des Äußeren Hochs zeigt, dass die Entwicklung der Vorderbogen-Becken seit dem oberen Miozän durch Blattverschiebungen geprägt wird. Die Mentawai-Störung lässt sich bis nördlich der Insel Simeulue verfolgen und war bis zum Ende des Miozäns in nördlicher Richtung mit der Sumatra-Störung verbunden. Dieser nördlichste Arm der Mentawai-Störung verlagerte sich in der Folge westwärts und initiierte die West-Andaman-Störung im Bereich des Aceh-Beckens. Ein lateraler Versatz verbindet die West-Andaman-Störung mit der Mentawai-Störung. In dieser transpressiven Situation bildete sich der Tuba-Rücken aus. Vom Treffpunkt der West-Andaman-Störung und des Tuba-Rückens zweigt eine dextrale Blattverschiebung in südsüdwestlicher Richtung ab und durchschneidet das Äußere Hoch und den Akkretionskeil. Dies führte südlich des Tuba-Rückens zu Extrusion und Ausbildung eines Randbeckens, das an seinem Westrand durch eine Überschiebung herausgehoben und in östlicher Richtung verkippt wurde. Die westwärtige Verlagerung von Blattverschiebungen im Aceh-Becken wurde von einer Verschiebung des sedimentären Ablagerungszentrums in nordwestlicher Richtung begleitet, was zur Bildung einer großen Diskordanz führte. Im Gegensatz dazu finden sich im Simeulue-Becken zwei Neogene Hauptdiskordanzen, was die unterschiedliche Entwicklung der Vorderbogen-Becken dokumentiert und zeigt, dass sie neben Subduktionsprozessen an aktiven Konvergenzzonen durch Deformationen entlang großer Blattverschiebungen kontrolliert wird.

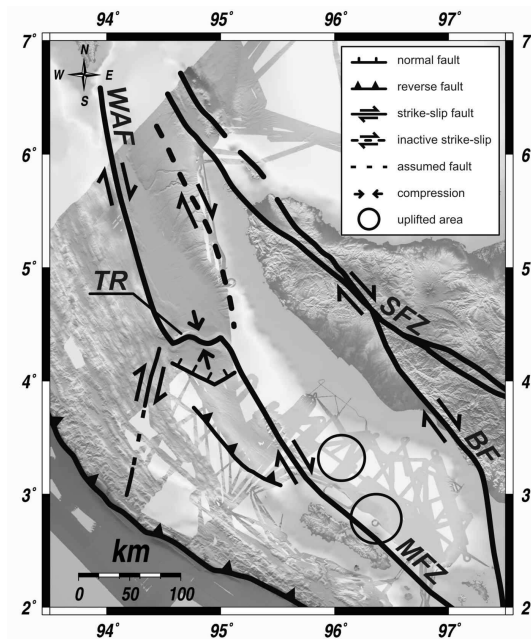


Abb. 16: Tektonische Strukturen im Untersuchungsgebiet. WAF = West-Andaman-Störung; SFZ = Sumatra-Störung; BF = Batee-Störung; MFZ = Mentawai-Störung; TR = Tuba-Rücken. Der nördliche Arm der Mentawai-Störung springt in westlicher Richtung auf die Position der West-Andaman-Störung. Ein transpressiver Versatz formt den Tuba-Rücken. Vom Treffpunkt der West-Andaman-Störung und des Tuba-Rückens verläuft eine dextrale Blattverschiebung in SSW-Richtung und schneidet das Äußere Hoch. Dies führt zu Extrusion eines Randbeckens, welches am Westrand durch eine Aufschubung herausgehoben und verkippt wird.

1.8 Das Kohlenwasserstoffsystem des Simeulue Beckens

Während der Sonneausfahrt SO-186-2 wurden im Simeulue Forearc-Becken ca. 650 km Mehrkanalseismik-, Fächerecholot-, Magnetik- und Gravimetriedaten im Tiefwasserbereich aufgenommen (Abbildung 17). Diese Daten zeigen u.a. deutliche „Bright-Spots“, die durch gasführende Sedimente verursacht werden. Die Gasführung wurde durch *Amplitude-versus-Offset* Untersuchungen und seismische Inversion nachgewiesen. Darüber hinaus sind zahlreiche Karbonatstrukturen sichtbar, die sich in heutigen Wassertiefen von 1000 m-1100 m befinden und von 500-800 m Sediment bedeckt sind. Die Karbonatstrukturen (Build-Ups) zeigen teilweise eine typische „Backstepping-Geometrie“, während andere als „Pinnacle-Strukturen“ ausgebildet sind.

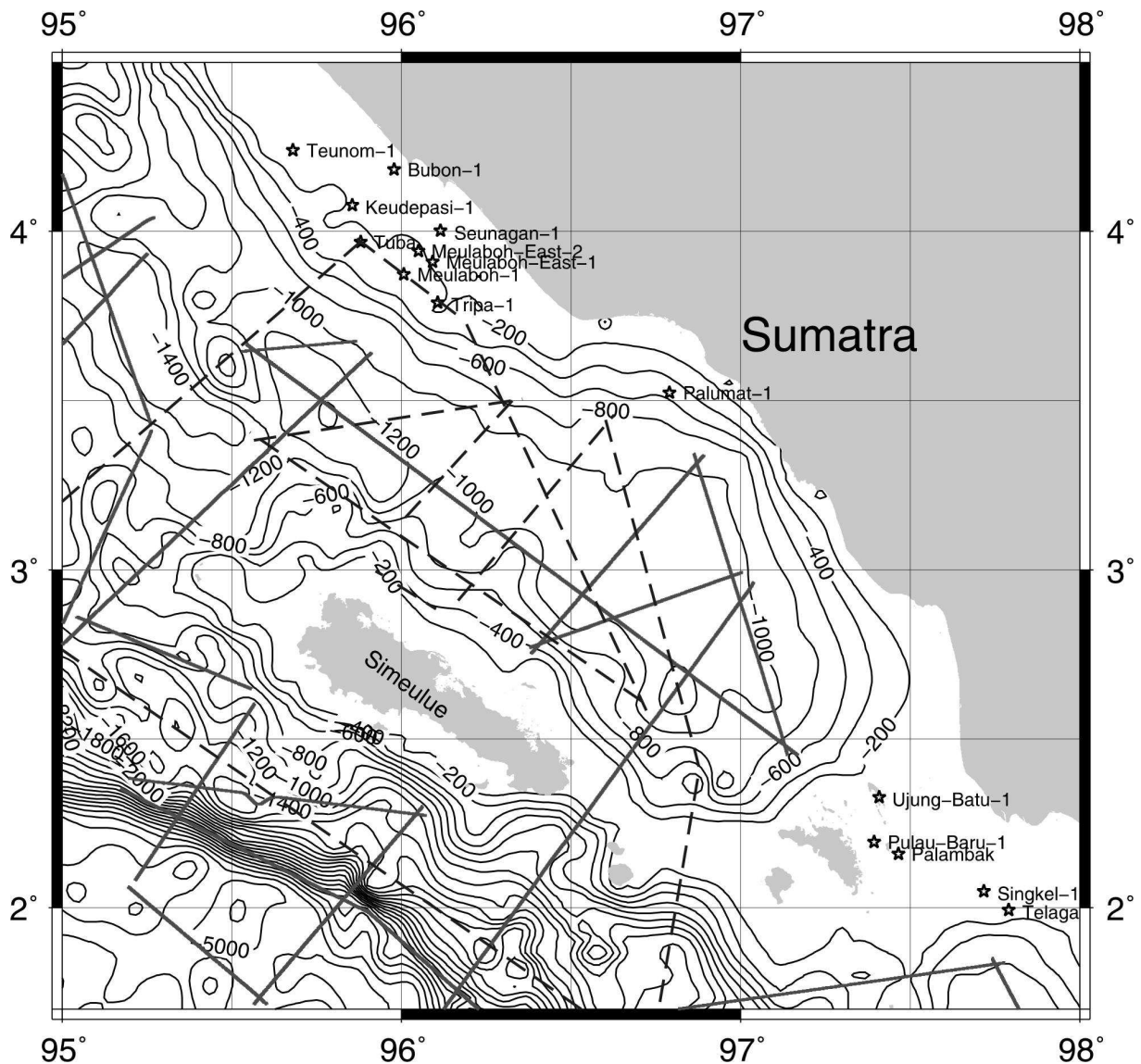


Abb. 17: Lage des Arbeitsgebietes, der Industriebohrungen und der seismischen Profile, die während der Sonnefahrten SO186 (durchgezogen) und SO189 (gestrichelt) in diesem Gebiet aufgenommen wurden.

Bei der Sonneausfahrt SO-189-1 wurden im gleichen Untersuchungsgebiet ca. 850 km Mehrkanalseismik-, Fächerecholot-, Magnetik- und Gravimetriedaten aufgenommen. Mit Hilfe der zusätzlichen Profile wurde ein Anschluss der seismischen Daten im Tiefwasserbereich an küstennahe Bohrungen erreicht.

Auf den seismischen Profilen wurden weitere Karbonatstrukturen entdeckt, die teilweise darüberliegende Bright-Spots aufweisen, so dass insgesamt mehr als 30 Karbonatstrukturen mit einer horizontalen Ausdehnung von weniger als 1 km bis über 10 km und einer Mächtigkeit zwischen 0,25 s (TWT) bis 0,415 s (TWT) in unseren seismischen Daten aufgezeichnet sind. Auffällig ist, dass sich die Bright-Spots am Rande einer Beckeneintiefung mit mehr als 6 km Sediment häufen. In diesem Depozentrum könnten Kohlenwasserstoffe generiert werden, die dann in strukturenhöhere Positionen (z.B. Karbonate) migrieren. Erdölmuttergesteine sind im Simeuleu-Becken bisher nicht erbohrt worden.

Die an Land befindlichen Sedimentbecken im Back-Arc-Bereich sind ergiebige Erdöl-/Erdgasprovinzen. Im Nordsumatra-Becken treten sowohl terrestrische als auch marine Muttergesteine auf. Im Zentralsumatra-Becken ist das wichtigste Erdölmuttergestein der lakustrine eozäne „Brown shale“ (Clure, 2005; Peters et al., 2005).

Gasgeochemische Untersuchungen an Sedimentproben zeigen, dass eine thermische Kohlenwasserstoffgenese aus vermutlich marinem Muttergestein stattgefunden hat. Um die Annahme der Kohlenwasserstoffgenese im Becken zu überprüfen wurde ein 3D-Modell des Simeuleu-Beckens erstellt und eine numerische Beckenmodellierung durchgeführt.

Der Wärmefluss im Simeuleu-Becken wurde in sechs Bohrungen durch 1D-Modelle bestimmt. Dabei variiert er zwischen 40 und 60 mW/m² mit der Ausnahme der Bohrung Teunom (100 mW/m²). Diese Spanne für den Wärmefluss wird durch Wärmeflussberechnungen aus der Tiefenlage von BSRs (bottom simulating reflector) bestätigt (37-74 mW/m²). Wärmeflussmessungen am Meeresboden zeigen Werte zwischen 47-107 mW/m², wobei die hohen Werte an aktiven Störungszonen gemessen wurden (Delisle and Zeibig, 2007). Zwei Wärmefluss Szenarien wurden für die Entwicklung des Simeuleu-Beckens gerechnet; eines mit 40 mW/m² und eines mit 60 mW/m².

Zusammenfassung

Die numerische Beckenmodellierung, die seismischen Untersuchungen und die gasgeochemischen Resultate zeigen folgende Ergebnisse:

Bright spots treten zahlreich in obermiozänen/pliozänen Sedimenten im Simeuleu-Becken auf und werden wahrscheinlich von gasführenden Schichten gebildet, was durch die AVO/AVA-Analysen bestätigt wird.

Der Wärmefluss im Becken beträgt zwischen 40 mW/m² und 60 mW/m², basierend auf den 1D-Modellierungen von sechs Bohrungen und BSR-Tiefenlagen. Höhere Wärmeflüsse wurden an aktiven Störungszonen gemessen.

Die Ergebnisse der Modellierung zeigen, dass eine Migration von Kohlenwasserstoffen vom Depozentrum aus in potenzielle Reservoirs möglich ist.

Die gasgeochemischen Untersuchungen der adsorbierten Kohlenwasserstoffgase sprechen für einen thermischen Ursprung des Gases aus einem marinen Muttergestein.

Die Karbonatstrukturen können als Reservoirs angesehen werden und wurden im 60 mW/m²-Modell mit Erdöl und Erdgas gefüllt; zusätzlich können obermiozäne/pliozäne Sedimente als Reservoirs vorhanden sein.

Im 40 mW/m²-Modell werden signifikant weniger Kohlenwasserstoffe gebildet. Diese Mengen reichen aus um die Bright-Spots zu erklären, eine deutliche Füllung der Karbonat-Reservoirs ist allerdings nicht zu erwarten.

1.9 Literaturverzeichnis

- Abercrombie, R. E., Antolik, M., and Ekström, G., 2003. The June 2000 Mw 7.9 earthquakes south of Sumatra: Deformation in the India-Australia Plate. *J. Geophys. Res.*, 108(B1), 2018, doi:10.1029/2001JB000674.
- Ammon, C.J., Ji, C., Thio, H-K., Robinson, D., Ni, S., Hjorleisdottir, V., Kanamori, H., Lay, T., Das, S., Helmberger, D., Ichinose, G., Polet, J., Wald, D., 2005. Rupture Process of the 2004 Sumatra-Andaman Earthquake. *Science* 308, 1133-1139, doi: 10.1126/science.1112260
- Andersen, O.B. and Knudsen, P., 2001. Global marine gravity field from the ERS-1 and GEOSAT geodetic mission altimetry, *J. Geophys. Res.*, 103(C4), 8129.
- Ballance, P. F., Scholl, D. W., Vallier, T. L., Stevenson, A. J., Ryan, H., and Herzer, R. H., 1989. Subduction of a late Cretaceous seamount of the Louisville Ridge at the Tonga Trench: A model of normal and accelerated tectonic erosion. *Tectonics* 8(5), 953-962.
- Briggs, R. W., Sieh, K., Meltzner, A. J., Natawidjaja, D., Galetzka, J., Suwargadi, B., Hsu, Y., Simons, M., Hananto, N., Suprihanto, I., Prayudi, D., Avouac, J.-P., Prawirodirdjo, L., and Bock, Y., 2006. Deformation and slip along the Sunda megathrust in the great 2005 Nias-Simeulue earthquake. *Science* 311, 1897-1901.
- Cande, S.C., LaBrecque, J.L., Larson, R.L., Pitman, W.C., Golovchenko, X., Haxby, W.F., 1989. Magnetic lineations of the world's ocean basins. LDGO contribution 4367, AAPG, Tulsa, Oklahoma.
- Clure, J., 2005. Fuel resources: oil and gas, in A. J. Barber, M. J. Crow, and J. S. Milsom, eds., *Sumatra: Geology, Resources and Tectonic Evolution*. Geological Society Memoirs, v. 31, Geological Society, London, p. 131-141, doi: 10.1144/GSL.MEM.2005.031.01.10
- Collot, J.-Y. and Fisher, M. A., 1989, Formation of forearc basins by collision between seamounts and accretionary wedges: An example from the New Hebrides subduction zone. *Geology* 17, 930-933.
- Delisle, G., and M. Zeibig, 2007. Marine Heat Flow Measurements in Hard Ground Offshore Sumatra. *EOS Transactions AGU* 88, 38-39.
- Deplus, C., Diament, M., Hébert, H., Bertrand, G., Dominguez, S., Dubois, J., Malod, J., Patriat, P., Pontoise, B., and Sibilla, J.-J., 1998. Direct evidence of active deformation in the eastern Indian oceanic plate. *Geology* 26, 131-134.
- DeShon, H. R., Engdahl, E. R., Thurber, C. H., Brudzinski, M., 2005. Constraining the boundary between the Sunda and Andaman subduction systems: Evidence from the 2002 Mw 7.3 Northern Sumatra earthquake and aftershock relocations of the 2004 and 2005 great earthquakes. *Geophys. Res. Lett.* 32, L24307, doi:10.1029/2005GL024188.
- Dominguez, S., Lallemand, S., Malavielle, J., and Schnuerle, P., 1998. Oblique subduction of the Gagua Ridge beneath the Ryukyu accretionary wedge system: Insights from marine observations and sandbox experiments. *Mar. Geophys. Res.* 20, 383-402.
- Engels, M., Barckhausen, U., Gee, J.S., 2007. A new towed marine vector magnetometer: methods and results from a Central Pacific cruise. Submitted to *Geophys. J. Int.*
- Franke, D., Schnabel, M., Ladage, S., Tappin, D.R., Neben, S., Djajadihardja, Y.S., Müller, C., Kopp, H., Gaedicke, C., 2008. The great Sumatra-Andaman earthquakes —Imaging the boundary between the ruptures of the great 2004 and 2005 earthquakes. *Earth Planet. Sci. Lett.* 269, 118–130, doi:10.1016/j.epsl.2008.01.047.
- Gaedicke, C., ed., 2006. Cruise Report SO186 Leg 2 SeaCause II, BGR Report, 0125999, 144 pp.
- Grevemeyer, I, Tiwari, V.M., 2006. Overriding plate controls spatial distribution of megathrust earthquakes in the Sunda-Andaman subduction zone. *Earth Planet. Sci. Lett.*, 251, 199-208, doi: 10.1016/j.epsl.2006.08.021
- Hampel, A., Adam, J., Kukowski, N., 2004. Response of the tectonically erosive south Peruvian forearc to subduction of the Nazca Ridge: Analysis of three-dimensional analogue experiments. *Tectonics* 23, TC5003, doi:10.1029/2003TC001585.

- Hébert, H., Deplus, C., Diament, M., 1996. Origin of the 90E Ridge and the Investigator Ridge deduced from the analysis of bathymetric and gravimetric data. *C. R. Acad. Sci. Paris*, 323, 105-112.
- Henstock, T. J., McNeill, L. C., Tappin, D. R., 2006. Seafloor morphology of the Sumatran subduction zone: Surface rupture during megathrust earthquakes? *Geology* 34, 485-488.
- Hilley, G. E., Arrowsmith, J. R., Stone, E., 2001. Inferring segment strength contrasts and boundaries along low-friction faults using surface offset data, with an example from the Cholame-Carrizo segment boundary along the San Andreas Fault, Southern California. *Bull. Seis. Soc. Am.* 91(3), 427-440.
- IOC, IHO, and BODC, 2003: Centenary Edition of the GEBCO Digital Atlas, published on CD-ROM on behalf of the Intergovernmental Oceanographic Commission and the International Hydrographic Organization as part of the General Bathymetric Chart of the Oceans, British Oceanographic Data Centre, Liverpool.
- Kennett, B. L. N., Cummins, P. R., 2005. The relationship of the seismic source and subduction zone structure for the 2004 December 26 Sumatra-Andaman earthquake *Earth Planet. Sci. Lett.* 239, 1-8.
- Kopp, H., and Flueh, E. R., eds., 2006, Cruise Report SO186 Leg 3 Seacause II, IFM-GEOMAR Report, 6, 205 pp.
- Krüger, F., Ohrnberger, M., 2005. Tracking the rupture of the Mw=9.3 Sumatra earthquake over 1,150 km at teleseismic distance. *Nature* 435, doi:10.1038/nature03696, 937-939.
- Ladage, S., Weinrebe, W., Gaedicke, C., Barckhausen, U., Flueh, E. R., Heyde, I., Krabbenhoft, A., Kopp, H., Fajar, S., and Djajadihardja, Y., 2006. Bathymetric survey images structure off Sumatra. *EOS* 87(17), 165-172.
- Laursen, J., Scholl, D. W., von Huene, R., 2002. Neotectonic deformation of the central Chile margin: Deepwater forearc basin formation in response to hot spot and seamount subduction. *Tectonics* 21(5), 1038, doi:10.1029/2001TC901023.
- Liu, C.-S., Curray, J.R. McDonald, J.M., 1983. New constraints on the tectonic evolution of the eastern Indian Ocean. *Earth Planet. Sci. Lett.*, 65, 331-342.
- National Geophysical Data Center, 2007, Marine Geophysical Trackline Data, DVD Version 5.0.10, World Data Center for Geophysics & Marine Geology, Boulder.
- Peters, K. E., Moldowan J. M., Walters C. C., 2005, *The biomarker guide; II, Biomarkers and isotopes in petroleum systems and Earth history.* Cambridge University Press, p. 475-1155.
- Prawirodirdjo, L, Bock, Y., McCaffrey, R., Genrich, J., Calais, E., Stevens, C., Puntodewo, S. S. O., Subarya, C., Rais, J., Zwick, P., Fauzi, 1997. Geodetic observations of interseismic strain segmentation at the Sumatra subduction zone. *Geophys. Res. Lett.* 24(21), 2601-2604.
- Royer, J.Y., Sandwell, D. T., 1989. Evolution of the eastern Indian Ocean since late Cretaceous: constraints from Geosat altimetry. *J. Geophys. Res.* 94, 13755-13782.
- Sabaka, T.J., Olsen, N., Purucker, M.E., 2004. Extending comprehensive models of the Earth's magnetic field with Ørsted and CHAMP data. *Geophys. J. Int.* 159, 521–547.
- Sandwell, D.T., Smith, W.H.F., 1997. Marine gravity anomaly from GEOSAT and ERS-1 satellite altimetry, *J. Geophys. Res.* 102, 10039-10054.
- Schmidt, S. Götze, H.-J., 1998: Interactive visualization and modification of 3D models using GIS functions, *Physics and Chemistry of the Earth*, 23 (3), 189-295.

2 Änderungen der Ziele des Vorhabens

Die Ziele des Vorhabens sind erreicht worden. Wegen der engen Verzahnung mit dem Vorhaben SO-189 SUMATRA konnten neben den ursprünglichen Zielen auch Aussagen zum Kohlenwasserstoffpotenzial des Simeulue-Beckens gemacht werden

3 Ergebnisse von dritter Seite mit Relevanz zum laufenden Projekt

Der Sumatra-Kontinentrand ist Ziel zahlreicher laufender internationaler Studien, deren Ergebnisse für unsere Arbeiten permanent mit berücksichtigt werden. Ein enger Austausch mit den internationalen Arbeitsgruppen wurde durch gegenseitige Teilnahme an Expeditionen (Stefan Ladage an US-Expedition, siehe auch Zwischenbericht 2007) verwirklicht.

4 Fortschreibung des Verwertungsplans

- Es sind keine Erfindungen/Schutzrechtsanmeldungen gemacht oder Schutzrechte erteilt worden.
- Wirtschaftliche Erfolgsaussichten sind derzeit nicht konkret.
- Wissenschaftliche Ergebnisse wurden in Publikationen und auf nationalen und internationalen Tagungen mit Kurzfassungen von Postern und Vorträgen verwertet. Diese sind Ansatzpunkte für zukünftige Forschungsarbeiten und eröffnen bzw. vertiefen unsere internationale wissenschaftliche Zusammenarbeit in der marinen Geophysik (aktive Kontinentalränder). Bisher erschienene und eingereichte Publikationen sind im Anhang gelistet. Publikationen mit peer-review Verfahren und ausgewählte Poster finden sich in Kopie im Anhang.
- Wissenschaftliche und wirtschaftliche Anschlussfähigkeit für eine mögliche nächste Phase: Eine weitergehende Untersuchung des Messgebietes, die Lücken schließt und offene Fragen angeht, wäre aus unserer Sicht eine sinnvolle nächste Phase.

Dr. Christoph Gaedicke
- Projektleiter *SeaCause* -

Hannover, den 27.03.2009

Anhang

Anhang I. Liste der Publikationen (peer-review Verfahren)

Die Publikationen liegen als Kopie bei. Publikationen, die den Projekten SO-186 SeaCause und SO-189 SUMATRA zugeordnet werden müssen, sind mit Stern * gekennzeichnet.

- * Berglar, K., Gaedicke, C., Lutz, R., Franke, D., and Djajadihardja, Y.S., 2008. Neogene subsidence and stratigraphy of the Simeulue forearc basin, Northwest Sumatra: *Marine Geology*, 253(1-2), p. 1–13 doi: 10.1016/j.margeo.2008.04.006.

- Franke, D., Schnabel, M., Ladage, S., Tappin, D.R., Neben, S., Djajadihardja, Y.S., Muller, C., Kopp, H., and Gaedicke, C., 2008. The great Sumatra-Andaman earthquakes – Imaging the boundary between the ruptures of the great 2004 and 2005 earthquakes: *Earth and Planetary Science Letters*, 269(1-2), p. 118–130 doi: 10.1016/j.epsl.2008.01.047.

- Kopp, H., Weinrebe, W., Ladage, S., Barckhausen, U., Klaeschen, D., Flueh, E.R., Gaedicke, C., Djajadihardja, Y., Grevemeyer, I., Krabbenhoft, A., Papenberg, C., and Zillmer, M., 2008. Lower slope morphology of the Sumatra trench system: *Basin Research*, 20(4), p. 519–529 doi: 10.1111/j.1365-2117.2008.00381.x.

- Ladage, S., Weinrebe, W., Gaedicke, C., Barckhausen, U., Flueh, E.R., Heyde, I., Krabbenhoft, A., Kopp, H., Fajar, S., and Djajadihardja, Y., 2006. Bathymetric Survey Images Structure off Sumatra: *Eos, Transactions American Geophysical Union*, 87(17), p. 165–172 doi: 10.1029/2006EO170001.

- * Lutz, R., Gaedicke, Chr., Berglar, K., Schlömer, S., Franke, D., Djajadihardja, Y. (eingereicht). *Petroleum Systems of the Simeulue Forearc Basin off Sumatra, Indonesia: AAPG Bulletin* (eingereicht 09.2008)

- * Berglar, K. Gaedicke, Chr. Franke, D., Ladage, S., Klingelhoef, F., Djajadihardja, Y. (2008, eingereicht). *Structural evolution and strike-slip tectonics off north-western Sumatra: Tectonophysics* (eingereicht 09/2008).

Anhang II. Liste der Diplomarbeiten

- Schauer, Michael (2007): *Morphotektonik des aktiven Kontinentalrandes von Nordsumatra, Indonesien*. Diplomarbeit, Leibniz-Universität Hannover.

- Glaubitz, Sabrina (2008): *Kartierung des Meeresbodens der konvergenten Plattengrenze vor Zentralsumatra*. Diplomkartierung, Leibniz-Universität Hannover.

- * Glaubitz, Sabrina (2009): *Herkunft, Mächtigkeit und Verteilung der Sedimente in der Tiefseerinne des Sundabogens*. Diplomarbeit, Leibniz-Universität Hannover.

Anhang III. Liste der öffentlichen Präsentation von Ergebnissen seit Projektbeginn bis Februar 2009 (Kurzfassungen für Poster und Vorträge)

Tagung	Autoren	Titel	Ort	Datum	Vortrag/ Poster
2005					
Fall Meeting - American Geophysical Union (2005)	<u>S. Ladage</u> , Chr. Gaedicke, U. Barckhasuen, D. Franke, I. Heyde, W. Weinrebe, H. Kopp, E. Flueh, Y. Djajadihardja, W. Soh, D. Tappin, C. Mueller	Great Sumatran Earthquakes: First Results of RV Sonne Cruise 186 SeaCause I	San Francisco	05.-09.12.2005	Poster
2006					
Collège de France (Kolloquium)	<u>Chr. Gaedicke</u>	The fore-arc structure off Sumatra and Java: Segmentation imaged in bathymetry and reflection seismics	Paris	22.03.2006	eingeladener Vortrag
Annual Meeting European Geophysical Union	<u>S. Ladage</u> , Chr. Gaedicke, Y.S. Djajadihardja & SO186 SeaCause TEAM	Great Sumatran Earthquakes - MCS images and bathymetry offshore Sumatra - first results of SeaCause II Leg1 cruise SO186	Wien	02.-07.04.2006	Vortrag
International Workshop on „Offshore Studies of the Andaman-Sumatran Earthquakes“	<u>S. Ladage & D. Tappin</u>	(Konferenzleitung)	Hannover	22.-23.05.2006	Organisation & Convenor
	<u>Chr. Gaedicke</u> , D. Franke, S. Ladage and SO186-2 Scientific Party (SeaCause Team)	New results and data sets from the RV Sonne SeaCause II cruise – the reflection seismic experiment	Hannover	22.-23.05.2006	Vortrag
	<u>W. Weinrebe</u> , S. Ladage, S. and the SeaCause / GITEWS working groups	Morphology of the continental margin off NW-Sumatra	Hannover	22.-23.05.2006	Vortrag

	U. Barckhausen & SeaCause-1 + 2 Scientific Parties	The segmentation of the subduction zone offshore Sumatra: Relations between upper and lower plate and implications for earthquake rupture areas	Hannover	22.-23.05.2006	Poster
	Berglar, K., Gaedicke, C., Lutz, R., Müller, C. & SO186-2 Scientific Party (SeaCause Team)	Seismostratigraphy and tectonics of NW Sumatran forearc basins – preliminary interpretation of MCS data	Hannover	22.-23.05.2006	Poster
	Berglar, K., Ladage, S., Schauer, M., Weinrebe, W. & Soh W	Bathymetry offshore Western Sumatra Compilation of German and Japanese Datasets	Hannover	22.-23.05.2006	Poster
	Dieter Franke, Christoph Gaedicke, Stefan Ladage & SO186-2 scientific party (SeaCause Team)	Seismic images of the segment boundary of the December 2004 and the March 2005 mega-thrust earthquakes	Hannover	22.-23.05.2006	Poster
	Heyde, I. & SeaCause Team	Marine gravity measurements offshore Sumatra and Java	Hannover	22.-23.05.2006	Poster
	Krabbenhoeft A., E. Flueh, H. Kopp, I. Grevemeyer, M. Zillmer, W. Weinrebe, C. Papenberg, C. Gaedicke, & the SeaCause & GITEWS working groups	Results from seismological and pressure data from stations placed around Simeulue Island during the SeaCause & GITEWS cruises	Hannover	22.-23.05.2006	Poster
	Lutz R., Chr. Gaedicke, K. Berglar & SO186-2 Scientific Party (SeaCause Team)	Petroleum System of the Simeulue forearc basin	Hannover	22.-23.05.2006	Poster
	I.Grevemeyer, Tilmann. F., Krabbenhöft, A., Flueh, E.R., Papenberg, C., Weinrebe, W., Zillmer, M., Kopp, H., and the SO186-3 Shipboard Scientific Party	Seismological study of aftershocks from the 2004 Mw=9.1 and 2005 Mw=8.6 Sumatran earthquakes from an offshore/onshore network at Simeulue island, Indonesia	Hannover	22.-23.05.2006	Poster
	M. Zillmer, H. Kopp, E.R. Flueh, I. Grevemeyer, A. Krabbenhoeft, C. Papenberg, W. Weinrebe, D. Franke:	Three wide-angle seismic experiments offshore Sumatra in March 2006 during cruise RV SONNE 186-3 in the frame of the SeaCause project	Hannover	22.-23.05.2006	Poster
21.Hydrographentag der Deutschen Hydrographischen Gesellschaft	W. Weinrebe, S. Ladage und SeaCause / GITEWS – Arbeitsgruppen	Bathymetrische Messungen mit FS SONNE am Kontinentalrand vor Sumatra	Magdeburg	14.06.2006	Vortrag extended Abstract

Jahrestagung Geologische Vereinigung	Chr. Gaedicke, D. Franke, S. Ladage & SO186-2 Scientific Party	Architecture of the source region of the December 2004 tsunami off northern Sumatra	Potsdam	26.-29.09.2006	Vortrag
GeoBerlin 2006, Deutsche Geologische Gesellschaft	M. Schauer, S. Ladage, W. Weinrebe, K. Berglar & C. Gaedicke	Morphotectonic of the Active Continental Margin off Northern Sumatra	Berlin	02.-04.10.2006	Poster
Fall Meeting - American Geophysical Union (2006)	C. Goldfinger, <u>S. Ladage</u> , L. McNeill, D. Tappin	Indian Ocean Tsunami: Two Years On Union Session	San Francisco	11.-15.12.2006	Convenor
	Chr. Gaedicke, <u>S. Ladage</u> , W. Soh, W. Weinrebe, D.R. Tappin, T. Henstock, L. McNeill, J.-C. Sibuet, F. Klingelhoefer, S. Singh, E. Flueh & Y. Djajadihardja	Bathymetry Offshore Sumatra – First Comprehensive map of International Data Sets.	San Francisco	11.-15.12.2006	Poster
	<u>Chr. Gaedicke</u> , D. Franke, S. Ladage, D.R. Tappin, B. Baranov, U. Barckhausen, K. Berglar, G. Delisle, Y. Djajadihardja, I. Heyde, R. Lutz, Khafid, Chr. Mueller, K. Nur Adi, J.O. Park, S. Neben, S. & E. Triarso	Imaging the Rupture Areas of the Giant Northern Sumatra Earthquakes: A Multidisciplinary Geophysical Experiment	San Francisco	11.-15.12.2006	eingeladener Vortrag
	H. Kopp, <u>W. Weinrebe</u> , S. Ladage, Chr. Gaedicke, E. Flueh, U. Barckhausen, I. Grevermeyer, A. Krabbenhoeft, C. Papenberg, & M. Zillmer	Geomorphic and seismotectonic segmentation of the Sumatra margin	San Francisco	11.-15.12.2006	Poster
	K. Berglar, <u>Chr. Gaedicke</u> , R. Lutz, S. Ladage, D. Franke & S. Neben	Tectonic and Sedimentary Evolution of the Simeulue Fore-Arc Basin, Northwest Sumatra	San Francisco	11.-15.12.2006	Vortrag
	<u>S. Ladage</u> , D. Franke, Chr. Gaedicke, I. Heyde & D.R. Tappin	Thrust Sheet Emplacement at the Northern Sumatra Margin – New Insights from the SeaCause Multichannel Reflection Seismic Experiment	San Francisco	11.-15.12.2006	Vortrag

	M. Schauer, S. Ladage, W. Weinrebe, K. Berglar, A. Krabbenhoeft, E. Flueh & Chr. Gaedicke	Morphotectonics of the Sumatra Margin -- Analysis of new Swath Bathymetry	San Francisco	11.-15.12.2006	Poster
	D. Franke, Chr. Gaedicke, S. Ladage, D. Tappin, S. Neben, A. Ehrhardt, Chr. Müller, Y. Djajadihardja	Contrasting structural styles of accretion along the Sumatra subduction zone	San Francisco	11.-15.12.2006	Poster
	U. Barckhausen & SeaCause Scientific Party	The segmentation of the subduction zone offshore Sumatra: Relations between upper and lower plate	San Francisco	11.-15.12.2006	Poster
	D.R. Tappin, S.; Ladage, L. McNeill, D.C. Mosher, Chr. Gaedicke, T. Henstock. & D. Franke	Landslides and mass Wasting Offshore Sumatra – Results from Marine Surveys Offshore of Sumatra	San Francisco	11.-15.12.2006	Vortrag
	I. Heyde, D. Franke & M. Schnabel	Marine gravity measurements offshore Sumatra	San Francisco	11.-15.12.2006	Poster
	M. Zillmer, H. Kopp, E. R. Flueh, A. Krabbenhoeft, I. Grevemeyer, D. Klaeschen, C. Papenberg, L. Planert, W. Weinrebe, C. Gaedicke, D. Franke,	Seismic Wide-angle Experiments Offshore Sumatra Using Ocean Bottom Seismometers	San Francisco	11.-15.12.2006	Poster
	F. Tilmann, E. R. Flueh, I. Grevemeyer, L. Hidayani, H. Kopp, B. Suwargadi, W. Triyoso, M. Heintz	First results from a combined marine and land passive seismic network near Simeulue island	San Francisco	11.-15.12.2006	Poster
	A. Krabbenhoeft, E. R. Flueh, H. Kopp, I. Grevemeyer, M. Zillmer, W. Weinrebe, C. Papenberg, T. Schoene, S. Roemer	Results From Pressure and Seismological Data From Stations Placed Offshore Sumatra During the SeaCause & GITEWS Cruises	San Francisco	11.-15.12.2006	Poster

2007					
Statusseminar Meeresforschung mit FS Sonne	<u>Kai Berglar</u> , Christoph Gaedicke, Rüdiger Lutz, Sönke Neben	Seismostratigraphie der Forearc-Becken Nordsumatras: Beckenentwicklung in einem obliquen Subduktionssystem – SO186- 2/SO189-1	Kiel	14.-16.02.2007	Vortrag
	<u>Christoph Gaedicke</u> , Stefan Ladage, Dieter Franke, Udo Barckhausen, Kai Berglar, Georg Delisle, Ingo Heyde, Rüdiger Lutz, Christian Müller, Michael Schauer, Anne Krabbenhöft, Ernst Flüh, Heidrun Kopp, Yusuf Djajadihardja, Boris Baranov, David Tappin, Leonardo Seeber, Jin-Oh Park & SeaCause Team	SO186 – SeaCause - Bathymetrie und Architektur offshore Sumatra: Ein Beitrag zum deutschen Tsunami- Frühwarnsystem für den indischen Ozean	Kiel	14.-16.02.2007	Vortrag
	<u>Ingo Heyde</u> , Udo Barckhausen & Bernd Schreckenberger	Erste Ergebnisse der Magnetik und Gravimetrie der Fahrten SO-186 und SO- 189 vor Sumatra	Kiel	14.-16.02.2007	Poster
	<u>H. Kopp</u> , W. Weinrebe, S. Ladage, C. Gaedicke, E. Flueh, U. Barckhausen, I. Grevemeyer, A. Krabbenhoeft, C. Papenberg & M. Zillmer	Geophysikalische Untersuchungen der Sumatra-Subduktionszone: Massentransfer und Seismotektonik (SO186 SeaCause)	Kiel	14.-16.02.2007	Vortrag
	<u>Stefan Ladage</u> , Dieter Franke , Christoph Gaedicke, David R. Tappin & Yusuf Djajadihardja	Aufbau und Struktur des Akkretionskeiles Nördlich Simeulue, Nord-Sumatra - SO186-2	Kiel	14.-16.02.2007	Vortrag
	<u>Rüdiger Lutz</u> , Kai Berglar, Christoph Gaedicke, Dieter Franke & Sönke Neben	Das Petroleumsystem im Simeulue Forearc- Becken (Nordsumatra) - SO186/SO189	Kiel	14.-16.02.2007	Poster
	<u>Michael Schauer</u> , Stefan Ladage, Wilhelm Weinrebe, David Tappin & Christoph Gaedicke	SO186 – Bathymetrie und Morphotektonik des aktiven Kontinentalrandes von Nord- Sumatra, Indonesien	Kiel	14.-16.02.2007	Poster

67. Jahrestagung der Deutsche Geophysikalische Gesellschaft	Kai Berglar, Christoph Gaedicke, Rüdiger Lutz, Stefan Ladage, Sönke Neben	Entwicklung der Forearc-Becken Nordsumatras	Aachen	26.-29.03.2007	Vortrag
	Kai Berglar, Christoph Gaedicke, Rüdiger Lutz, Stefan Ladage, Dieter Franke, Sönke Neben	Tektonische und sedimentäre Entwicklung des Simeulue Forearc-Beckens, Nordwestsumatra	Aachen	26.-29.03.2007	Poster
	Dieter Franke, Christoph Gaedicke, Stefan Ladage, David Tappin, Sönke Neben, Axel Ehrhardt, Chr. Müller, Yusuf Djajadihardja	Contrasting structural styles of accretion along the Sumatra subduction zone	Aachen	26-29.3.2007	Poster
	Stefan Ladage, Dieter Franke, Christoph Gaedicke, Kai Berglar, Ingo Heyde, David Tappin, Yusuf Djajadihardja	Structural Architecture of the Northern Sumatra Accretionary Complex – Results from the “SeaCause” Marine Geophysical Survey with R/V SONNE	Aachen	26-29.3.2007	Vortrag
	Kai Berglar, Christoph Gaedicke, Rüdiger Lutz, Stefan Ladage, Sönke Neben	Entwicklung der Forearc-Becken Nordsumatras	Aachen	26-29.3.2007	Vortrag
	Kai Berglar, Christoph Gaedicke, Rüdiger Lutz, Stefan Ladage, Dieter Franke, Sönke Neben	Tektonische und sedimentäre Entwicklung des Simeulue Forearc-Beckens, Nordwestsumatra	Aachen	26-29.3.2007	Poster
	Ingo Heyde, Udo Barckhausen & Bernd Schreckenberger	Marine Magnetik- und Schweremessungen an der Subduktionszone vor Sumatra	Aachen	26-29.3.2007	Poster
	Michael Schauer, Stefan Ladage, Wilhelm Weinrebe, Kai Berglar, Ernst Flueh, Heidrun Kopp, Anne Krabbenhöft, Christoph Gaedicke	Seafloor Morphology and Structures of the Sunda Trench off Sumatra	Aachen	26-29.3.2007	Poster
	H. Kopp, W. Weinrebe, S. Ladage, D. Klaeschen, U. Barckhausen, E. R. Flueh, C. Gaedicke, M. D. Yusuf	Bathymetry data reveal morphotectonic segmentation of the Sumatra margin	Aachen	26-29.3.2007	Poster

AAPG Hedberg Conference	Rüdiger Lutz, Kai Berglar, Christoph Gaedicke, Dieter Franke	Petroleum Systems Modelling in the Simeulue Forearc Basin	Den Haag	06.-09.05.2007	Poster
International Conference 2007 and 97th Annual Meeting of the Geologische Vereinigung e.V.	Franke, D., M. Schnabel, C. Gaedicke, D.R. Tappin, S. Ladage, S. Neben, H. Kopp, C. Müller & Y. Djajadihardja	Segment boundary revealed: key to understanding the great Sumatra-Andaman earthquakes. Tear in the subducting oceanic plate limits propagation of December 2004 and March 2005 mega-thrusts	Bremen	1-5.10.2007	Vortrag
European Geosciences Union General Assembly 2007	S. Brune, A.Y. Babeyko, S.V. Sobolev, S. Harig, A. Androsof, J., Behrens, S. Ladage	Hazard assessment of underwater landslide-generated tsunamis for the Padang region, Indonesia	Wien	15.-20.4.2007	Poster
	Heidrun Kopp, Wilhelm Weinrebe, Stefan Ladage, Udo Barckhausen, Dirk Klaeschen, Ernst Flueh, Christoph Gaedicke, C.; Yusuf Djajadiradja, Seacause & GITEWS Teams	Lower plate impact on earthquake rupture segmentation on the Sumatra margin	Wien	15.-20.4.2007	Poster
	M Zillmer, D Klaeschen, H Kopp, E Flueh, I. Grevemeyer, A Krabbenhoft, C Papenberg, L Planert, W Weinrebe	Tomography of OBS data and prestack-depth migration of MCS data from the Sumatra continental margin	Wien	15.-20.4.2007	Poster
97. Jahrestagung der Geologischen Vereinigung	Kai Berglar, Christoph Gaedicke, Rüdiger Lutz, Stefan Ladage, Sönke Neben	Tectonic framework of the forearc basins off northwest Sumatra – Neogene basin evolution in an oblique setting	Bremen	01.-05.10.2007	Poster
	Franke, D, M. Schnabel, C. Gaedicke, D.R. Tappin, S. Ladage, S. Neben, H. Kopp, C. Müller & Y. Djajadihardja	Tear in the subducting oceanic plate limits propagation of December 2004 and March 2005 mega-thrusts earthquakes.	Bremen	01.-05.10.2007	Vortrag

Fall Meeting - American Geophysical Union (2007)	M Zillmer, D. Klaeschen, <u>H. Kopp</u> , E. Flueh, A. Krabbenhoeft, C. Papenberg, L. Planert, W. Weinrebe, D. Franke, C. Gaedicke, Y. Djajadihardja	Firstarrival Tomography of Seismic OBS Data and Prestack Depth Migration of MCS Data from the Sumatra Continental Margin	San Francisco	10.-14.12.2007	Poster
	<u>Schnabel</u> , M, Damm, VFranke, D, Ladage, S, Neben, S	The Subducting Investigator Fracture Zone Offshore Siberut as Imaged by Seismic Tomography.	San Francisco	10.-14.12.2007	Poster
	<u>Ladage</u> , S, Franke, D, Schnabel, M, Gaedicke, C, Neben, S, Djajadihardja, Y S	Seismic image of the segment boundary of the Sumatra Dec. 2004 and March 2005 megathrust earthquakes	San Francisco	10.-14.12.2007	Poster
	Patton, J R, Goldfinger, C, Morey, A, Wynn, R B, Stoner, J, Ikehara, K, Hanifa, U, Djajadihardja, Y, Ladage, S, Viscaino, A, Gracia, E	Possible Earthquake Generated Turbidites along the Sumatra Margin	San Francisco	10.-14.12.2007	Vortrag
	H. Kopp, D. Hindle	Structure and Evolution of the Accretionary Margin of Java-Sumatra. Seismic Data and Numerical Modeling Comparisons	San Francisco	10.-14.12.2007	Vortrag

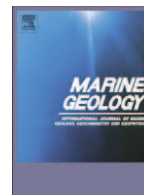
2008					
Kolloquium Universität Greifswald	Christoph Gaedicke	Geodynamik, Georisiko- und Kohlenwasserstoffpotenzial des aktiven Plattenrandes von Sumatra -- Ergebnisse von Expeditionen mit FS Sonne	Greifswald	10.01.2008	eingeladener Vortrag
Kolloquium Universität Freiburg	Heidrun Kopp	Marine Geophysical Investigations of a Subduction System: Tectonic and Geodynamic Evolution of the Sunda-Banda margin, Indonesia	Freiburg	Feb. 2008	eingeladener Vortrag
Kolloquium IFREMER	Stefan Ladage	Deformation Processes Along the Northern Sumatra Margin	Brest	15.02.2008	eingeladener Vortrag
68. Jahrestagung der Deutsche Geophysikalische Gesellschaft	Hauke Thöle, Christoph Gaedicke, Stefan Ladage, Yusuf Djajadihardja	Morphological and structural features of the Siberut fore-arc basin offshore southern Sumatra	Freiburg	03.-07.03.2008	Poster
	<u>Sabrina Glaubitz</u> , Stefan Ladage, Christoph Gaedicke, Wilhelm Weinrebe, Yusuf Djajadihardja	Morphotectonic of the accretionary prism off southern Sumatra	Freiburg	03.-07.03.2008	Poster
AAPG 2008 Annual Convention and Exhibition	<u>Kai Berglar</u> , Rüdiger Lutz, Christoph Gaedicke, Dieter Franke, Yussuf Djajadihardja	Seismic Stratigraphy and Petroleum System in the Simeulue Forearc Basin, Northern Sumatra	San Antonio, Texas	20.-23.04.2008	Poster
European Geosciences Union General Assembly 2008	Tilmann, FJ; Grevemeyer, I; Suwargadi, B; <u>Kopp, H</u> ; Flueh, E	The seismic/aseismic transition as seen in aftershocks of the 28 Mar 2005 Nias and 26 December 2004 Aceh-Andaman earthquakes	Vienna	13.-18. 04. 2008	Vortrag
Geophysikalisches Aktions Programm GAP	Heidrun Kopp	Getting to the bottom (and deeper): Multiscale studies of subduction zone processes	Kiel	1.-4. 05. 2008	Eingeladener Vortrag
Fall Meeting - American Geophysical Union (2008)	Tilmann, F., Grevemyer, I., Suwargadi, B., Kopp, H., Flueh, E., R.	The updip seismic/aseismic transition as seen by aftershocks of the 28 March 2005 Nias and 26 December 2004 Aceh-Andaman earthquakes	San Francisco	12.-19.12.2008	Poster

2009					
Statusseminar Meeresforschung mit FS Sonne	H. Kopp, W. Weinrebe, S. Ladage, U. Barckhausen, D. Klaeschen, E. R. Flueh, C. Gaedicke, Y. Djajadihardja, I. Grevemeyer, A. Krabbenhoeft, C. Papenberg, M. Zillmer,	Morphologische Untersuchungen des Plattenrandes vor Sumatra	Bremerhaven	12.-13.02.2009	Poster
	R. Lutz, K. Berglar, Ch. Gaedicke, D. Franke, S. Schlömer	Kohlenwasserstoffpotenzial des Simeulue Forearc-Beckens (Nordsumatra) – SO186/SO189	Bremerhaven	12.-13.02.2009	Poster
	Christoph Gaedicke, Dieter Franke, Michael Schnabel, Stefan Ladage, Sönke Neben, Heidrun Kopp	Segementierung der abtauchenden Platte - Schlüssel zum Verständnis der Sumatra- Andaman Erdbeben - SO186/SO189	Bremerhaven	12.-13.02.2009	Vortrag
	Hauke Thöle, Christoph Gaedicke, Stefan Ladage, Kai Berglar, Yusuf Djajadihardja	Die Mentawai Störungszone im Forearc- bereich von der Westküste Sumatras, Indonesien	Bremerhaven	12.-13.02.2009	Poster
	Christoph Gaedicke, Dieter Franke, Michael Schnabel, Stefan Ladage, Sönke Neben, Heidrun Kopp, Yusuf Djajadihardja	Abtauchende Bruchzone der Indischen Platten verursacht Segmentgrenze der Sumatra-Andaman Erdbeben - SO186/SO189	Bremerhaven	12.-13.02.2009	Vortrag
	Kai Berglar, Christoph Gaedicke, Dieter Franke, Stefan Ladage, Frauke Klingelhoefter, Yusuf Djajadihardja	Strukturelle Entwicklung und Blattverschiebungstektonik vor Nordwestsumatra - SO186/SO189	Bremerhaven	12.-13.02.2009	Poster

Anhang IV. Publikationen

Publikation

- * Berglar, K., Gaedicke, C., Lutz, R., Franke, D., and Djajadihardja, Y.S., 2008. Neogene subsidence and stratigraphy of the Simeulue forearc basin, Northwest Sumatra: *Marine Geology*, 253(1-2), p. 1–13 doi: 10.1016/j.margeo.2008.04.006.



Neogene subsidence and stratigraphy of the Simeulue forearc basin, Northwest Sumatra

Kai Berglar^{a,*}, Christoph Gaedicke^a, Rüdiger Lutz^a, Dieter Franke^a, Yusuf S. Djajadihardja^b

^a Federal Institute for Geosciences and Natural Resources, Stilleweg 2, D-30655 Hannover, Germany

^b Agency for the Assessment & Application of Technology, Jl. M.H. Thamrin No.8, Jakarta 10340, Indonesia

ARTICLE INFO

Article history:

Received 10 December 2007

Received in revised form 15 April 2008

Accepted 18 April 2008

Keywords:

Subduction

Forearc basin

Seismic stratigraphy

Sumatra

Simeulue

ABSTRACT

Interpretation of new multi-channel seismic data reveals the Neogene subsidence history of the Simeulue forearc basin, located off northwestern Sumatra. The trench-parallel elongated basin extends over 260 km in NW–SE direction and 100 km in SW–NE direction. Maximum water depth is about 1300 m and the Neogene sedimentary fill shows a thickness of up to 5 s two-way traveltime. We identified three stages of subsidence evolution after the formation of a regional basal Neogene unconformity which are characterized by changing accumulation space, sedimentation rates, source areas and tectonic phases. An Early/Mid Miocene stage is marked by occurrence of subsidence in several half grabens forming along the western border of the basin. During the Late Miocene/Pliocene this small scale subsidence changed to a steadily subsiding trench-parallel trough. The present setup of the forearc region under the influence of strike-slip faults due to oblique subduction is active at least since this time as evidenced by wrench faulting. At the end of this stage subsidence expanded significantly eastwards drowning a large carbonate platform that evolved in the then shallow southern and eastern parts of the basin. Presently, the central part of the Simeulue basin is subject to inversion, probably related to reactivation of Early/Mid Miocene half grabens.

© 2008 Elsevier B.V. All rights reserved.

1. Introduction

Forearc basins are prominent elements of subduction zones and evolve between the magmatic arc and the accretionary prism. They are areas of strong subsidence and serve as traps for sediments derived from the arc region. Such basins often contain a sedimentary column of several kilometers. As their subsidence evolution is directly influenced by subduction processes, the stratigraphy depicts an important record of the plate margin evolution.

The Simeulue forearc basin is one of several depositional basins situated off Sumatra along the Sunda Arc. The latter is a classical convergent margin system that stretches over 5000 km from Java in the south to Burma in the north (Fig. 1). It is the geological expression of the convergence between the Indo-Australian and Eurasian Plates where oceanic lithosphere is being subducted beneath the Indonesian Archipelago as well as the Andaman and Nicobar Islands. The Simeulue forearc basin is bordered to the west by Simeulue Island, a part of the consolidated outer arc high of the subduction zone. The Banyak Islands separate the Simeulue basin from the southerly located Nias basin. To the north the Aceh basin can be clearly distinguished by a ridge-like structure in between and a change in water depth of more than 1500 m (Izart et al., 1994). The Simeulue basin itself is trench-parallel elongated and extends over 260 km in NW–SE direction and 100 km in SW–

NE direction. It contains a Neogene sedimentary fill of up to 5 s two-way traveltime (TWT) and consists of a deep water area with a maximum water depth of about 1300 m followed to the east by the slope of the basin and the shallow water inner shelf at the transition to the Sumatran mainland (Fig. 2). The Simeulue basin is relatively unexplored in a petroleum geologic context. Few wells were drilled in the 1970s at the northeastern edge of the basin in water depths less than 100 m and described by Karig et al. (1979), Rose (1983) and Beaudry and Moore (1985). Later research based on single channel reflection seismic data was conducted by Malod et al. (1993) and Izart et al. (1994).

This paper discusses the subsidence history of the Simeulue forearc basin on the basis of geophysical data acquired during two joint Indonesian–German surveys in 2006. Based upon seismic stratigraphy we present a model for the Neogene subsidence and stratigraphic basin evolution and examine its decisive factors.

2. Regional setting

Along the Sunda arc the oceanic Indo-Australian Plate subducts beneath the Eurasian Plate. The rate and direction of convergence of the Indo-Australian Plate with respect to the Eurasian Plate show a decreasing and slightly anticlockwise trend from southeast to northwest (Fig. 1). Based upon GPS measurements Prawirodirdjo and Bock (2004) proposed convergence rates of 65 mm/y (N17°E) south of Java and 51 mm/y (N11°E) off northern Sumatra. The model NUVEL-1A

* Corresponding author. Tel.: +49 511 643 2149; fax: +49 511 643 3663.

E-mail address: kai.berglar@bgr.de (K. Berglar).

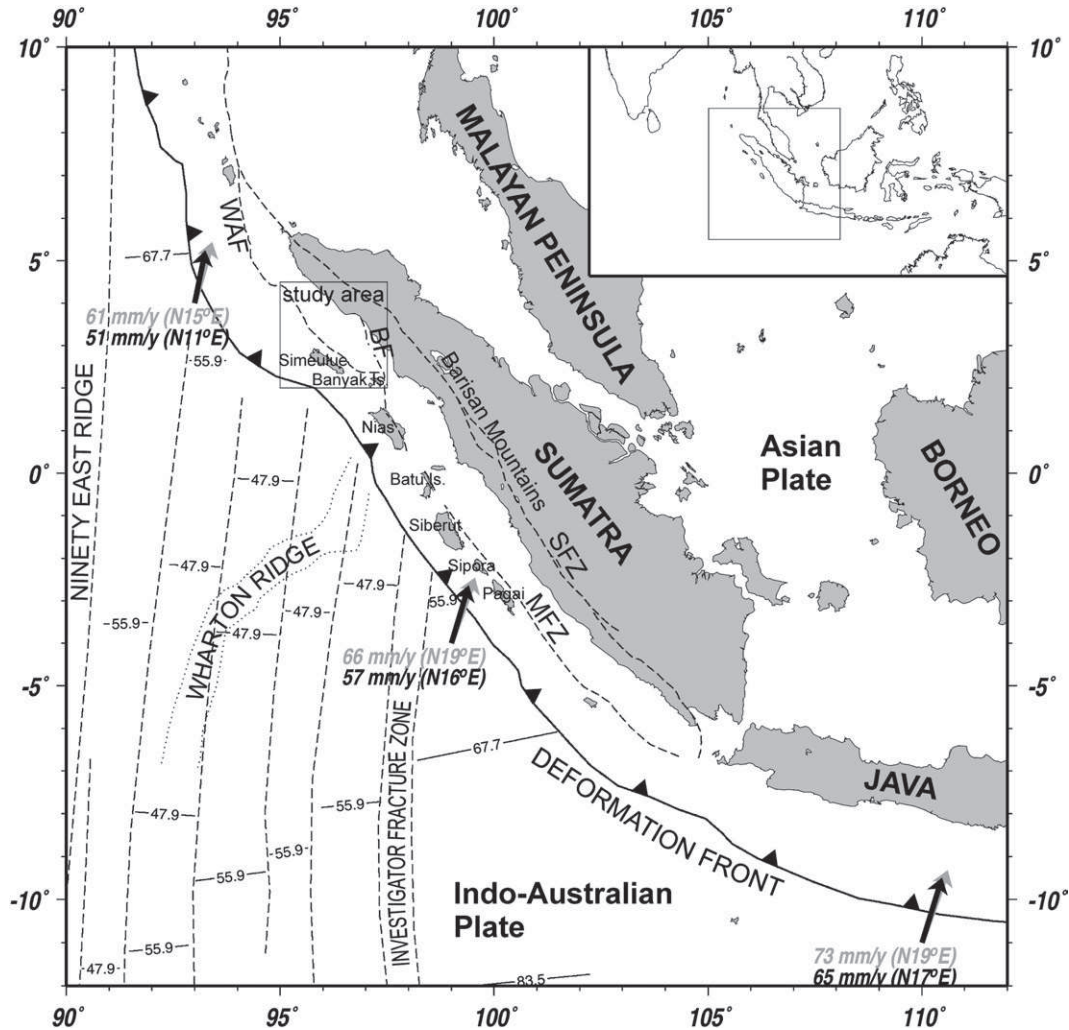


Fig. 1. Regional tectonic setting of the Sumatran subduction zone. Sumatran Fault Zone (SFZ), Mentawai Fault Zone (MFZ), Batee Fault (BF), West Andaman Fault (WAF) and deformation front are based on Sieh and Natawidjaja (2000). Ages of the oceanic crust are after Müller et al. (1997) and Deplus et al. (1998). Gray arrows indicate relative plate movements based on NUVEL-1A (DeMets et al., 1994), black arrows based on CGPS (Prawirodirdjo and Bock, 2004).

(DeMets et al., 1994), using geomagnetic time scale, gives values of 73 mm/y (N19°E) and 61 mm/y (N15°E) respectively.

Due to the curvature of the margin the plate convergence gradually changes from nearly perpendicular subduction off Java to highly oblique subduction off northern Sumatra (Moore et al., 1980). This results in slip partitioning along the northwestern Sunda island arc and the development of arc-parallel strike-slip faults. The most pronounced strike-slip shear zone is the Sumatran Fault Zone (McCarthy and Elders, 1997; Sieh and Natawidjaja, 2000) located on the Sumatran mainland along the volcanic arc which forms the Barisan Mountains (Fig. 1). The Sumatran Fault Zone accommodates most of the right-lateral stress of the relative plate motion. However, a smaller amount of the arc-parallel stress is taken up by right-lateral strike-slip fault systems along the western edges of the forearc basins, namely the Mentawai Fault Zone and West Andaman Fault (Diament et al., 1992; Malod and Kemal, 1996; McCaffrey, 1991). The Mentawai Fault Zone extends from the Sunda Strait up to south of Nias Island where it is probably connected with the Sumatran Fault Zone along the Batee Fault (Milsom et al., 1995). The West Andaman Fault proceeds southwards from the Andaman Islands to the Simeulue basin (Curry, 2005). As pointed out by Curry et al. (1979) the Sumatran forearc acts as a sliver plate bounded to the west by the trench, below by the subducting plate, and to the east by the Sumatran Fault Zone. As a

consequence the forearc sliver consists of elongated strips moving to the northwest. This was further refined by Malod and Kemal (1996) proposing two forearc microplates between the outer arc high and the Mentawai Fault Zone, separated by the Batee Fault. The western border of the northern microplate is represented by the West Andaman Fault.

Besides strain partitioning, subducting ridges on the oceanic plate – namely the Wharton Ridge and the Investigator Fracture Zone – may have had an effect on the deformation of the forearc and may have accounted for segmentation into several forearc basins off northern and central Sumatra.

3. Data acquisition and processing

Data used in this study were acquired during two cruises with the German research vessel SONNE in 2006 (SO186-2 SeaCause and SO189-1 SUMATRA). Approximately 1500 km of multi-channel seismic (MCS) data were obtained in the area of the Simeulue basin (Fig. 2). Shot distance was 50 m and we used a digital 240 channel streamer of 3 km length with a receiver spacing of 12.5 m, towed at a water depth of 6 m. The acoustic signal was generated by a tuned G-gun array of 16 units with a total volume of 50.8 l operating at air pressure of 14.5 MPa. Data were recorded with a sampling interval of 2 ms and 14 s length. Stacking velocities were picked at regular

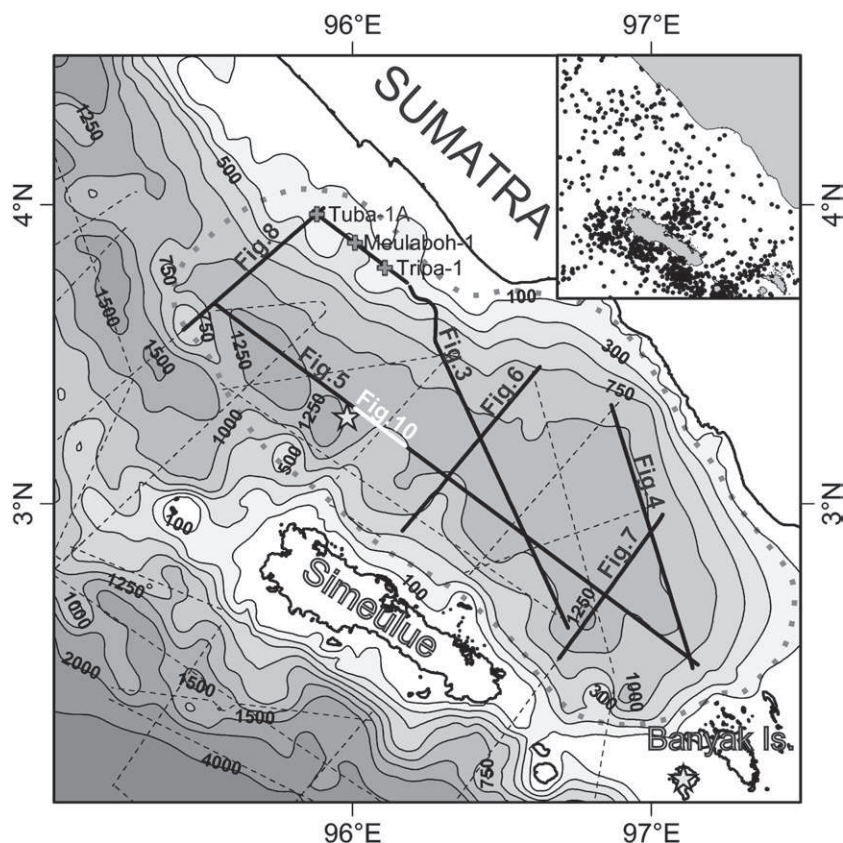


Fig. 2. Bathymetric map of the Simeulue basin (Smith and Sandwell, 1997). The dotted gray line indicates the extent of the Simeulue basin. Dashed lines show the location of acquired seismic sections, solid bold lines the location of Figs. 3 to 8 and 10. Crosses denote positions of wells used for chronostratigraphic calibration. Stars display the epicenter locations of the December 2004 (north of Simeulue) and March 2005 (Banyak Islands) mega-earthquakes. The sketch shows earthquake epicenter locations ($m_b > 4$) since 2000. All earthquake locations are from USGS NEIC.

intervals of 3 km along every line. Pre-stack processing included resampling to 4 ms, trace editing, CMP-sort (nominal 30-fold coverage, 6.25 m spacing), Ormsby bandpass filter (6–12–60–160 Hz), polygon f - k filter (window of 60 traces and 1 s length), zerophase spiking deconvolution (52 ms operator length, 1 s design window beginning shortly below seabottom reflection), amplitude correction for spherical divergence based on stacking velocities ($1/(t \times v^2)$), normal moveout correction (40% stretch mute), and Radon velocity filter for multiple suppression (rejecting velocities differing more than $\pm 20\%$ of corresponding stacking velocity). After stack we applied a space and time variant Ormsby bandpass filter (upper window: 10–20–60–100 Hz, lower window: 6–12–50–100 Hz), a minimum phase predictive deconvolution and a post-stack Kirchhoff time migration with 90% of stacking velocities. From the interpreted 2-D profiles grids were calculated using the Schlumberger-GeoQuest CPS-3 convergent gridding algorithm for the major stratigraphic boundaries (spacing: 200 m) and used for generation of TWT-isopach maps. Such maps may be of limited use for estimation of sedimentation rates as they do not consider compaction, erosion or density of the sediments. Also the accuracy of the grids is constricted by limited density of the data. Nevertheless, they provide insights into the three-dimensional setting of the study area. In addition high resolution parametric echosounder recordings (difference frequency of 3.5 kHz) were evaluated. The data were resampled to 8 kHz, bandpass filtered (1.75–2.1–3.8–4 kHz) and the envelope seismic attribute applied for visualization.

4. Chronostratigraphic calibration

Chronostratigraphic calibration of the data was accomplished using three wells located on the northwestern inner shelf of the

Simeulue basin (Fig. 2), drilled by Union Oil Company of California in the 1970s (Tuba-1A, Meulaboh-1 and Tripa-1). These wells were reviewed by several authors (Beaudry and Moore, 1985; Karig et al., 1979; Rose, 1983) with partially contradicting interpretations (see e.g. Meulaboh-1 well; Fig. 3, upper section). The borehole had a total depth of 3072 m and the lowermost section was described by all authors of pre-Neogene age, ranging from Eocene to Oligocene. Recrystallized belemnites may also indicate Jurassic strata, but it is more likely they have been reworked into the Paleogene (Rose, 1983). The latter author described steeply dipping sediments in the Eocene to Oligocene which are overlain unconformably by the successive strata of Miocene age. The basal Miocene strata were described as a thin sequence of nearshore marine and non-marine clastics containing coal beds. Sparse fossil recovery led to a tentative age of Mid Miocene or possibly latest Early Miocene according to Rose (1983). Above, a carbonate complex that is overlain by mudstone or shale was described by all three authors. This succession was reported to have an Early Miocene age by Beaudry and Moore (1985) and by Karig et al. (1979), whereas Rose (1983) interpreted a Mid Miocene age. These mudstones are unconformably (Beaudry and Moore, 1985) overlain by another carbonate complex of reportedly Late Miocene (Beaudry and Moore, 1985; Rose, 1983) or Pliocene age (Karig et al., 1979). Further differentiation was done by Beaudry and Moore (1985) describing an additional unconformity between the Pliocene and Pleistocene.

For a rough correlation of the seismic image with the well data the migrated time section was depth-stretched using interval velocities derived from seismic processing. The result shows a reasonable match between the marker horizons and the unconformities in the seismic image with those reported from the well (Fig. 3, upper section). In particular, we were able to correlate two distinct groups of high-

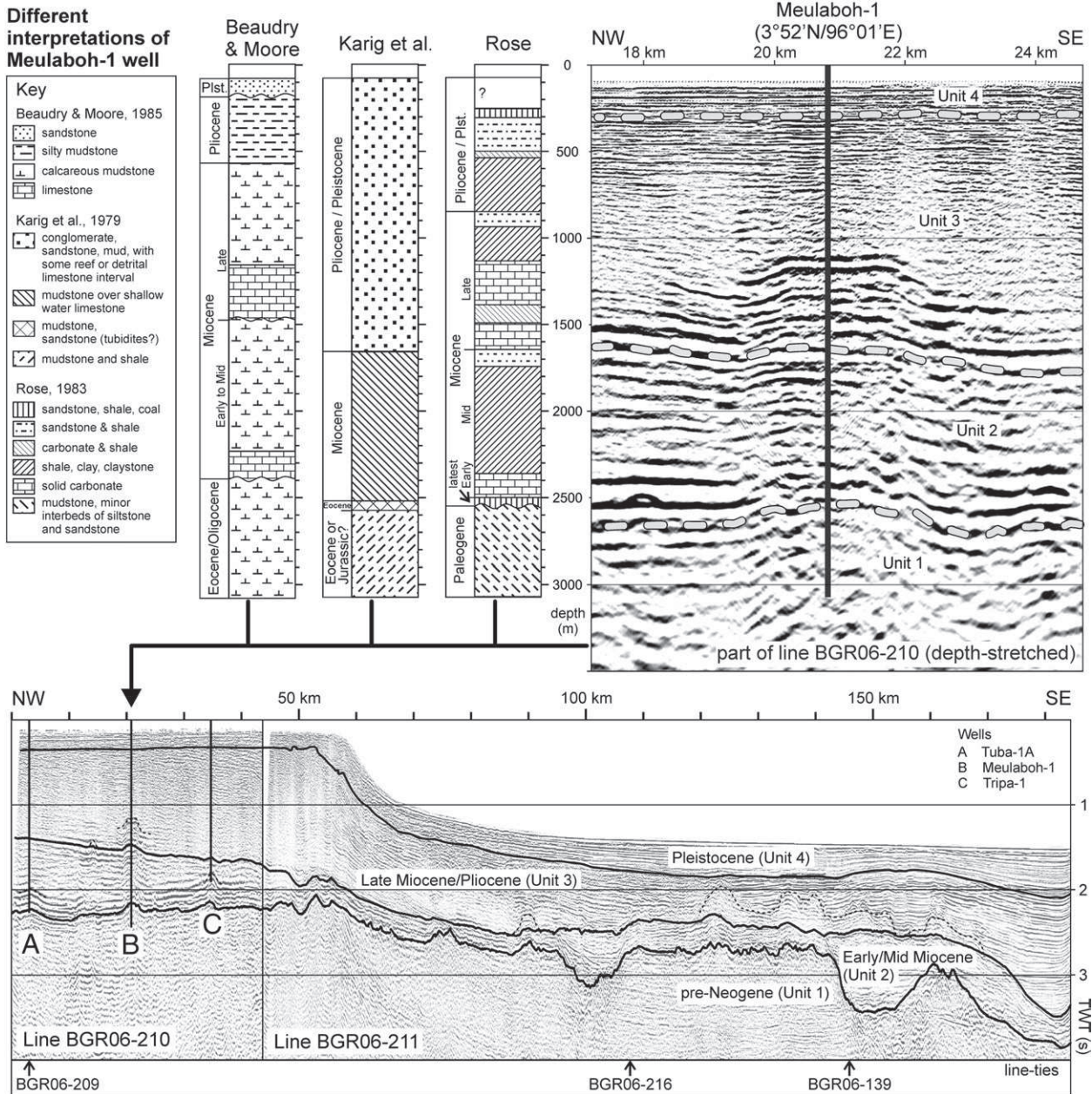


Fig. 3. Chronostratigraphic calibration of seismic lines. The upper part of the figure depicts available interpretations of Meulaboh-1 well and a depth-stretched seismic section covering the well location. Mismatch between water depths given in bathymetric (Fig. 2) and well data are due to limitation of bathymetry derived from satellite altimetry in shallow water. The lower portion of the figure illustrates the continuation of unconformities into the deeper basin part and the major units identified. See Fig. 2 for location of MCS profile.

amplitude and low-frequency reflectors, interpreted as carbonate complexes, with the reported carbonates from the well. The interpretation of carbonates in the seismic image is further supported by the mound-like shape of the upper reflectors and a velocity pull-up below, resulting from higher travel times in the carbonate rocks with respect to those of the surrounding sedimentary strata. The reflectors above the upper carbonate complex are dipping slightly southeastwards and may indicate an aggrading/prograding system. Atop, a group of parallel reflectors give a good match to the Pleistocene sediments described by Beaudry and Moore (1985).

All available wells are located at the inner shelf of the basin in shallow water below 100 m depth. However, it was possible to unequivocally trace the unconformities and their correlating conformities into the deeper basin parts (Fig. 3, lower section). The boundary between pre-Neogene and Miocene rocks was identified in unison by all groups interpreting the well data (Beaudry and Moore, 1985; Karig

et al., 1979; Rose, 1983). It is obviously an unconformity of regional extent, as it was also found in forearc basins off central and southern Sumatra and south of Java (Karig et al., 1980; Schlüter et al., 2002; Susilohadi et al., 2005; van der Werff, 1996). We correlated this unconformity with a distinct high-amplitude reflector that also marks a significant change in seismic facies and was found to be present in all our MCS sections across the forearc basin.

The Mid-Late Miocene boundary is equally distinct in our seismic data. At the eastern basin edge it is developed as an erosional surface with overlying build-up structures indicating subaerial exposure and shallow water environment respectively. In deep water regions a flexured surface with thick onlapping strata above can be observed, denoting areas of subsidence and rapid sedimentary fill.

The boundary between the Pliocene and the Pleistocene is clearly visible in the area of the shallow inner shelf where it is characterized by parallel reflectors overlying basinward-dipping

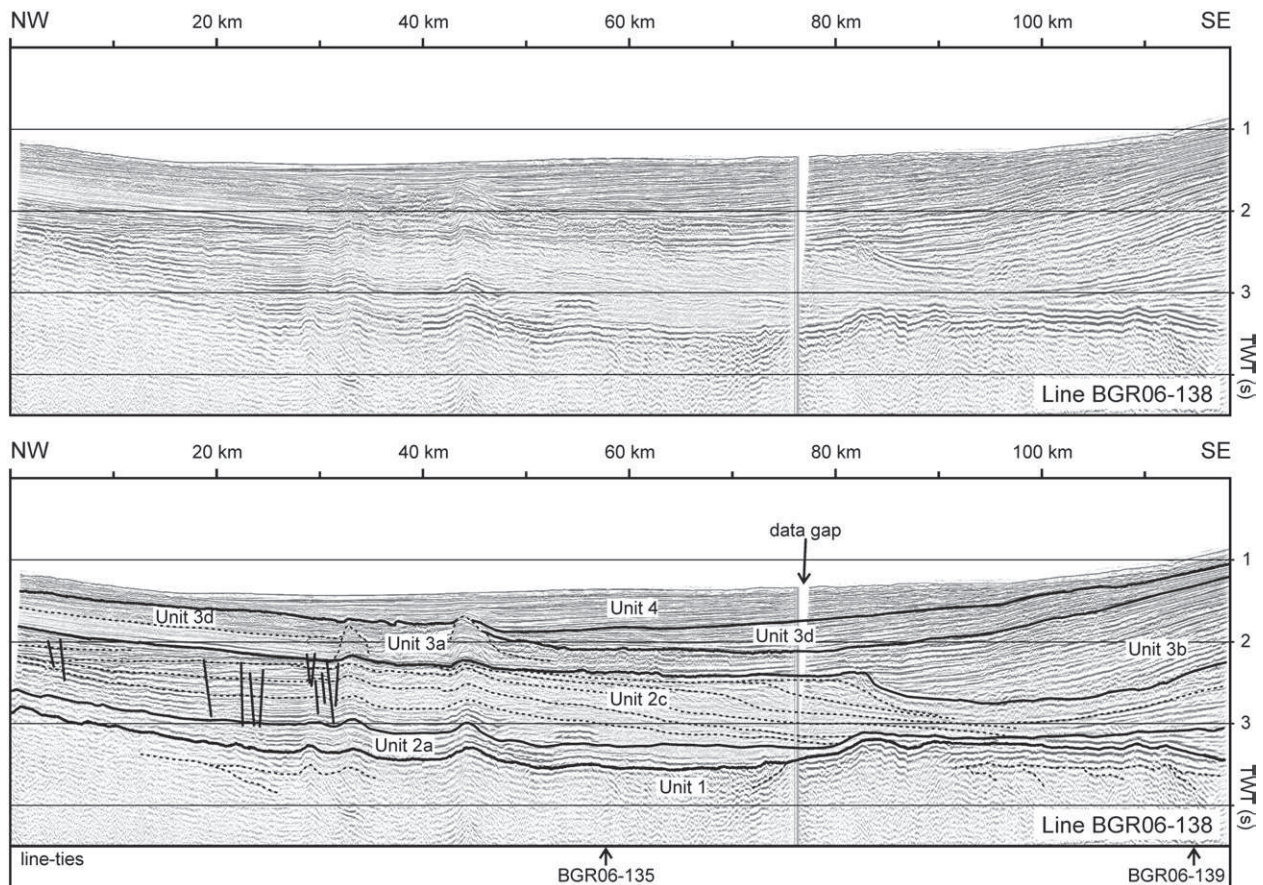


Fig. 4. MCS profile covering the southeastern part of the Simeulue basin. A large prograding body (Unit 2c) is covered by sediments derived from the opposite direction (Unit 3b), presumably from the rapidly emerging Banyak Island located at southern border of the Simeulue basin. See Fig. 2 for location of profile.

prograding facies. It can be traced into the deep water basin parts where it correlates with young onlapping strata indicating the latest phase of subsidence.

5. Seismic stratigraphy

In the MCS data we identified three major unconformities in the Simeulue basin. By correlating these with industry wells (see Section 4) we dated them as Early Miocene, base Late Miocene and base Pleistocene age. Based on these unconformities we defined four major stratigraphic units, which we further divided into subunits. The subunits do not necessarily represent different ages of the strata, but account for diverse depositional conditions. The main reason for this approach was to achieve a clear differentiation between shallow water, platform and deep water environments.

5.1. Pre-Neogene Unit 1

The acoustic basement is represented by the pre-Neogene succession. Its internal geometry is not clearly imaged in the MCS data, but along some profiles reflectivity can be observed in its uppermost parts. Especially in undeformed areas a band of parallel low-frequency high-amplitude reflectors is visible. Here, these reflections are concordant to their upper boundary and overlie an angular unconformity above steeply dipping older strata (Fig. 4, km 20, km 90–120; Fig. 5, km 210–220; Fig. 6, km 45 and km 65). Chaotic, hummocky and wavy reflectors seem to be connected to later subsidence and deformation, so this internal configuration is presumably rather an expression of deformation than of a sedimentary process.

5.2. Early and Mid Miocene Unit 2

The seismic facies of the Early and Mid Miocene succession reflects differentiated basin evolution in the Simeulue area. The following subunits have been identified:

5.2.1. Unit 2a

Unit 2a consists of parallel to sub-parallel high-amplitude reflectors of high continuity, concordantly overlying the basal Neogene unconformity. The thickness of this unit varies from 100 ms TWT (Fig. 4) to about 300 ms TWT (Fig. 7). Small buildup-like structures occasionally formed atop (Fig. 7, km 45–50; Fig. 8, km 65) indicating that Unit 2a is restricted to areas under shallow water conditions. The eastern slope of the basin was located approximately 30–40 km westwards during the time of deposition compared to its present day position (Figs. 6 to 8). At the edge of the former shallow water areas reef complexes terminate this unit (Fig. 6, km 45; Fig. 7, km 35) and lead over to deep water environments. Existing paleomorphology is leveled out by Unit 2a.

5.2.2. Unit 2b

The internal reflection pattern of Unit 2b is composed of parallel to sub-parallel continuous reflectors which are onlapping on their lower boundary. Occurrence of Unit 2b is restricted to the area west of the shallow depositional environment of Unit 2a indicating the location of a local depocenter which is narrowing northwards. Maximum thickness of up to 3 s TWT can be found in the central part of the basin (Fig. 5, km 90). The internal configuration exhibits several onlapping sequences showing phases of increased subsidence. Deformation of Unit 2b can be observed throughout the Simeulue basin and is caused by subsequent

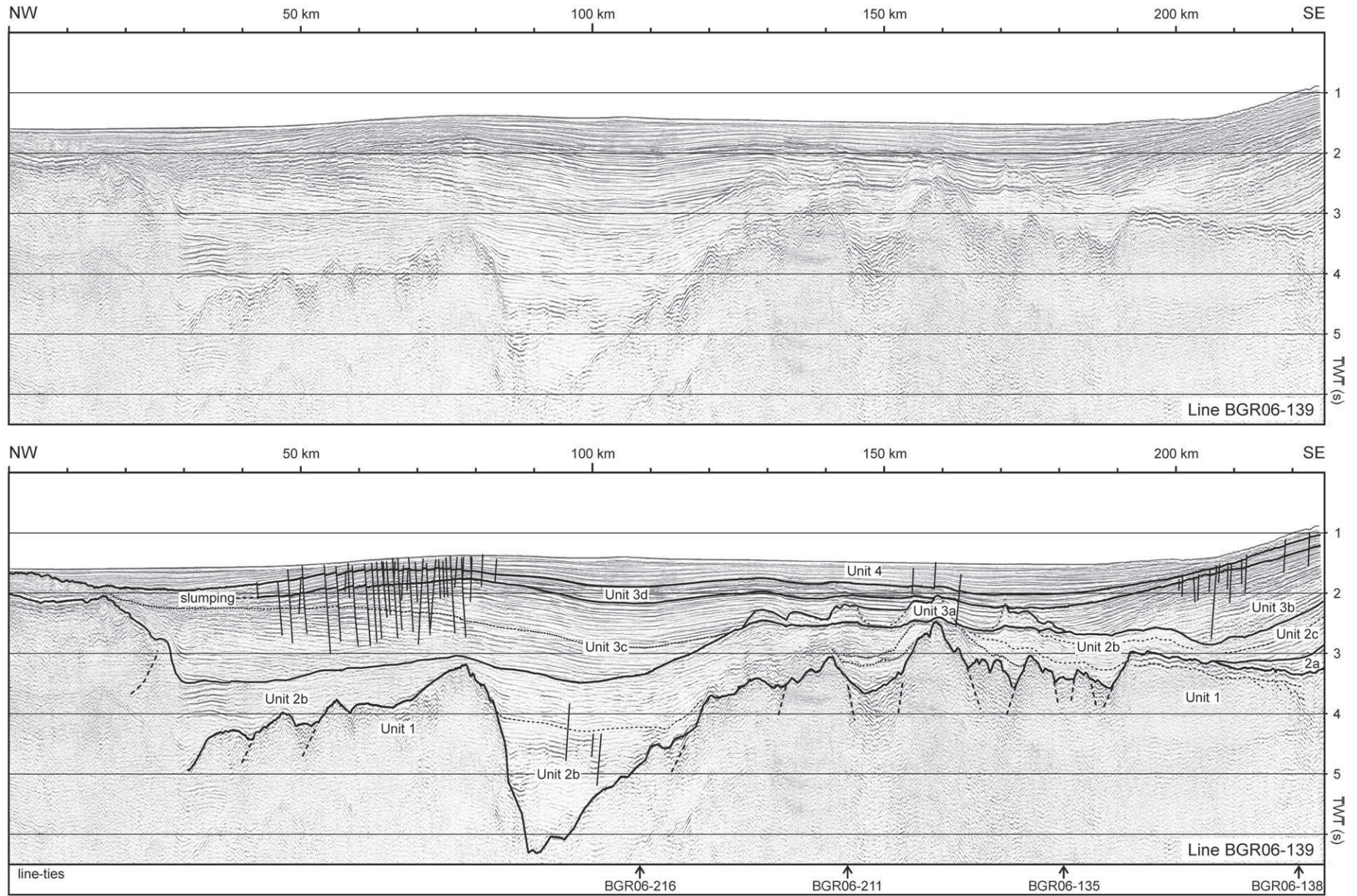


Fig. 5. MCS profile along the main axis of the Simeulue basin. Early and Mid Miocene deformation is reflected in the half graben faulting of Unit 1. The southeastern section is located at the Late Miocene/Pliocene location of the inner shelf of the basin where a carbonate platform evolved (Unit 3a). Recent uplift and associated normal faulting and erosion might be caused by reactivation of the Early/Mid Miocene half grabens. See Fig. 2 for location of profile.

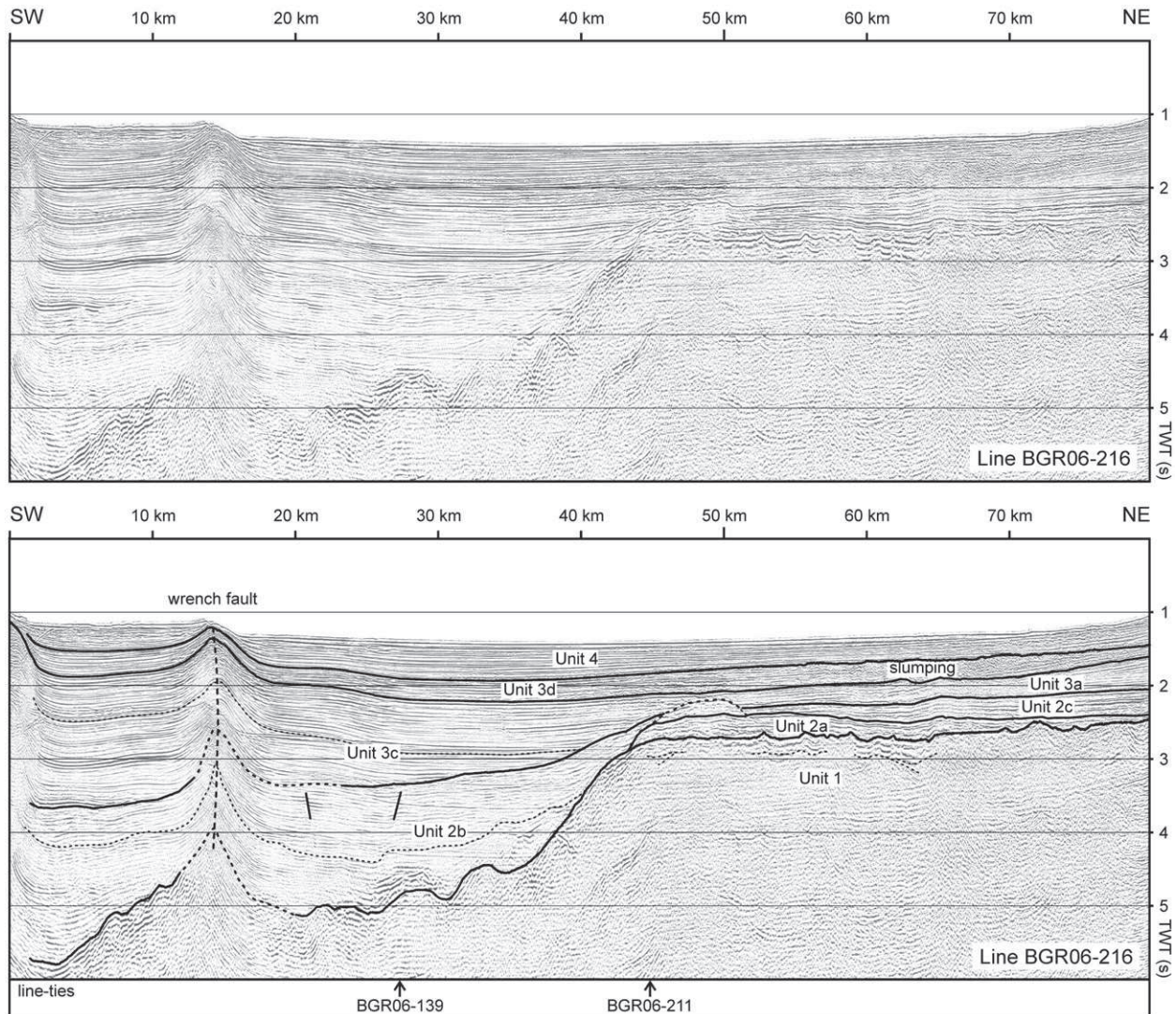


Fig. 6. MCS profile across the central part of the Simeulue basin perpendicular to the main axis of the basin. Neogene sediment thickness of the Simeulue basin is maximal at its central-western border with 4 s TWT. Wrench faulting results in uplift of this area since the Late Miocene/Pliocene and the paleo-shelf break gets buried (Unit 3d) and subsidence expanded eastwards. See Fig. 2 for location of profile.

subsidence and development of normal faults (e.g. Fig. 5, km 90–100; Fig. 6, km 20–28; Fig. 7, km 25).

5.2.3. Unit 2c

Unit 2c overlies the shallow water sediments of Unit 2a. In the southern part of the Simeulue basin it is characterized by basinward prograding, downlapping reflection patterns. This unit reflects a large sedimentary body of up to 1 s TWT thickness with internal sigmoidal configuration in the shallow area of the basin exhibiting a southward direction of progradation (Figs. 4 and 7). In the southernmost part of the basin Unit 2c interfingers with Unit 2b (Fig. 5, km 210). In the central (Fig. 6) and northern (Fig. 8) part of the basin the reflectors of Unit 2c are sub-parallel and of good to moderate continuity.

5.3. Late Miocene and Pliocene Unit 3

The Late Miocene and the Pliocene are characterized by an exceedingly expanded depocenter, the development of a large platform with patch reefs in the eastern and southern Simeulue basin during the Late Miocene and a high sedimentary input from the onshore regions. The shelf of the basin evolved into its present form during this time with continuously prograding and aggrading sequences.

5.3.1. Unit 3a

Unit 3a is characterized by isolated mounded bodies with low-amplitude internal reflectors. Below these pinnacles velocity pull-ups are present. Their occurrence is focused on the shallow areas of the eastern and southern Simeulue basin. This mound-like bodies interfinger with the surrounding units differently. Well stratified (Fig. 5, km 130–180), hummocky (Fig. 4, km 30–50) or chaotic reflection patterns (Fig. 7, km 40–50) on the former inner shelf of the basin indicate locally diverse sedimentation environments. The maximum thickness of the patch reefs is about 0.5 s TWT (Fig. 7, km 38).

5.3.2. Unit 3b

Unit 3b is composed of downlapping strata with an internal pattern of parallel to sub-parallel reflectors of good continuity. This unit is restricted to the southern part of the Simeulue basin where it reaches a thickness of up to 1 s TWT (Figs. 4 and 5). The northward direction of progradation suggests the Banyak Islands as the source area. With continued progradation the patch reefs of Unit 3a were buried (Fig. 5).

5.3.3. Unit 3c

Analog to Unit 2b this Late Miocene/Pliocene unit is an onlapping basin fill facies restricted to the western basin part where strong

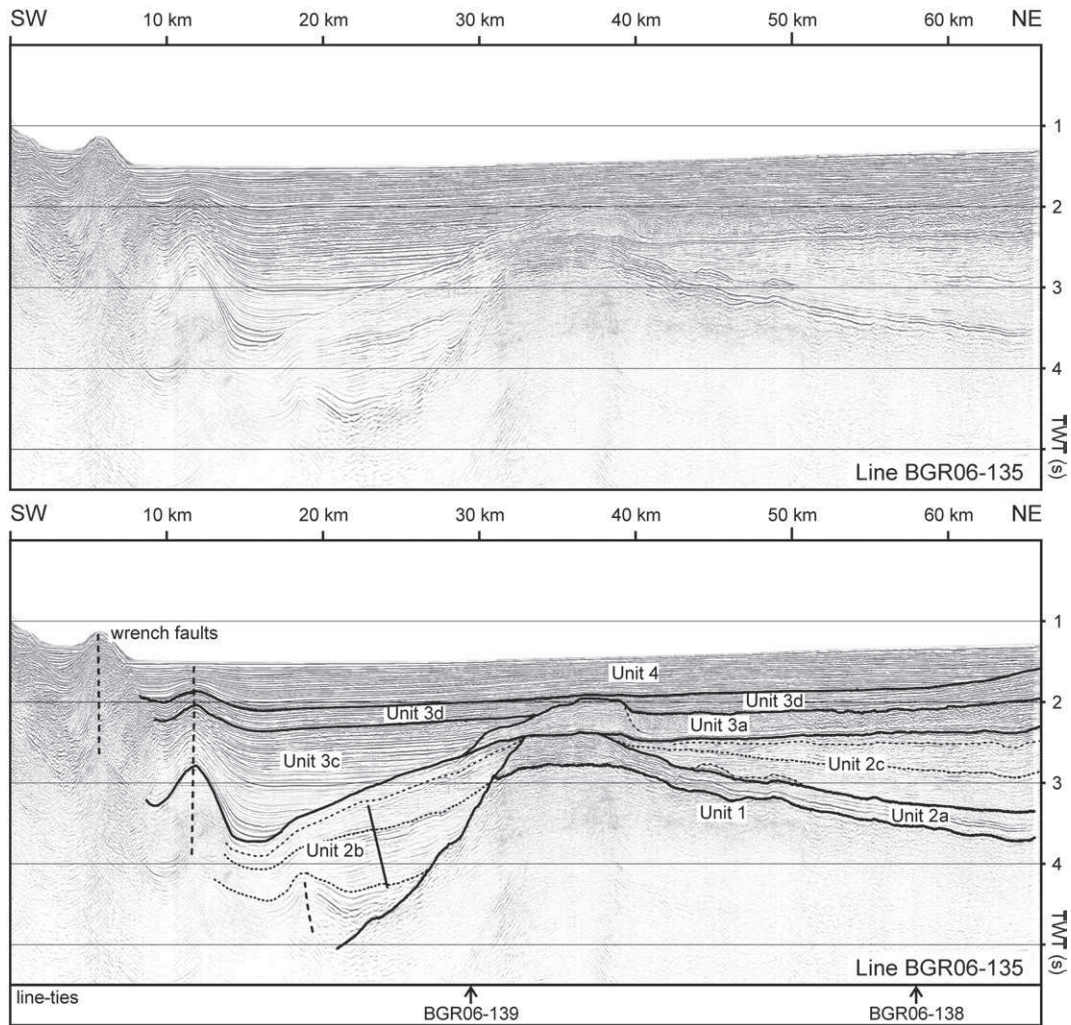


Fig. 7. MCS profile across the southern part of the Simeulue basin perpendicular to the main axis of the basin. The eastern basement block rotated after deposition of Unit 2a deforming the lower section of Unit 2b. Shortly after initiation of wrench faulting in Late Miocene/Pliocene time at the western border of the basin (upper part of Unit 3c) subsidence extended several tens of km eastward. See Fig. 2 for location of profile.

subsidence occurred resulting in a sedimentary package of up to 1.2 s TWT thickness. It consists of well stratified reflectors with good continuity in the southern basin part (Figs. 6 and 7). To the north, the reflections are increasingly discontinuous (Fig. 8).

5.3.4. Unit 3d

Unit 3d is the upper succession of Unit 3c, but spreads over the entire basin with a maximum thickness of 0.4 s TWT. The patch reefs of Unit 3a were completely buried by this sedimentary unit. In the northern (Fig. 8) and central (Fig. 6) Simeulue basin the upper part of this unit is characterized by a chaotic reflection pattern merged with stratified reflectors in the direction of the inner shelf.

5.4. Pleistocene to recent Unit 4

The Pleistocene to recent sediments are characterized by a well stratified onlapping configuration. They reflect the present-day depocenter which shows a northward narrowing triangular form. Recent sedimentation in the Simeulue basin is confined to a large area in the southern basin part (thickness of 0.6 s TWT, Fig. 7) and a narrow region in the north (thickness of 0.4s TWT, Fig. 8), whereas the central basin part is currently subject to inversion, indicated by erosional truncation of the uppermost layers (Fig. 5). The northern depocenter is

distinguished by a westward shift of sedimentation and a bypass of sediments on the slope of the basin (Fig. 8).

6. Discussion of subsidence history and tectonic structures

The subsidence evolution of the Simeulue forearc basin is documented by its sedimentary volume. Analogous to the sedimentary units we divide the subsidence evolution into four major stages, characterized by changing accumulation space, sedimentation rates, source areas and tectonic phases.

6.1. Pre-Neogene

The acoustic basement in the seismic sections is formed by pre-Neogene successions. It was penetrated by several wells in the Sumatran forearc basins and “presumably consists of several thousand feet of folded sedimentary rocks deposited at the continental margin of Sundaland” (Rose, 1983). Where distinct, our seismic sections show mainly faulted and heavily deformed strata. According to de Smet and Barber (2005) the pre-Neogene unit was affected by a regional horst and graben stage which influenced the entire Sunda mainland from the Late Eocene to Early Oligocene. In their interpretation the basement below the present-day forearc basin was part of a stable

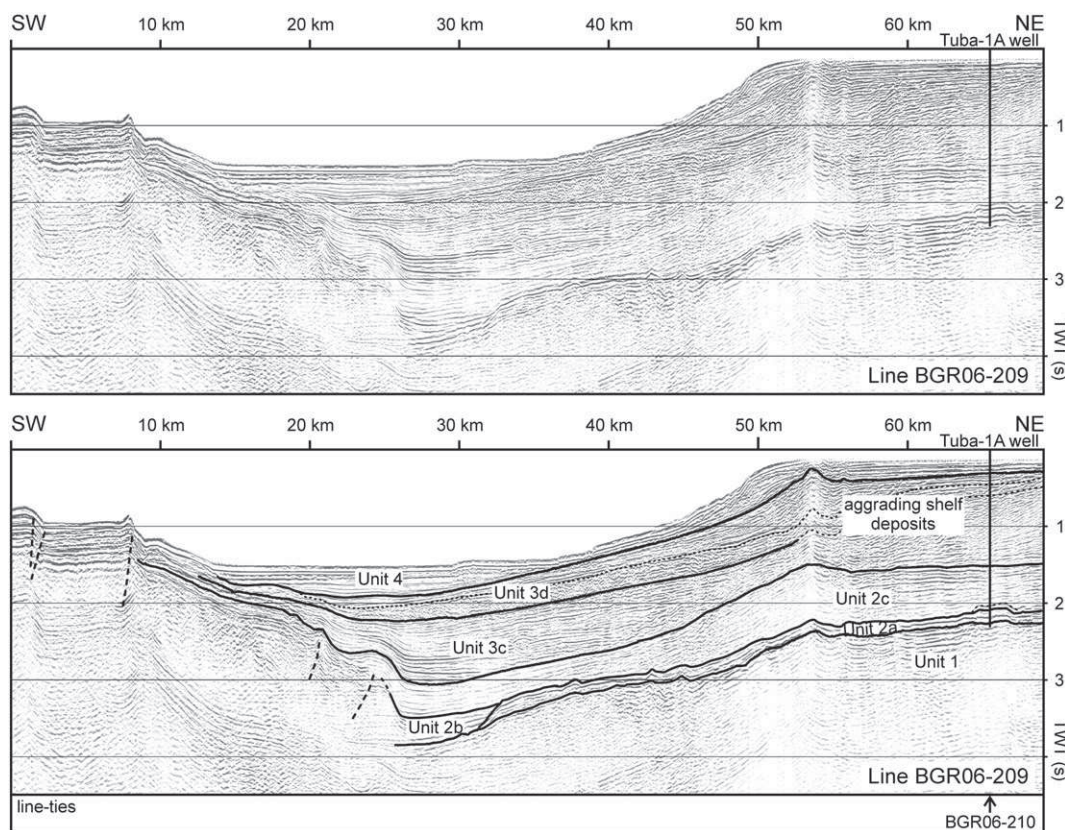


Fig. 8. MCS profile across the northern part of the Simeulue basin perpendicular to the main axis of the basin. The shelf evolved to its present shape since the Late Miocene with aggrading deposits of Unit 3. The Pleistocene to recent sedimentation shifted westwards with a sedimentary bypass on the slope. See Fig. 2 for location of profile.

continental shelf reaching landwards to the volcanic arc. Other authors proposed that the acoustic basement is made up of sediments of a subduction system of late Mesozoic to early Tertiary age, evidenced by mélangé complexes exposed on the Banyak Islands (Karig et al., 1979) and the outer arc islands of Nias, Pagai and Sipora and by volcanics and intrusives intersecting these sediments (Simandjuntak and Barber, 1996). Paleogene subduction took place at the western Sumatran border according to several plate tectonic reconstructions (Hall, 1997; Longley, 1997; Morley, 2002). Thus these models imply an extensive oceanward migration of the subduction zone to its present location. A combination of both aspects was presented by Kopp and Kukowski (2003), suggesting sediments of an older forearc basin overlying rocks originating from the arc framework corresponding to the stable continental shelf from de Smet and Barber (2005). In this scenario the location of the forearc basin stayed more or less steady since the Paleogene.

On the base of our data distinguishing between these scenarios is not possible. However, in our data an angular unconformity in the upper part of the pre-Neogene section is overlain by parallel high-amplitude reflectors (Fig. 4, km 90–120; Fig. 5, km 210–220; Fig. 6, km 45–65) which represent the latest Paleogene sediments. As this high-amplitude reflector succession shows a good continuity in areas without later deformation, it may indicate a late Paleogene decrease in subduction rate and tectonic stabilization contemporaneously taking place to a change from horst and graben architecture to regional sag due to thermal subsidence throughout Sundaland (de Smet and Barber, 2005; Simandjuntak and Barber, 1996).

The Paleogene succession ends with an unconformity observed throughout the subduction zone off Sumatra (Beaudry and Moore, 1985; Izart et al., 1994; Karig et al., 1979; Karig et al., 1980; Malod et al., 1993; Rose, 1983; Schlüter et al., 2002; Susilohadi et al., 2005). The regional scale of this unconformity indicates either a global sea level lowstand or a reorganization of the tectonic setting between the Sunda- and Indo-

Australian Plates resulting in subaerial exposure or shallow water conditions. We consider the latter more likely because a major change in relative plate motions approximately 40 Ma ago was triggered by the termination of oceanic subduction beneath the Indian–Eurasian collision zone (Hall, 1998; Longley, 1997) and also induced the extinction of the Wharton spreading center (Fig. 1).

6.2. Early and Mid Miocene

Our data reveal that the lower and middle Miocene succession, represented by Unit 2, is characterized by rapid subsidence in the trenchward, western area of the Simeulue basin (Unit 2b). In the eastern part of the basin a stable platform was present confined to the west by a carbonate barrier displayed by build-up structures in the seismic sections (Unit 2a; Figs. 6 and 7). The width of the rapidly subsiding trough is highly variable from about 25 km in the south (Fig. 7), 40 km in the central part (Fig. 6) to 10 km in the north (Fig. 8) of the Simeulue basin. This is due to the formation of half grabens of different structural behaviour. These half grabens strike mainly in SW–NE direction as revealed by a line running along the main axis of the basin (Fig. 5). Here, a series of half graben structures with vertical offsets indicating normal faults bounding the grabens to the NW are clearly imaged while lines running perpendicular to the main axis of the basin do not image these offsets and faults (Figs. 6 to 8). The TWT-isopach map of Unit 2 (Fig. 9A) shows several maxima along the western basin border. The hinge of these in-line arranged depressions is located at the western edge of the stable platform (Unit 2b). This narrow and trench-parallel series of depressions can be most reasonably explained as the result of flexural subsidence due to load of the evolving accretionary prism (Matson and Moore, 1992). The half graben structures may express erratic thicknesses and load of the accreted material in front of the Simeulue basin, reactivating weakened zones of the Eocene/Oligocene regional Horst and Graben stage described by de Smet and Barber (2005) or Hall et al.

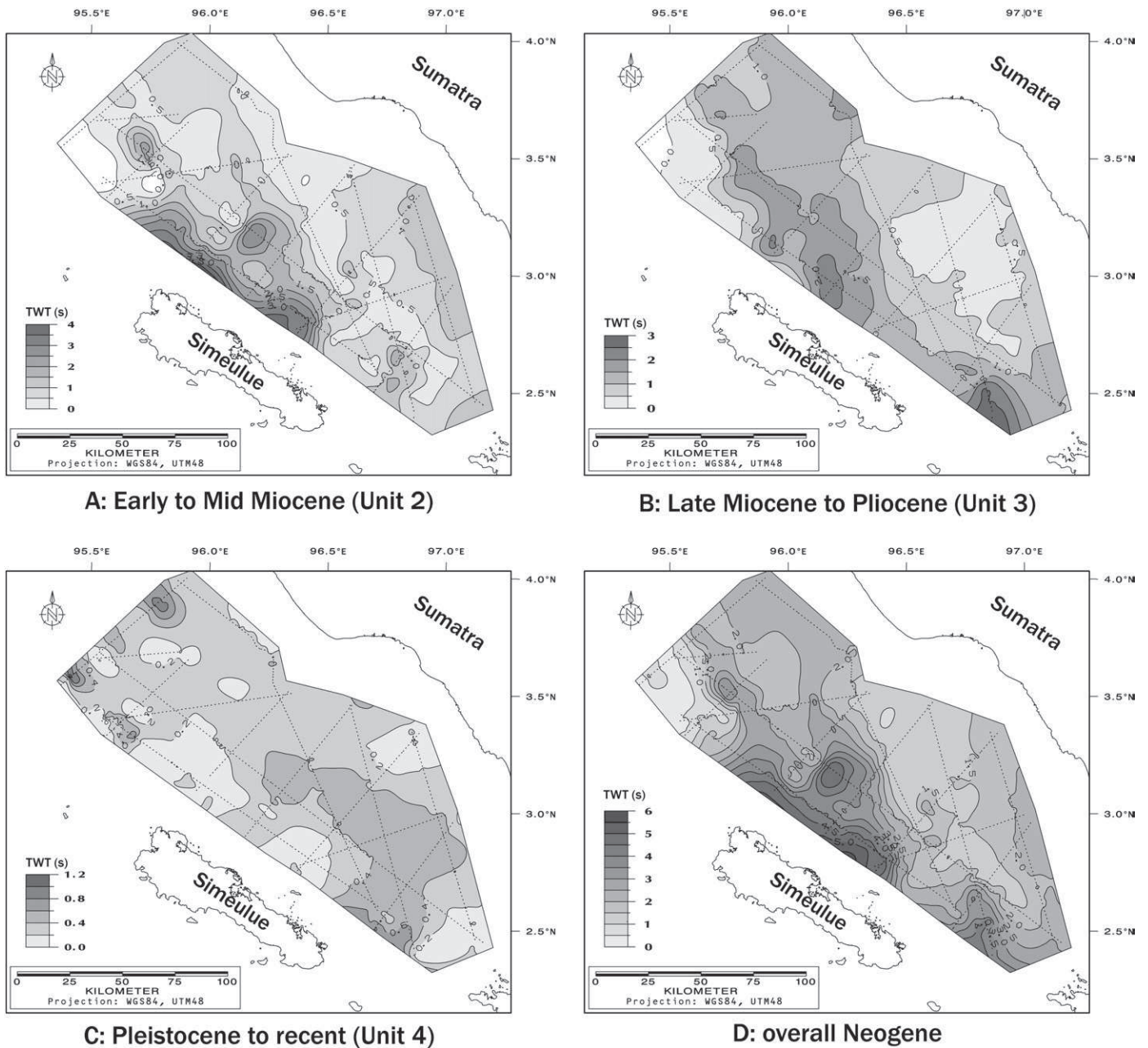


Fig. 9. TWT-isopach map of Neogene sediments in the Simeulue basin. Dotted lines indicate location of MCS profiles used for grid calculation. The Early to Mid Miocene succession shows several maxima lined up along the western border of the basin. The Late Miocene/Pliocene TWT thickness is more regular over a greater area and the maximum TWT thickness shifted eastward from Pliocene to Pleistocene times. Overall Neogene sediments have their maximum TWT thickness northeast of Simeulue Island.

(1993). Fig. 9A also shows a NNW–SSE trend for Unit 2, which might be introduced by the gridding process but nevertheless, this does not change the general picture of the basin geometry described above.

Unit 2a is described by Rose (1983) as basal Miocene clastics, consisting of nearshore marine and non-marine mudstone, sandstone, silt and minor coal beds. It is conformably overlain by a carbonate sequence in the Meulaboh-1 well (Fig. 3). Small scale buildup structures can be identified atop Unit 2a (e.g. Fig. 7, km 42–50). As patch reefs indicate shallow water conditions, we confirm the interpretation of Rose (1983) that this sequence may represent the base of a first Miocene transgressive–regressive cycle in the forearc basin which coincides with a transgressional phase described for the whole Sumatran forearc region (Barber and Crow, 2005).

After the deposition of Unit 2a, the pre-Miocene basement in the southernmost Simeulue basin rotated in landward direction resulting in accumulation space for the prograding Unit 2c on the inner shelf of the

basin (Fig. 7). This rotation is also evidenced by a compressional anticline in the lower section of the basin fill Unit 2b (Fig. 7, km 20) which therefore can be temporally correlated with its shallow water counterpart Unit 2a and also allows the correlation of the upper section of Unit 2b with Unit 2c. As Unit 2c consists of gently inclined sigmoidal clinoforms prograding in a more or less southward direction into a tectonically induced depression (Fig. 4), we consider the Sumatran mainland as the likely source area. The sediments probably represent the lobe of deltaic deposits as some reflections in the upper part of Unit 2c indicate a seaward prograding direction (Fig. 7, km 40–50), pointing towards a curved expanding sedimentary body.

In the northern basin part Unit 2c represents shelf sediments deposited during the Early and Mid Miocene with a more or less continuous sedimentation of shale, clay and claystone (Rose, 1983), indicating a transgressive environment following the deposition of the basal Miocene clastics of Unit 2a. Beaudry and Moore (1985) presented

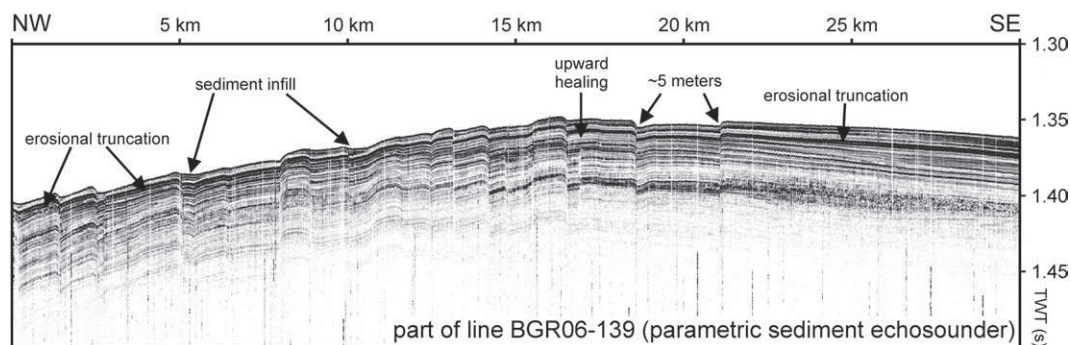


Fig. 10. Parametric echosounder recording showing recent normal faulting at the hinge of an anticline caused by reactivation of Early/Mid Miocene half graben structures. Youngest faults generate escarpments of about 5 m. An earlier phase of uplift is indicated by a buried erosional surface. See Fig. 2 for location of profile.

three MCS sections extending farther to the east onto the inner shelf of the basin in this area. They described a landward thinning and disappearance of the lower and middle Miocene successions supporting the transgressive character of Unit 2c.

6.3. Late Miocene and Pliocene

In the Late Miocene/Pliocene the Simeulue basin is characterized by the development of a carbonate platform composed of buildups. These buildups are observed over a wide area of the southern and the eastern basin edges (Unit 3a). As such bodies presumably represent patch reefs (Akbar et al., 2001; Beaudry and Moore, 1981) they indicate shallow water environment. A prominent basin shelf break evolved in the east during this time characterized by aggrading and prograding deposits (Figs. 3 and 8).

Subsidence continued in the northern and the trenchward region of the Simeulue basin. In contrast to the initial situation during the Early/Mid Miocene, subsidence was no longer focused on the half grabens. Rather the entire area subsided more or less consistently (Fig. 9B) generating accumulation space for the well stratified basin fill facies of Unit 3c. A local maximum of sediment thickness can be observed northeast of Simeulue Island which was also shown by Izart et al. (1994). This unit is well-defined to the trenchward dipping underlying strata by a distinct unconformity with onlap configuration. The change from several smaller areas of subsidence to one combined region may be due to a more regular flexural response caused by a westward progradation of the trench and the subsequent consolidation of the accretionary wedge at the western basin border. It got superseded by trenchward accreted material and now forms the distinct present day outer arc high including Simeulue Island.

Platform Unit 3a was successively drowned in northwestern direction by prograding strata (Unit 3b; Figs. 4 and 5). As Unit 3b is not present in the northern Simeulue basin, this massive sedimentary influx is most suitably explained by a rapid emergence of the nearby Banyak Islands, which was probably caused by movements along the Batee Fault, a major splay of the Sumatran Fault Zone, climaxing in this time (Harbury and Kallagher, 1991). Before the Late Miocene there was obviously no sediment source area to the south of the Simeulue basin as indicated by the nearly reverse direction of progradation of the Early/Mid Miocene Unit 2c (Fig. 4). The increased subsidence with aggrading deposits from the Sumatran mainland in the arcward part of the basin (Fig. 3, km 0–60; Fig. 8, km 50–70) marks this depositional sequence as synorogenic to an increased uplift of the Barisan Mountains on the Sumatran mainland (de Smet and Barber, 2005).

At the end of the Late Miocene/Pliocene time the forearc basins off Sumatra underwent major subsidence (Barber and Crow, 2005). In the Simeulue area subsidence expanded eastwards for several tens of kilometers in the central (Fig. 6) and southern (Fig. 7) part of the basin. The basin fill facies of Unit 3c was succeeded by Unit 3d drowning the last remnants of the carbonatic platform.

The western border of the basin was characterized by strong tectonic deformation during Late Miocene/Pliocene time. Initiation of wrench faulting parallel to the western basin border is documented by upward healing anticlines showing internal onlap of Unit 3c onto the fault (Fig. 6, km 15; Fig. 7, km 12). Farther north, the deformational style was different with reverse faulting resulting in deformation and upward-bending of the basin fill sediments (Fig. 8, km 20–30). These wrench faults likely display the northward continuation of the Mentawai Fault Zone (Diament et al., 1992) as proposed by Malod and Kemal (1996) and therefore mark the initial formation of a sliver plate in the forearc region off northern Sumatra due to oblique subduction.

6.4. Pleistocene to Recent

The Pleistocene to recent subsidence evolution of the forearc basins off Sumatra is a continuation of the Late Miocene/Pliocene situation of strong subsidence (de Smet and Barber, 2005). In the Simeulue basin the general Pliocene setup is continued but is now characterized by local uplift (Fig. 5, km 50–90) dividing the basin in two separated areas of sedimentation. The smaller northern subbasin shows a westward shift of the main axis of the depocenter (Fig. 8). Here, the deep water sediments consist of a relatively undisturbed basin fill facies. Adjacent to the east, the slope of the basin exhibit a bypass of sediments. Farther eastwards, in the shallow inner shelf of the basin, the seismic reflection pattern indicates a transgressive environment. We do not have seismic sections that cross the slope and inner shelf of the southern subbasin. However, bathymetric data (Smith and Sandwell, 1997) suggest a similar situation with a well-defined basin slope break (Fig. 2). The deep water area containing basin fill facies is considerably larger in the south (Fig. 9C) and coincides in extent with the Late Miocene/Pliocene Unit 3d.

The inversion of the central part of the basin from the Pleistocene onwards may be related to reactivation of Early Miocene half graben structures. This spatially confined tectonic zone occurs together with a distinct clustering of earthquake epicenters northeast of Simeulue Island (Fig. 2) which suggest a link with the subducting oceanic plate. A segment boundary confining the ruptures of Dec 2004 and March 2005 earthquakes is proposed at this position (Ammon, 2006; Briggs et al., 2006; Engdahl et al., 2007; Franke et al., 2008; Gahalaut et al., 2006; Konca et al., 2007; Meltzner et al., 2006). Recent normal faulting at the top of the anticline (Fig. 5, km 45–90) formed by the uplift is evidenced by high resolution sediment echosounder data (Fig. 10) where active faults produce escarpments of about 5 m (assumed sound speed in water of 1500 m/s). Presently inactive faults are identified by a sedimentary infill leveling bathymetric steps.

7. Conclusions

The structural and subsidence history of the Simeulue basin can be divided into four stages closely related to the evolution of the Sumatran subduction zone:

- 1) At the end of the Paleogene the forearc area off Sumatra was uplifted and subsequently eroded resulting in a regional scale erosional surface which separates the Paleogene and Neogene sediments. The uplift was probably caused by a major plate tectonic reorganization some 40 My ago due to the Indian–Eurasian collision, which can be temporally correlated with the extinction of the Wharton spreading center. Whether the Paleogene rocks originated from an older subduction system or were part of a stable continental shelf remains unclear.
- 2) During the Early and Mid Miocene hinged half graben structures with a general SW–NE strike evolved in the western Simeulue basin. They may have been caused by lithospheric flexure due to the load of the accreted material in front of the Simeulue basin (Matson and Moore, 1992) which resulted in narrow depocenters along the western border of the basin. The sedimentary succession in the eastern shallow part of the basin represents a transgressive–regressive cycle starting with continentally influenced coal bearing layers followed by a marine carbonatic facies. Local tectonic influence is documented by landward tilting of the basement in the southern part of the Simeulue basin resulting in accumulation space for prograding deltaic sediments.
- 3) During the Late Miocene and Pliocene the small scale subsidence pattern with several discrete depocenters changed to a consistently subsiding trough along the western basin border occupied by basin fill sediments. This was probably related to a consolidation of the accretionary wedge and the formation of the distinct outer arc high. A large carbonate platform with widespread buildup structures evolved on the shelf of the basin. This platform was successively drowned by prograding strata derived from the Sumatran mainland and the rapidly emerging Banyak Islands along the Batee Fault (Harbury and Kallagher, 1991). During the last phase of the Late Miocene/Pliocene stage subsidence extended several tens of kilometers in the direction of Sumatra. This probably was associated with the initiation of strike-slip faulting at the western border of the basin.
- 4) During the Pleistocene and extending to recent times subsidence across the Simeulue basin was relatively uniform except for the central basin part where uplift and subsequent normal faulting occurred. This inversion was possibly caused by a reactivation of Early/Mid Miocene half graben structures.

Acknowledgements

The authors express their gratitude to all colleagues making this work possible by organizing the projects and by collecting and processing the data. In particular we thank the ship's masters Lutz Mallon and Oliver Meyer and the crews of FS SONNE for their unfailing cooperation and support during the SeaCause and SUMATRA cruises. We are indebted to two anonymous reviewers and the editor for their helpful and constructive reviews and comments. We thank Michael Schnabel and Hans Keppler for the corrections and suggestions on the manuscript. We are grateful to Ingo Heyde and Ewald Lüschen for their helpful notes on magnetic anomalies and seismic processing, respectively. We would also like to thank Stefan Ladage and Dave Tappin for an interesting discussion about forearc basins. The first author wishes to thank his Ph.D. advisor Jutta Winsemann for her encouragement and support. The research projects were carried out with grants 03G0186A (SeaCause) and 03G0189A (SUMATRA) of the Federal Ministry of Education and Research (BMBF), Germany.

References

- Akbar, M., Vissarpragada, B., Alghamdi, A.H., Allen, D., Herron, M., Carnegie, A., Dutta, D., Olesen, J.-R., Chourasiya, R.D., Logan, D., Steif, D., Netherwood, R., Russell, S.D., Saxena, K., 2001. A snapshot of carbonate reservoir evaluation. *Oilfield Rev.* 12 (4), 20–41.
- Ammon, C.J., 2006. Megathrust investigations. *Nature* 440 (7080), 31–32. doi:10.1038/440031a.

- Barber, A.J., Crow, M.J., 2005. Structure and structural history. In: Barber, A.J., Crow, M.J., Milsom, J.S. (Eds.), *Sumatra: Geology, Resources and Tectonic Evolution*. Geological Society of London, London, pp. 175–233. doi:10.1144/GSL.MEM.2005.031.01.13.
- Beaudry, D., Moore, G.F., 1981. Seismic-stratigraphic framework of the forearc basin off central Sumatra, Sunda Arc. *Earth Planet. Sci. Lett.* 54 (1), 17–28. doi:10.1016/0012-821X(81)90065-0.
- Beaudry, D., Moore, G.F., 1985. Seismic stratigraphy and Cenozoic evolution of West Sumatra forearc basin. *Am. Assoc. Petrol. Geol. Bull.* 69 (5), 742–759.
- Briggs, R.W., Sieh, K., Meltzner, A.J., Natawidjaja, D., Galetzka, J., Suwargadi, B., Hsu, Y.-J., Simons, M., Hananto, N., Suprihanto, I., Prayudi, D., Avouac, J.-P., Prawirodirdjo, L., Bock, Y., 2006. Deformation and slip along the Sunda Megathrust in the Great 2005 Nias-Simeulue earthquake. *Science* 311, 1897–1901. doi:10.1126/science.1122602.
- Curry, J.R., Moore, D.G., Lawver, L.A., Emmel, F.J., Raitt, R.W., Henry, M., Kieckhefer, R., 1979. Tectonics of the Andaman Sea and Burma. *Am. Assoc. Petrol. Geol. Mem.* 29, 2479–2489.
- Curry, J.R., 2005. Tectonics and history of the Andaman Sea region. *J. Asian Earth Sci.* 25 (1), 187–232. doi:10.1016/j.jseae.2004.09.001.
- de Smet, M.E.M., Barber, A.J., 2005. Tertiary stratigraphy. In: Barber, A.J., Crow, M.J., Milsom, J.S. (Eds.), *Sumatra: Geology, Resources and Tectonic Evolution*. Geological Society of London, London, pp. 86–97. doi:10.1144/GSL.MEM.2005.031.01.07.
- DeMets, C., Gordon, R.G., Argus, D.F., Stein, S., 1994. Effect of recent revisions to the geomagnetic reversal time scale on estimates of current plate motions. *Geophys. Res. Lett.* 21 (20), 2191–2194. doi:10.1029/94GL02118.
- Deplus, C., Diament, M., Hebert, H., Bertrand, G., Dominguez, S., Dubois, J., Malod, J., Patriat, P., Pontoise, B., Sibilla, J.-J., 1998. Direct evidence of active deformation in the eastern Indian oceanic plate. *Geology* 26 (2), 131–134. doi:10.1130/0091-7613(1998)026<0131:DEOADI>2.3.CO;2.
- Diament, M., Harjono, H., Karta, K., Deplus, C., Dahrin, D., Zen Jr., M.T., Gerard, M., Lassal, O., Martin, A., Malod, J., 1992. Mentawai fault zone off Sumatra; a new key to the geodynamics of western Indonesia. *Geology* 20 (3), 259–262. doi:10.1130/0091-7613(1992)020<0259:MFZOSA>2.3.CO;2.
- Engdahl, E.R., Villaseñor, A., DeShon, H.R., Thurber, C.H., 2007. Teleseismic relocation and assessment of seismicity (1918–2005) in the region of the 2004 Mw 9.0 Sumatra–Andaman and 2005 Mw 8.6 Nias Island great earthquakes. *Bull. Seismol. Soc. Am.* 97 (1A), S43–S61. doi:10.1785/0120050614.
- Franke, D., Schnabel, M., Ladage, S., Tappin, D.R., Neben, S., Djajadihardja, Y.S., Müller, C., Kopp, H., Gaedicke, C., 2008. The great Sumatra–Andaman earthquakes – imaging the boundary between the ruptures of the great 2004 and 2005 earthquakes. *Earth Planet. Sci. Lett.* 269 (1–2), 118–130. doi:10.1016/j.epsl.2008.01.047.
- Gahalaut, V.K., Nagarajan, B., Catherine, J.K., Kumar, S., 2006. Constraints on 2004 Sumatra Andaman earthquake rupture from GPS measurements in Andaman Nicobar Islands. *Earth Planet. Sci. Lett.* 242 (3–4), 365–374. doi:10.1016/j.epsl.2005.11.051.
- Hall, D.M., Duff, B.A., Courbe, M.C., Seubert, B.W., Siahaan, M., Wirabudi, A.D., 1993. The Southern Fore-Arc Zone of Sumatra: Cainozoic Basin-Forming Tectonism and Hydrocarbon Potential. *Proc. Annu. Conv. Indones. Pet. Assoc.* 22, 319–344.
- Hall, R., 1997. Cenozoic plate tectonic reconstructions of SE Asia. In: Fraser, A.J., Matthews, S.J., Murphy, R.W. (Eds.), *Petroleum Geology of Southeast Asia*. Geological Society of London, London, pp. 11–23.
- Hall, R., 1998. The plate tectonics of Cenozoic SE Asia and the distribution of land and sea. In: Hall, R., Holloway, J.D. (Eds.), *Biogeography and Geological Evolution of SE Asia*. Backhuys Publishers, Leiden, The Netherlands, pp. 99–131.
- Harbury, N.A., Kallagher, H.J., 1991. The Sunda outer-arc ridge, North Sumatra, Indonesia. *J. Southeast Asian Earth Sci.* 6 (3–4), 463–476. doi:10.1016/0743-9547(91)90088-F.
- Izart, A., Mustafa Kemal, B., Malod, J.A., 1994. Seismic stratigraphy and subsidence evolution of the northwest Sumatra fore-arc basin. *Mar. Geol.* 122 (1–2), 109–124. doi:10.1016/0025-3227(94)90207-0.
- Karig, D.E., Suparka, S., Moore, G.F., Hehanussa, P.E., 1979. Structure and Cenozoic evolution of the Sunda Arc in the central Sumatra region. In: Watkins, J.S., Montadert, L., Dickerson, P.W. (Eds.), *Geological and geophysical investigations of continental margins*. American Association of Petroleum Geologists, Tulsa, pp. 223–237.
- Karig, D.E., Lawrence, M.B., Moore, G.F., Curry, J.R., 1980. Structural framework of the fore-arc basin, NW Sumatra. *J. Geol. Soc.* 137 (1), 77–91. doi:10.1144/gsjgs.137.1.0077.
- Konca, A.O., Hjørleifsdóttir, V., Song, T.-R.A., Avouac, J.-P., Helmberger, D.V., Ji, C., Sieh, K., Briggs, R., Meltzner, A., 2007. Rupture Kinematics of the 2005 Mw 8.6 Nias-Simeulue earthquake from the joint inversion of seismic and geodetic data. *Bull. Seismol. Soc. Am.* 97 (1A), S307–S322. doi:10.1785/0120050632.
- Kopp, H., Kukowski, N., 2003. Backstop geometry and accretionary mechanics of the Sunda margin. *Tectonics* 22 (6), 1072. doi:10.1029/2002TC001420.
- Longley, I.M., 1997. The tectonostratigraphic evolution of SE Asia. In: Fraser, A.J., Matthews, S.J., Murphy, R.W. (Eds.), *Petroleum Geology of Southeast Asia*. Geological Society of London, London, pp. 311–339.
- Malod, J.A., Kemal, B.M., Beslier, M.O., Deplus, C., Diament, M., Karta, K., Mauffret, A., Patriat, P., Pubellier, M., Regnaud, H., Arifonang, P., Zen, M.T., 1993. Deformation of the fore-arc basin northwest off Sumatra: a response to oblique Subduction. SUMANTA cruise (Baruna Jaya III, 1991). In: Zen, M.T. (Ed.), 10th anniversary of the French–Indonesian cooperation in oceanography, ocean research, technology and maritime industry, Jakarta, pp. 59–68.
- Malod, J.A., Kemal, B.M., 1996. The Sumatra Margin; oblique subduction and lateral displacement of the accretionary prism. In: Hall, R., Blundell, D. (Eds.), *Tectonic Evolution of Southeast Asia*. Geological Society of London, London, pp. 19–28.
- Matson, R.G., Moore, G.F., 1992. Structural influences on Neogene subsidence in the central Sumatra fore-arc basin. In: Watkins, J.S., Zhiqiang, F., McMillen, K.J. (Eds.), *Geology and Geophysics of Continental Margins*. American Association of Petroleum Geologists, Tulsa, pp. 157–181.
- McCaffrey, R., 1991. Slip vectors and stretching of the Sumatran fore arc. *Geology* 19 (9), 881–884. doi:10.1130/0091-7613(1991)019<0881:SVASOT>2.3.CO;2.

- McCarthy, A.J., Elders, C.F., 1997. Cenozoic deformation in Sumatra; oblique subduction and the development of the Sumatran fault system. In: Fraser, A.J., Matthews, S.J., Murphy, R.W. (Eds.), *Petroleum Geology of Southeast Asia*. Geological Society of London, London, pp. 355–363.
- Meltzner, A.J., Sieh, K., Abrams, M., Agnew, D.C., Hudnut, K.W., Avouac, J.-P., Natawidjaja, D.H., 2006. Uplift and subsidence associated with the great Aceh-Andaman earthquake of 2004. *J. Geophys. Res.* 111, B02407. doi:10.1029/2005JB003891.
- Milsom, J., Baizar, S., Sipahutar, J., 1995. Basin formation in the Nias area of the Sumatra forearc, western Indonesia. *Bull. Geol. Soc. Malays.* 37, 285–299.
- Moore, G.F., Curray, J.R., Moore, D.G., Karig, D.E., 1980. Variations in geologic structure along the Sunda fore arc, northeastern Indian Ocean. *Am. Geophys. Union Monogr.* 23, 145–160.
- Morley, C.K., 2002. A tectonic model for the Tertiary evolution of strike-slip faults and rift basins in SE Asia. *Tectonophysics* 347 (4), 189–215. doi:10.1016/S0040-1951(02)00061-6.
- Müller, R.D., Roest, W.R., Royer, J.-Y., Gahagan, L.M., Sclater, J.G., 1997. Digital isochrons of the world's ocean floor. *J. Geophys. Res.* 102 (B2), 3211–3214. doi:10.1029/96JB01781.
- Prawirodirdjo, L., Bock, Y., 2004. Instantaneous global plate motion model for 12 years of continuous GPS observations. *J. Geophys. Res.* 109, B08405. doi:10.1029/2003JB002944.
- Rose, R.R., 1983. Miocene carbonate rocks of Sibolga Basin, Northwest Sumatra. *Proc. Annu. Conv. Indones. Pet. Assoc.* 12, 107–125.
- Schlüter, H.U., Gaedicke, C., Roeser, H.A., Schreckenberger, B., Meyer, H., Reichert, C., Djajadihardja, Y., Prexl, A., 2002. Tectonic features of the southern Sumatra–western Java forearc of Indonesia. *Tectonics* 21 (5), 1047. doi:10.1029/2001TC901048.
- Sieh, K., Natawidjaja, D., 2000. Neotectonics of the Sumatran Fault, Indonesia. *J. Geophys. Res.* 105 (B12), 28,295–28,326. doi:10.1029/2000JB900120.
- Simandjuntak, T.O., Barber, A.J., 1996. Contrasting tectonic styles in the Neogene orogenic belts of Indonesia. In: Hall, R., Blundell, D. (Eds.), *Tectonic Evolution of Southeast Asia*. Geological Society of London, London, pp. 185–201.
- Smith, W.H.F., Sandwell, D.T., 1997. Global sea floor topography from satellite altimetry and ship depth soundings. *Science* 277 (5334), 1956–1962. doi:10.1126/science.277.5334.1956.
- Susilohadi, S., Gaedicke, C., Erhardt, A., 2005. Neogene structures and sedimentation history along the Sunda forearc basins off southwest Sumatra and southwest Java. *Mar. Geol.* 219 (2–3), 133–154. doi:10.1016/j.margeo.2005.05.001.
- van der Werff, W., 1996. Variation in forearc basin development along the Sunda Arc, Indonesia. *J. Southeast Asian Earth Sci.* 14 (5), 331–349. doi:10.1016/S0743-9547(96)00068-2.

Publikation

Franke, D., Schnabel, M., Ladage, S., Tappin, D.R., Neben, S., Djajadihardja, Y.S., Muller, C., Kopp, H., and Gaedicke, C., 2008. The great Sumatra-Andaman earthquakes – Imaging the boundary between the ruptures of the great 2004 and 2005 earthquakes: *Earth and Planetary Science Letters*, 269(1-2), p. 118–130 doi: 10.1016/j.epsl.2008.01.047.

The great Sumatra–Andaman earthquakes — Imaging the boundary between the ruptures of the great 2004 and 2005 earthquakes

Dieter Franke ^{a,*}, Michael Schnabel ^a, Stefan Ladage ^a, David R. Tappin ^b, Sönke Neben ^a, Yusuf S. Djajadihardja ^c, Christian Müller ^a, Heidrun Kopp ^d, Christoph Gaedicke ^a

^a Federal Institute for Geosciences and Natural Resources (BGR), Stilleweg 2, 30655 Hannover, Germany

^b British Geological Survey, Kingsley Dunham Centre, Keyworth, Nottingham, NG12 5GG, United Kingdom

^c Agency for the Assessment & Application of Technology (BPPT), Jl. M.H. Thamrin no. 8, Jakarta 10340, Indonesia

^d IFM-Geomar, Wischhoffstr. 1-3, Kiel, Germany

Received 27 April 2007; received in revised form 28 January 2008; accepted 28 January 2008

Available online 16 February 2008

Editor: R.D. van der Hilst

Abstract

Segmentation along convergent margins controls earthquake magnitude and location, but the physical causes of segment boundaries, and their impact on earthquake rupture dynamics, are still poorly understood. One aspect of the 2004 and 2005 great Sumatra–Andaman earthquakes is their abrupt termination along a common boundary. This has led to speculation on the nature of the boundary, its origin and why it was not breached.

For the first time the boundary has been imaged and, with newly acquired marine geophysical data, we demonstrate that a ridge on the subducting Indo-Australian oceanic crust may exert a control on margin segmentation. This suggests a lower plate influence on margin structure, particularly its segmentation. The ridge is masked by the sedimentary cover in the trench. Its most likely trend is NNE–SSW. It is interpreted as a fracture zone on the subducting oceanic plate. A ramp or tear along the eastern flank of the subducting fracture zone beneath Simeulue Island may be considered as an intensification factor in terms of rupture propagation barrier.

© 2008 Elsevier B.V. All rights reserved.

Keywords: subduction; earthquakes; segmentation; seismic data; Sumatra

1. Introduction

Rupture propagation during earthquakes along convergent margins may commonly be confined to discrete along-strike structural segments. However, it is recognised that rupture propagation across such segment boundaries can result in megathrust earthquakes of considerable destructive power that may generate transoceanic tsunamis. The control on earthquake propagation exerted by segment boundaries is well established (Spence, 1977; Ando, 1975) but the physical causes are poorly understood. As a result we cannot fully determine seismic and

tsunami hazard along convergent margins globally. Several mechanisms are recognised as influencing segmentation. These include: discontinuities in the geometry of the subducting plate such as slab tears (Spence, 1977; Aki, 1979); topographic anomalies within the subducting plate, such as ridges, fracture zones and seamount chains (Kodaira et al., 2000; Cummins et al., 2002; Bilek et al., 2003; Collot et al., 2004), major structures crossing the over-riding plate (Ryan and Scholl, 1993; Collot et al., 2004) and large-scale variations in the buoyancy of the subducting plate related to its thermal age (Yáñez and Cembrano, 2004).

In the instance of the great Indian Ocean earthquakes of 2004/5 the southern boundary of the December 26th 2004 event is clearly delineated (e.g. Ammon et al., 2005; Bilham, 2005; Krüger and Ohrnberger, 2005; Lay et al., 2005; Gahalaut et al., 2006). Significantly, this boundary also delineates the northern

* Corresponding author. Tel.: +49 511 643 3235; fax: +49 511 643 3663.
E-mail address: Dieter.Franke@bgr.de (D. Franke).

termination of the March 28th 2005 earthquake (e.g. Ammon, 2006; Subarya et al., 2006). A large-scale structure near Simeulue Island (Fig. 1) has been suggested as a control on the ruptures, but its specific nature is unknown. Singh et al. (2005) and Kamesh Raju et al. (2007) propose an upper plate control on the segment boundary with the West Andaman Fault as a key structure controlling rupture propagation. DeShon et al. (2005) propose that the boundary of the southern Andaman microplate, in the vicinity of Simeulue Island is a diffuse deformation zone, and that this developing plate boundary served as a barrier to rupture propagation. Dewey et al. (2007) propose a lower plate control, suggesting that a distortion of the plate interface at depth beneath the forearc may be the cause. More specifically, Subarya et al. (2006) suggest that a boundary has formed due to distortion of the plate interface, related to a north–south trending fracture zone on the incoming oceanic plate.

The aim of this study, therefore, is to characterize the plate interface and structural architecture in the vicinity of the segment boundary between the December 26th 2004 and March 28th 2005 mainshocks. To this end, during 2006, we acquired swath bathymetry, multichannel reflection seismic (MCS), and

wide-angle/refraction seismic data. Along trench-parallel profiles these data image the oceanic plate subducting beneath the forearc as well as upper plate structures. On the oceanic plate there is a broad N–S trending ridge entering the accretionary wedge SW of Simeulue. The influence of this ridge on segmentation of the upper plate is discussed.

2. Tectonic setting

Along the convergent margin off Sumatra the oceanic Indo-Australian Plate subducts under the Eurasian Plate (Fig. 1). As the former plate moves northward, convergence becomes increasingly oblique from south to north. In the vicinity of the December 2004 epicentre the azimuth of convergence is N10°E at 4°N, 95°E, (Delescluse and Chamot-Rooke, 2007). The result is large-scale strain partitioning with trench-normal and trench-parallel shear components. Along the leading edge of the Eurasian Plate, the trench-parallel shear results in large-scale, dextral strike-slip fault systems within the forearc basins and on Sumatra. Along the plate margin continental sliver plates have formed (Malod and Kemal, 1996; Simandjuntak and Barber,

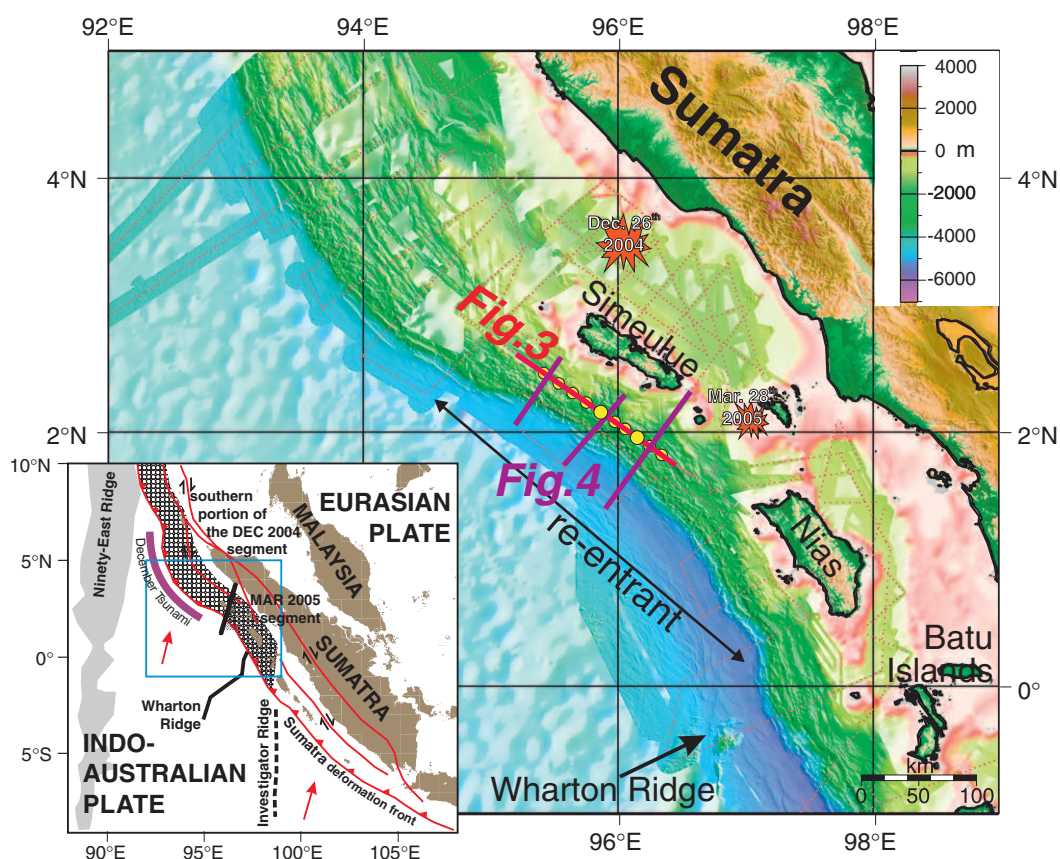


Fig. 1. Bathymetry off Sumatra underlain by satellite altimetry (Smith and Sandwell, 1997). Yellow dots mark positions of ocean-bottom hydrophone/seismometer stations and enlarged the two example stations shown in Fig. 2. Light red dashed lines give location of MCS profiles acquired during RV Sonne cruises and thick red and purple lines indicate location of multichannel seismic profile shown in Figs. 3 and 4, respectively. The locations of the initiation of rupture of the December 26th 2004 and March 28th 2005 great Sumatra–Andaman earthquakes are indicated. The only striking feature entering the subduction zone is the extinct Wharton spreading ridge southwest of Nias Island. The inset shows the tectonic situation with the Sumatra deformation front (red line with teeth) and major structures on- and offshore. The red arrows indicate the convergence direction of the Indo-Australian and Eurasian plates. The December 2004 and March 2005 rupture zones are indicated by different shades. The location of major structures on the Indo-Australian oceanic plate as the Ninetyeast, Wharton and Investigator ridges are indicated.

1996; McCarthy and Elders, 1997; Baroux et al., 1998; Sieh and Natawidjaja, 2000).

Off central Sumatra the convergent margin is mainly linear (Fig. 1), but farther north, in the region of the December 2004 and March 2005 ruptures, it becomes markedly arcuate along an area we here term the ‘re-entrant’ (Fig. 1). Northwest of the re-entrant a change in morphology and structure of both the accretionary prism and the oceanic plate takes place. To the northwest, the Sumatra deformation front continues as a salient, with its apex offset ~ 150 km to the west (Henstock et al., 2006; Fig. 1). The outboard slope of the accretionary prism is a pronounced feature with steep gradients of approximately 4° to 8° passing from 4500 m at the base to 1500 m at the top, where it forms an irregular plateau with water depths as shallow as 200 m. There is no distinct outer arc high. The accretionary prism is 140 km wide with a structural trend generally parallel to the margin (Sibuet et al., 2007). At the re-entrant the architecture of the March 2005 rupture segment, is remarkably different to that in the north. The width of the accretionary prism decreases to 100 km (from the deformation front to the West Andaman fault), the wide plateau seen in the north disappears, and the more usual tapered form of an accretionary prism is present. There is an outer arc high on which are located a chain of small islands, of which Simeulue is the most northerly (Fig. 1). The region between Nias and Simeulue islands forms a broad northeast facing re-entrant.

3. Methodology

3.1. Wide-angle/refraction seismics

To obtain reliable velocity and structural information on the deeper section of the accretionary wedge we acquired wide-angle/refraction seismic data along two MCS profiles; BGR06-208a and BGR06-135 (Fig. 1). Line BGR06-208a is situated southwest of Simeulue Island. It is parallel to the trench and at a mean distance of about 34 ± 2 km from the toe of the accretionary prism. Along this line, ten ocean-bottom hydrophones/seismometers were deployed with a mean separation of 15 km (Fig. 1). 1763 shots were fired at intervals of about 106 m, resulting in a total length of profile of 186 km. The wide-angle seismic instruments recorded energy from an offset range of at least -60 to 60 km (see Fig. 2 and Supplements 1 and 2 in Appendix A). At all 10 stations we recorded well defined refracted waves from within the sedimentary column (Pg) of the accretionary prism as well as clear wide-angle reflections of the subducting oceanic crust (PcP).

We constructed velocity–depth models by applying a tomographic method — tomo2d, (Korenaga et al., 2000) which inverts traveltimes from both refracted and reflected waves. The result is a velocity–depth-distribution and the position of the seismic reflection from the subducted oceanic crust. The modelling sequence for line BGR06-208a is as follows. For the compilation

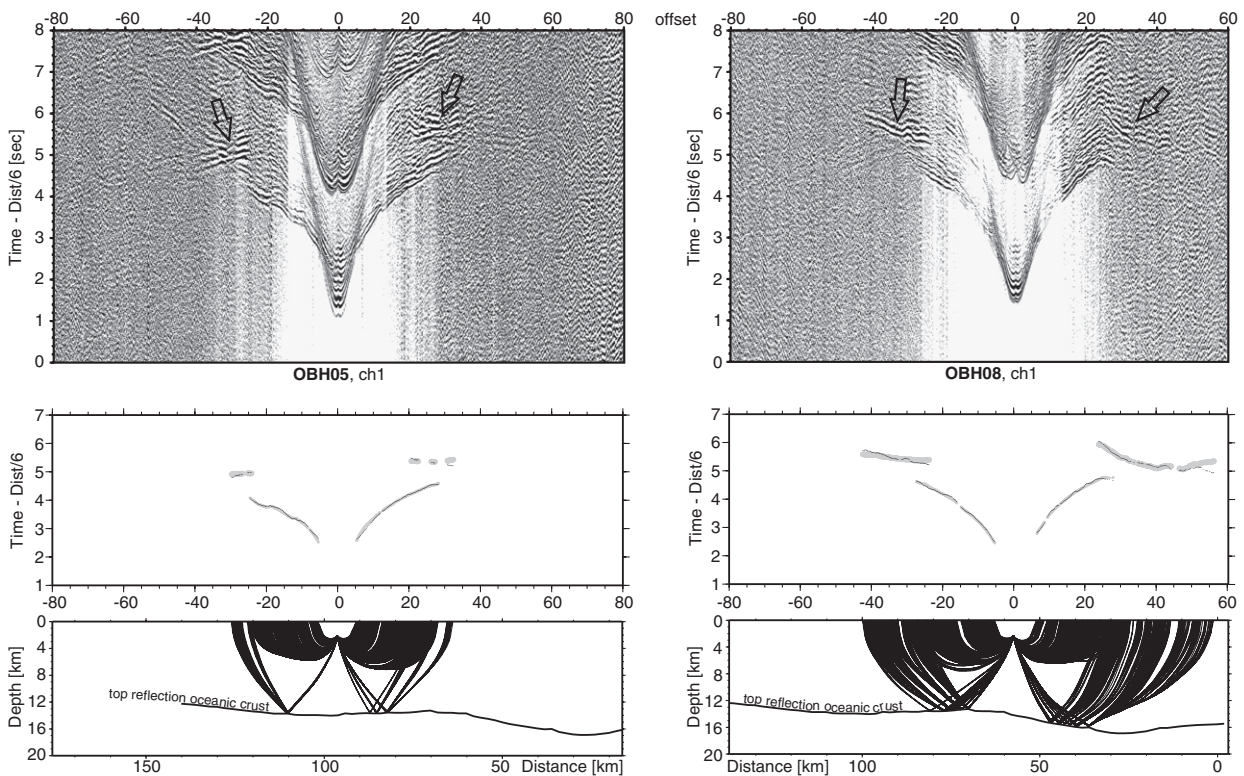


Fig. 2. Two example seismic sections from ocean-bottom stations (top), observed and calculated traveltimes (middle) and rays corresponding to the calculated traveltimes (bottom). The profile kilometre scale (Distance) corresponds to that of Fig. 3 while the offset scale is referring to the shot-receiver distance. OBH05 (left) is located above the flat lying oceanic crust while OBH08 (right) is located above a depth step of the oceanic crust. A major difference in the wide-angle reflection from the top oceanic crust is distinct in the seismograms (see arrows). The location of the two stations is marked in Fig. 1 as enlarged yellow dots. Seismograms, calculated rays and traveltimes of all remaining eight stations are shown in Supplements 1 and 2 in Appendix A.

of the starting model, we constrained the depth of the sea bottom with bathymetric data and used a 1-D velocity model with a constant gradient along the whole profile. The inversion was run in two steps. Firstly, inversion of the refracted waves through the sedimentary column provided a detailed velocity–depth model of the upper 6 to 8 km below sealevel. Between these depths the refracted waves, calculated as diving waves, reached their turning point and travelled back to the surface. Secondly, the traveltimes for reflected waves were calculated. The results provide both the seismic velocities between the well-constrained upper sedimentary section and the top of the oceanic crust at a depth of about 12 to 16 km together with the depth and profile of the oceanic crust. The top oceanic crust reflection is shown in Fig. 3 (top) only for those regions where there is a good coverage of seismic rays and where the location of crust is well constrained.

The RMS misfit of the PcP phases is in the range of accuracy by which the traveltimes of the PcP phases could be picked. This misfit is less than 100 ms and gives an error in the depth determination of the oceanic crust reflector of less than 300 m. The traveltimes of the Pg-phases are better resolved than those from the PcP, with a misfit of less than 40 ms. From these results we consider the velocity model and depth to the oceanic crust to be well defined.

To confirm that the structures imaged are within the spatial resolution of the data, we performed checkerboard tests (Supplement 3 in Appendix A). The final velocity model, as obtained by the tomography, was tested with superimposed velocity anomalies of systematically decreasing size. A set of first arrival times and reflection phases together with corresponding ray paths were generated and formed the input for another tomography using the given source–receiver configuration. If the perturbed model can be reproduced by the tomography the size of the velocity anomalies are within the vertical and horizontal resolution of the data. In this way we are able to resolve velocity variations with a dimension of less than 20×8 km. At the southeastern end of line BGR06-208a, the top oceanic crust reflector is more than 3 km deeper than in the centre of the profile (Fig. 3). The deeper location of the top oceanic crust reflector was found over a distance of 40 km, i.e. twice the horizontal resolution of better than 20 km. This proves that the depth change identified is not a velocity artefact caused by variations in the overlying sedimentary sequence. In fact there is a uniform velocity structure in the sediments resting on the subducting oceanic crust (Fig. 3). A constant depth for the subducting oceanic crust would only be possible if there were a distinct, and very large, low velocity zone (i.e. a very strong velocity inversion) in the sediments above the section where we identify the deeper oceanic crust (profile km 0–70). Such a velocity inversion is not possible.

To address the question of velocity–depth ambiguity, we systematically varied the depth kernel weighting parameter (Korenaga et al., 2000). The final velocity model shown in Fig. 3 was calculated with a weighting parameter of unity, which corresponds to equal weighting of velocity and depth nodes. Decreasing the weighting parameter should lead to smaller depth variations with larger velocity variations. However, even with an implausible kernel weighting parameter as small as 0.1 (where the

velocity perturbations are very much greater than the perturbation of the depth of the resulting reflector), the top of the oceanic crust in the final model shows a depth change of 2 km towards the southeast.

The second wide-angle/refraction seismic line BGR06-135 runs perpendicular to the trench in SW–NE direction. The line extends for 215 km from the oceanic plate to the Simeulue forearc basin. We recorded at a total of 31 ocean-bottom stations. Due to higher ships speed a shooting interval of 60 s resulted in an average shot spacing of about 120 m. Here we only concentrate on the western, seaward, part of the line and use traveltimes of refracted waves from 13 stations to derive the velocity–depth model. PcP phases from 5 stations constrain velocities at greater depth down to the subducting oceanic crust.

We used a similar modelling procedure for this wide-angle/refraction line as for line BGR06-208a. The resulting model provides seismic velocities for the trench fill and for the accretionary prism up to 60 km landward of the prism toe. The prism sediments have values of 4.0 km/s at a depth of 3 km below seafloor, and reach a value of 5.5 km/s at about 13 km below seafloor.

The results from the two wide-angle/refraction seismic lines provided an initial velocity model for the depth migration of the MCS lines (Section 3.2). Reflections beneath the top oceanic crust were recorded only occasionally in the wide-angle data. Thus the deeper parts of the velocity model are based mainly on extrapolation and, therefore, are tentative. In the MCS processing, in order to avoid any migration artefacts, we smoothed these velocity models in the crustal area with a vertical window of 3 km. Thus there are minor differences between the wide-angle and the MCS velocity models.

3.2. Multichannel reflection seismics (MCS)

During our marine surveys over the 2004 and 2005 rupture zones a comprehensive dataset of some 9000 line kilometres of MCS data were acquired together with gravity and magnetics data. MCS data were acquired with a 240 channel, 3 km streamer (offset to near group: 150 m; maximum offset: 3,137.5 m), and a tuned airgun array comprising 16 airguns with a total capacity of 50.8 L. Record length was 14 s with a sample interval of 2 ms. A shot interval of 50 m resulted in a fold of 30.

Processing of four MCS lines was performed up to full Kirchhoff prestack-depth migration and included the production and correction via MVA (migration velocity analysis) of a depth velocity model. After testing various combinations of processing parameters the following sequence was regarded as optimal. Prestack processing included geometry editing, deconvolution, true amplitude recovery, and filtering. Reduction of water-bottom multiples (a major challenge) was achieved by applying a parabolic radon filter and inner trace mutes. Stacking velocities, at an average distance interval of 3 km, were determined for the reference poststack time migrated sections. The initial depth model was derived from the wide-angle/refraction seismic data along the lines BGR06-135 and BGR06-208a and from smoothed DMO velocities, adjusted and calibrated at the cross point with the refraction seismic line for lines BGR06-117 and

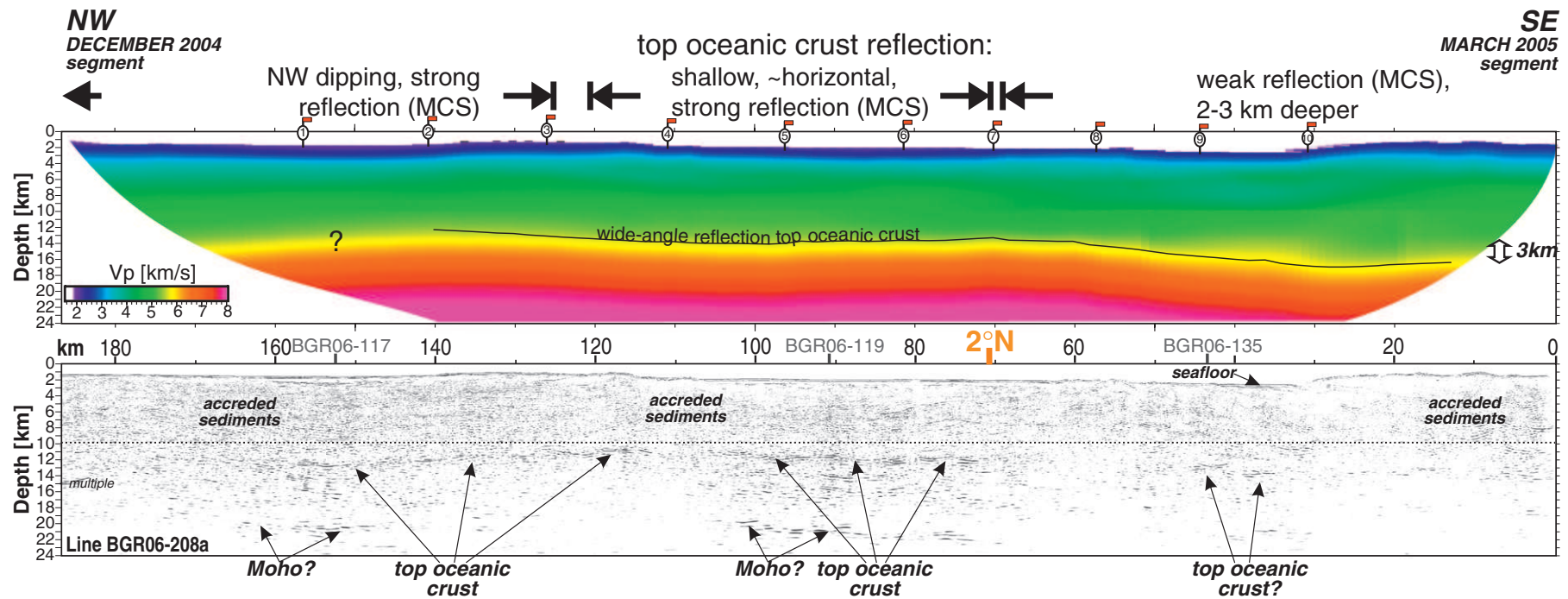


Fig. 3. Velocity–depth model (top) as derived from wide-angle/refraction seismic data and a prestack-depth migrated multichannel seismic line (bottom). Line BGR06-208a runs margin parallel from the December 2004 segment across the segment boundary and extending SE-ward on the March 2005 segment. The location of the profile is indicated as thick red line in Fig. 1. Top: The inversion of the refracted waves from 10 ocean-bottom stations revealed a detailed velocity–depth model of the model’s upper 6 to 8 km. The traveltimes from reflected waves gave a detailed image of the seismic velocities down to the top of the oceanic crust at a depth of about 12 to 16 km. We resolve the shape of the subducting oceanic plate along the profile (black line). In the SE (km 70 to 15) a distinct depth step of the subducting oceanic crust of more than 3 km is resolved. Bottom: The top reflection from the subducting oceanic crust is well imaged north of 2°N (profile km 160–70). It shows a dip to the NW from about 11 km depth to 12.5 km depth (profile km 120 to 160). The reflection vanishes at the NW end of the line, where the initial velocity model for depth migration is poorly controlled. In the centre of the line (profile km 70–120) the strong reflective top of the oceanic crust lies continuously at a shallow depth of 11 to 12 km. Southeast of 2°N (profile km 70–20) only weak reflections are visible, which are located at 2 to 3 km greater depth.

-119. The upper parts of the velocity fields were iteratively improved via MVA until the migrated CRP gathers were flat. Quality control included a detailed evaluation of congruence between the poststack migrated sections and the time-converted prestack-depth migrated sections. Kirchhoff time migration, based on smoothed interval velocities derived from stacking velocities, completed the poststack migration sequence for the reference time migrated lines as well as for the additional lines not depth migrated. Finally, time and space variant signal filtering, time varying scaling and, along some sections, a smooth *fx*-deconvolution completed the poststack processing sequence.

3.3. Bathymetry

Swath bathymetry was acquired by the RV Sonne using a 12 kHz Simrad EM 120 and by the HMS Scott using 12 kHz SASS-IV system (Henstock et al., 2006, Ladage et al., 2006). At the northern edge of the study area we added multibeam data from cruise MD149 (Sibuet et al., 2007). The swath data was compiled and merged to provide a complete map of the area off northern Sumatra (Figs. 1 and 6). Interpretations of the swath bathymetry were integrated with geodetic data to provide an overall picture of the structure of the boundary between the 2004/2005 earthquakes located in the vicinity of Simeulue Island.

4. Results

4.1. Image of the plate interface

The margin-parallel line BGR06-208a (Fig. 3) crosses the boundary between the two earthquake ruptures of 2004 and 2005 in the vicinity of Simeulue Island. It lies 34 ± 2 km landward of the deformation front. From the wide-angle seismic data the velocity–depth model resolves the top oceanic crust between line kilometres 15 and 140 (Fig. 3 — top). Only at the margins is the ray coverage insufficient to image the reflection. The oceanic crust is subhorizontal at a depth of about 12 km along the central part of the line. To the southeast over a distance of 40 km the ocean crust depth gradually increases by more than 3 km (Fig. 3 — top; profile km 60–20; south of 2°N). Since the velocities of the overlying, accreted sediments are uniform along the line the depth change is not an artefact due to velocity pull-down.

The MCS data provides complementary insights into the finer detail of the sedimentary prism, together with the crustal structure than available from the wide-angle seismic data. Reflections of the sedimentary prism and the underlying oceanic crust allow refinement of the coarse interpretations based on the refraction results. Conversely, the refraction models provide a constraint on interpretations of the MCS (Mooney and Brocher, 1987).

On the MCS data, the profile of the subducting oceanic crust is seen to be broadly similar to that on the wide-angle seismics (Fig. 3 — bottom). However, there are distinct regions of strongly reflective oceanic crust alternating with regions of weaker reflections. In the centre of the line (Fig. 3 — bottom; profile km 70–120) the strongly reflective top of the oceanic crust lies

continuously at a shallow depth of 11 to 12 km. To the northwest the strongly reflective oceanic crust dips slightly from about 11 km to 12.5 km depth (Fig. 3 — bottom; profile km 120 to 160). The oceanic crust reflection is not imaged at the northwestern end of the line where the initial velocity model for depth migration is poorly controlled.

Southeast of 2°N (Fig. 3 — bottom; profile km 70) there are no MCS reflections from the top of the oceanic crust for some 20 km. This absence of reflections is where, on the wide-angle seismic data, there is a gradual increase in depth of the oceanic crust. Further south at km 45 on the MCS line, the oceanic crust reappears as a weak, discontinuous reflection about 2 km deeper than in the central part of profile. The change in reflectivity is not due to any change in the character of the overlying sediments because these can be traced across this region.

In the region traversed by the seismic line the deformation front is slightly curved because it is located in the broad re-entrant region between Nias and Simeulue islands. However, the change in the depth of the oceanic crust cannot be attributed to an oblique relationship between the orientation of the seismic line and the deformation front. Even if there was some limited obliquity between the orientation of the seismic line and the dip of the slab, given an average dip of the oceanic crust of about 5° an offstrike distance of 2 km either up or down the slab would result in a depth change of the top oceanic crust of less than 200 m.

From both seismic datasets we can identify an increase in depth along the strike of the oceanic crust of between 2 km (MCS) and 3 km (wide-angle data). Due to the MCS streamer length of 3000 m, absolute oceanic crust depth values are probably better resolved from the wide-angle seismic data. The observed variations in slab depth are due to a prominent structural relief in the lower plate. The location of the change in slab depth coincides with the segment boundary outlined by the aftershock distribution (Ammon, 2006). The depth change is limited to a 40 km wide region of the lower plate at approximately 2°N and 96°E.

4.2. Structural architecture and domains along the margin

Southwest of Simeulue, towards the trench, we acquired MCS data along three dip lines that cross the accretionary prism. These lines are shown in Fig. 4 arranged relatively to the line-ties with BGR06-208a.

Profile BGR06-117 (Fig. 4A) is located in the southern region of the December 2004 earthquake rupture. The line extends for some 72 km across the trench and accretionary prism at the northwestern tip of the re-entrant. Along the line the trench fill is more than 4 km (3.4 s TWT) thick and at the seabed completely levels out the oceanic crust relief. The fill consists of continuous parallel to sub-parallel reflections cut by palaeochannels. The seismic character is typical of turbidite facies. A series of conjugate normal faults cuts the entire trench fill. The oceanic crust can be traced beneath the frontal accretionary prism. It dips at about 4°. At the tie-point with line BGR06-208a, some 34 km northeast of the toe of the accretionary prism, the oceanic crust is at a depth of ~12.5 km. Almost all the sedimentary cover on the incoming plate is offscraped and deformed at the prism toe. Thus almost all incoming sediment is

accreted to the frontal prism. Within 12 km of the prism toe there is a doubling of the sediment thickness resting on the subducting plate. This increase in sediment thickness results in an extraordinarily steep prism slope of 15° . The increase in thickness is accompanied by frontal collapse structures.

MCS line BGR06-119 is located 60 km to the SSE of BGR06-117, just offshore and perpendicular to Simeulue Island. At the southwest end of the line, the top of the oceanic crust is at 7 km depth. Beneath the prism toe this depth increases to about 8 km (Fig. 4B). Oceanic crust depths are considerably shallower (~ 2 km) than on line BGR06-117 (Fig. 4A). Along line BGR06-119 the oceanic crust entering the subduction zone shows a similar normal fault pattern to that on line BGR06-117. However, the trench fill is only 2 km thick and slightly more wedge-shaped as it passes towards the accretionary prism. Normal faults penetrate the lower trench fill but heal upwards. Above a 500 m elevated graben shoulder in the oceanic crust a popup structure delineates the youngest outboard deformation. Again, there is frontal accretion of almost the whole trench fill at the prism toe, thus the incoming sediments are basally detached. However, the resulting frontal toe of the accretionary wedge is broader than further north and not as steeply dipping. The oceanic crust dips gently beneath the trench at the toe but the dip increases beneath the slope. About 32 km from the toe of the prism it reaches a depth of ~ 11.5 km at the line-tie with line BGR06-208a. Here the oceanic crust dips $\sim 6^\circ$.

MCS line BGR06-135 runs from SW to NE from the oceanic plate to the eastern part of the Simeulue Basin (Fig. 4C). It is located in the northern region of the March 2005 rupture. The profile lies at the apex of the broad re-entrant located off of Simeulue and Nias Island. The trench fill is strongly wedge-shaped, thickening from 1 km in the southwest to 4 km at the deformation front. Again, the trench fill and oceanic crust are normally faulted. In the lower section of the accretionary prism there is imbricate thrusting of the accreted sediment similar in style to that on line BGR06-119 and also seen further south (Schlüter et al., 2002; Susilohadi et al., 2005). The oceanic crust reflection is discontinuous but can be traced for more than 70 km to the northeast of the deformation front (Fig. 4C). There is an increase in depth of the oceanic crust from 9 km at the deformation front to ~ 13 km at the line-tie with line BGR06-208a. This corresponds to a slab dip of 6.7° beneath the frontal accretionary prism.

Comparing the three cross-profiles we establish an increase in slab dip from the north (4°) to the south (6.7°) beneath the frontal prism slope. This trend is accompanied by decreasing seabed slope angle of the frontal accretionary prism. Large seabed slope angles in the north coincide with the accretion of a thick sedimentary column whereas the thinner incoming sedimentary pile south of Simeulue Island corresponds with lower slope angles.

5. Discussion

5.1. Origin of slab relief

The simplest hypothesis to explain the shallow depth oceanic slab north of 2° identified on our data, would be a broad rise on

the lower plate created as the Indo-Australian Plate is subducted beneath the 300 km long re-entrant. The re-entrant (Fig. 1) extends as far south as Nias Island and interaction with the overriding Eurasian plate along this feature would result in a rise in the oceanic plate with the apex approximately located midway between Nias and Simeulue islands. However, there are several inconsistencies in this explanation that lead us to consider a different source to be more likely. Our seismic profiles show that the shallowest slab reflections are in the northern third of the re-entrant, offshore of Simeulue. The shallow slab section here is only 60 km long and the dips at either end resolved by our data are too steep to be explained by a rise of longer (300 km) wavelength. The opposing dip directions at the ends of the slab suggest a smaller, more local, source. Moreover, on line BGR06-135, located at the apex of the re-entrant, there is an oceanic crust that is more steeply landward dipping (Fig. 4C) than to the north (Figs. 4A and B). This would not be expected if the shallow slab was formed by a broad rise on oceanic crust subducting along the re-entrant. We conclude, therefore, that the narrow width and steep marginal dips of the shallow slab reflection cannot be explained by a broad rise on the slab that has formed by broad-scale subduction beneath the re-entrant. Rather, the data support the subduction of an elongated, narrow high on the subducting plate.

For the origin of the narrow high we refer to the Indo-Australian Plate offshore of Sumatra, the structure of which is reasonably well established (Cande et al., 1989; Deplus et al., 1998; Milsom, 2005; Delescluse and Chamot-Rooke, 2007). Dominant structures on the plate are E–W trending extinct spreading ridges, or N–S trending fracture zones. However, on the oceanic plate off Simeulue Island along strike from the feature we identify, neither spreading ridges nor fracture zones are evident on our high-resolution bathymetry nor on satellite altimetry (Smith and Sandwell, 1997). Further south, where the sedimentary cover thins, several fracture zones are imaged on gravity and magnetic data and the satellite altimetry (Smith and Sandwell, 1997). Morphologically, these fracture zones appear as complex structures of alternating topographic highs and lows (Ladage et al., 2006). Their width (30–50 km) and relief (~ 500 –2000 m) are of same order of magnitude as the rise observed in our seismic data south of Simeulue. The Investigator Fracture Zone, which trends approximately north–south at 98°E , has an estimated elevation of up to 2000 m (Milsom, 2005).

North of the re-entrant, at 93.2°E and 93.6°E , Sibuet et al. (2007) propose that north–south oriented tectonic lineaments on the incoming plate are related to palaeo-fracture zones. These authors suggest that these fracture zones have been subducted and are influencing upper plate deformation, being reactivated with left-lateral slip during the December 2004 mainshock. Another fracture zone, further south of those identified by Sibuet et al. (2007), can also be mapped from magnetic anomaly patterns (Cande et al., 1989; Barckhausen, 2006) and traced into the area off Simeulue. A fracture zone at this location was also inferred by Newcomb and McCann (1987). It projects almost exactly onto the location of the elevated oceanic crust we identify along line BGR06-208a (Fig. 3). In conclusion, we suggest that it is this fracture zone, now deeply buried beneath

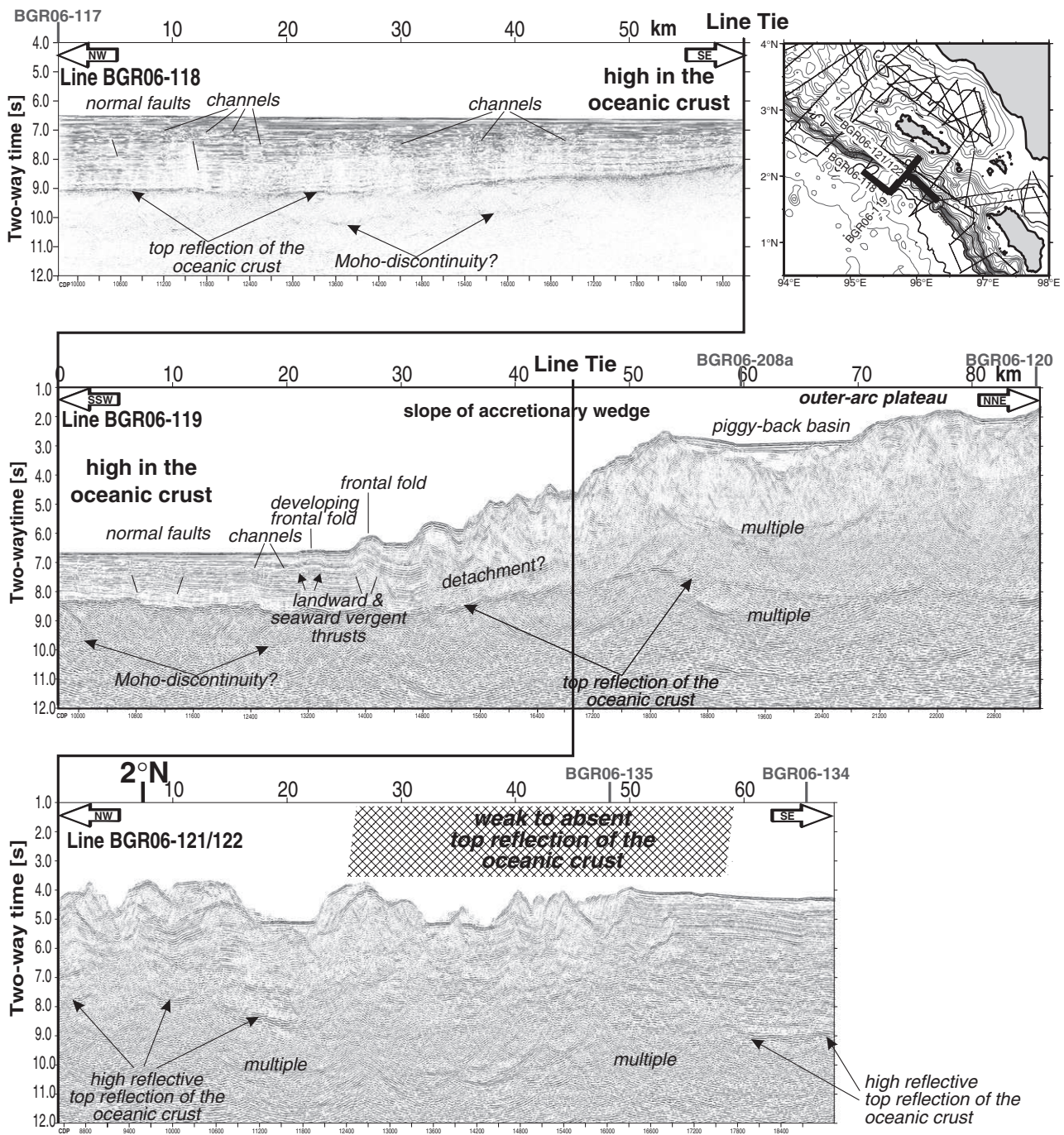


Fig. 5. Time migrated seismic sections from the trench and frontal slope of the accretionary prism. Line BGR06-118 (top) runs margin parallel in the trench SW of Simeulue Island. The oceanic basement shallows remarkably from 9.1 s (TWT) in the NW to 8.25 s (TWT) in the SE, at the intersection with line BGR06-119. Along line BGR06-119 landward and seaward verging thrusts at the deformation front and a frontal fold are developed. The composite line BGR06-121/122 runs in strike with the slope and shows a pointed depth variation in the subducting oceanic crust from 7.8 s (TWT) in the NW to 9.0 s (TWT) about 70 km to the SE. Both locations are about 20 km landward of the toe of the accretionary prism. At both ends of the line the top oceanic crust reflection is highly reflective while the reflection becomes weak to absent in the centre (profile km 26–58).

trench sediment, that is the source of the shallow flat slab we identify on line BGR06-208a.

5.2. Orientation of shallow slab/fracture zone

The question remains, what is the orientation of the shallow slab, and does this support a fracture zone origin? Fig. 3 shows a

slightly NW dipping oceanic crust reflection in the NW part of line BGR06-208a. As this is at the edge of the velocity–depth model, the increase in depth of the oceanic crust to the NW is not well constrained. However, in this region, but further to the southwest on line BGR06-118 (Fig. 5 — top) we observe a similar depth trend in the oceanic crust seaward of the accretionary prism. Seismic line BGR06-118 is about 60 km

SW of the prism toe and oriented parallel to the trench as well as to line BGR06-208a. The top of the oceanic crust is well imaged and dips to the NW, as on line BGR06-208a. It shallows over a distance of 30 km from 9.1 s (TWT) in the NW to 8.25 s (TWT) in the SE (Fig. 5 — top) where it intersects line BGR06-119 (Fig. 5 — middle). Its relief at seabed is masked by the drape of the trench fill sediments. A line connecting the relief in the oceanic crust identified along line BGR06-118 with the increase in depth of the oceanic crust to the NW along the margin-parallel line BGR06-208a would strike NNE.

Turning to composite line BGR06-121/122 (Fig. 5 — bottom). This line is margin parallel and located between the toe of the accretionary prism and line BGR06-208a. At the cross tie between lines BGR06-119 and BGR06-121/122 the oceanic crust is at a depth of 7.8 s (TWT). At the southern end of BGR06-121/122, about 70 km to the south, it is at 9.0 s (TWT) (Fig. 5, bottom). The sedimentary thickness is 4 s (TWT) at the northwestern end of the line whereas it is up to 5 s (TWT) in the southeast. Although the seabed relief is more irregular in the northwest (smoother in the southeast) the water depths on average remain the same along the line. However, although the top oceanic crust reflection is clearly imaged at both ends of the line, between km 25 and 58 it disappears. Both locations are about 20 km landward of the toe of the accretionary prism. In the SE part of the profile the back limb of an anticline is imaged showing smooth topography and subhorizontal strata. It is therefore surprising that the highly reflective top oceanic crust reflection becomes weak to absent northeast of km 58, where it still underlies the subhorizontal strata (Fig. 5 — bottom).

We consider the absence of the reflection to be attributable to the same cause as on line BGR06-208a. Allowing for the difference in sediment thickness along line BGR06-121/122, that would result in a velocity pull-up in the southeast, in the southeast the oceanic crust reflection is about 2.5 km deeper than in the northwest. A line connecting the locations of weak oceanic crust reflections as well as the increase in depth from composite line BGR06-121/122 and line BGR06-208a would strike NNE towards Simeulue (Fig. 6 — top).

5.3. Links between lower and upper plates

GPS measurements on Simeulue Island (Subarya et al., 2006, Briggs et al., 2006) reveal vertical uplift in the north during the earthquake of December 2004 and uplift in the south of the island during the March 2005 event. The differential uplift defines a saddle in the middle of the island. It is taken as evidence for a major basement structure that may control rupture termination and a segment boundary (Briggs et al., 2006). Projecting the trend of the slab rise (fracture zone) on our seismic data onto Simeulue Island reveals a close alignment with the saddle identified by Briggs et al. (2006), with a trend of NNE–SSW (\sim N10°). The proposed NNE trend identified on our data also projects onto the nucleation point of the December 2004 earthquake (Fig. 6 — top). Consideration of the uplift on Simeulue in the context of our interpretations of an increase in depth of the oceanic crust seen in our wide-angle/refraction and MCS data may reflect a common cause.

Relative plate convergence between the Indo-Australian and Eurasian plates is parallel to the general trend of the strike of the extinct fracture zones (Subarya et al., 2006; Simons et al., 2007). Assuming a constant plate motion vector for the past 5 million years (Hall, 2002; Delescluse and Chamot-Rooke, 2007) the location of the collision between an N–S oriented fracture zone and the convergent margin has remained stationary. This coincidence between the relative plate vector and the strike of the extinct fracture zones results in the deformation of the upper plate during subduction of the fracture zone ridge remaining stationary also. It is surmised that such deformation over an extended time period would produce a significant structural change in the over-riding plate, such as a major tectonic boundary. There appears to be no large-scale evidence of this structural change on Simeulue Island, nor on the accretionary prism. However, offshore of Simeulue Island, to the southwest, there are several submarine canyons. These canyons are aligned with tectonic lineaments striking N–S (Fig. 6 — bottom; Ladage et al., 2006). They may be an expression of local tectonic deformation due to the deformation identified on our seismic data and on Simeulue. Their presence may reflect a pervasive structural control by the oceanic plate on upper plate deformation. Therefore, we propose that off Simeulue the structural relief of a subducting extinct fracture zone entering the accretionary wedge at about 2°N contributes to or is a major control on segmentation of the forearc. DeShon et al. (2005) suggest that the southern boundary of the Andaman microplate is located in the vicinity of Simeulue Island. Although the evidence is equivocal, it may also be that this boundary was initiated by subduction of the fracture zone.

However, the evidence suggests that NNE–SSW oriented fracture zones on the oceanic plate are influencing deformation on the over-riding plate, imparting structures that are oriented in the same direction. Previously, the orientation of the segment boundary was inferred to be orthogonal to the plate boundary (Newcomb and McCann, 1987; Ammon et al., 2005; Bilham, 2005). In this regard the aftershock distribution is ambiguous but, however, in terms of orientation of the segment boundary, does not discount an alternative trend of NNE–SSW (Fig. 6).

5.4. Simeulue segment boundary

Fracture zones and other structural discontinuities on the downgoing plate are first-order candidates for the initiation of segmentation and earthquake rupture termination between the 2004 and 2005 earthquakes (e.g. Subarya et al., 2006). Our data lends support to this interpretation. The shallow slab we identify is 60 km wide and elevated for about 1 km towards the NW and for some 3 km towards the SE. As an extinct fracture zone, it is comparable in width and height, to the Investigator Ridge, another N–S trending fracture zone on the Indo-Australian Plate. Located further south, the Investigator Ridge, where it collides with the accretionary wedge at 89°E, 2.5°S, has a width of 30–50 km and an elevation of about 1 km. Perhaps significantly, the collision zone of this feature correlates with the boundary between the 1797 and 1833 great earthquakes (northern end) and the 1861 great earthquake (southern end)

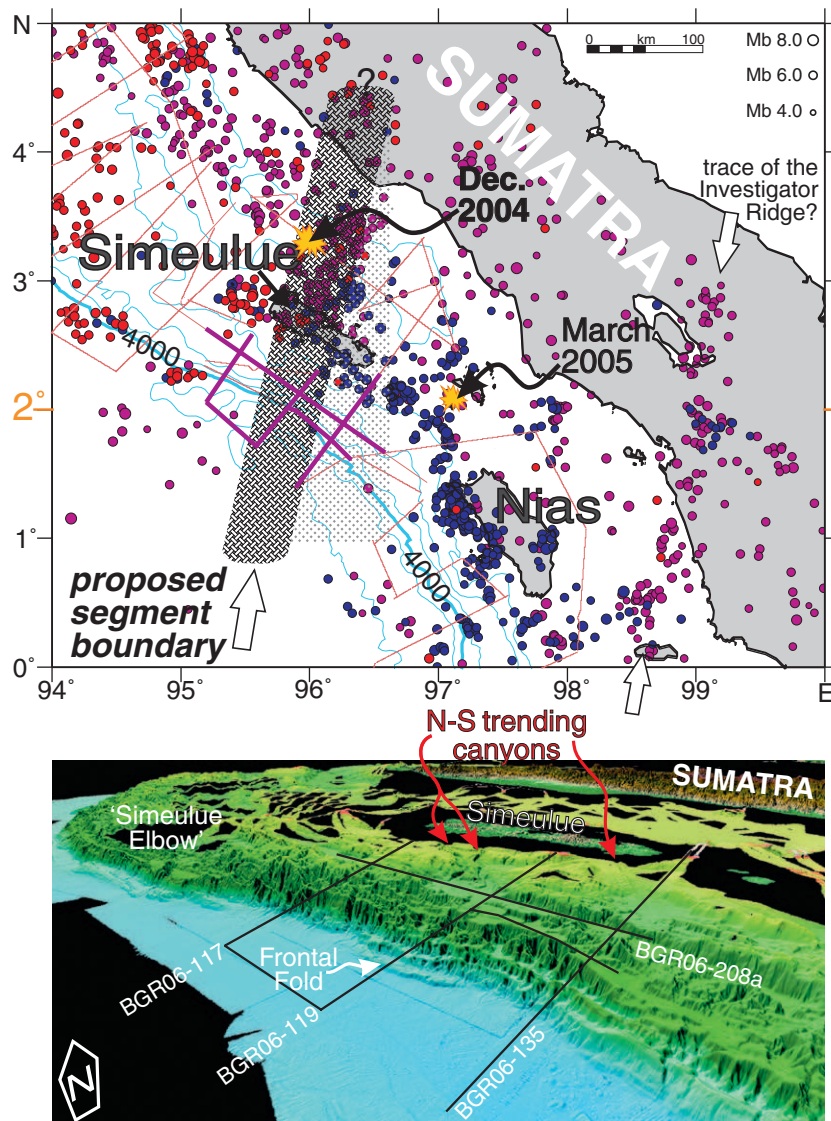


Fig. 6. NNE extent of the proposed segment boundary as revealed by the seismic data (upper panel) and enlarged bathymetric map of the broad re-entrant south of Simeulue Island (lower panel). Top: Seismicity before December, 26th 2004 is shown in purple, aftershocks of the 2004 mainshock in red, and aftershocks of the 2005 mainshock in blue (Engdahl et al., 2007). The distribution of the earthquakes is not in contradiction to the proposed trend of the segment boundary. The likely trace of the subducting Investigator Ridge indicated by an elongated cluster of epicentres is also marked. Purple lines mark the location of the reflection seismic lines shown in Figs. 3, 4 and 5. Bottom: Swath bathymetry shown with a vertical exaggeration of 2. Location of the seismic lines discussed in the text is indicated. The slope off Simeulue Island is cut by canyons striking N–S, probably linked to structures of the subducting plate, most likely a fracture zone.

offshore of southern Sumatra (Fauzi et al., 1996; Sieh and Natawidjaja, 2000; Rivera et al., 2002).

A particular feature of the Simeulue fracture zone that may contribute to its effect on margin segmentation is its size and asymmetry. The relief of the fracture zone is far greater than that of the other prominent fracture zones and ridges (including the Investigator Ridge) on the Indo-Australian plate. The eastern flank of the ridge off Simeulue is at 3 km high much higher than the western flank. This height is twice that of the Investigator Ridge.

This relief across a fracture zone could be a function of the juxtaposition of crust of significantly different ages. The general age of the oceanic crust, however, is Eocene and, assuming

symmetrical spreading, there is an age difference of ~ 2 Ma (Cande et al., 1989). The resulting seafloor depth difference will, therefore, be only of the order of 100–200 m, a difference that cannot account for the overall relief observed across the fracture zone.

Alternatively a fault or tear at the eastern flank of the proposed fracture zone could explain the depth difference of 3 km we observe. Modelling the wide-angle seismic data reveals that the top of the subducting oceanic crust gradually increases in depth (Fig. 3 — top). However, the spatial resolution is limited due to the layout of the wide-angle seismic experiment and the modelling algorithm used. An abrupt depth change like a steep ramp or tear would also be resolved as smooth transition with this acquisition configuration.

The interpretation of this feature as a fault or tear is supported by the MCS data. These show weak and discontinuous reflections on both margin-parallel lines BGR06-208a and BGR06-122 east of the topographic high of the proposed fracture zone (Figs. 3 and 5). This reflection character would not be expected if it were merely a gradual change in slab depth. Rather, it favours a faulted and dissected eastern flank of the Simeulue fracture zone.

The N–S to NNE–SSW striking fracture zones on the Indo-Australian plate between the Ninetyeast ridge and Sumatra are activated and reactivated as left-lateral strike-slip faults (Deplus et al., 1998). Close to the trench these are additionally reactivated as normal faults caused by flexural bending of the oceanic plate as it descends into the subduction zone (Schauer et al., 2006; Graindorge et al., 2007). The fracture zone off of Simeulue we consider to be similarly reactivated and dip-slip movements along the eastern flank have resulted in the observed step in the oceanic slab. Faulting along the eastern edge of this fracture zone possibly penetrates the entire oceanic slab. The result could be a tear in the subducting plate as slab dip increases beneath the accretionary prism. This may be an answer, as to why the Simeulue fracture zone is such a prominent barrier to rupture propagation.

6. Conclusions

Interpretation of a suite of marine geophysical data including wide-angle seismic and multichannel reflection seismic reveals a ridge on the subducting oceanic crust, entering the accretionary wedge off Sumatra located at 95.6°E, 2°N. The western flank of the ridge is about 1 km high whereas the eastern flank is up to 3 km. Trench sediments up to 5 km in thickness mask the topographic relief of the oceanic crust so that the ridge is not visible on the bathymetric data. The ridge is about 60 km wide and strikes in NNE–SSW direction. It extends beneath the accretionary wedge and likely also beneath Simeulue Island.

The projection of the ridge beneath the accretionary wedge and further under the forearc basins plots onto the common segment boundary of the 2004 and 2005 mainshocks. This relationship implies a structural control of the downgoing ridge on the segment boundary between the huge ruptures of the December 2004 and the March 2005 earthquakes. The trend of the ridge is parallel to fracture zones on the Indo-Australian plate and we consider such a fracture zone, buried by thick sediments as likely origin of the ridge.

The ridge on the oceanic crust contributes to or is a major control on the initiation of the segment boundary. The step in the slab across the eastern flank of the proposed ridge/fracture zone could be the result of either a gradual, oblique ramp or a shallow slab tear. However, the gradual depth change of 3 km as derived by wide-angle/refraction seismic data coincides with a significant change in the reflectivity of the oceanic crust reflection in the multichannel seismic data. We consider that this may reflect a dissected and faulted subducting oceanic crust. Dip-slip movements along the eastern flank of the subducting fracture zone beneath Simeulue may be considered as intensification factor in terms of rupture propagation barrier.

Acknowledgements

We are indebted to the Government of Indonesia (BPPT) as Indonesian partner providing the permission for the investigations in its territorial water. We thank ship's masters and their crew for operating RV Sonne. We are grateful to Petrologic Geophysical Service GmbH, Hannover, Germany for providing support in performing the prestack-depth migration. The SASS multibeam data was acquired by HMS SCOTT, a UK Royal Navy Survey Vessel during Marine Scientific Research coordinated by the Joint Environment Directorate of Defence Intelligence, and the data was processed by the United Kingdom Hydrographic Office. David Tappin publishes with the permission of the Executive Director of the British Geological Survey. We thank Robert Engdahl for providing hypocentre data. Helpful comments by two anonymous reviewers are kindly acknowledged. The German Ministry for Research and Education (BMBF) supported the study (grants 03G0186A and 03G0189A). This is publication no. 2 of the SeaCause project.

Appendix A. Supplementary data

Supplementary data associated with this article can be found, in the online version, at doi:10.1016/j.epsl.2008.01.047.

References

- Aki, K., 1979. Characterization of barriers on an earthquake fault. *J. Geophys. Res.* 84, 6140–6148.
- Ammon, C.J., 2006. Megathrust investigations (News and Views). *Nature* 440 (7080), 31–32.
- Ammon, C.J., Ji, C., Thio, H.-K., Robinson, D., Ni, S., Hjorleifsdottir, V., Kanamori, H., Lay, T., Das, S., Helmberger, D., Ichinose, G., Polet, J., Wald, D., 2005. Rupture process of the 2004 Sumatra–Andaman earthquake. *Science* 308, 1133–1139.
- Ando, M., 1975. Source mechanisms and tectonic significance of historical earthquakes along the Nankai Trough, Japan. *Tectonophysics* 27, 119–140.
- Barckhausen, U., 2006. The segmentation of the subduction zone offshore Sumatra: relations between upper and lower plate. *EOS Trans. AGU* 87 (52) (Fall Meet. Suppl., Abstract U53A–0029).
- Baroux, E., Avouac, J.-P., Bellier, O., Sébrier, M., 1998. Slip-partitioning and forearc deformation at the Sunda-Trench, Indonesia. *Terra Nova* 10 (3), 139–144.
- Bilek, S.L., Schwartz, S.Y., DeShon, H.R., 2003. Control of seafloor roughness on earthquake rupture behaviour. *Geology* 31, 455–458.
- Bilham, R., 2005. A flying start, then a slow slip. *Science* 308, 1126–1127.
- Briggs, R.W., Sieh, K., Meltzner, A.J., Natawidjaja, D., Galetzka, J., Suwargadi, B., Hsu, Y.-J., Simons, M., Hananto, N., Suprihanto, I., Prayudi, D., Avouac, J.-P., Prawirodirdjo, L., Bock, Y., 2006. Deformation and slip along the Sunda megathrust in the great 2005 Nias–Simeulue earthquake. *Science* 311, 1897–1901.
- Cande, S.C., LaBrecque, J.L., Larson, R.L., Pitman, W.C., Golovchenko, X., Haxby, W.F., 1989. Magnetic Lineations of the World's Ocean Basins. LDGO Contribution 4367. AAPG, Tulsa, Oklahoma.
- Collot, J.-Y., Marcaillou, B., Sage, F., Michaud, F., Agudelo, W., Charvis, P., Graindorge, D., Gutscher, M.-A., Spence, G., 2004. Are rupture zone limits of great subduction earthquakes controlled by upper plate structures? Evidence from multichannel seismic reflection data acquired across the northern Ecuador–southwest Colombia margin. *J. Geophys. Res.* 109, B11103. doi:10.1029/2004JB003060.
- Cummins, P.R., Baba, T., Kodaira, S., Kaneda, Y., 2002. The 1946 Nankai earthquake and segmentation of the Nankai Trough. *Phys. Earth Planet. Inter.* 132, 75–87.

- Delescluse, M., Chamot-Rooke, N., 2007. Instantaneous deformation and kinematics of the India–Australia Plate. *Geophys. J. Int.* 168 (2), 818–842. doi:10.1111/j.1365-246X.2006.03181.x.
- DeShon, H.R., Engdahl, E.R., Thurber, C.H., Brudzinski, M., 2005. Constraining the boundary between the Sunda and Andaman subduction systems: evidence from the 2002 Mw 7.3 Northern Sumatra earthquake and aftershock relocations of the 2004 and 2005 great earthquakes. *Geophys. Res. Lett.* 32, L24307. doi:10.1029/2005 GL024188.
- Deplus, C., Diament, M., Hebert, H., Bertrand, G., Dominguez, S., Dubois, J., Malod, J., Patriat, P., Pontoise, B., Sibilla, J.-J., 1998. Direct evidence of active deformation in the eastern Indian oceanic plate. *Geology* 26, 131–134.
- Dewey, J.W., Benz, H., Choy, G., Earle, P., Presgrave, B., Sipkin, S., Tarr, A.C., Wald, D., 2007. Seismicity associated with the Sumatra–Andaman Islands earthquake of 26 December 2004. *Bull. Seismol. Soc. Am.* 97 (1A), 25–42.
- Engdahl, E.R., Villasenor, A., DeShon, H.R., Thurber, C., 2007. Teleseismic relocation and assessment of seismicity (1918–2005) in the region of the 2004 Mw 9 Sumatra–Andaman and 2005 M 8.7 Nias great earthquakes. *Bull. Seismol. Soc. Am.* 97, 43–61. doi:10.1785/0120050614.
- Fauzi, F., McCaffrey, R., Wark, R.D., Sunaryo, P.Y., Haryadi, P., 1996. Lateral variation in slab orientation beneath Toba Caldera, northern Sumatra. *Geophys. Res. Lett.* 23, 443–446.
- Gahalaut, V.K., Nagarajan, B., Catherine, J.K., Kumar, S., 2006. Constraints on 2004 Sumatra–Andaman earthquake rupture from GPS measurements in Andaman–Nicobar Islands. *EPSL* 242, 365–374.
- Graindorge, D., Klingelhoefer, F., Gutscher, M.-A., Sibuet, J.-C., McNeill, L., Henstock, T., Dean, S., Tappin, D., Dessa, J.-X., Singh, S., 2007. Lower plate control of upper plate deformation at the toe of the NW Sumatra convergent margin from swath bathymetry. *Geophys. Res. Abstr.* 9, 05979 SRef-ID: 1607-7962/gra/EGU2007-A-05979.
- Hall, R., 2002. Cenozoic geological and plate tectonic evolution of SE Asia and the SW Pacific: computer-based reconstructions, model and animations. *J. Asian Earth Sci.* 20 (4), 353–431.
- Henstock, T.J., McNeill, L.C., Tappin, D.R., 2006. Seafloor morphology of the Sumatran subduction zone: surface rupture during megathrust earthquakes? *Geology* 34, 485–488.
- Kamesh Raju, K.A., Murty, G.P.S., Amarnath, Dileep, Kumar, M.L.M., 2007. The west Andaman fault and its influence on the aftershock pattern of the recent megathrust earthquakes in the Andaman–Sumatra region. *Geophys. Res. Lett.* 34, L03305. doi:10.1029/2006GL028730.
- Kodaira, S., Takahashi, N., Nakanishi, A., Miura, S., Kaneda, Y., 2000. Subducted seamount imaged in the rupture zone of the 1946 Nankaido earthquake. *Science* 289, 104–106.
- Korenaga, J., Holbrook, W.S., Kent, G.M., Kelemen, P.B., Detrick, R.S., Larsen, H.-C., Hopper, J.R., Dahl-Jensen, T., 2000. Crustal structure of the southeast Greenland margin from joint refraction and reflection seismic tomography. *J. Geophys. Res.* 105, 21591–21614.
- Krüger, F., Ohrnberger, M., 2005. Tracking the rupture of the Mw=9.3 Sumatra earthquake over 1,150 km at teleseismic distance. *Lett. Nature*. doi:10.1038/nature03696.
- Ladage, S., Gaedicke, C., Barckhausen, U., Heyde, I., Weinrebe, W., Flueh, E.R., Krabbenhoft, A., Kopp, H., Fajar, S., Djajadihardja, Y., 2006. Bathymetric survey images structure off Sumatra. *EOS Trans. AGU* 87 (17), 165.
- Lay, T., Kanamori, H., Ammon, C.J., Nettles, M., Ward, S.N., Aster, R.C., Beck, S.L., Bilek, S.L., Brudzinski, M.R., Butler, R., DeShon, H.R., Ekström, G., Satake, K., Sipkin, S., 2005. The Great Sumatra–Andaman earthquake of 26 December 2004. *Science* 308, 1127–1133.
- McCarthy, A.J., Elders, C.F., 1997. Cenozoic deformation in Sumatra: oblique subduction and the development of the Sumatran Fault System. In: Fraser, A.J., Matthews, S.J., Murphy, R.W. (Eds.), *Petroleum Geology of Southeast Asia*. *Geol. Soc. Spec. Publ.*, vol. 126, pp. 355–363.
- Malod, J.A., Kemal, B.M., 1996. The Sumatra margin: oblique subduction and lateral displacement of the accretionary prism. In: Hall, R., Blundell, D. (Eds.), *Tectonic Evolution of Southeast Asia*. *Geol. Soc. Spec. Publ.*, vol. 106, pp. 19–28.
- Milsom, J., 2005. Seismology and neotectonics (Chapter 2). In: Barber, A.J., Crow, M.J., Milsom, J.S. (Eds.), *Sumatra*. *Geol. Soc. Mem.*, vol. 31, pp. 8–15.
- Mooney, W.D., Brocher, T.M., 1987. Coincident seismic reflection/refraction studies of the continental lithosphere: a global review (paper 6R0778). *Rev. Geophys. Space Phys.* 25, 723–742.
- Newcomb, K.R., McCann, W.R., 1987. Seismic history and seismotectonics of the Sunda arc. *J. Geophys. Res.* 92, 421–439.
- Rivera, L., Sieh, K., Helmberger, D., Natawidjaja, D., 2002. A comparative study of the Sumatran subduction-zone earthquakes of 1935 and 1984. *Bull. Seismol. Soc. Am.* 92, 1721–1736.
- Ryan, H.F., Scholl, D.W., 1993. Geologic implications of great interplate earthquakes along the Aleutian arc. *J. Geophys. Res.* 98, 22135–22146.
- Schauer, M., Ladage, S., Weinrebe, W., Berglar, K., Krabbenhoft, A., Flueh, E., Gaedicke, C., 2006. Morphotectonics of the Sumatra margin — analysis of new swath bathymetry. *EOS Trans. AGU* 87 (52) (Fall Meet. Suppl., Abstract U53A–0033).
- Schlüter, H.U., Gaedicke, C., Roeser, H.A., Schreckenberger, B., Meyer, H., Reichert, C., Djajadihardja, Y., Prexl, A., 2002. Tectonic features of the southern Sumatra–western Java fore-arc of Indonesia. *Tectonics* 21, 1047. doi:10.1029/2001TC901048.
- Sibuet, J.-C., Rangin, C., Le Pichon, X., Singh, S., Cattaneo, A., Graindorge, D., Klingelhoefer, F., Lin, J.-Y., Malod, J., Maury, T., Schneider, J.-L., Sultan, N., Umber, M., Yamaguchi, H., “Sumatra aftershocks” team, 2007. 26th December 2004 great Sumatra–Andaman earthquake: co-seismic and postseismic motions in northern Sumatra. *Earth Planet. Sci. Lett.* doi:10.1016/j.epsl.2007.09.005.
- Sieh, K., Natawidjaja, D., 2000. Neotectonics of the Sumatran fault, Indonesia. *J. Geophys. Res.* 105 (B12), 28295–28326.
- Simandjuntak, T.O., Barber, A.J., 1996. Contrasting tectonic styles in the Neogene orogenic belts of Indonesia. In: Hall, R., Blundell, D. (Eds.), *Tectonic Evolution of Southeast Asia*. *Geol. Soc. Spec. Publ.*, vol. 106, pp. 185–201.
- Simons, W.J.F., Socquet, A., Vigny, C., Ambrosius, B.A.C., Haji Abu, S., Promthong, Chaiwat, Subarya, C., Sarsito, D.A., Matheussen, S., Morgan, P., Spakman, W., 2007. A decade of GPS in Southeast Asia: resolving Sundaland motion and boundaries. *J. Geophys. Res.* 112, B06420. doi:10.1029/2005JB003868.
- Singh, S.C., et al., 2005. Sumatra earthquake research indicates why rupture propagated northward. *EOS Trans. AGU* 86 (48), 497.
- Smith, W.H.F., Sandwell, D.T., 1997. Global seafloor topography from satellite altimetry and ship depth soundings. *Science* 277, 1957–1962.
- Spence, W., 1977. The Aleutian arc: tectonic blocks, episodic subduction, strain diffusion, and magma generation. *J. Geophys. Res.* 82, 213–230.
- Subarya, C., Chlieh, M., Prawirodirdjo, L., Avouac, J.-P., Bock, Y., Sieh, K., Meltzner, A.J., Natawidjaja, D.H., McCaffrey, R., 2006. Plate-boundary deformation associated with the great Sumatra–Andaman earthquake. *Nature* 440, 46–51.
- Susilohadi, S., Gaedicke, C., Ehrhardt, A., 2005. Neogene structures and sedimentation history along the Sunda forearc basins off southwest Sumatra and southwest Java. *Mar. Geol.* 219, 133–154.
- Yáñez, G., Cembrano, J., 2004. Role of viscous plate coupling in the late Tertiary Andean tectonics. *J. Geophys. Res.* 109, B02407. doi:10.1029/2003JB002494.

Publikation

Kopp, H., Weinrebe, W., Ladage, S., Barckhausen, U., Klaeschen, D., Flueh, E.R., Gaedicke, C., Djajadihardja, Y., Grevemeyer, I., Krabbenhoeft, A., Papenberg, C., and Zillmer, M., 2008. Lower slope morphology of the Sumatra trench system: Basin Research, 20(4), p. 519–529 doi: 10.1111/j.1365-2117.2008.00381.x.

Lower slope morphology of the Sumatra trench system

H. Kopp,* W. Weinrebe,* S. Ladage,† U. Barckhausen,† D. Klaeschen,* E. R. Flueh,* C. Gaedicke,† Y. Djajadihardja,‡ I. Grevemeyer,* A. Krabbenhoft,* C. Papenberg* and M. Zillmer*¹

*IFM-GEOMAR Leibniz-Institute of Marine Sciences, Kiel, Germany

†BGR, Federal Institute for Geosciences and Natural Resources, Hannover, Germany

‡BPPT, Agency for the Assessment and Application of Technology, Jakarta, Indonesia

ABSTRACT

At convergent margins, the structure of the subducting oceanic plate is one of the key factors controlling the morphology of the upper plate. We use high-resolution seafloor mapping and multichannel seismic reflection data along the accretionary Sumatra trench system to investigate the morphotectonic response of the upper plate to the subduction of lower plate fabric. Upper plate segmentation is reflected in varying modes of mass transfer. The deformation front in the southern Enggano segment is characterized by neotectonic formation of a broad and shallow fold-and-thrust belt consistent with the resumption of frontal sediment accretion in the wake of oceanic relief subduction. Conversely, surface erosion increasingly shapes the morphology of the lower slope and accretionary prism towards the north where significant oceanic relief is subducted. Subduction of the Investigator Fracture Zone and the fossil Wharton spreading centre in the Siberut segment exemplifies this. Such features also correlate with an irregularly trending deformation front suggesting active frontal erosion of the upper plate. Lower plate fabric extensively modulates upper plate morphology and the large-scale morphotectonic segmentation of the Sumatra trench system is linked to the subduction of reactivated fracture zones and aseismic ridges of the Wharton Basin. In general, increasing intensity of mass-wasting processes, from south to north, correlates with the extent of oversteepening of the lower slope (lower slope angle of 3.8° in the south compared with 7.6° in the north), probably in response to alternating phases of frontal accretion and sediment underthrusting. Accretionary mechanics thus pose a second-order factor in shaping upper plate morphology near the trench.

INTRODUCTION

The eastern Indian Ocean is dominated by the Wharton Basin, which is limited to the west by the Ninetyeast Ridge, to the north and east by the Sunda trench along Sumatra and Java and by the Broken Ridge at ~30°S (Fig. 1, inset panel). Seafloor of the Wharton Basin was generated between 85 and 45 Ma at the Wharton Ridge that consists of east-west-trending segments of a fossil spreading axis (Liu *et al.*, 1983; Royer & Sandwell, 1989) (Fig. 1, inset panel). Bathymetric features are prominent in the Wharton Basin (Stein *et al.*, 1989) and trend in a N–S direction (black lines in Fig. 1) following fossil transform faults that are currently being reactivated as left-lateral strike-slip faults (Deplus *et al.*, 1998; Abercrombie *et al.*, 2003). Four N5°E-trending faults occur in the western Wharton Basin

between the Ninetyeast Ridge and the Investigator Fracture Zone and enter the Sunda Trench at ~93, 94, 96 and 97°E (Sandwell & Smith, 1997; Hébert, 1998) (Fig. 1). The morphologic expression of the 93 and 94°E fault zones is covered by Nicobar Fan sediment deposits in the northern extension of the Wharton Basin NW of Simeulue Island. The 96°E Fracture Zone shows considerable basement relief as evidenced in seismic data (Franke *et al.*, 2008). An additional fracture zone is visible in the bathymetry, crossing the Wharton Ridge and entering the trench at 97°E (Barckhausen & SeaCause Scientific Party, 2006) (Fig. 1). To the SE, the Investigator Fracture Zone at 98.25°E outcrops at the seafloor and comprises four individual ridges of parallel trend of up to 1900 m relief and ~120 km total width.

Fracture zone geometry has been documented from seismic and magnetic data. (Barckhausen & SeaCause Scientific Party, 2006; Franke *et al.*, 2008). Magnetic spreading anomalies, which trend E–W in the Wharton Basin, are offset left-laterally by the fracture zones (Cande *et al.*, 1989). Seafloor age contrast is greatest across the

Correspondence: Heidrun Kopp, IFM-GEOMAR Leibniz-Institute of Marine Sciences, Kiel, Germany. E-mail: hkopp@ifm-geomar.de

¹ Present address: Institut de Physique du Globe, Strasbourg, France.

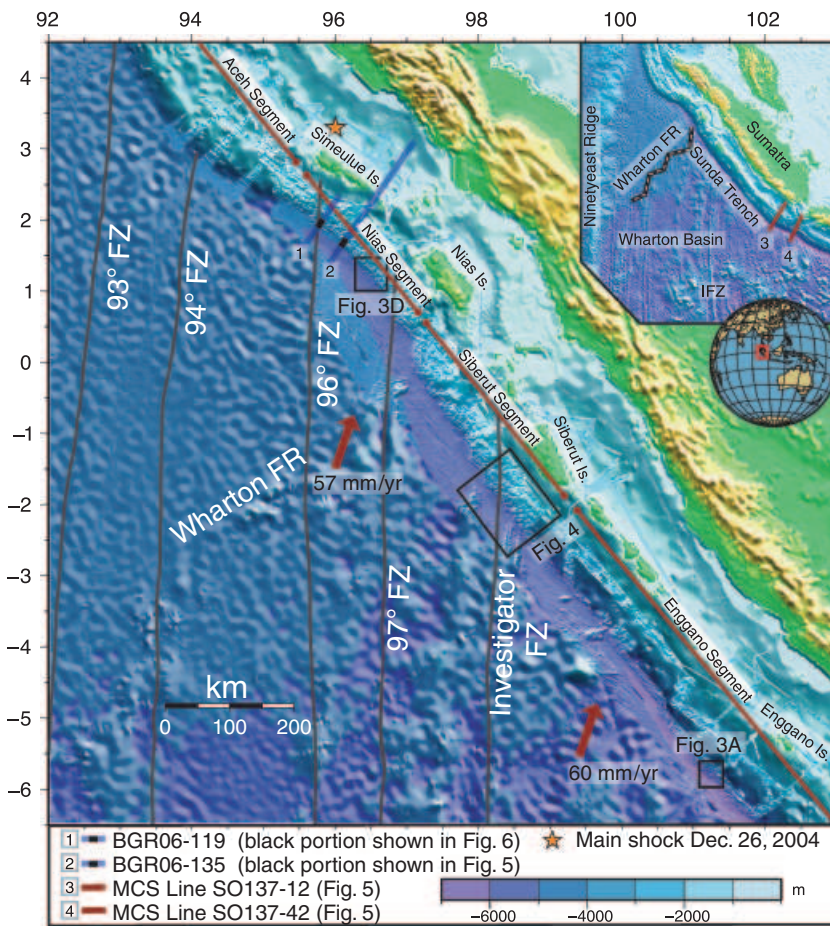


Fig. 1. Composite bathymetric map of the Sumatra trench system: The global satellite altimetry (Sandwell & Smith, 1997) is overlain by high-resolution swath mapping data. The bathymetry data were acquired using RV Sonne's 12 kHz Simrad EM120 echosounder system. The extent of the Enggano, Nias and Siberut segments discussed in the text is shown by red bars. Location of multichannel seismic lines presented in Figs 5 and 6 is indicated. Black boxes show location of data presented in Figs 3 and 4. Fracture zones are from Cande *et al.* (1989). IFZ, Investigator Fracture Zone; FR, fossil ridge; FZ, fracture zone.

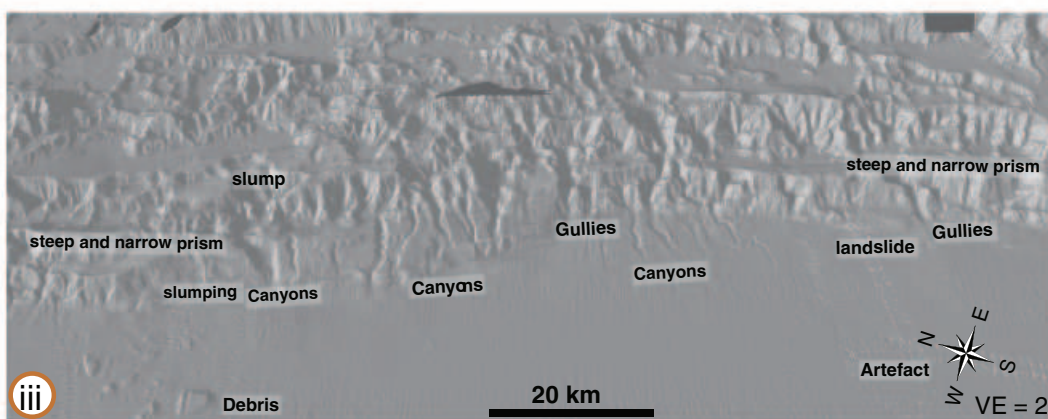
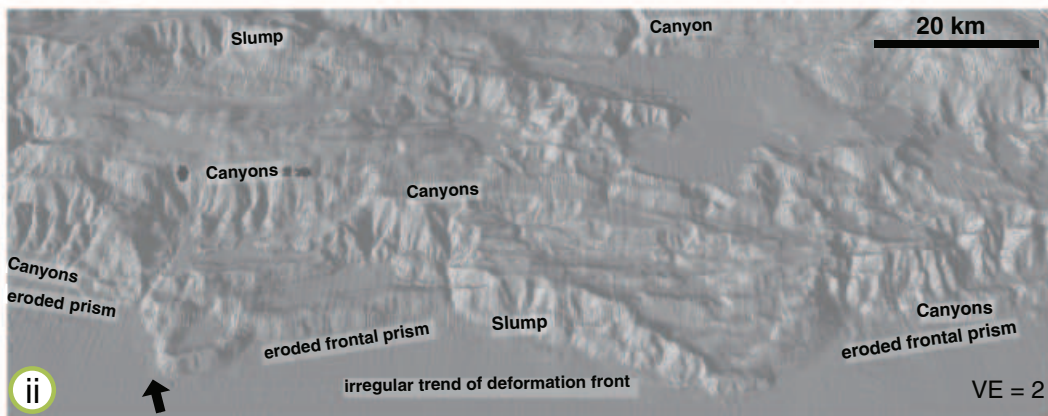
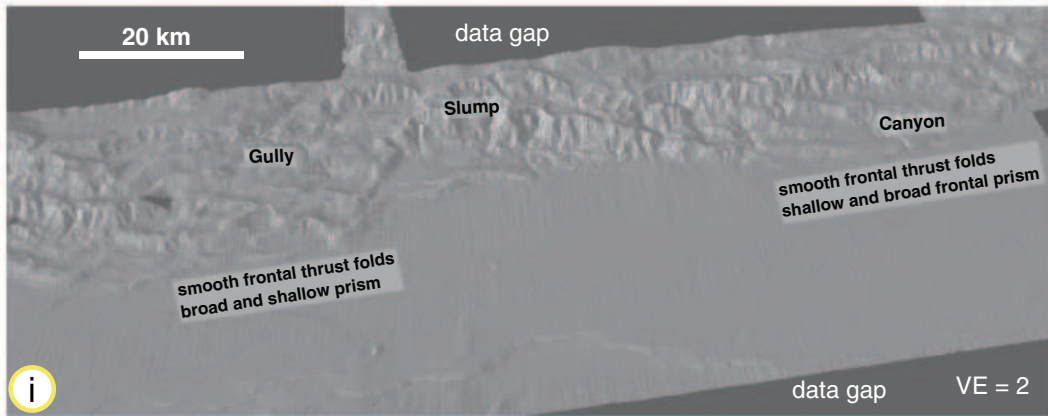
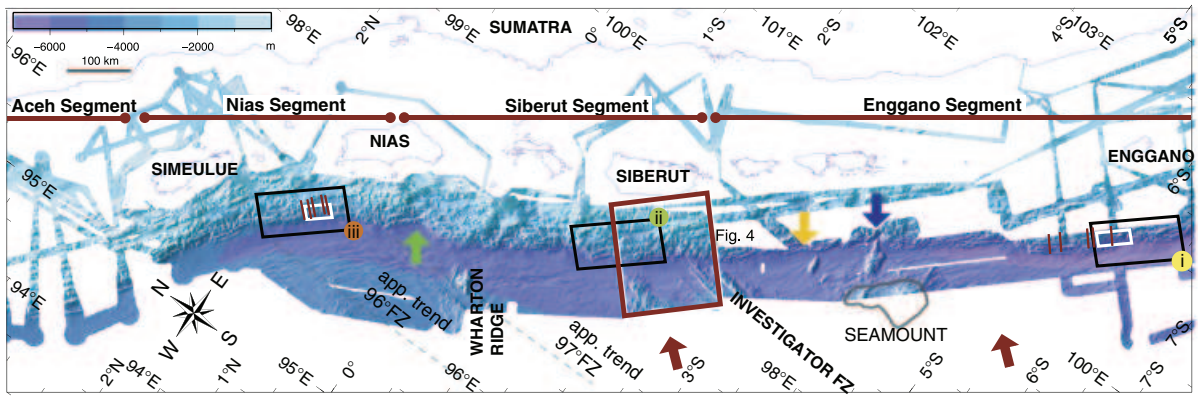
Investigator Fracture Zone, where the magnetic data to the east of the fracture zone correlates to anomalies of Chrons 31–29 (68–64 Ma) from south to north. To the west, anomalies 21–23 (47–52 Ma) are identified, resulting in age differences across the Investigator Fracture Zone of up to 15 m.y. (Gaedicke, 2006).

The scientific objective of this study is to investigate the effect of the incoming basement structure on the evolution of the upper plate. The lower slope, forming the outermost part of the upper plate, linearly responds to the subducting plate impact and thus poses the focus of our investigations. The lower slope of convergent margins defines a morphological province and covers the area of the upper plate immediately landward of the trench. In an accretionary setting such as the Sumatra margin, the lower slope of tentimes comprises imbricate thrust slices formed by

frontally accreted sediment and thus displays a more rugged topography compared with the landward portion of the prism (Kopp *et al.*, 2001). Oceanic plate fabric exerts a first-order control on the morphology of the lower slope of the accretionary prism.

The seafloor mapping described in Kopp & Flueh (2006) provides the bathymetric data used in this study. Seafloor mapping concentrated on the surface contact zone between upper and lower plates (i.e. the deformation front) south–west of the Sumatran forearc islands of Simeulue, Nias, Siberut and Enggano (Fig. 2) to geographically complement bathymetric mapping to the NW conducted by HMS Scott along the southern part of the rupture zone of the 26 December 2004 Banda Aceh earthquake (Henstock *et al.*, 2006). The high-resolution bathymetric mapping reveals a morphological segmentation of

Fig. 2. Swath survey covering the Sumatra trench and deformation front (top panel). Black boxes indicate location of data examples shown in panels (i)–(iii). A segmentation of the upper plate's lower slope is observed based on morphotectonic variations along the margin: in the southern Enggano Segment, nascent fold-and-thrust belts are the geomorphic expression of frontal sediment accretion (e.g. yellow arrow) (panel i). Conversely, the Siberut segment experiences re-working of the lower slope due to subduction of bathymetric features. Frontal erosion results in an irregular trend of the deformation front where landward offsets correspond to the entry of pronounced lower plate fabric into the trench (e.g. green arrow) (panel ii). In the northern Nias segment, extensive surface erosion of the steep and narrow active accretionary prism is manifested in slumps and ramified gully systems (panel iii). Upper plate material and debris is displaced to several kilometres onto the trench. White boxes indicate location of data shown in Fig. 3 (a, d). Short red lines show position of across slope tracks of Fig. 3 (c, f). Large red square displays location of data shown in Fig. 4. Blue arrow indicates entry point of a seamount in the Enggano segment. Red arrows indicate convergence.



the upper plate that correlates with incoming plate structure (Fig. 2). In addition, we show multi-channel seismic reflection data to unravel the internal structure of the lower slope. We discuss how material transfer by cyclical frontal and basal accretion and mass-wasting processes shape the lower slope morphology.

DATA

Bathymetric mapping

The bathymetry data were acquired from October 2005 to March 2006 using RV Sonne's Simrad echosounder system (Ladage *et al.*, 2006). The EM120 system is a multibeam echosounder providing accurate bathymetric mapping of areas at depths down to 11 000 m. This system is composed of two transducer arrays fixed to the ship's hull. It sends successive frequency-coded acoustic signals. Data acquisition is based on successive emission-reception cycles of this signal. The nominal sonar frequency is 12 kHz with an angular coverage sector of up to 150° and 191 beams per ping. The emission beam is 150° wide across track, and 2° along track direction. The reception is obtained from 191 beams, with widths of 2° across track and 20° along track. Thus the actual footprint of a single beam has a dimension of $2 \times 2^\circ$. Achievable swath width on a flat bottom will normally be up to six times the water depth dependent on the character of the seafloor. The angular coverage sector and beam pointing angles may be set to vary automatically with depth according to achievable coverage. This maximizes the number of usable beams. The beam spacing is normally equidistant with equiangle available.

For depth measurements, 191 isolated depth values are obtained perpendicular to the track for each ping. Using the two-way-travel-time and the beam angle known for each beam, and taking into account the ray bending due to refraction in the water column by sound speed variations, depth is calculated for each beam. A combination of amplitude (for the central beams) and phase (slant beams) is used to provide a measurement accuracy practically independent of the beam pointing angle.

Multibeam bathymetry data processing

Generally, processing of multibeam data requires two sequences of processing steps: a profile-oriented sequence followed by an area-based processing. The profile-oriented processing of the EM-120 data comprises the merging with navigation data to compute the geographic position, interpolating missing navigation values, the calculation of the water depth and position of the footprints of the beams by raytracing through the water-column taking into account the sound velocity profile, and removing artefacts and erroneous data points. Area-based processing comprises the calculation of a digital terrain model (DTM) and the visualization of the data in various different presentations. For these purposes several software packages were used [SIMRAD applications, the academic

software packages MB-System (Caress & Chayes, 1996) and GMT (Wessel & Smith, 1995)].

Seismic multichannel data

Multichannel seismic reflection data were collected during RV SONNE cruise SO-137 (lines SO137-12 and SO137-42) (Kopp *et al.*, 2001) and SO186 (line BGR06-135) (Franke *et al.*, 2008). Profile SO137-12 is located ~75 km SE of the island of Enggano offshore southern Sumatra (Profile 2 in inset panel of Fig. 1). Profile SO137-42 was shot further SE offshore the Sunda Strait (Profile 3 in inset panel of Fig. 1), trending in a SW-NE direction. Both lines were acquired on 120 channels using a 3500-m-long source-receiver offset. Seismic signals were generated by a tuned set of 20 airguns grouped in two identical linear sub-arrays. The total volume of the array is 51.2 L (3.124 cu. in.). A shot interval of 50 m and a hydrophone spacing of 25 m were chosen, resulting in a common depth point (CDP) distance of 12.5 m and a maximum fold of 30. Pre-processing included frequency filtering after an amplitude balancing and trace editing of the shot gathers. An enhanced signal resolution was achieved by a two-gated predictive deconvolution. An iterative migration procedure was applied, which uses seismic velocities constrained by focusing analyses and common reflection point gathers (Mackay & Abma, 1993) as well as velocity information gained from corresponding wide-angle data. The energy of a reflection point in the subsurface is focused using a range of velocities until an optimal image is achieved, which provides the highest energy at zero-offset. Using an ideal velocity, the reflection position will be corrected. This in turn will yield better constraints on velocities during the next iteration and ray paths are determined more accurately. Pre-stack depth migration thus images complex dipping structures even in the presence of a strong lateral velocity gradient far better than conventional post-stack migration.

Line BGR06-135 was acquired offshore northern Sumatra (Profile 1 in Fig. 1) SE of Simeulue Island. Data were recorded on 240 channels spaced 12.5 m apart at a shot-point interval of 50 m. The resulting CDP distance is 6.25 m with a nominal coverage of 30. A G-Gun airgun array of 16 airguns subdivided into two sub-array consisting of four two-gun clusters was used as seismic source [total volume of 50.8 L (3.100 cu. in.)]. Pre-processing as described above included a post-stack time migration for line BGR06-135.

LOWER SLOPE MORPHOLOGY AND SUBDUCTION OF OCEANIC PLATE RELIEF

The various bathymetric data sets acquired by RV Sonne yield a continuous seafloor swath map of the trench and deformation front from Simeulue Island off northern Sumatra to southern Sumatra at around 7°S, covering an

extent of more than 1300 km (Fig. 2). These new data reveal a highly segmented regional morphology of the lower slope. The morphology of the lower slope and how this interacts with oceanic relief being subducted is described in three segments (Enggano segment, Siberut segment and Nias segment in Fig. 2). We follow the nomenclature of Ladage *et al.* (2006) for the segment names, which are termed after nearby islands (Fig. 1). Taking the segments in turn from SE to NW a qualitative description is given and quantitative parameters are derived.

Enggano segment

Segment definition and limits

The Enggano segment off southern Sumatra extends for ~600 km from the Sunda Strait (7°S) to where the Investigator Fracture Zone is currently being subducted (~2.5°S). A broad and shallow frontal accretionary prism defines this segment (Fig. 2i), which displays a moderate surface gradient (Fig. 3b). It is characterized by the growth of a smooth fold-and-thrust-belt through active frontal accretion as evidenced in seismic data (Kopp *et al.*, 2001; Schlüter *et al.*, 2002). Evidence for large-scale frontal erosion or surface erosion, as discussed below for the Siberut and Nias segments, is scarce along the Enggano segment, where frontal accretion is the dominating process shaping the geomorphology of the upper plate.

Qualitative description of morphology

The active frontal accretionary prism shows a lateral extent of ~20 km as identified from depth-migrated multi-channel data in conjunction with velocity information obtained from refraction data (Kopp & Kukowski, 2003). Slope morphology is distinguished by the presence of young and relatively smooth frontal thrust folds (Figs 2 and 3a). Evidence for landslides or material transport paths such as canyon systems dissecting the lower slope are infrequent along this margin segment and key slope failure features such as slumps, rockslides and topples are scarce or absent (Fig. 2). Indications for major current erosional processes are only found where an isolated, irregularly shaped seamount of 25 km in diameter impinges on the margin at 99.6°E/3.8°S (blue arrow in Fig. 2, upper panel). It causes frontal erosion of the lower slope, locally scarring the margin toe. Away from the seamount collision zone though, trench material is frontally accreted and sub-parallel nascent thrust folds develop at the slope base with a singular fold length of 20–70 km (e.g. yellow arrows in Fig. 2, upper panel).

Quantitative morphology

The Enggano segment displays an overall smooth and coherent appearance with a mean surface slope α of 3.8° of the lower slope (Fig. 3c). This value is obtained by averaging the gradient perpendicular to the trench axis along five tracks over a distance of 15 km from the deformation

front (red bars in Fig. 2, upper panel). We re-sampled the bathymetry grid in steps of 0.004° and subsequently averaged the data along the five tracks. As our morphological investigations focus on the deformation front and lower slope, it would not be feasible to use a longer distance as this would result in an underestimate of surface slope α and an overestimate of plate dip β (Wang & Hu, 2006). This results from the fact that the plate dip β is not defined by a straight line, but shows a curved trend as the oceanic plate is thrust underneath the upper plate. Simultaneously, the surface slope will shallow due to compaction and lithification of the prism. Thus, the taper angle changes from the lower slope to the shallower portion of the forearc. For investigations limited to the lower slope portion of the prism, taking an average value across the entire forearc would bias both the surface slope angle α as well as the plate dip β .

Siberut segment

Segment definition and limits

Lower slope morphology changes abruptly where the ridges composing the Investigator Fracture Zone dissect the trench sediments at 98.25°E/2°S (Fig. 2, upper panel). This marks the southern limit of the Siberut segment, which is defined by frontal erosion of the lower slope due to subduction of oceanic plate relief. The geomorphology of the upper plate is profoundly modulated by the subducted bathymetric elevations (Fig. 4). The segment extends northward to the location of the Wharton fossil ridge re-entrant at 97°E/0.2°N. The smooth fold-and-thrust belt of the Enggano segment has been frontally eroded along the Siberut segment by the northward migration of the Investigator Fracture Zone as well as the Wharton Ridge, resulting in an irregular trend of the deformation front (Figs 2 and 4).

Qualitative description

The Investigator Fracture Zone affects the structure and morphology of the oceanic lithosphere in a zone of ~120 km width. In the trench and on the outer rise, the Investigator Fracture Zone outcrops along four individual parallel ridges (IFZ Ridge 1–4 in Fig. 4), ranging from ~1100 to 1900 m height above the trench. The four ridges show lateral widths of ~40 km (IFZ Ridge 1), 5 km (IFZ Ridge 2), 15 km (IFZ Ridge 3) and 10 km (IFZ Ridge 4) (Fig. 4) in the surveyed trench area and reach water depth of 4313, 4461, 3850 and 3777 m, respectively. Isolated seamounts are observed on top of the ridges and on their flanks (black arrows in Fig. 4) as well as in the more diffuse area of altered crust, which displays remnants of the original spreading fabric (white arrows in Fig. 4).

The lower slope has extensively been re-worked and the frontal accretionary prism partially eroded as the Wharton Ridge and the Investigator Fracture Zone migrated along the trench (Figs 2 and 4), resulting in kinks in the trend of the deformation front (stippled line in Fig. 4). Most

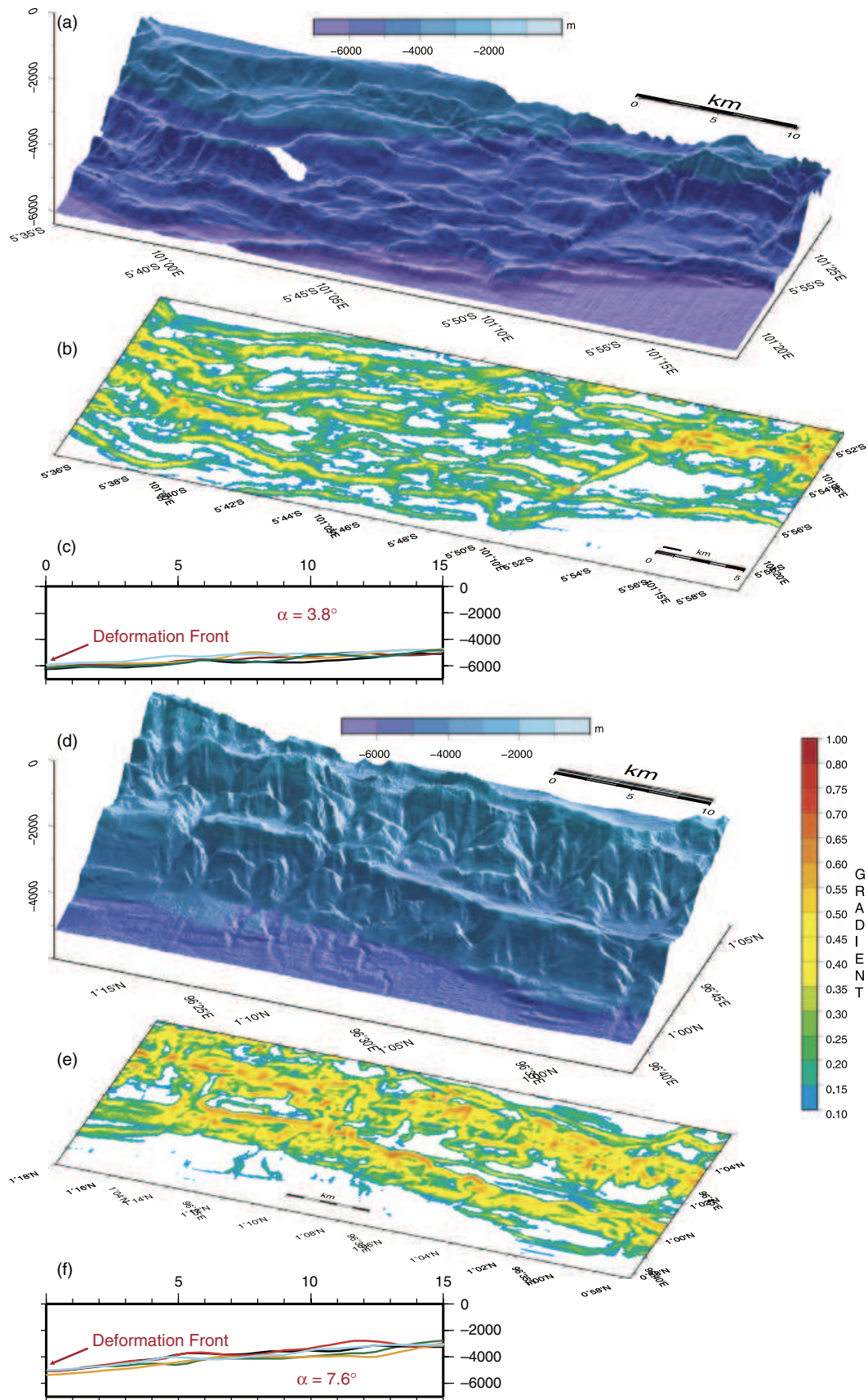


Fig. 3. High-resolution bathymetry in the Enggano (a) and Nias (d) segments (compare black boxes in Fig. 1 or white boxes in Fig. 2 for location) and corresponding projected gradients (b and e). The surface slope angle α is obtained by averaging the slope angle across five tracks perpendicular to the trench axis over a distance of 15 km from the deformation front (c and f, location shown by red lines in Fig. 2). The increased slope angle in the northern Nias segment (e) corresponds to an increase in surface slope gradient (f).

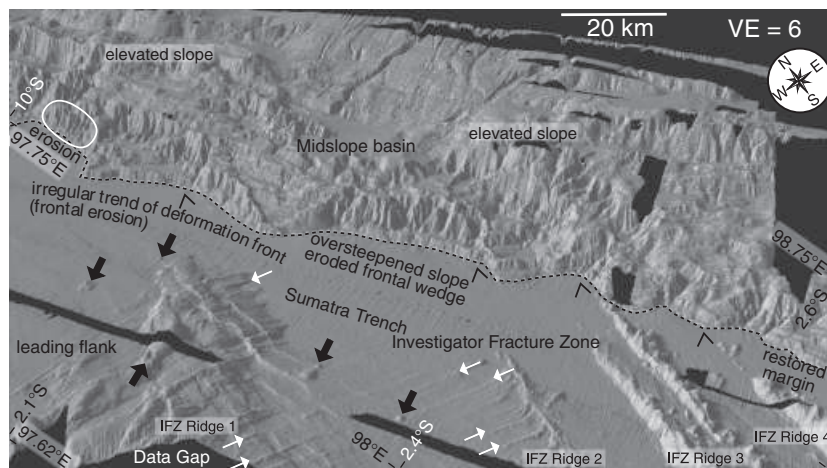


Fig. 4. Perspective view of the entry point of the Investigator Fracture Zone (IFZ) into the Sumatra trench. The IFZ consists of four individual ridges (IFZ Ridge 1–4) and migrates northwards along the Sumatra trench. The geomorphology of the upper plate is profoundly modulated by the subducted bathymetric elevations. To the south, margin healing after the passage of the IFZ is manifested in juvenile frontal thrust folds as frontal sediment accretion recommences. The margin segment currently affected by the subduction of the IFZ shows ubiquitous evidence of erosion. The frontal accretionary wedge has in parts completely been eroded, resulting in an irregular trend of the deformation front (stippled line) and local oversteepening of the lower slope (white ellipse). Alternating zones of uplift (local highs on an elevated slope) and subsidence are generated as the IFZ migrates along the margin. Thick black arrows show isolated volcanoes. White arrows indicate original spreading fabric. Open arrows point to kinks in the deformation front associated with the subduction of the individual ridges.

striking is the step-wise retreat of the deformation front in response to frontal erosion along this segment (black arrow in Fig. 2ii). Offsets of the deformation front and thus volumes of eroded material are closely associated with the entry of the individual ridges composing the Investigator Fracture Zone (open arrows in Fig. 4). The magnitude of the offsets primarily correlates to the geographical width of the ocean floor topography. The northernmost 40-km-wide ridge (IFZ Ridge 1) causes a 5 km retreat of the lower slope normal to the deformation front, whereas the 10-km-wide ridge (IFZ Ridge 4) results in a deformation front offset of only 2 km. The wider ridges cause a more pronounced landward retreat of the deformation front, irrespective of their height. A broad (~100 km width scale) landward retreat of the deformation front and forearc high, upon which the smaller-scale offsets or kinks related to the subduction of discrete ridges might be superimposed, is not observed. Trench sediment supply is thus sufficient to restore the lower slope and margin wedge after cessation of erosive processes after a ridge propagates northward, rebuilding the frontal fold-and-thrust belt as described above for the Enggano segment and as observed immediately south of IFZ Ridge 4 in Fig. 4.

Quantitative description

Kinematic considerations yield a current migration velocity for the Investigator Fracture Zone of 4.0–4.5 cm year⁻¹ along the margin. Owing to the variable angle of the segmented Wharton Ridge with the trench (Fig. 1, inset), the lateral migration velocity of the northward-migrating abandoned spreading centre is highly erratic. Segments perpendicular to the convergence vector migrate at a fast

rate (exceeding the convergence rate), whereas the offset segments which trend nearly parallel to the convergence vector have an almost stationary entry point to the trench (as observed in the bathymetry data) (compare also Hampel, 2002).

The current entry of the Wharton Ridge into the trench is marked by a 13-km-deep embayment where the lower slope has been eroded (green arrow in Fig. 2, upper panel). Several mid-slope basins are neighbouring local elevations along the slope (Fig. 4) and by analogy represent remnant tectonic imprints of oceanic relief subduction as observed along other margins and in sandbox modelling (Collot & Fisher, 1989; Dominguez *et al.*, 1998, Laursen *et al.*, 2002). Uplift of the margin wedge occurs over the leading flank of the subducting Wharton Ridge, whereas a mid-slope basin south of Nias at 0.5°N/97.5°E (landward of the embayment shown by the green arrow in Fig. 2, upper panel) originates from subsidence over the trailing flank (Hampel *et al.*, 2004). Equivalent structures are also witnessed offshore Siberut where the Investigator Fracture Zone impinges on the margin (Fig. 4). Only detailed analysis of seismic data would allow to evaluate if these basins are solely related to depocentres forming on top of the moving thrust sheets as observed e.g. along the Enggano segment (Fig. 5b) or if they are additionally enhanced by basal erosion.

Where incipient subduction of pronounced lower plate fabric has eroded the frontal wedge, the lower slope shows inclination angles in excess of 10° (e.g. white ellipse in Fig. 4). It is not feasible to average lower slope angles or gradients along this margin segment, as the lower slope has been intensely re-worked and extremely steep portions of the lower slope lie adjacent to shallower

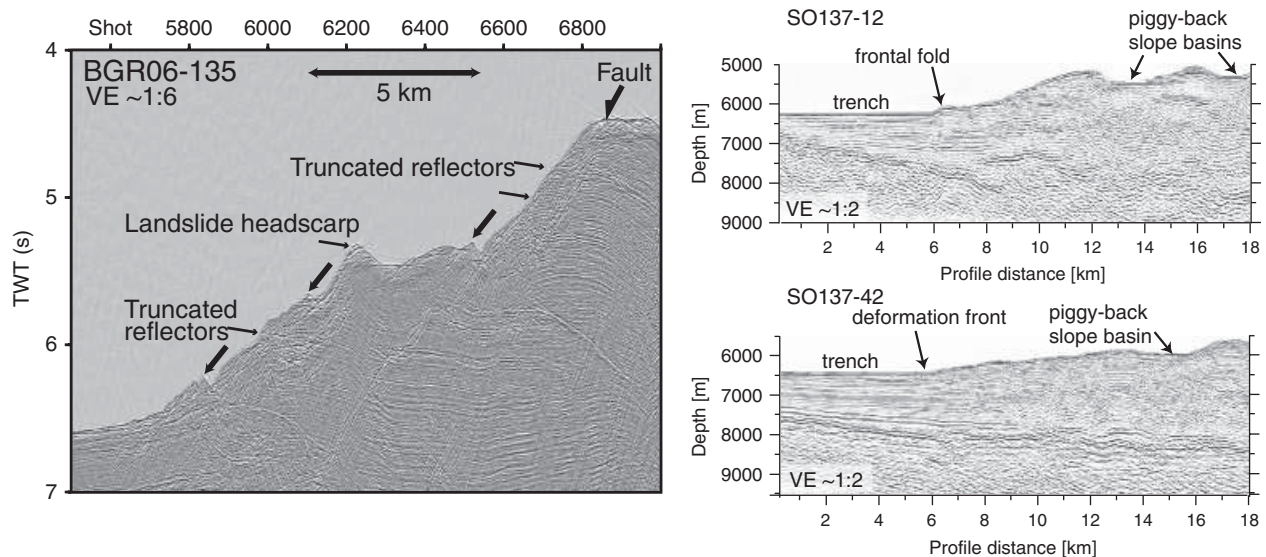


Fig. 5. Truncated reflectors in the time-migrated section of the lower slope on MCS Line BGR06-135 in the northern Nias segment (see Fig. 1 for location) indicate surface erosion and mass wasting processes resulting in slumps (thick black arrows). Jumbled and chaotic reflectors characterize the slump masses on top of the active folds, which are linked to landslide headscarps. Reflection profiles SO137-12 and SO137-42 (modified from Kopp & Kukowski, 2003) (see Fig. 1 inset for location) are located in the Enggano Segment offshore southern Sumatra and off the Sunda Strait, respectively, and are characterized by the evolution of relatively smooth frontal folds and a shallower lower slope compared with the Nias segment. Evidence for prominent surface erosion of the frontal folds is not recognized on these seismic lines. MCS data were acquired by the BGR, Hannover, Germany during SONNE cruises SO137 and SO186.

sections, resulting in erratic variations of the lower slope geometry (Fig. 4).

Nias segment

Segment definition and limits

Slope morphology changes again to the NW of the Wharton Ridge in the Nias segment (Figs 2 and 3). The Nias segment is defined by a narrow and steep frontal prism compared with the shallow and broad prism of the Enggano segment (Fig. 2i and iii). The deformation front shows a uniform trend, without the kinks and offsets resulting from frontal erosion as observed in the Siberut segment. The lower slope consists of steep thrust folds, which show extensive geomorphic evidence of surface erosion, corresponding to Morphology B of Henstock *et al.* (2006), which is characterized by widespread and complex erosion.

Qualitative description

Although the frontal accretionary prism along the Nias segment is still intact (Fig. 2), the morphology along this margin segment has a generally much rougher appearance than along the Enggano segment and shows a higher gradient of the lower slope compared with the southern area (Fig. 3c and f). Collapse structures such as slumps are ubiquitous along the lower slope. Ladage *et al.* (2006) conclude that the frontal folds along the Nias segment may be older or may not have been tectonically reactivated compared with the nascent frontal thrust folds in the Enggano segment. This is based on the observation of short tributaries to the trench, cross-cutting the frontal folds in the Nias

segment (Fig. 2iii). This pattern may only have developed during or after the folding events (Ladage *et al.*, 2006) and is not observed in the southern Enggano segment. The prism is narrower and steeper along the Nias segment compared with the adjacent segments (Ladage *et al.*, 2006). An extensive transverse pattern of downslope gullies and rills dissects the prism into the trench and supplies material to the trench by transverse mass wasting (Fig. 2iii). Transport of material in the canyons occurs over a distance of more than 10 km towards the ocean basin (Fig. 2iii). The seaward faces of frontal folds show slope failure in the form of slumping as described by Henstock *et al.* (2006) for the lower slope located north of Simeulue. Debris flows deposit material on the trench fill, including blocks of 100 m height, which are displaced to more than 15 km seaward of the deformation front (Fig. 2iii). Sediment transport paths are mainly short and restricted to the fold limbs and tributaries do not generally cross-cut the entire accretionary prism. Evidence for erosion also comes from seismic data. MCS profiles acquired in the Nias segment (Fig. 5a), the Enggano segment (Fig. 5b) and off the Sunda Strait (Fig. 5c) show striking dissimilarities, reflecting the distinct morphotectonic regimes. The time-migrated seismic reflection line of the Nias segment is characterized by truncated reflectors indicative of downslope mass wasting (Fig. 5a) as evidenced in slump masses, which have accumulated downslope from landslide headscarps.

Quantitative description

The lower slope shows an increased surface gradient along this segment compared with the southern Enggano

segment. The slope angle takes the value of $\alpha = 7.6^\circ$ (Fig. 3f) averaged over a distance of 15 km along five tracks perpendicular to the deformation front (red bars in Fig. 2, upper panel). This corresponds to slope values inferred from seismic data acquired off Nias (Line 7 of Moore & Curray, 1980). In the Nias segment, water depth decreases from 4950 m in the trench to 3375 m at 8 km from the deformation front along Line BGR06-135. Conversely, off southern Sumatra, MCS lines SOI37-12 and SOI37-42 (Kopp & Kukowski, 2003) show little evidence of down-slope material transport across the well-developed fold-and-thrust belt. The seafloor ascends by 1000 m over a distance of 8 km from the frontal fold along profile SOI37-12 and by only 700 m over the same distance on line SOI37-42.

DISCUSSION

Surface erosion offshore Simeulue and Nias (Fig. 2) correlates with the increase in frontal slope angle (Fig. 3) from the Enggano segment to the Nias segment. The steeper morphology of the Nias segment is reflected in the increased gradient (Fig. 3b and e) of the seafloor. On a regional scale, the seafloor gradient of the southern Enggano segment is only half of that in the northern Nias segment.

Changes in the surface slope angle at a convergent margin may be attributed to modifications in material strength caused by variations in physical properties such as porosity or fluid pressure (Lallemand *et al.*, 1994). Compression and dewatering are most prevalent in the frontal prism, where the trench material is initially deformed and fluid expulsion occurs along fluid pathways. (von Huene *et al.*, 1998). These processes may be invoked to explain commonly observed arcward changes in surface slope (Kopp & Kukowski, 2003; Fisher *et al.*, 2007) in the context of critical wedge mechanics (Davis *et al.*, 1983). However, lateral variations along trench strike as observed between the Enggano, Siberut and Nias segments are more difficult to explain by systematic changes in physical properties in a single margin.

Episodic wedge growth by frontal and basal accretion poses an alternative explanation for surface slope adjustments along trench strike. Cyclical accretion with alternating phases of frontal accretion and sediment underplating has been simulated in analogue experiments (Gutscher *et al.*, 1998). Episodic underthrusting of sediment sheets or duplexes underneath the frontal accretionary prism will cause a steepening of the frontal slope and thus facilitate surface erosion. During this phase, growth of the prism by sediment accretion occurs in the vertical dimension (i.e. uplift). Conversely, imbricate thrusting during frontal accretion will advance the frontal accretionary prism trenchwards, lowering the surface slope and reducing the overburden. Both mechanisms, frontal accretion and basal accretion, may occur at a single margin (e.g. Alaska) and result in a high variation of the surface slope angle of the lower slope. Whereas frontal accretion and the formation of imbricate thrust slices is the dominant process off south-

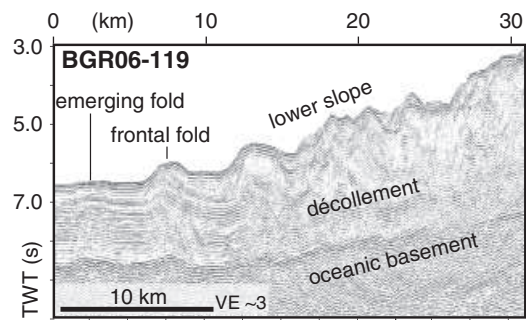


Fig. 6. MCS line BGR06-119 (modified from Franke *et al.*, 2008) shows a subduction channel sandwiched between the décollement and the oceanic basement. Approximately one-third of the trench sediment fill is currently underthrust beneath the lower slope and frontal prism. Cyclical phases of imbricate thrusting and sediment underthrusting strongly affect the lower slope surface gradient. Line BGR06-119 was processed at BGR, Hannover, Germany.

ern Sumatra as documented in MCS Lines SOI37-12 and SOI37-42 (Fig. 5), about one-third of the trench fill is currently subducted underneath the lower slope along MCS Line BGR06-119 (Franke *et al.*, 2008) (Fig. 6). A layered sheet of sediment sandwiched between the detachment and the oceanic basement is traced for at least 20 km beyond the frontal fold. This material is currently trapped in the subduction channel and transported beyond the deformation front. Underthrusting of sediment concurs with an increase in surface slope and a retreat of the deformation front as shown from sandbox modelling (Gutscher *et al.*, 1998). This process continues until the overburden of the steep frontal prism reaches a critical value, hindering further underthrusting. In addition, the coefficient of basal friction plays a crucial role with high basal friction resulting in steeper angles. Increased basal friction has been proposed by Fisher *et al.* (2007) to occur in the frontal prism offshore Banda Aceh (northern Sumatra). Thus underthrusting of sediment sheets in a high friction setting may explain the increased surface slope in the Nias segment compared with the Enggano segment, where the formation of imbricate thrust slices by frontal accretion and the observed low basal friction (Kopp & Kukowski, 2003) decrease the surface slope. The opening of the frontal taper leads to an oversteepening of the lower slope in the Nias and Siberut segments and thus facilitates surface erosion as witnessed in the bathymetric data. The variation in deformation mode and surface slope between the Enggano and Nias segments thus suggest a change in the accretionary mechanics from frontal accretion in the south (Kopp *et al.*, 2001) to underthrusting as the dominating process in the north. An important observation in this context is the along-strike change in sediment supply to the trench offshore Sumatra. The trench off Simeulue Island is found at a water depth of < 4900 m, whereas it reaches water depths of more than 6200 m to the SE in the Enggano segment. Axial material transport in the trench is manifested in channel systems of up to 280 km length, as

for example observed originating south of the Investigator Fracture Zone entry point. The Investigator Fracture Zone poses an effective barrier to the axial material transport in the trench, where the trench fill is declining from ~2500 m in the NW (Line BGR06-135 in Fig. 1) to 1300 m to the SE of Enggano Island (Kopp *et al.*, 2001; Kopp & Kukowski 2003). As the sediment supply exceeds the subduction channel capacity along the entire length of the Sumatra trench, it remains unresolved if and to what degree the variation in sediment supply influences the mechanical mode of accretion.

Accelerated frontal erosion in the central Siberut segment results from the subduction of the pronounced oceanic basement relief of the Wharton Ridge and Investigator Fracture Zone. This segment encompasses the most deformed and in parts largely eroded frontal prism along the Sumatra margin and local slope angles are approaching or are in excess of the angle of repose. Restoration of the margin toe in the southern Enggano segment after the passage of the Investigator Fracture Zone occurs by frontal sediment accretion. Imbricate thrusting at the deformation front lowers the oversteepened surface slope and favours the seaward growth of a fold-and-thrust-belt as imaged in the bathymetric and seismic data.

ACKNOWLEDGEMENTS

We would like to thank our Indonesian partners, namely the BPPT (Agency for the Assessment and Application of Technology), Jakarta for their continuous assistance. The SeaCause and GITEWS projects, on which this study is based, are supported by the German Ministry of Education and Science BMBF, grants 03G0186 and 03TSU01. The offshore data were acquired by the RV SONNE. The support of the vessel's captains and their crews is warmly acknowledged. We would furthermore like to thank all participants of the related cruises for their professional help at sea. MCS data were acquired by the BGR, Hannover, Germany. Line BGR06-119 was processed at BGR, Hannover, Germany. We wish to thank editors J. K. Hillier and F. Tilmann and reviewer L. McNeill for their constructive and critical reviews, which have greatly improved an earlier version of the manuscript.

REFERENCES

- ABERCROMBIE, R.E., ANTOLIK, M. & EKSTRÖM, G. (2003) The June 2000 Mw 7.9 earthquakes south of Sumatra: deformation in the India–Australia plate. *J. Geophys. Res.*, **108**(B1), 2018, doi: 10.1029/2001JB000674.
- BARCKHAUSEN, U. & SEACAUSE SCIENTIFIC PARTY (2006) The segmentation of the subduction zone offshore Sumatra: relations between upper and lower plate, *EOS Trans. AGU*, **87**(52), Fall Meet. Suppl., Abstract U53A-0029.
- CANDE, S.C., LABRECQUE, J.L., LARSON, R.L., PITMAN, W.C., GOLOVCHENKO, X. & HAXBY, W.F. (1989) Magnetic lineations of World's Ocean Basins. *Amer. Ass. Petrol. Geol.*, Tulsa.
- CARESS, D.W. & CHAYES, D.N. (1996) Improved processing of Hydrosweep DS multibeam data on the R/V Maurice Ewing. *Mar. Geophys. Res.*, **18**, 631–650.
- COLLOT, J.-Y. & FISHER, M.A. (1989) Formation of forearc basins by collision between seamounts and accretionary wedges: an example from the New Hebrides subduction zone. *Geology*, **17**, 930–933.
- DAVIS, D., SUPPE, J. & DAHLEN, F.A. (1983) Mechanics of fold-and-thrust belts and accretionary wedges: cohesive coulomb theory. *J. Geophys. Res.*, **88**, 1153–1172.
- DEPLUS, C., DIAMENT, M., HÉBERT, H., BERTRAND, G., DOMINGUEZ, S., DUBOIS, J., MALOD, J., PATRIAT, P., PONTOISE, B. & SIBILLA, J.-J. (1998) Direct evidence of active deformation in the eastern Indian oceanic plate. *Geology*, **26**, 131–134.
- DOMINGUEZ, S., LALLEMAND, S., MALAVIELLE, J. & SCHNUEERLE, P. (1998) Oblique subduction of the Gagua Ridge beneath the Ryukyu accretionary wedge system: insights from marine observations and sandbox experiments. *Mar. Geophys. Res.*, **20**, 383–402.
- FISHER, D., MOSHER, D., AUSTIN, J.A., GULICK, S., MASTERLARK, T. & MORAN, K. (2007) Active deformation across the Sumatran forearc over the December 2004 Mw 9.2 rupture. *Geology*, **35**(2), 99–102, doi: 10.1130/G22993A.1.
- FRANKE, D., SCHNABEL, M., LADAGE, S., TAPPIN, D.R., NEBEN, S., DJAJADIHARDJA, Y., MUELLER, C., KOPP, H. & GAEDICKE, C. (2008) The great Sumatra–Andaman earthquakes—imaging the boundary between the ruptures of the great 2004 and 2005 earthquakes. *Earth Planet. Sci. Lett.*, **269**, 1–2, doi: 10.1016/j.epsl.2008.01.047.
- GAEDICKE, C. (Ed). (2006) Cruise Report SO186 Leg 2 Seacause II, *BGR Report*, 0125999, 144pp.
- GUTSCHER, M.-A., KUKOWSKI, N., MALAVIELLE, J. & LALLEMAND, S. (1998) Episodic imbricate thrusting and underthrusting: analog experiments and mechanical analysis applied to the Alaskan Accretionary Wedge. *J. Geophys. Res.*, **103**, 10161–10176.
- HAMPEL, A. (2002) The migration history of the Nazca Ridge along the Peruvian active margin: a re-evaluation. *Earth Planet. Sci. Lett.*, **203**, 665–679.
- HAMPEL, A., ADAM, J. & KUKOWSKI, N. (2004) Response of the tectonically erosive south Peruvian forearc to subduction of the Nazca Ridge, Analysis of three-dimensional analogue experiments. *Tectonics*, **23**, TC5003, doi: 10.1029/2003TC001585.
- HÉBERT, H. (1998) Etudes géophysiques d'une dorsale naissante (dorsale d'Aden à l'Ouest de 46°E) et d'une dorsale fossile (dorsale de Wharton): implications sur les processus de l'accrétion océanique, et la déformation intraplaque de l'Océan Indien, PhD Thesis, University of Paris, 372pp.
- HENSTOCK, T.J., MCNEILL, L.C. & TAPPIN, D.R. (2006) Seafloor morphology of the Sumatran subduction zone: surface rupture during megathrust earthquakes? *Geology*, **34**, 485–488.
- KOPP, H. & FLUEH, E.R. (Eds). (2006) Cruise Report SO186 Leg 3 Seacause II, *IFM-GEOMAR Rep.*, **6**, 205pp.
- KOPP, H., FLUEH, E.R., KLAESCHEN, D., BIALAS, J. & REICHERT, C. (2001) Crustal structure of the central Sunda margin at the onset of oblique subduction. *Geophys. J. Int.*, **147**, 449–474.
- KOPP, H. & KUKOWSKI, N. (2003) Backstop geometry and accretionary mechanics of the Sunda margin. *Tectonics*, **22**(6), 1072, doi: 10.1029/2002TC001420.
- LADAGE, S., WEINREBE, W., GAEDICKE, C., BARCKHAUSEN, U., FLUEH, E.R., HEYDE, I., KRABENHOEFT, A., KOPP, H., FAJAR, S. & DJAJADIHARDJA, Y. (2006) Bathymetric survey images structure off Sumatra. *EOS*, **87**(17), 165–172.

- LALLEMAND, S., SCHNÜRLE, P. & MALLAVIELLE, J. (1994) Coulomb theory applied to accretionary and nonaccretionary wedges: possible causes for tectonic erosion and/or frontal accretion. *J. Geophys. Res.*, **99**, 12033–12055.
- LAURSEN, J., SCHOLL, D.W. & VON HUENE, R. (2002) Neotectonic deformation of the central Chile margin: deepwater forearc basin formation in response to hot spot and seamount subduction. *Tectonics*, **21**(5), 1038, doi: 10.1029/2001TC901023.
- LIU, C., CURRAY, J.R. & McDONALD, J.M. (1983) New constraints on the tectonic evolution of the eastern Indian Ocean. *Earth Planet. Sci. Lett.*, **65**, 331–342.
- MACKAY, S. & ABMA, R. (1993) Depth focusing analysis using wavefront-curvature criterion. *Geophysics*, **58**, 1148–1156.
- MOORE, G.F. & CURRAY, J. (1980) Structure of the Sunda trench lower slope off Sumatra from multichannel seismic reflection data. *Mar. Geophys. Res.*, **4**, 319–340.
- ROYER, J.Y. & SANDWELL, D.T. (1989) Evolution of the eastern Indian ocean since late cretaceous: constraints from Geosat altimetry. *J. Geophys. Res.*, **94**, 13755–13782.
- SANDWELL, D.T. & SMITH, W.H.F. (1997) Marine gravity anomaly from Geosat and ERS-1 altimetry. *J. Geophys. Res.*, **102**(B1), 10039–10054.
- SCHLÜTER, H.U., GAEDICKE, C., ROESER, H.A., SCHRECKENBERGER, B., MEYER, H., REICHERT, C., DJAJADIHARDJA, Y. & PREXL, A. (2002) Tectonic features of the southern Sumatra-western Java forearc of Indonesia. *Tectonics*, **21**(5), 1047, doi: 10.1029/2001TC901048.
- STEIN, C.A., CLOETHINGH, S. & WORTEL, R. (1989) Seasat-derived gravity constraints on stress and deformation in the northeastern Indian Ocean. *Geophys. Res. Lett.*, **16**, 823–826.
- VON HUENE, R., KLAESCHEN, D., GUTSCHER, M.-A. & FRUEHN, J. (1998) Mass and fluid flux during accretion at the Alaska margin. *Geol. Soc. Am. Bull.*, **110**(4), 468–482.
- WANG, K. & HU, Y. (2006) Accretionary prisms in subduction earthquake cycles: the theory of dynamic Coulomb wedge. *J. Geophys. Res.*, **111**, B06410, doi: 10.1029/2005JB004094.
- WESSEL, P. & SMITH, W.H.F. (1995) New Version of the Generic Mapping Tools Released, EOS Trans. AGU, **76**, 329.

Manuscript received 29 January 2008; Manuscript accepted 25 July 2008

Publikation

Ladage, S., Weinrebe, W., Gaedicke, C., Barckhausen, U., Flueh, E.R., Heyde, I., Krabbenhoeft, A., Kopp, H., Fajar, S., and Djajadihardja, Y., 2006. Bathymetric Survey Images Structure off Sumatra: *Eos, Transactions American Geophysical Union*, 87(17), p. 165–172 doi: 10.1029/2006EO170001.

Bathymetric Survey Images Structure off Sumatra

PAGES 165, 168

Fault rupture models and aftershock activities of both the 26 December 2004 M_w 9.3 and the 28 March 2005 M_w 8.7 earthquakes postulate a strong structural segmentation of the Sumatra fore arc, or the region between a subduction trench and the volcanic arc. The 2004 earthquake rupture propagated some 1200–1400 kilometers to the northwest from the epicenter along the plate boundary. Yet the rupture ended abruptly at a southern boundary crosscutting the upper plate from the trench to the island of Simeulue. Similarly, the rupture plane and aftershock distribution of the 2005 earthquake are confined to a zone some 300–400 kilometers around the epicenter off Nias Island, clearly distinguishable from the northern rupture zone.

To investigate this along strike structural segmentation, offshore of the northwestern Sumatran islands of Simeulue, Nias, and Siberut new bathymetric swath mapping has been conducted that covers the main structural units from the deep-sea trench to the outer arc high of the Sumatra subduction zone (Figure 1). The first bathymetric images, seen here, reveal a multitude of morphological features depicting the structural setting of the fore arc.

This bathymetric survey is the first part of two multidisciplinary geophysical-geological projects named 'SeaCause' and 'Sumatra.' During this survey, 20 ocean-bottom seismometers and hydrophones were deployed around Simeulue Island. These stations recorded the ongoing aftershock activity until March 2006. This network of ocean-bottom seismometers and hydrophones will allow precise determination of the aftershock epicenters and deliver valuable information to delineate the segment boundary in the area.

The target of this experiment is to identify the subduction interface and its along-strike variations, especially concerning the development of a detachment, giving clues about the degree of coupling of the upper and lower plates. Concurrent with all seismic profiling,

gravimetric and magnetic surveys are performed, as well as swath mapping and high-resolution subbottom profiling. The investigations will be completed with rock and sediment sampling of the fore arc and trench in August–September 2006. The projects are conducted in close international collaboration with scientists from France, Germany, Indonesia, Japan, Russia, the United Kingdom,

and the United States. The geoscientific data and results will be utilized for implementation of the German Indian Ocean Tsunami Early Warning System (GITEWS).

First Results of Bathymetric Mapping

The first images of the bathymetry acquired to date cover the area offshore the islands of Simeulue, Nias, and Siberut, as well as a vast part of the deep-sea trench along Sumatra (Figure 1). The frontal slope of the upper continental plate can reach a 15° inclination angle, and frontal collapse structures and underwater landslides are prevalent.

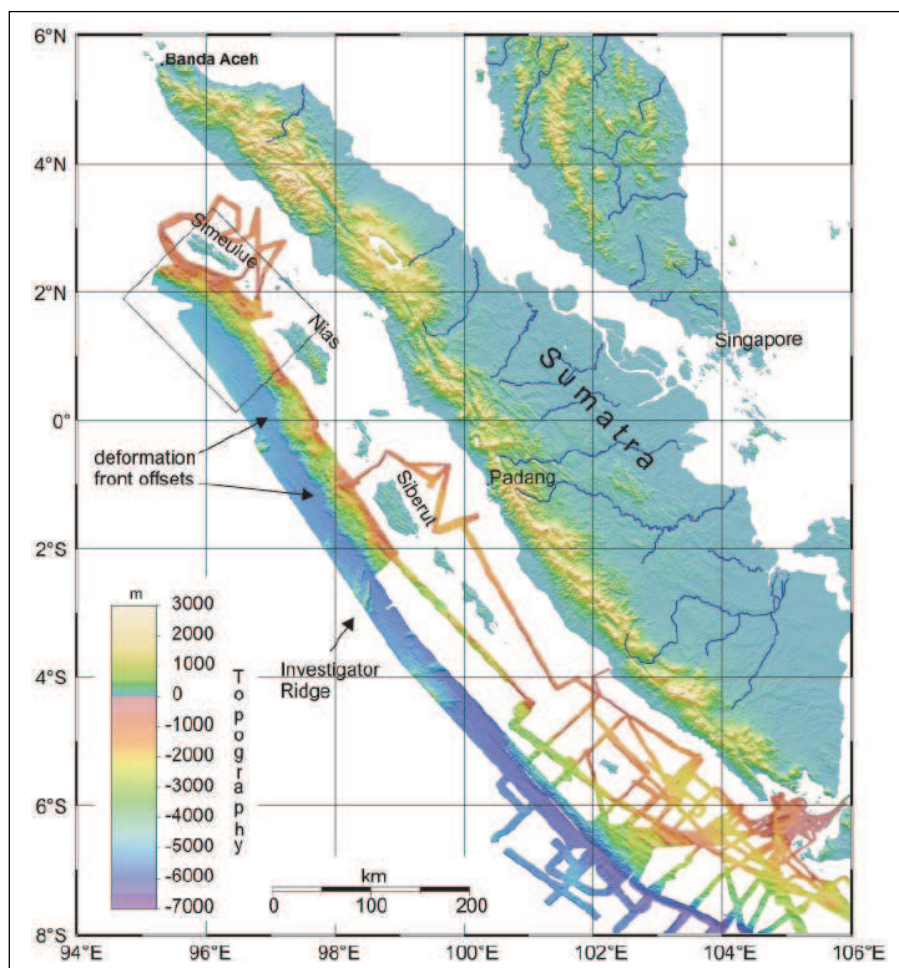


Fig. 1. Compilation of bathymetric data offshore Sumatra. Data are from SeaCause I cruise SO186 carried out with the German R/V Sonne in October 2005 as well as from former cruises (SO184, SO137-139). Topography is from digital elevation data of the Shuttle Radar Topography Mission SRTM30 data set. The black box indicates the three-dimensional view shown in Figure 2.

Despite this, morphologically most striking is a prominent 15-kilometer oblique offset of the base of the slope and deformation front offshore Nias. Preliminary interpretation indicates that this feature delineates one of two first-order segment boundaries of the upper plate, which may act as a boundary during earthquake propagation and aftershock distribution. Supporting evidence is that the axis of the outer arc high (i.e., the fore-arc island chain axis) also experiences an eastward shift in this region, indicating that segmentation may affect the whole outer fore arc and not merely the lower slope units. This segment is termed the Nias segment, and accordingly the adjoining northern one is termed the Aceh-Simeulue segment and the southern one the Siberut segment, because of their proximity to nearby islands.

The lower slope is built up of a few frontal folds at the deformation front. Piggyback basins, which evolve during folding and uplift between the folds, trap the gross part of sediments coming from upslope (Figure 2). Larger midslope basins appear offshore Simeulue and Siberut. These basins each are fed by two canyons up to 200 meters deep commencing from the islands. The overall picture of the lower slope and outer fore arc from the map view so far is that it is lacking a significant accretionary prism, an important observation in respect to the possible modes of subduction and coupling/decoupling along the subduction plate interface.

Furthermore, the slope exhibits secondary features, for instance, in the Siberut segment, where the lower slope units are obliquely crosscut by a set of north-south (N-S) trending offsets of the deformation front. This segment seems to be affected by the recent subduction of the Investigator Ridge on the oceanic plate, an extinct, also N-S trending fracture zone system built up of a set of four ridges up to 200 meters high. The Investigator Ridge can be traced through the trench fill, as it is only partly buried by trench sediments.

Continuing beneath the slope, the subducted ridge modulates the relief of the lower slope. In fact, it is presumed that the N-S trending oblique faults developed in response to subduction of this ridge and led to tectonic overprint of the lower slope. Geometrically, it even appears that the Nias-Siberut segment boundary coincides with the northern extent of the Investigator Ridge. Thus, an important influence of the crustal structure of the oceanic plate on the development of the fore arc has to be considered.

A further observation is that the frontal folds at the deformation front of the Nias segment are crosscut by a dense, transverse pattern of short tributaries to the trench. In front of these, smaller sediment aprons are piled on top the trench fill. This setting provides a clue to the timing of events. The tributaries crosscutting the folds may only have developed during or after the folding events. Thus, the frontal folds of the Nias segment may be older than in the other segments or may not have been tectonically reactivated recently.

In contrast, in the Siberut segment to the south the frontal folds are intact, with trap-

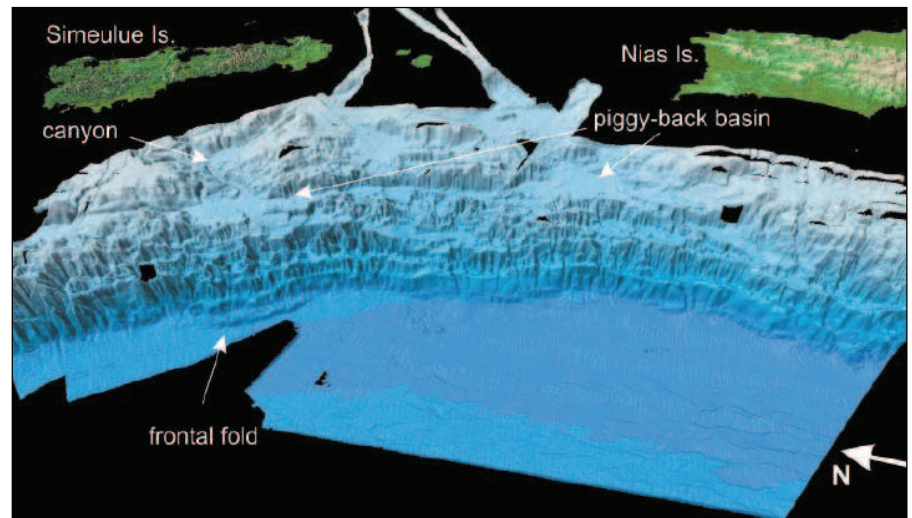


Fig. 2. Bathymetry in three-dimensional view off the islands of Simeulue and Nias. The bathymetry depicts the structural inventory of the deep-sea trench (more than 6000 meters deep) and the steep lower slope with a small accretionary complex. The middle slope is dominated by piggy-back basins, fed by canyons, following tectonic lineaments.

ping of sediments in piggyback basins. Farther north in the Aceh-Simeulue segment, the deformation front differs significantly [Henstock *et al.*, 2005]. Here a frontal, slightly southward plunging anticline, possibly above a protothrust, is developing in the trench fill in sequence in front of other (stacked) folds in the slope unit. This incipient anticline at the moment is likely the best candidate for the tsunami-generating structure on the seafloor [Moran *et al.*, 2005]. The absence of a comparable, recently active fold in the Nias segment could therefore be a possible clue as to why the March 2005 earthquake did not cause a mentionable tsunami. Resolving these issues remains a demanding task for the international geoscientific community.

Current Developments and Future Research

At the end of March 2006, geophysical profiling within the SeaCause project offshore Sumatra was completed. A dense net of about 40 multichannel reflection seismic profiles with a three-kilometer-long digital streamer imaged the subseafloor structures of the subduction zone traversing the oceanic plate, the trench, and lower to upper slope units with the outer arc high, as well as parts of the fore-arc basins. Along selected profiles, ocean-bottom seismometers and hydrophones were deployed to conduct refraction seismic studies to identify the velocity structure, and to image even deeper structures. Furthermore, at the base of the slope along short trench-parallel profiles, near-incidence reflection seismic experiments were conducted with ocean-bottom seismometers and hydrophones. Data from this suite of experiments is currently being processed. The geophysical and geological investigations offshore Sumatra will be carried on from August to September during the Sumatra cruise, and will focus on the evolution of the fore-arc basins.

Detailed knowledge of the tectonic setting of the plate boundary is essential for earthquake and tsunami hazard assessment in the

region. Moreover, this bathymetric data set is a prerequisite for modeling tsunami wave propagation and predicting run up heights offshore Sumatra for different earthquake scenarios. However, further detailed bathymetric mapping of the shallower fore arc basins is needed to incorporate local topography in the models, which will help hazard mitigation analysts identify vulnerable areas.

Close coordination of ongoing and future geoscience research projects offshore Sumatra is necessary to efficiently employ available resources. This is a focus of the upcoming 22–24 May workshop “Offshore studies of the Andaman-Sumatran Earthquakes,” in Hanover, Germany. For details, visit <http://www.bgr.bund.de/EN/Sumatraws> or e-mail sumatraws@bgr.de

Acknowledgments

We thank Dirk Hebbeln and Tim Jennerjahn, Bremen, for providing bathymetric data of cruise SO184. This is publication number 1 of the SeaCause and number 3 of the GITEWS projects, funded by the German Ministry of Education and Science, grants 03G0186 and 03TSU01.

References

- Henstock, T., L. McNeill, and D. Tappin (2005), Recent seafloor deformation at the 26 December 2004 Indian Ocean earthquake rupture zone: Results from the HMS Scott 2005 survey, *Geophys. Res. Abstr.*, 7, 11183.
- Moran, K., J. A. Austin, and D. R. Tappin (2005), Survey presents broad approach to tsunami studies, *Eos Trans. AGU*, 86(44), 430.

Author Information

Stefan Ladage, Christoph Gaedicke, Udo Barckhausen, and Ingo Heyde, Federal Institute for Geosciences and Natural Resources-BGR, Hanover, Germany, Email: s.ladage@bgr.de; Wilhelm Weinrebe, Ernst R. Flueh, Anne Krabbenhoft, and Heidrun Kopp, Leibniz-Institute of Marine Sciences, IFM-GEO-MAR, Kiel, Germany; Suryono Fajar and Yusuf Djajidhardja, Agency for the Assessment and Application of Technology, BPPT, Jakarta, Indonesia.

Publikation

- * Berglar, K. Gaedicke, Chr. Franke, D., Ladage, S., Klingelhofer, F., Djajadihardja, Y. (2008, eingereicht). Structural evolution and strike-slip tectonics off north-western Sumatra: Tectonophysics (eingereicht 09/2008).

Structural evolution and strike-slip tectonics off north-western Sumatra

Kai Berglar^a, Christoph Gaedicke^a, Dieter Franke^a, Stefan Ladage^a, Frauke Klingelhofer^b, Yusuf S. Djajadihardja^c

^aFederal Institute for Geosciences and Natural Resources (BGR), Stilleweg 2, D-30655 Hanover, Germany

^bIfremer Centre de Brest, B.P. 70, 29280 Plouzané cedex, France

^cAgency for the Assessment & Application of Technology, Jl. M.H. Thamrin No.8, Jakarta 10340, Indonesia

Corresponding Author

Kai Berglar
Bundesanstalt für Geowissenschaften und Rohstoffe
Federal Institute for Geosciences and Natural Resources
Stilleweg 2, D-30655 Hanover, Germany
kai.berglar@bgr.de
Tel: +49 511 643 2149, Fax: +49 511 643 3663

Abstract

Based on new multi-channel seismic data, swath bathymetry, and sediment echosounder data we present a model for the interaction between strike-slip faulting and forearc basin evolution off north-western Sumatra between 2°N and 7°N. We examined seismic sequences and sea floor morphology of the Simeulue- and Aceh forearc basins and the adjacent outer arc high. We found that strike-slip faulting controls the forearc basin evolution since the Late Miocene. The Mentawai Fault Zone extends up to north of Simeulue Island and was most probably connected farther northwards to the Sumatran Fault Zone until the end of Miocene. In the following, this northern branch jumped westwards, initiating the West Andaman Fault in the Aceh area. The connection to the Mentawai Fault Zone is a left-hand step-over. In this transpressional setting the Tuba Ridge developed. We found a right-lateral strike-slip fault running from the conjunction of the West Andaman Fault and the Tuba Ridge in SSW-direction crossing the outer arc high. As a result, extrusion formed a marginal basin north of Simeulue Island which is tilted eastwards by uplift along a thrust fault in the west. The shift of strike-slip movement in the Aceh segment is accompanied by a relocation of the depocenter of the Aceh Basin in northwestern direction forming one major Neogene unconformity. The Simeulue Basin bears two major Neogene unconformities documenting, that differences in subsidence evolution along the northern Sumatran margin are linked to both forearc-evolution related to subduction processes and to deformation along major strike-slip faults.

Keywords: oblique subduction, strike-slip, forearc basin, Sumatra, Mentawai Fault Zone, West Andaman Fault

1. Introduction

Oblique convergence of colliding plates is a common feature at convergent margins. Partitioning of strain results in two major structural components: One that is perpendicular to the trench, represented by folds and thrusts in the accretionary prism, and a second component, accommodating the oblique convergence in strike-slip faults parallel to the trench (Beck et al., 1993; Beck, 1983; Fitch, 1972; Malod and Mustafa Kemal, 1996; McCaffrey, 1991). Examples of such strike-slip motions are the Liquine-Ofqui Fault (Cembrano et al., 1996) and Atacama Fault (Cembrano et al., 2005) in Chile or the Queen Charlotte/Fairweather fault system in Alaska (Doser and Lomas, 2000). Studying such major strike-slip systems is crucial to understand the evolution of oblique margins and their behavior in terms of forearc basin evolution.

The study area is located off north-western Sumatra between 2°N and 7°N, covering the offshore region between the Mentawai Fault Zone and West Andaman Fault and the Sumatran Fault Zone (Fig. 1). The right-lateral offshore fault systems and the onshore Sumatran Fault Zone accommodate the trench-parallel component of the oblique convergence between the Indo-Australian and the Eurasian Plates (Diament et al., 1992; Malod and Mustafa Kemal, 1996; Samuel and Harbury, 1996; Sieh and Natawidjaja, 2000). The study area includes the Simeulue- and Aceh forearc basins and parts of the outer arc high. The studied basins show a change in water depth from about 1300 m in the Simeulue Basin to about 2800 m in the Aceh Basin and are clearly separated by an anticlinal structure that is elevated above the seafloor and referred to as Tuba Ridge by Malod et al. (1993).

The main purpose of this work is the assessment of the structural evolution of the strike-slip fault system and its relation to the forearc basin evolution off northern Sumatra based on the combined analysis of reflection seismic data, swath bathymetry and high resolution parametric echosounder data. The availability of a nearly complete swath bathymetric map in combination with a dense grid of seismic datasets of different resolutions allows us to address the questions of when strike-slip movements started and if these movements have had a notable influence on the evolution of the forearc basins. Our data make it possible to distinguish the interaction of the Mentawai Fault Zone and the West Andaman Fault in the Simeulue area which is not yet fully understood.

2. Tectonic evolution of the western Sunda Arc

Along the Sunda arc the oceanic Indo-Australian Plate subducts beneath the continental Eurasian Plate. The rate and direction of convergence of the Indo-Australian Plate with respect to the Eurasian Plate show a decreasing and slightly anticlockwise trend from southeast to northwest (Fig. 1). Based upon GPS measurements Prawirodirdjo and Bock (2004) proposed convergence rates of 61 mm/y (N17°E) off the Sunda Strait and 51 mm/y (N11°E) off northern Sumatra. The plate motion model NUVEL-1A (DeMets et al., 1994) gives values of 70 mm/y (N20°E) and 61 mm/y (N15°E) respectively. It is discussed that a clockwise rotation of Sumatra and Malaya of about 20° relative to Eurasia since the Late Miocene (Ninkovich, 1976; Nishimura et al., 1986) or Oligocene (Holcombe, 1977) was caused by the collision and indentation of India into Eurasia (Daly et al., 1991; Longley, 1997) and is the reason for a northward increasing obliquity of the subduction along the Sunda Arc. However, the curvature of the margin results in a plate convergence that gradually changes from nearly perpendicular subduction off Java to highly oblique subduction off northern Sumatra (Moore et al., 1980). Along the northwestern Sunda Arc slip partitioning and the development of arc-parallel strike-slip faults took place. The most prominent strike-slip shear zone is the Sumatran Fault Zone located on the Sumatran mainland along the volcanic arc (Bellon et al., 2004) which forms the Barisan Mountains (Fig. 1). The Sumatran Fault Zone accommodates most of the right-lateral

stress of the relative plate motion and is proposed to be active since the Mid Miocene (McCarthy and Elders, 1997). However, a distinct amount of arc-parallel stress is taken up by right-lateral strike-slip fault systems along the western edges of the forearc basins, namely the Mentawai Fault Zone and West Andaman Fault (Diament et al., 1992; Malod and Mustafa Kemal, 1996; McCaffrey, 1991). The Mentawai Fault Zone extends from the Sunda Strait in the south to at least the Island of Nias at about 1.5°N where it is probably connected with the Sumatran Fault Zone along the Batee Fault (Milsom et al., 1995). Likely the Mentawai Fault Zone extends farther north into the Simeulue Basin (Diament et al., 1992). The West Andaman Fault extends southwards from the Andaman Islands to the Simeulue Basin along the western border of the Aceh Basin (Curry, 2005). As pointed out by Curry et al. (1979) the Sumatran forearc acts as a sliver plate bounded to the west by the trench, below by the subducting plate, and to the east by the Sumatran Fault Zone. As a consequence the forearc sliver consists of elongated strips moving to the northwest. This was further refined by Malod and Kemal (1996) proposing two forearc microplates between the outer arc high and the Mentawai Fault Zone, separated by the Batee Fault. The western border of the northern microplate is represented by the West Andaman Fault.

3. Methodology

We had approximately 2800 km of multi-channel seismic (MCS) data available in the study area from a total of more than 9700 km acquired during two research cruises with RV SONNE in 2006. Shot distance was 50 m and we used a digital 240-channel streamer of 3 km length with a receiver spacing of 12.5 m, towed at a water depth of 6 m. The acoustic signal was generated by a tuned G-gun array of 16 units comprising a total volume of 50.8 l operated at air pressure of 14.5 MPa. Data were recorded with a sampling interval of 2 ms and 14 s length. Stacking velocities were picked at regular intervals of 3 km along every line. Pre-stack processing included resampling to 4 ms, trace editing, CMP-sort (nominal 30-fold coverage, 6.25 m spacing), Ormsby bandpass filter (6-12-60-160 Hz), polygon f-k filter (window of 60 traces and 1 s length), zerophase spiking deconvolution (52 ms operator length, 1 s design window beginning shortly below seabottom reflection), amplitude correction for spherical divergence based on stacking velocities ($1/(t \times v^2)$), normal moveout correction (40% stretch mute), and Radon velocity filter for multiple suppression (rejecting velocities differing more than $\pm 20\%$ of corresponding stacking velocity). After stack we applied a space and time variant Ormsby bandpass filter (upper window: 10-20-60-100 Hz, lower window: 6-12-50-100 Hz), a minimum phase predictive deconvolution and a post-stack Kirchhoff time migration with 90% of stacking velocities.

Additionally, digitized scans converted to Segy-format from single-channel recordings acquired during the SUMENTA cruises in the early 90s (Izart et al., 1994; Malod et al., 1993; Malod and Mustafa Kemal, 1996) were available with a total length of about 4800 km in the study area.

Together with the MCS data, high resolution parametric echosounder data (difference frequency of 3.5 kHz) were recorded with the ATLAS PARASOUND system at a sampling rate of 40 kHz. The data were resampled to 8 kHz, bandpass filtered (1.75-2.1-3.8-4 kHz) and the envelope seismic attribute applied for visualization.

The swath bathymetric data is a compilation of Japanese (Soh, 2006), British (Henstock et al., 2006; Tappin et al., 2007), French (Graindorge et al., 2008; Sibuet et al., 2007), US-American (RR0705, Cruise Report, 2007) and German (Ladage et al., 2006) datasets recorded in the area during several cruises. The bathymetric datasets were provided either in different native binary multibeam-system formats or as dumped grid data in xyz-ascii format. The data were used as delivered, i.e. no further editing was performed, and merged using the MB-System software package (Caress and Chayes, 1996). For gridding, the different surveys were given priorities by

a weighting scheme based on aerial coverage and data quality to minimize artifacts and inconsistencies in regions of overlap. Gridding was performed with a grid spacing of 100 m and maps plotted with the GMT software package (Wessel and Smith, 1991).

4. Structural Analysis

The evaluated area off northern Sumatra covers three basin domains: The Aceh Basin, the Simeulue Basin and a smaller basin located northwest of Simeulue Island. For clarity, we introduce the name Tuba Basin for this depression (Fig. 1).

A morphological analysis of the seafloor based on bathymetric data was carried out to identify tectonic structures. 2-D MCS data was used to determine the type and time of activity of the structures. We used simultaneously recorded high-resolution echosounder data to verify if such structures affected the uppermost sedimentary layers thus indicating recent activity.

4.1 Aceh Basin

The Aceh Basin is the northernmost forearc basin off Sumatra and is located in the conjunction between the West Andaman Fault and the Sumatran Fault Zone. It has a northward narrowing triangular shape covering an area of about 6600 km² with the northern tip reaching up to the island of Greater Nicobar (Fig. 1). From there, the basin spans southward for about 260 km where it is bordered by the Tuba Ridge (Fig. 1; Mosher et al., 2008). In E-W direction the basin has a width from the West Andaman Fault to the inner slope of about 65 km. To the east, the inner slope leads over to the Sumatran mainland and, offshore the northern tip of Sumatra, the Sumatran Fault Zone. The basin is filled with well stratified sedimentary sequences of an average thickness of 2 s two-way traveltime (TWT) that increases southwards. The architecture of the Aceh Basin is quite uniform in the south, while it becomes complex in the north.

The western border of the Aceh Basin is coincident with the West Andaman Fault. Bathymetry (Fig. 2A) shows a NNW-SSE-striking, mainly linear feature with a well defined main fault and several subordinate fault lines imaged as anticlines. These branch off into both the forearc basin and the outer arc high. The inset in Fig. 3 shows the typical expression of the main fault line of the West Andaman Fault along the Aceh Basin, a small depression filled syntectonically with westward dipping sediments. It is enframed at both sides by anticlines of about 6 km in width. The easternmost anticline is built up by the entire Neogene sedimentary column of the Aceh Basin. The deformation affected the youngest sediments indicating a recent activity of the West Andaman Fault, also evidenced by fault plane solutions (Kamesh Raju et al., 2007).

In the entire basin the base of the well stratified sediments is formed by a distinct unconformity (Figs. 3, 4 and 5). This unconformity is of regional extent and was probably caused by uplift and subsequent erosion of the forearc area off Sumatra. It was interpreted in all forearc basins along the Sumatran trench as of Oligocene/Early Miocene age (Beaudry and Moore, 1985; Izart et al., 1994; Karig et al., 1979; Karig et al., 1980; Malod et al., 1993; Rose, 1983; Schlüter et al., 2002; Susilohadi et al., 2005; van der Werff, 1996). From this widespread extent and the narrow position to the Simeulue Basin where the age is proved by drilling we propose that the basal unconformity in the Aceh Basin is also of base Neogene age. On top of the basal unconformity two well layered sedimentary sequences are divided by an angular unconformity. Sequence A has a maximum thickness of 4 s (TWT) in the southern Aceh Basin near the Tuba Ridge (Fig. 5). Farther north, it thins to 1.4 s (TWT) and is trenchward rotated (Fig. 3). Sequence B is horizontally layered and onlaps the unconformity below. The main depocenter of sequence B is located in the central Aceh Basin (Fig. 3) with a maximum thickness of about 1.3 s (TWT). The whole depocenter of the Aceh Basin shows a northward migrating trend of subsidence over time.

Fig. 6A spans over 120 km from the West Andaman Fault to the Sumatran Fault Zone and covers the northern part of the Aceh Basin and the area adjacent to the east. Again, the main line of the West Andaman Fault is developed as a narrow synsedimentary filled depression (km 7). The deformed area at the transition to the forearc basin is composed of uplifted and deformed sediments. The narrow depocenter contains two sedimentary sequences above the acoustic basement (km 17-33). The lower one is confined to the eastern part of the basin (km 25-33) and is subdivided into two subsections. Sub-parallel reflectors dominate in the basal section. The upper section contains westward dipping reflectors, downlapping on the sediments below. The upper sequence of the basin is well layered and downlaps onto the lower sequence in the east. Here, this sequence shows a divergent reflection pattern, indicating a deposition syntectonically to subsidence (km 25-30).

In the area between the Aceh Basin and the Sumatran Fault Zone to the east an erosional truncation separates deformed sediments from a package with sub-parallel configuration atop. The internal configuration of the sediments below the erosional truncation point to a deposition in a basin setting and we refer to this area as Paleo Aceh Basin. Incisions of a channel (see Fig. 1) are visible on the profile shown in Fig. 6A from km 50-58. Below these incisions an older sedimentary basin is imaged (km 40-60). It contains two major sedimentary sequences with the upper onlapping on the lower one and is bounded to the east by an extensional fault (km 59). A distinguishing of the individual sedimentary sequences was impossible with the data at hand. The sedimentary fill might either be interpreted as consisting of only sequence B (similar the northern Aceh Basin) or as sequences A and early B (similar the southern Aceh Basin). We tentatively interpret the erosional truncation as separating sequence A from early sequence B because of the distinct onlapping reflection pattern also found in the southern Aceh Basin and because we observe a general westwards migration of the western border of the northern Aceh Basin.

Further eastwards sediments below the erosional truncation are strongly folded. Folding can be followed on seismic sections (Fig. 6B) on a line across the area east of the Aceh Basin in southern direction to the eastern edge of the Tuba Ridge. We interpret a non-active strike-slip fault similar to the Sumatran Fault Zone and West Andaman Fault.

4.2 Tuba Basin

The Tuba Basin is a narrow depression to the south of the Aceh Basin. It is separated from the latter by the Tuba Ridge, a zone of compressional uplift. Fig. 5 shows the large anticline of the Tuba Ridge from km 58-75 uplifting the basin sediments for more than 700 m to the south and 1000 m to the north over the surrounding ocean floor. The Tuba Basin is trench-parallel elongated, and extends over 160 km in NW-SE direction with a maximum width of about 70 km, totaling in an area of about 6000 km². To the west it is confined by the outer arc high which is cut by a right-lateral strike-slip fault running from the western end of the Tuba Ridge in SSW-direction (Fig. 2B). The northern part of the basin is occupied by a depression covering an area of approximately 1200 km² with side lengths of about 27 km and 50 km. Here, the seafloor is at a maximum water depth of about 2200 m whereas it reaches depths of 1700 m in the southerly located area. The sedimentary infill is generally thin with a maximum thickness of about 1.2 s (TWT; Fig. 7). The northern depression is bounded to the south by normal faults and crossed by a W-E striking escarpment of about 80 m (Figs. 2B and 5, km 83 and inset). Most likely this part of the Tuba Basin was disconnected from the Aceh Basin by the formation of the Tuba Ridge because reflectors of sequence A, though heavily folded and dragged, can be followed through the Tuba Ridge into the northern Tuba Basin (Fig. 5).

Bathymetry of the southern basin part (Fig. 2C) shows a steady northwest-directed inclination with a slope angle of about 1.4° (Fig. 7) from the outer arc high in the west to the eastern

boundary of the basin where the recent depocenter is located (Figs. 7, km 45-55 and 8, km 32-40). Tilting of the basin is documented by a circular buildup structure on the ocean floor (Figs. 2C and 8, km 15-20) which exhibits the same inclination. Several folds with a NW-SE strike are distinct in the bathymetric map, the most prominent at the border to the outer arc high (Fig 2C). The seismic image shows a steep high-amplitude reflector band below this fold (Fig 7, km 6-12) which we interpret as a thrust fault. Uplift along this fault may have resulted in a tilting of the western part of the Tuba Basin and subsequent deformation of the sedimentary succession. The reflection pattern of the sequences and basement of the Tuba Basin differ from the other forearc basins and are merely typical for the outer arc high.

4.3 Simeulue Basin

With an area of about 15,000 km², the Simeulue Basin is the largest forearc basin off northern Sumatra. It is a northward narrowing, trench-parallel elongated depression and extends over 260 km in NW-SE direction and approximately 100 km in SW-NE direction. The maximum water depth is about 1300 m (Berglar et al., 2008). The basin contains a sedimentary succession of Early Miocene to recent age (Beaudry and Moore, 1985; Berglar et al., 2008; Karig et al., 1979; Rose, 1983) of up to 5 s (TWT). It is bounded to the south by the Banyak Islands and to the west by Simeulue Island and a ridge-like structure separating it from the Tuba Basin. To the east a well defined slope and shelf passes into the Sumatran mainland.

The stratigraphy and subsidence of the Simeulue Basin was described in detail by Berglar et al. (2008): The base of the stratified sediments is formed by the regional basal Neogene unconformity. Atop, three major stages of subsidence and deposition were identified. Subsidence in the Simeulue Basin was initiated during the Early and Middle Miocene in the western part of the basin where half grabens formed. A second major stage took place during the Late Miocene and Pliocene when the accretionary wedge west of the basin consolidated and formed the distinct outer arc high. This resulted in a consistently subsiding trough along the western border of the basin and a broad shelf in the eastern part. The last phase of the second stage was characterized by a westward shift of the depocenter probably associated with the initiation of strike-slip faulting. The Pleistocene to recent stage shows relatively uniform subsidence across the basin except for the central part where uplift and subsequent normal faulting at the crests of the uplifted areas occurred.

The Simeulue Basin is characterized by two styles of deformation, namely large anticlines with normal faulting at the crest and strike-slip related faulting and folding. Fig. 9 (km 108-128) shows an example of an anticline with subsequent normal faulting. The faults penetrate from the ocean floor down to Early Miocene sediments on top of an anticline of about 70 km in width. The crest is subject to erosion exposing Pliocene sediments. The deep reaching normal faults and the size of the anticline suggest uplift of the basement. Bathymetry (Fig. 2D) reveals the surficial shape of the anticline as semicircular in northeastern direction towards the basin, pointing to either a NE-dipping crest line or a dome-like architecture of this area of uplift. The SW-NE strike of the normal faults follow the axis of the anticline (Fig. 2D).

An example of strike-slip related faulting and folding is the elongated structure of NW-SE strike separating the Simeulue- and Tuba Basins north of Simeulue Island (Fig. 2C). Seismic sections (Figs. 8, km 48-63 and 9, km 0-20) depict a positive flower structure of about 15 km in width and 800 m in height. We interpret this structure as the main line of the transpressional fault continuing the Mentawai Fault Zone north of the Banyak Islands up to the east of the Tuba Ridge. The deformation extends farther into the Simeulue Basin as documented by blind reverse faults deforming the basin sediments (Fig. 8, km 70-80). Fig. 2D shows a large channel circuiting a fold; similar anticlines are located to the NW as well as on Simeulue Island.

The transition from the outer arc high south of Simeulue Island into the southwestern basin part is illustrated on Figs. 2E and 10. There, a series of wrench faults is observed. Interfingering sedimentary packages (Fig. 10, km 15-20) depict the alternating intensity of deformation and uplift of wrench faults that resulted in changing direction of sediment supply into the basin. The northeastern wrench fault on Fig. 10 (km 25-30) exhibits onlapping reflectors with upwards decreasing angles marking the initiation of deformation in Late Miocene to Pliocene time (bold line). The recent activity of this fault is revealed by uplift and erosion of youngest sediments imaged in subbottom profiler data (inset).

5. Discussion

An earlier interpretation based on single-channel seismic data proposed a common stratigraphy for the entire forearc basin region off northern Sumatra (Izart et al., 1994). These authors correlated sedimentary sequences from the Nias Basin, previously described by Beaudry and Moore (1981) and Matson and Moore (1992) in the south to the Aceh Basin in the north. However, we propose that the basin evolution differs significantly from south to north.

The stratigraphic framework of the Simeulue Basin established by Berglar et al. (2008) was calibrated with published data of exploration wells (Beaudry and Moore, 1985; Karig et al., 1979; Rose, 1983) and the temporal delimitation of identified tectonic structures is well constrained. The Simeulue Basin evolved in three major stages. To distinguish in detail the sedimentary sequences in the Aceh Basin, we reviewed the old seismic data and combined them with our newly acquired MCS data. In contrast to the Simeulue Basin we found only two main stages. Independently from the stratigraphic position of the sedimentary fill in the Aceh Basin, this is a clear indication of the different evolution of the forearc basins. The evolution of the forearc basins is apparently much more complex than previously assumed.

The main depocenter of sequence A is located in the southern Aceh Basin. Recently, this part was subject to uplift and folding, as documented by exposure and subsequent erosion of sequence A (Fig. 5). Since this uplift, the depocenter moved considerably northwards while the southern part is sediment-starved. The age of unconformity A/B in the Aceh Basin is not determinable without doubt by sequence stratigraphy. It may be either of Mid Miocene age, as the oldest major Neogene unconformity in the Simeulue Basin, or considerably younger.

Strike-slip movements are a direct consequence of the oblique convergence of colliding plates and thus are of regional extent. We propose that these strike-slip movements in the forearc basins off Sumatra can be used to tie the evolution scenarios for the basins. In the Simeulue Basin the initiation of strike-slip movement started earliest in the Late Miocene (Fig. 10; Berglar et al., 2008). In the Aceh Basin sequence B can clearly be associated with the initiation of strike-slip movement along the West Andaman Fault. Here, strike-slip faulting replaced a former, now inactive fault, as e.g. imaged on Fig. 6A (km 70-80) and the depocenter of the northern Aceh Basin probably migrated westward over time. If our assumption is right, the unconformity between sequence A and B in the Aceh Basin then would approximately be at the Miocene/Pliocene boundary. The onset of movements along the West Andaman Fault thus resulted in a significant north- and westward shift of the depocenter in the Aceh Basin. Extensional faulting (Fig. 6A, km 33 and 59) at the eastern edges of the narrow half graben like depocenters and the westward dip of sequence A (Fig. 3) may be explained by the slightly curved geometry of the West Andaman Fault resulting in a releasing bend.

The two major forearc basins in the study area, namely the Simeulue- and the Aceh Basins, thus evolved step by step. While subsidence continued in the Aceh Basin (sequence A) a major Mid/Late Miocene unconformity in the Simeulue Basin marks differences in basin evolution. With the initiation of strike-slip faulting, subsidence expanded considerably eastwards in the

Simeulue Basin, but the Mentawai Fault Zone itself affected only the westernmost part of the basin. In contrast, the sediments of the northern Aceh Basin were deformed by the northward continuation of the Mentawai Fault Zone. The cessation of this northernmost fault section (Fig. 11) and subsequent jump of strike-slip movement initiated the West Andaman Fault. The Aceh Basin adapted to the structural reorganization by erosion of the Paleo Aceh Basin and a shift of the depocenter to the west and north to the recent position.

The complex evolution of the Simeulue Basin is also documented in the interaction of two different styles of deformation: (1) Uplift and subsequent erosion accompanied by deep reaching normal faults, and (2) strike-slip faulting and folding along the western border of the basin.

(1) Uplift and basin inversion starting in the Pleistocene is probably related to reactivation of Early Miocene half graben structures responsible for the initial Neogene subsidence of the basin (Berglar et al., 2008). The recent activity is proven by bathymetric steps with SW-NE strike caused by the normal faults at the crest of the anticlines (Fig. 2D). Two bottom simulating reflectors (Fig. 9, km 115-123) may indicate a rapid recent uplift, where the gas hydrates did not had time to adjust to the changes of the gas hydrate stability zone (Foucher, 2002; Popescu et al., 2006; Posewang and Mienert, 1999). The deep reaching normal faults visible on seismic sections (Fig. 9) suggest an activation related either to changes in dip of the subducting oceanic crust (Franke et al., 2008) or to local changes in plate coupling resulting in inhomogeneous compensation of tectonic slip (Ammon, 2006; Ammon et al., 2005; Briggs et al., 2006).

(2) Strike-slip deformation led to primary faulting along the main fault line and secondary folding to both sides of the main fault. The main fault line along the western boundary of the Simeulue Basin is imaged on Figs. 2D, 8 and 9. As the location and trend at the western rim of the forearc basin is similar to that of the Mentawai Fault Zone in the southerly located Bengkulu Basin (Diament et al., 1992) we attribute the strike-slip fault in the Simeulue Basin to this system. The secondary folds are sigmoidal shaped, with their axis more or less parallel to the main fault line and lengths of about 10-20 km (Figs. 2C-E, 9 and 10). These are the surficial expression of wrench faults typically found along the Sumatran forearc basins (Diament et al., 1992). Fig. 9 shows several structures related to wrench faulting. Km 58-70 is occupied by an area of local uplift. As revealed by the bathymetric data (Fig. 2D), this is an anticline which is cut along strike by the seismic section. It has a visible length of about 12 km on the surface and a sigmoidal shaped hinge line. Directly south of this anticline onshore topography depicts a similar shaped structure on Simeulue Island, but with a mirrored form. The striking similarity of both structures led us to interpret the position of the trend of the main Mentawai fault line between these folds, along the eastern shelf off Simeulue Island.

The Mentawai Fault Zone is connected to the West Andaman Fault by the Tuba Ridge (Figs. 2B and 5). In our view the Tuba Ridge is a transpressional uplifted area of a left-hand step-over in the right-lateral strike-slip system. A second, SSE-trending right-lateral strike-slip fault meets the West Andaman Fault at its southernmost tip at the transition to the Tuba Ridge (Fig. 11), similarly described by Seeber et al. (2007). This fault is traceable on bathymetry data across the entire outer arc high and accretionary prism to the Sumatra Trench. In this regime the northern Tuba Basin to the south of the Tuba Ridge extruded in southward direction leading to deeply seated extensional normal faults evident in our seismic data (Fig. 5, km 75-100). Overlying sediments are recently affected and the uppermost strata is teared (Figs. 2B and 5, inset). A thrust fault bordering the southern Tuba Basin to the west (Figs. 2C, 7 and 8) gives evidence for recent compression and tilting in that part of the basin. The Tuba Basin is bordered in landward direction by ridges which act as barriers hindering sediments to enter the basin making determination of timing of deformation difficult. Because even the uppermost strata were subject of thrusting and folding (Figs. 7 and 8) we speculate that the thrust fault and minor reverse faults within the basin are active.

6. Conclusion

From these findings we conclude the following evolution scenario for the strike-slip systems and the forearc basins off NW Sumatra: Since their initiation in the Late Miocene strike-slip faults control the forearc basin evolution off northern Sumatra. The northern branch of the Mentawai Fault Zone is traceable along the western boundary of the Simeulue Basin. Until the Miocene/Pliocene boundary the Mentawai Fault Zone was most probably connected to the Sumatran Fault Zone. Until that time the depocenter of the northern Aceh Basin was located further eastwards. In the Lower Pliocene the Aceh section of the Mentawai Fault Zone jumped westward or left-hand to the position of the West Andaman Fault. The shift of the fault was accompanied by a west- and northward shift of the depocenter in the Aceh Basin. The Tuba Ridge is a result of compression at this left-hand step-over. This ridge and the Mentawai Fault Zone isolate the Tuba Basin from terrigenous sediment sources leading to its recent sediment starved setting. A NNE-SSW trending right-lateral strike-slip fault cuts from the Sumatra Trench through the accretionary prism and outer arc high. Interaction of this fault with the West Andaman Fault leads to subsidence and extrusion of the northern Tuba Basin, the southern Tuba Basin is tilted by uplift along a thrust fault. Initiation of strike-slip movement in the Simeulue Basin is accompanied by an expansion of subsidence for several kilometers in the direction of Sumatra. Recent inversion is observed in the Simeulue Basin which we attribute either to change in dip of the oceanic crust or to changes in coupling of the upper and lower plates.

Acknowledgements

The authors express their gratitude to all colleagues making this work possible by organizing the projects and by collecting and processing the data. In particular we thank the ship's masters Lutz Mallon and Oliver Meyer and the crews of RV SONNE for their cooperation and support during the SeaCause and SUMATRA cruises. We are grateful to The Agency for the Assessment and Application of Technology (BPPT) and Indonesian Government for their support and permission for the scientific investigation in Indonesian waters. We thank Ingo Heyde and Ewald Lüschen for their helpful notes on magnetic anomalies and seismic processing, respectively. We appreciate Michael Schnabel for corrections and suggestions on the manuscript. The research projects were carried out with grants 03G0186A (SeaCause) and 03G0189A (SUMATRA) of the Federal Ministry of Education and Research (BMBF), Germany.

References

- Ammon, C.J., 2006. Megathrust investigations. *Nature* 440(7080), 31–32. doi: [10.1038/440031a](https://doi.org/10.1038/440031a).
- Ammon, C.J., Ji, C., Thio, H.K., Robinson, D., Ni, S., Hjorleifsdottir, V., Kanamori, H., Lay, T., Das, S., Helmberger, D., Ichinose, G., Polet, J., Wald, D., 2005. Rupture Process of the 2004 Sumatra-Andaman Earthquake. *Science* 308(5725), 1133–1139. doi: [10.1126/science.1112260](https://doi.org/10.1126/science.1112260).
- Beaudry, D., Moore, G.F., 1981. Seismic-stratigraphic framework of the forearc basin off central Sumatra, Sunda Arc. *Earth and Planetary Science Letters* 54(1), 17–28. doi: [10.1016/0012-821X\(81\)90065-0](https://doi.org/10.1016/0012-821X(81)90065-0).
- Beaudry, D., Moore, G.F., 1985. Seismic stratigraphy and Cenozoic evolution of West Sumatra forearc basin. *The American Association of Petroleum Geologists Bulletin* 69(5), 742–759.

- Beck, M.E., Rojas, C., Cembrano, J., 1993. On the nature of buttressing in margin-parallel strike-slip fault systems. *Geology* 21(8), 755–758. doi: [10.1130/0091-7613\(1993\)021<0755:OTNOBI>2.3.CO;2](https://doi.org/10.1130/0091-7613(1993)021<0755:OTNOBI>2.3.CO;2).
- Beck, M.E., 1983. On the mechanism of tectonic transport in zones of oblique subduction. *Tectonophysics* 93(1-2), 1–11. doi: [10.1016/0040-1951\(83\)90230-5](https://doi.org/10.1016/0040-1951(83)90230-5).
- Bellon, H., Maury, R.C., Sutanto, Soeria-Atmadja, R., Cotten, J., Polve, M., 2004. 65 m.y.-long magmatic activity in Sumatra (Indonesia), from Paleocene to Present. *Bulletin de la Societe Geologique de France* 175(1), 61–72. doi: [10.2113/175.1.61](https://doi.org/10.2113/175.1.61).
- Berglar, K., Gaedicke, C., Lutz, R., Franke, D., Djajadihardja, Y.S., 2008. Neogene subsidence and stratigraphy of the Simeulue forearc basin, Northwest Sumatra. *Marine Geology* 253(1-2), 1–13. doi: [10.1016/j.margeo.2008.04.006](https://doi.org/10.1016/j.margeo.2008.04.006).
- Briggs, R.W., Sieh, K., Meltzner, A.J., Natawidjaja, D., Galetzka, J., Suwargadi, B., Hsu, Y.j., Simons, M., Hananto, N., Suprihanto, I., Prayudi, D., Avouac, J.P., Prawirodirdjo, L., Bock, Y., 2006. Deformation and Slip Along the Sunda Megathrust in the Great 2005 Nias-Simeulue Earthquake. *Science* 311(5769), 1897–1901. doi: [10.1126/science.1122602](https://doi.org/10.1126/science.1122602).
- Caress, D., Chayes, D., 1996. Improved processing of Hydrosweep DS multibeam data on the R/V Maurice Ewing. *Marine Geophysical Researches* 18, 631–650. doi: [10.1007/BF00313878](https://doi.org/10.1007/BF00313878).
- Cembrano, J., González, G., Arancibia, G., Ahumada, I., Olivares, V., Herrera, V., 2005. Fault zone development and strain partitioning in an extensional strike-slip duplex: A case study from the Mesozoic Atacama fault system, Northern Chile. *Tectonophysics* 400(1-4), 105–125. doi: [10.1016/j.tecto.2005.02.012](https://doi.org/10.1016/j.tecto.2005.02.012).
- Cembrano, J., Herve, F., Lavenu, A., 1996. The Liquine Ofqui fault zone: a long-lived intra-arc fault system in southern Chile. *Tectonophysics* 259(1-3), 55–66. doi: [10.1016/0040-1951\(95\)00066-6](https://doi.org/10.1016/0040-1951(95)00066-6).
- Curry, J.R., Moore, D.G., Lawver, L.A., Emmel, F.J., Raitt, R.W., Henry, M., Kieckhefer, R., 1979. Tectonics of the Andaman Sea and Burma. In: J.S. Watkins, L. Montadert, P.W. Dickerson (Eds.), *Geological and geophysical investigations of continental margins*. Memoir, vol. 29, American Association of Petroleum Geologists, Tulsa, OK, pp. 189–198.
- Curry, J.R., 2005. Tectonics and history of the Andaman Sea region. *Journal of Asian Earth Sciences* 25(1), 187–232. doi: [10.1016/j.jseaes.2004.09.001](https://doi.org/10.1016/j.jseaes.2004.09.001).
- Daly, M., Cooper, M., Wilson, I., Smith, D., Hooper, B., 1991. Cenozoic plate tectonics and basin evolution in Indonesia. *Marine and Petroleum Geology* 8(1), 2–21. doi: [10.1016/0264-8172\(91\)90041-X](https://doi.org/10.1016/0264-8172(91)90041-X).
- DeMets, C., Gordon, R.G., Argus, D.F., Stein, S., 1994. Effect of recent revisions to the geomagnetic reversal time scale on estimates of current plate motions. *Geophysical Research Letters* 21(20), 2191–2194. doi: [10.1029/94GL02118](https://doi.org/10.1029/94GL02118).
- Deplus, C., Diament, M., Hebert, H., Bertrand, G., Dominguez, S., Dubois, J., Malod, J., Patriat, P., Pontoise, B., Sibilla, J.J., 1998. Direct evidence of active deformation in the eastern Indian oceanic plate. *Geology* 26(2), 131–134. doi: [10.1130/0091-7613\(1998\)026<0131:DEOADI>2.3.CO;2](https://doi.org/10.1130/0091-7613(1998)026<0131:DEOADI>2.3.CO;2).
- Diament, M., Harjono, H., Karta, K., Deplus, C., Dahrin, D., Zen, M. T., J., Gerard, M., Lassal, O., Martin, A., Malod, J., 1992. Mentawai fault zone off Sumatra: A new key to the geodynamics of western Indonesia. *Geology* 20(3), 259–262. doi: [10.1130/0091-7613\(1992\)020<0259:MFZOSA>2.3.CO;2](https://doi.org/10.1130/0091-7613(1992)020<0259:MFZOSA>2.3.CO;2).
- Doser, D.I., Lomas, R., 2000. The transition from strike-slip to oblique subduction in Southeastern Alaska from seismological studies. *Tectonophysics* 316(1-2), 45–65. doi: [10.1016/S0040-1951\(99\)00254-1](https://doi.org/10.1016/S0040-1951(99)00254-1).
- Fitch, T.J., 1972. Plate Convergence, Transcurrent Faults, and Internal Deformation Adjacent to Southeast Asia and the Western Pacific. *Journal of Geophysical Research* 77(23), 4432–4460. doi: [10.1029/JB077i023p04432](https://doi.org/10.1029/JB077i023p04432).
- Foucher, J.P., 2002. Observation and tentative interpretation of a double BSR on the Nankai Slope. *Marine Geology* 187(1-2), 161–175. doi: [10.1016/S0025-3227\(02\)00264-5](https://doi.org/10.1016/S0025-3227(02)00264-5).

- Franke, D., Schnabel, M., Ladage, S., Tappin, D.R., Neben, S., Djajadihardja, Y.S., Muller, C., Kopp, H., Gaedicke, C., 2008. The great Sumatra-Andaman earthquakes – Imaging the boundary between the ruptures of the great 2004 and 2005 earthquakes. *Earth and Planetary Science Letters* 269(1-2), 118–130. doi: [10.1016/j.epsl.2008.01.047](https://doi.org/10.1016/j.epsl.2008.01.047).
- Graindorge, D., Klingelhoefer, F., Sibuet, J.C., McNeill, L., Henstock, T.J., Dean, S., Gutscher, M.A., Dessa, J.X., Permana, H., Singh, S.C., Leau, H., White, N., Carton, H., Malod, J.A., Rangin, C., Aryawan, K.G., Chaubey, A.K., Chauhan, A., Galih, D.R., Greenroyd, C.J., Laesanpura, A., Prihantono, J., Royle, G., Shankar, U., 2008. Impact of the lower plate on upper plate deformation at the NW Sumatran convergent margin from seafloor morphology. *Earth and Planetary Science Letters* (In Press). doi: [10.1016/j.epsl.2008.04.053](https://doi.org/10.1016/j.epsl.2008.04.053).
- Henstock, T.J., McNeill, L.C., Tappin, D.R., 2006. Seafloor morphology of the Sumatran subduction zone: Surface rupture during megathrust earthquakes? *Geology* 34(6), 485–488. doi: [10.1130/22426.1](https://doi.org/10.1130/22426.1).
- Holcombe, C.J., 1977. Earthquake foci distribution in the Sunda Arc and the rotation of the backarc area. *Tectonophysics* 43(3-4), 169–180. doi: [10.1016/0040-1951\(77\)90115-9](https://doi.org/10.1016/0040-1951(77)90115-9).
- Izart, A., Mustafa Kemal, B., Malod, J.A., 1994. Seismic stratigraphy and subsidence evolution of the Northwest Sumatra fore-arc basin. *Marine Geology* 122(1-2), 109–124. doi: [10.1016/0025-3227\(94\)90207-0](https://doi.org/10.1016/0025-3227(94)90207-0).
- Kamesh Raju, K.A., Murty, G.P.S., Amarnath, D., Kumar, M.L.M., 2007. The West Andaman Fault and its influence on the the aftershock pattern of the recent megathrust earthquakes in the Andaman-Sumatra region. *Geophysical Research Letters* 34(3), L03305. doi: [10.1029/2006GL028730](https://doi.org/10.1029/2006GL028730).
- Karig, D.E., Suparka, S., Moore, G.F., Hehanussa, P.E., 1979. Structure and Cenozoic evolution of the Sunda Arc in the central Sumatra region. In: J.S. Watkins, L. Montadert, P.W. Dickerson (Eds.), *Geological and geophysical investigations of continental margins. Memoir, vol. 29*, American Association of Petroleum Geologists, Tulsa, OK, pp. 223–237.
- Karig, D.E., Lawrence, M.B., Moore, G.F., Curray, J.R., 1980. Morphology and shallow structure of the lower trench slope off Nias Island, Sunda Arc. In: D.E. Hayes (Ed.), *The tectonic and geologic evolution of Southeast Asian seas and islands. Geophysical Monograph, vol. 23*, American Geophysical Union, Washington, DC, pp. 179–208.
- Ladage, S., Weinrebe, W., Gaedicke, C., Barckhausen, U., Flueh, E.R., Heyde, I., Krabbenhoef, A., Kopp, H., Fajar, S., Djajadihardja, Y., 2006. Bathymetric Survey Images Structure off Sumatra. *Eos, Transactions American Geophysical Union* 87(17), 165–172. doi: [10.1029/2006EO170001](https://doi.org/10.1029/2006EO170001).
- Longley, I.M., 1997. The tectonostratigraphic evolution of SE Asia. In: A.J. Fraser, S.J. Matthews, R.W. Murphy (Eds.), *Petroleum Geology of Southeast Asia. Special Publications, vol. 126*, Geological Society, London, pp. 311–339. doi: [10.1144/GSL.SP.1997.126.01.19](https://doi.org/10.1144/GSL.SP.1997.126.01.19).
- Malod, J.A., Mustafa Kemal, B., Beslier, M.O., Deplus, C., Diament, M., Karta, K., Mauffret, A., Patriat, P., Pubellier, M., Regnault, H., Aritonang, P., Zen, M. T., J., 1993. Deformations du bassin d'avant-arc au nord-ouest de Sumatra: une reponse a la subduction oblique. *Comptes Rendus de l'Academie des Sciences de Paris, Série 2* 316(6), 791–797.
- Malod, J.A., Mustafa Kemal, B., 1996. The Sumatra Margin: oblique subduction and lateral displacement of the accretionary prism. In: R. Hall, D. Blundell (Eds.), *Tectonic Evolution of Southeast Asia. Special Publications, vol. 106*, Geological Society, London, pp. 19–28. doi: [10.1144/GSL.SP.1996.106.01.03](https://doi.org/10.1144/GSL.SP.1996.106.01.03).
- Matson, R.G., Moore, G.F., 1992. Structural influences on Neogene subsidence in the central Sumatra fore-arc basin. In: J.S. Watkins, F. Zhiqiang, K.J. McMillen (Eds.), *Geology and geophysics of continental margins. Memoir, vol. 53*, American Association of Petroleum Geologists, Tulsa, OK, United States, pp. 157–181.
- McCaffrey, R., 1991. Slip vectors and stretching of the Sumatran fore arc. *Geology* 19(9), 881–884. doi: [10.1130/0091-7613\(1991\)019<0881:SVASOT>2.3.CO;2](https://doi.org/10.1130/0091-7613(1991)019<0881:SVASOT>2.3.CO;2).
- McCarthy, A.J., Elders, C.F., 1997. Cenozoic deformation in Sumatra: oblique subduction and the development of the Sumatran fault system. In: A.J. Fraser, S.J. Matthews, R.W. Murphy

- (Eds.), *Petroleum Geology of Southeast Asia*. Special Publications, vol. 126, Geological Society, London, pp. 355–363. doi: [10.1144/GSL.SP.1997.126.01.21](https://doi.org/10.1144/GSL.SP.1997.126.01.21).
- Milsom, J., Sain, B., Sipahutar, J., 1995. Basin formation in the Nias area of the Sumatra forearc, western Indonesia. *Bulletin Geological Society of Malaysia* 37, 285–299.
- Müller, R.D., Roest, W.R., Royer, J.Y., Gahagan, L.M., Sclater, J.G., 1997. Digital isochrons of the world's ocean floor. *Journal of Geophysical Research* 102(B2), 3211–3214. doi: [10.1029/96JB01781](https://doi.org/10.1029/96JB01781).
- Moore, G.F., Curray, J.R., Moore, D.G., Karig, D.E., 1980. Variations in geologic structure along the Sunda Fore Arc, northeastern Indian Ocean. In: D.E. Hayes (Ed.), *The tectonic and geologic evolution of Southeast Asian seas and islands*. Geophysical Monograph, vol. 23, American Geophysical Union, Washington, DC, pp. 145–160.
- Mosher, D., Austin Jr., J., Fisher, D., Gulick, S., 2008. Deformation of the northern Sumatra accretionary prism from high-resolution seismic reflection profiles and ROV observations. *Marine Geology* 252(3-4), 89–99. doi: [10.1016/j.margeo.2008.03.014](https://doi.org/10.1016/j.margeo.2008.03.014).
- Ninkovich, D., 1976. Late cenozoic clockwise rotation of Sumatra. *Earth and Planetary Science Letters* 29(2), 269–275. doi: [10.1016/0012-821X\(76\)90130-8](https://doi.org/10.1016/0012-821X(76)90130-8).
- Nishimura, S., Nishida, J., Yokoyama, T., Hehuwat, F., 1986. Neo-tectonics of the Strait of Sunda, Indonesia. *Journal of Southeast Asian Earth Sciences* 1(2), 81–91. doi: [10.1016/0743-9547\(86\)90023-1](https://doi.org/10.1016/0743-9547(86)90023-1).
- Popescu, I., M., Batist, D., Lericolais, G., Nouze, H., Poort, J., Panin, N., Versteeg, W., Gillet, H., 2006. Multiple bottom-simulating reflections in the Black Sea: potential proxies of past climate conditions. *Marine Geology* 227(3-4), 163–176. doi: [10.1016/j.margeo.2005.12.006](https://doi.org/10.1016/j.margeo.2005.12.006).
- Posewang, J., Mienert, J., 1999. The enigma of double BSRs: indicators for changes in the hydrate stability field? *Geo-Marine Letters* 19(1-2), 157–163. doi: [10.1007/s003670050103](https://doi.org/10.1007/s003670050103).
- Prawirodirdjo, L., Bock, Y., 2004. Instantaneous global plate motion model for 12 years of continuous GPS observations. *Journal of Geophysical Research* 109, B08405. doi: [10.1029/2003JB002944](https://doi.org/10.1029/2003JB002944).
- Rose, R.R., 1983. Miocene carbonate rocks of Sibolga Basin, Northwest Sumatra. *Proceedings Indonesian Petroleum Association* 12, 107–125.
- RR0705, 2007. Cruise Report: Paleoseismologic Studies of the Sunda Subduction Zone. Oregon State University Active Tectonics Laboratory, United States; Agency for the Assessment and Application of Technology, Indonesia. <http://www.activetectonics.coas.oregonstate.edu/sumatra/report/index.html>.
- Samuel, M.A., Harbury, N.A., 1996. The Mentawai fault zone and deformation of the Sumatran Forearc in the Nias area. In: R. Hall, D. Blundell (Eds.), *Tectonic Evolution of Southeast Asia*. Special Publications, vol. 106, Geological Society, London, pp. 337–351.
- Schlüter, H.U., Gaedicke, C., Roeser, H.A., Schreckenberger, B., Meyer, H., Reichert, C., Djajadihardja, Y., Prexl, A., 2002. Tectonic features of the southern Sumatra-western Java forearc of Indonesia. *Tectonics* 21(5), 1047. doi: [10.1029/2001TC901048](https://doi.org/10.1029/2001TC901048).
- Seeber, L., Mueller, C., Fujiwara, T., Arai, K., Soh, W., Djajadihardja, Y.S., Cormier, M.H., 2007. Accretion, mass wasting, and partitioned strain over the 26 Dec 2004 Mw9.2 rupture offshore Aceh, northern Sumatra. *Earth and Planetary Science Letters* 263(1-2), 16–31. doi: [10.1016/j.epsl.2007.07.057](https://doi.org/10.1016/j.epsl.2007.07.057).
- Sibuet, J.C., Rangin, C., Le Pichon, X., Singh, S., Cattaneo, A., Graindorge, D., Klingelhoefer, F., Lin, J.Y., Malod, J., Maury, T., Schneider, J.L., Sultan, N., UMBER, M., Yamaguchi, H., 2007. 26th December 2004 great Sumatra-Andaman earthquake: Co-seismic and post-seismic motions in northern Sumatra. *Earth and Planetary Science Letters* 263(1-2), 88–103. doi: [10.1016/j.epsl.2007.09.005](https://doi.org/10.1016/j.epsl.2007.09.005).
- Sieh, K., Natawidjaja, D., 2000. Neotectonics of the Sumatran Fault, Indonesia. *Journal of Geophysical Research* 105(B12), 28,295–28,326. doi: [10.1029/2000JB900120](https://doi.org/10.1029/2000JB900120).
- Soh, W., 2006. Seismic and Tsunami Tectonics of 26th Dec. 2004 Sumatra-Andaman Clarified in the Urgent Study. *Blue Earth Special Issue* 1, 14–17.

- Susilohadi, S., Gaedicke, C., Erhardt, A., 2005. Neogene structures and sedimentation history along the Sunda forearc basins off southwest Sumatra and southwest Java. *Marine Geology* 219(2-3), 133–154. doi: [10.1016/j.margeo.2005.05.001](https://doi.org/10.1016/j.margeo.2005.05.001).
- Tappin, D., McNeill, L., Henstock, T., Mosher, D., 2007. Mass wasting processes - offshore Sumatra. In: V. Lykousis, D. Sakellariou, J. Locat (Eds.), *Submarine Mass Movements and Their Consequences. Advances in Natural and Technological Hazards Research*, vol. 27, Springer Netherlands, pp. 327–336. doi: [10.1007/978-1-4020-6512-5_34](https://doi.org/10.1007/978-1-4020-6512-5_34).
- van der Werff, W., 1996. Variation in forearc basin development along the Sunda Arc, Indonesia. *Journal of Southeast Asian Earth Sciences* 14(5), 331–349. doi: [10.1016/S0743-9547\(96\)00068-2](https://doi.org/10.1016/S0743-9547(96)00068-2).
- Wessel, P., Smith, W., 1991. Free software helps map and display data. *Eos, Transactions American Geophysical Union* 72(41), 441. doi: [10.1029/90EO00319](https://doi.org/10.1029/90EO00319).

Figure Captions

Figure 1:

Bathymetric map off northern Sumatra. Lines indicate positions of seismic sections (Figs. 3-10), boxes of detailed bathymetry (Fig. 2). Land image is derived from SRTMv2 data, light bathymetric background from the GEBCO One Minute Grid. The inset shows the regional tectonic setting of the Sumatran subduction zone. IFZ = Investigator Fracture Zone. Sumatran Fault Zone (SFZ), Mentawai Fault Zone (MFZ), Batee Fault (BF), West Andaman Fault (WAF) and deformation front are based on Sieh and Natawidjaja (2000). Ages of the oceanic crust are after Müller et al. (1997) and Deplus et al. (1998) in million years. Gray arrows indicate relative plate movements based on NUVEL-1A (DeMets et al., 1994), black arrows based on CGPS (Prawirodirdjo and Bock, 2004).

Figure 2:

Detailed bathymetric maps of the study area. Letter order is from NW to SE (note different scale of maps). See Fig. 1 for location of maps and color scale.

A: Aceh Basin. The West Andaman Fault (WAF) is a mainly linear feature with subordinate faults branching off both into the forearc basin and outer arc high.

B: Southern Aceh- and northern Tuba Basins. The Tuba Ridge connects the West Andaman Fault and Mentawai Fault Zone (MFZ) through a left-hand step-over. A right-lateral strike-slip fault cuts the outer arc high resulting in extrusion of the northern Tuba Basin.

C: Southern Tuba- and northern Simeulue Basins. The Mentawai Fault Zone developed a positive flower structure separating the basins. The Tuba Basin is tilted eastwards by uplift along a thrust fault at the western boundary.

D: Western Simeulue Basin and part of Simeulue Island. Sigmoidal shaped anticlines indicate the main line of the Mentawai Fault Zone on the eastern shelf off Simeulue Island. Normal faults with SW-NE strike are located at the crest of a semicircular uplifted area.

E: Southwestern Simeulue Basin. The transition of the outer arc high to the basin is characterized by wrench-fault related anticlines.

Figure 3:

MCS profile across the central Aceh Basin. Older sediments (A) are tilted westwards and the depocenter moved trenchward (B). The inset illustrates the typical expression of the West Andaman Fault (WAF) in the Aceh segment. See Fig. 1 for location of profile.

Figure 4:

MCS profile across the southern Aceh Basin. Older basin sediments (A) are uplifted and deformed by the West Andaman Fault (WAF), leaving little sedimentation space for Sequence B. See Fig. 1 for location of profile.

Figure 5:

MCS profile covering the southern Aceh Basin, Tuba Ridge and northern Tuba Basin. Older sediments of the northern Tuba Basin belonged to the depocenter of the Aceh Basin before the formation of the Tuba Ridge. Sediment echosounder data (inset) show tear of youngest sediments due to extrusion. See Fig. 1 for location of profile.

Figure 6:

A: MCS profile from the West Andaman Fault (WAF) to the Sumatran Fault Zone (SFZ). Sediments of sequence A are deformed by an older strike-slip fault. The depocenter of the Aceh Basin moved westward over time.
B: Single-channel seismic profile located on the eastern slope of the Aceh Basin showing the non-active strike-slip fault. See Fig. 1 for location of profiles.

Figure 7:

MCS profile across the central part of the Tuba Basin perpendicular to the main axis of the basin. A thrust fault uplifting and tilting the western part of the basin is clearly imaged. Sediments are deformed by reverse faults due to tilting. See Fig. 1 for location of profile.

Figure 8:

MCS profile covering the southern Tuba- and northwestern Simeulue Basins. In between, the Mentawai Fault Zone (MFZ) developed a positive flower structure. The Tuba Basin is sediment starved and more than 300 m deeper than the Simeulue Basin. An eastward inclined buildup-structure indicates uplift along a thrust fault tilting the Tuba Basin and resulting in compression and reverse faulting. See Fig. 1 for location of profile.

Figure 9:

MCS profile across the western part of the Simeulue Basin parallel to the main axis of the basin. The Mentawai Fault Zone (MFZ) is developed as a positive flower structure. An anticline with normal faulting at the crest indicates recent uplift (inset with sediment echosounder data). Note the "double" BSR in the uplifted region. See Fig. 1 for location of profile.

Figure 10:

MCS profile covering the southwestern part of the Simeulue Basin and adjacent outer arc high. Alternating intensity of wrench faulting is documented by interfingering sedimentary packages caused by changing direction of sediment supply. The inset with sediment echosounder recordings illustrates recent uplift of youngest sediments. The solid line marks the initiation of the easternmost wrench fault. See Fig. 1 for location of profile.

Figure 11:

Tectonic structures in the working area. WAF = West Andaman Fault; SFZ = Sumatran Fault Zone; BF = Batee Fault; MFZ = Mentawai Fault Zone; TR = Tuba Ridge. The northern branch of the Mentawai Fault Zone jumped westwards to the position of the West Andaman Fault. A transpressional step-over formed the Tuba Ridge. A right-lateral strike-slip fault runs from the conjunction of the West Andaman Fault and Tuba Ridge in SSW-direction crossing the outer arc high, resulting in extrusion of the Tuba Basin which is tilted eastwards by uplift along a thrust fault.

Figure 1:

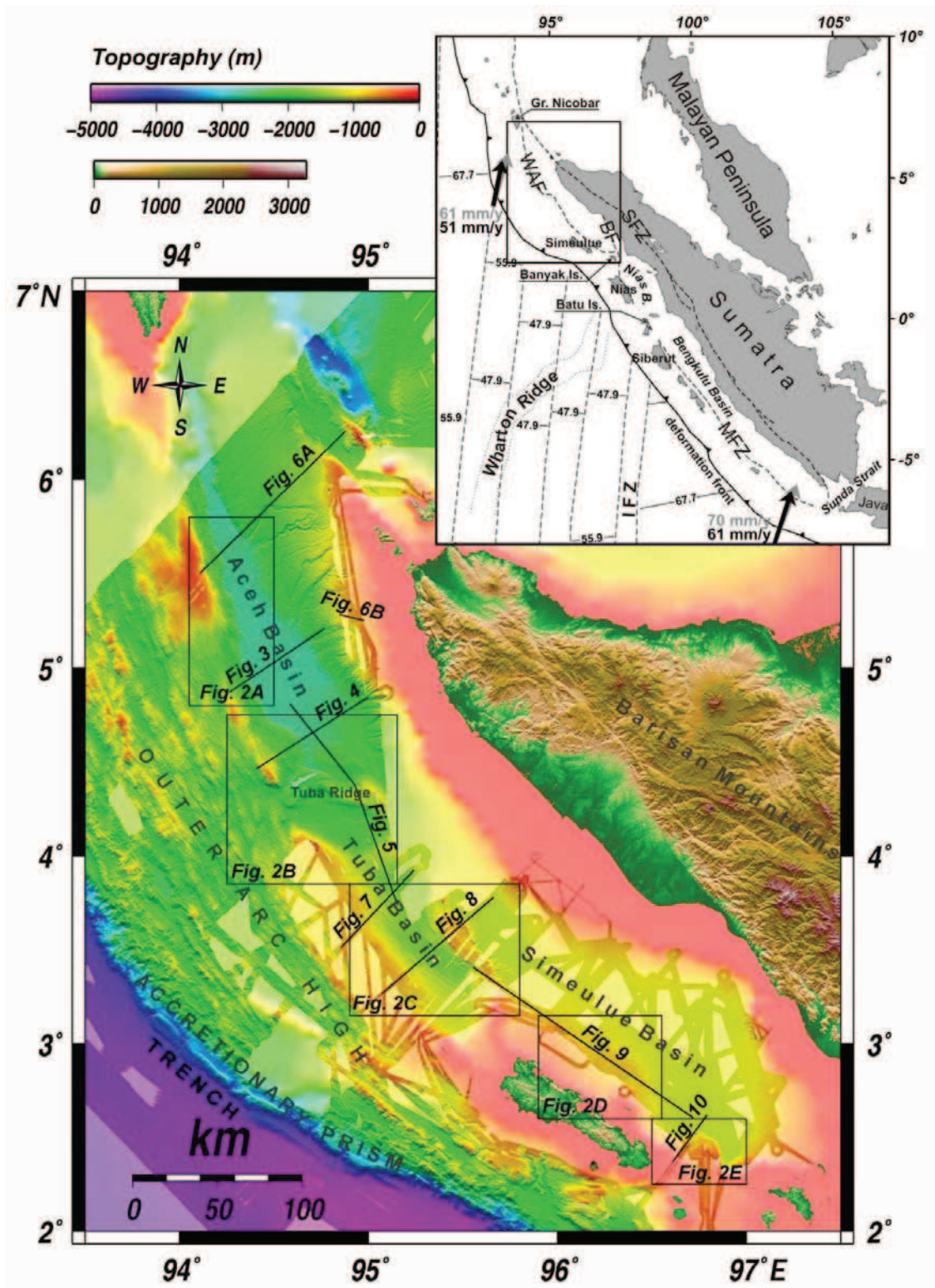


Figure 2:

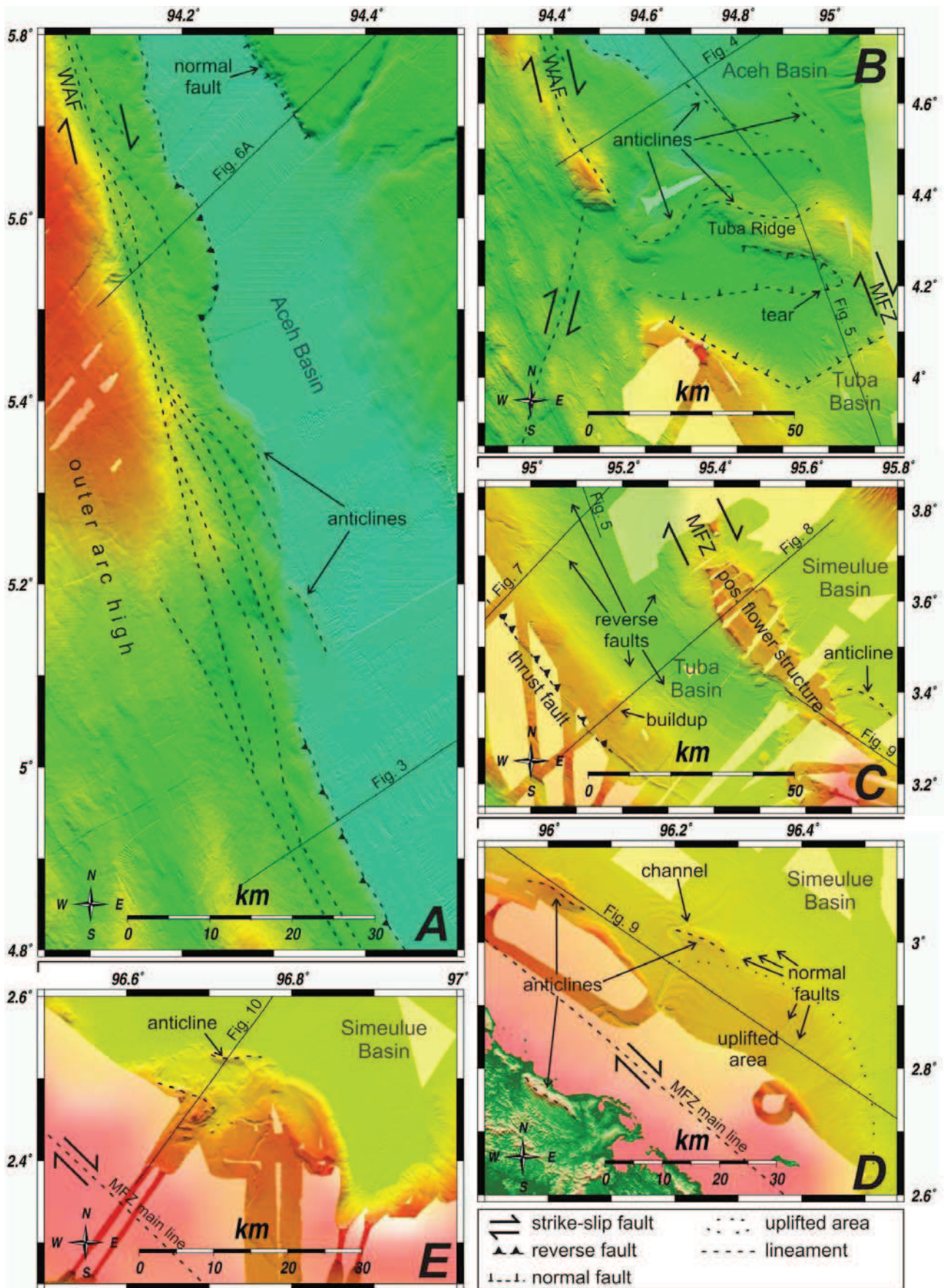


Figure 3:

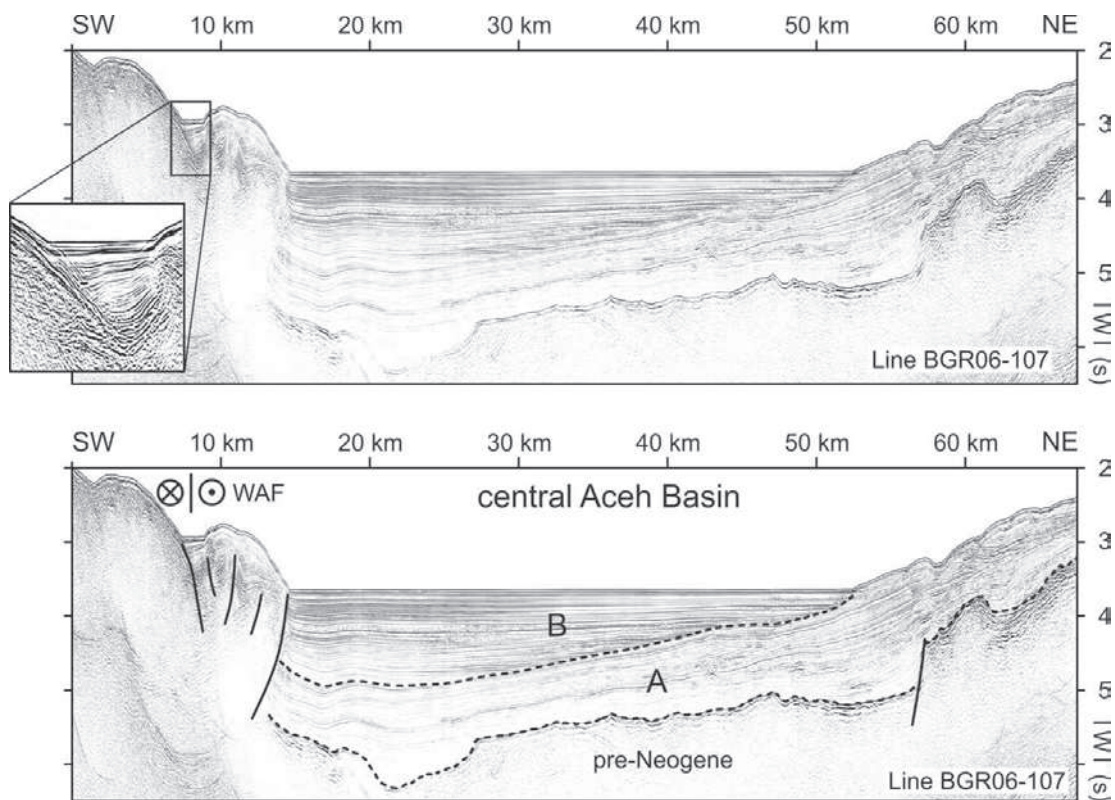


Figure 4:

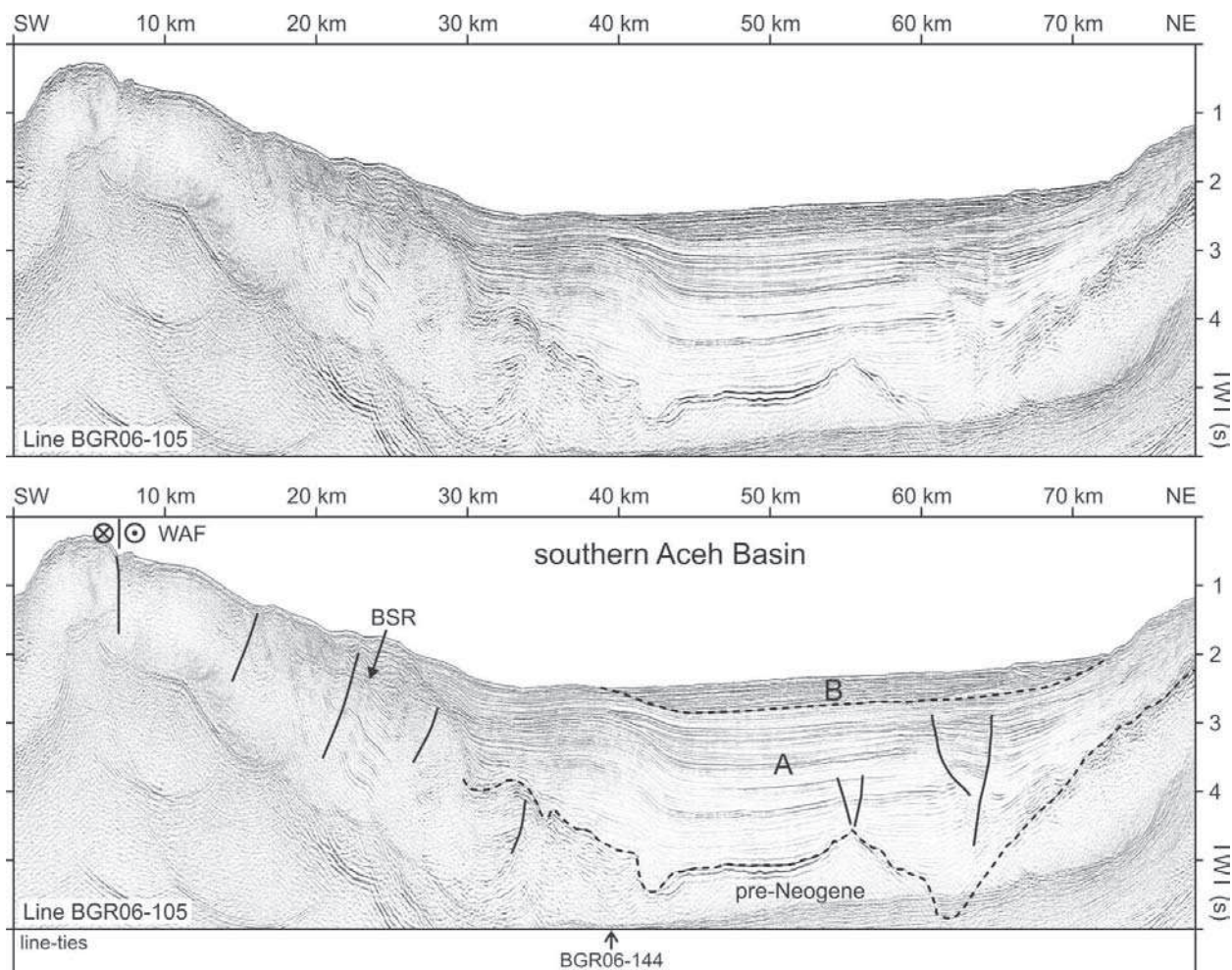


Figure 5:

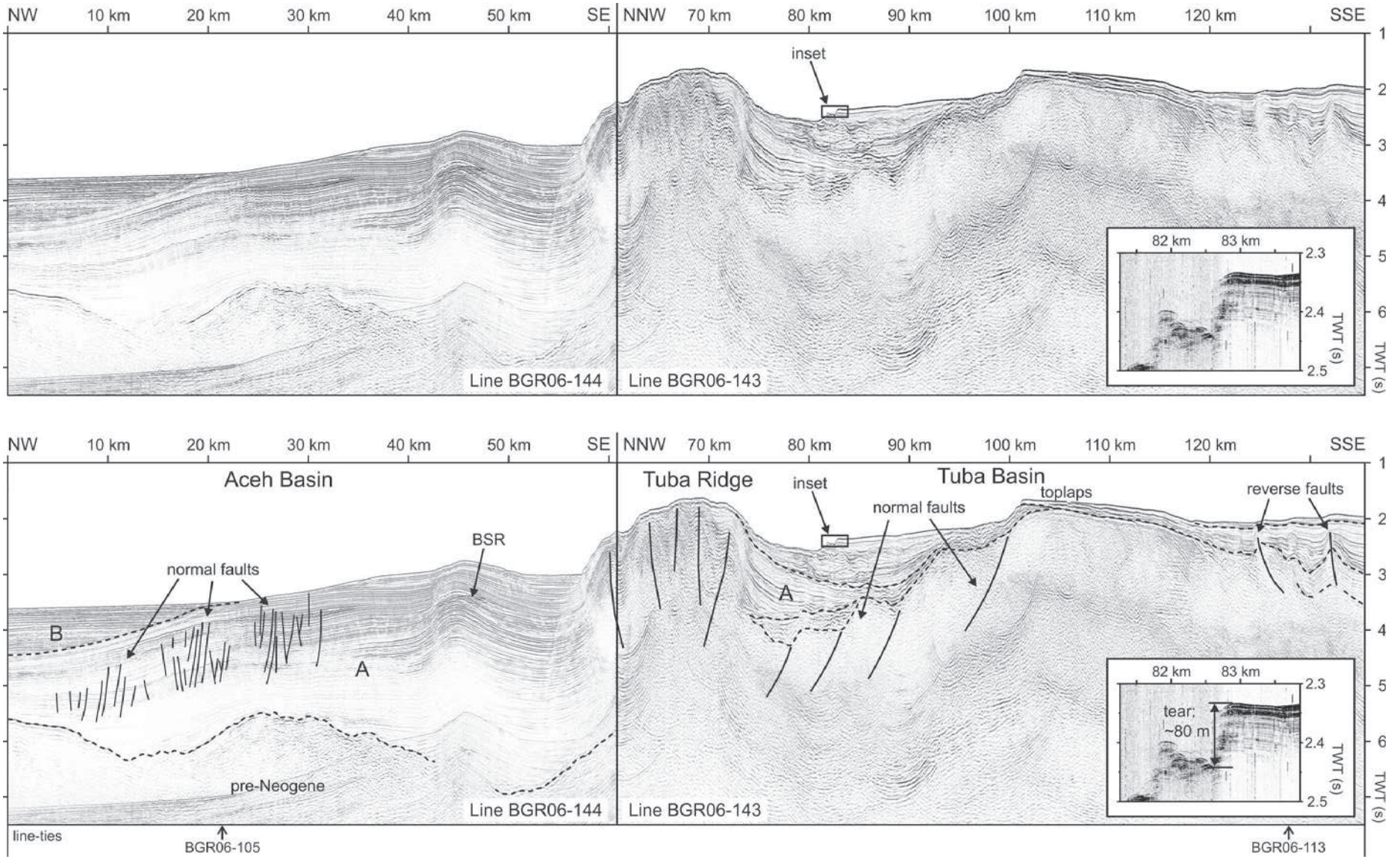


Figure 6:

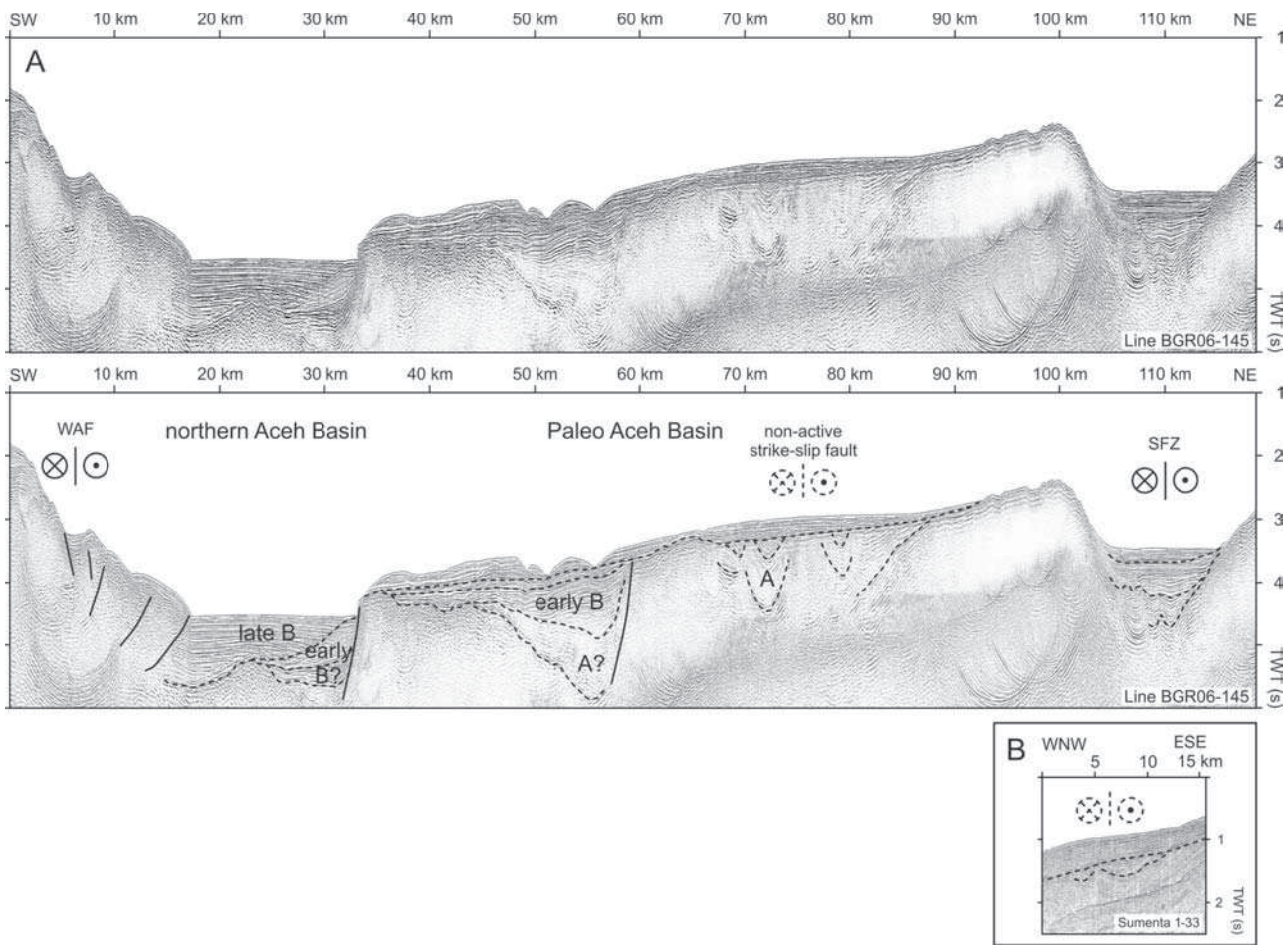


Figure 7:

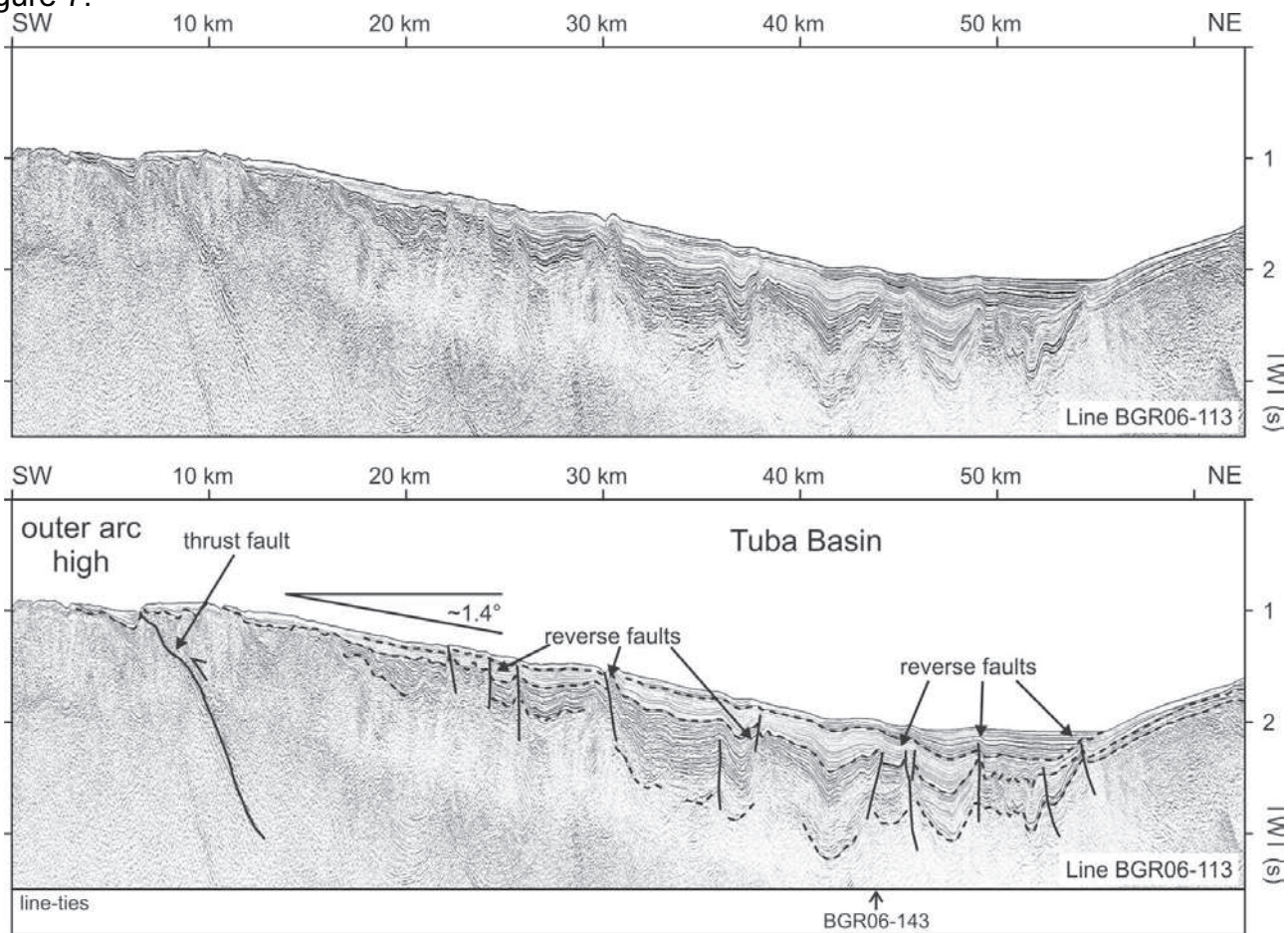


Figure 8:

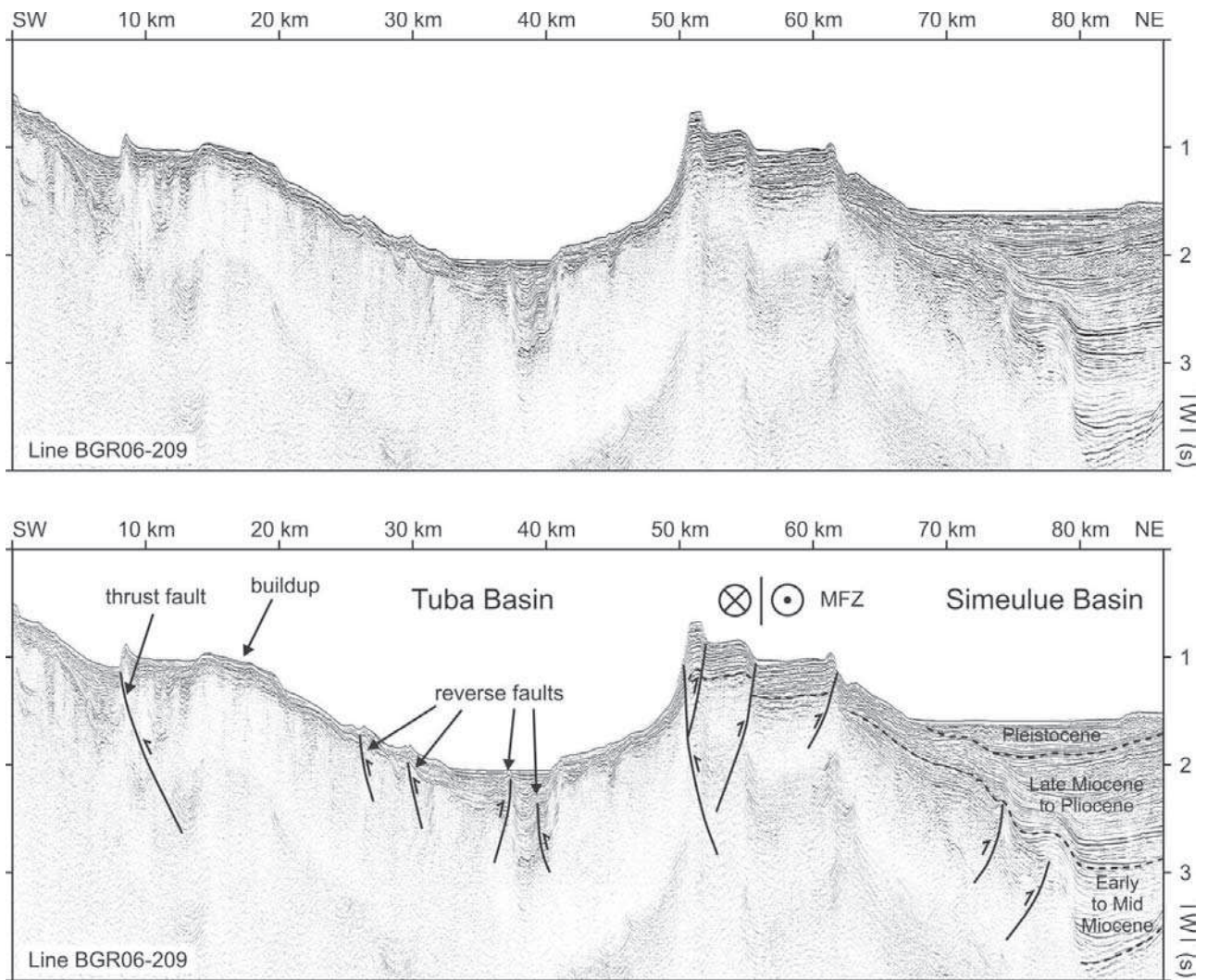


Figure 9:

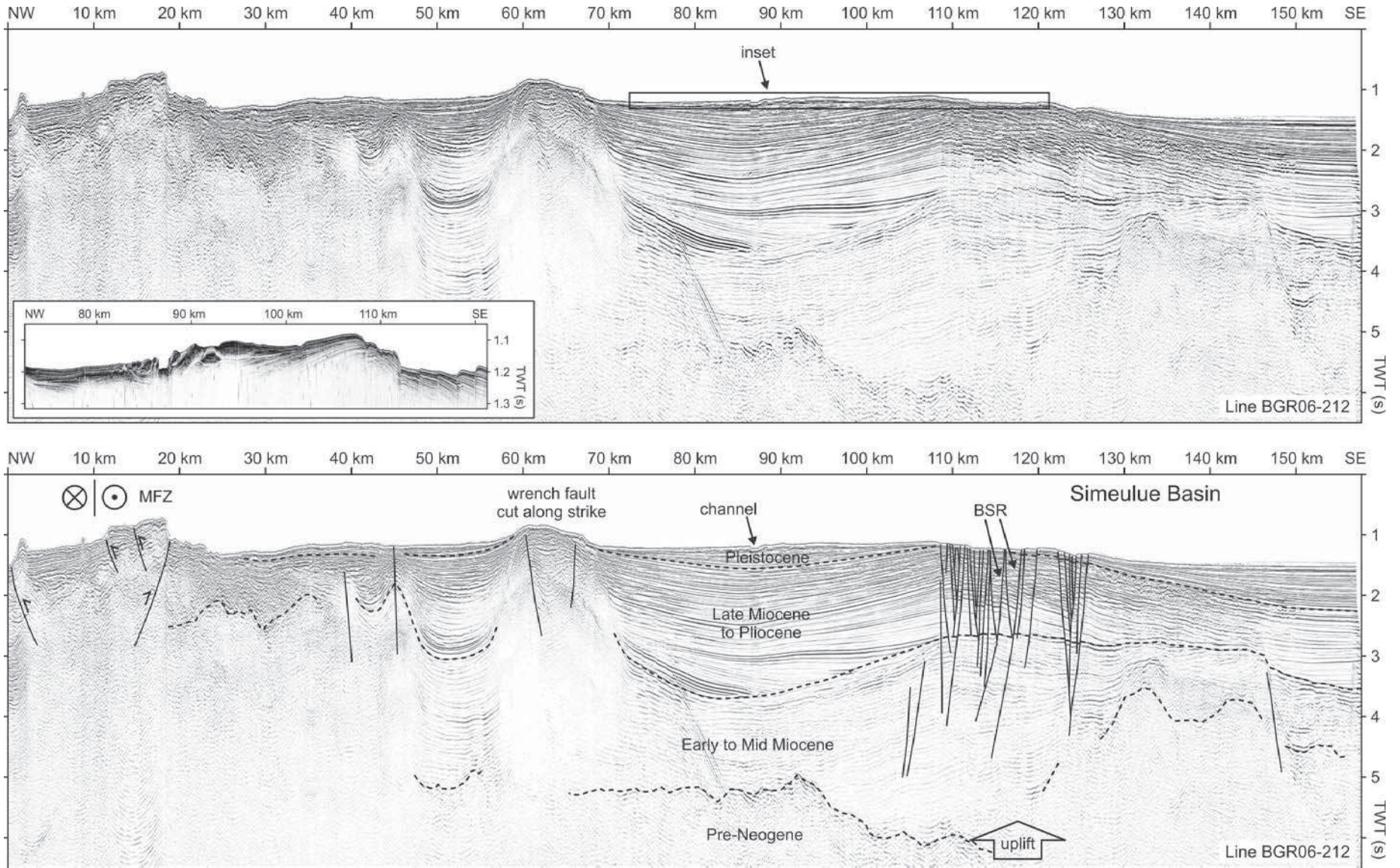


Figure 10:

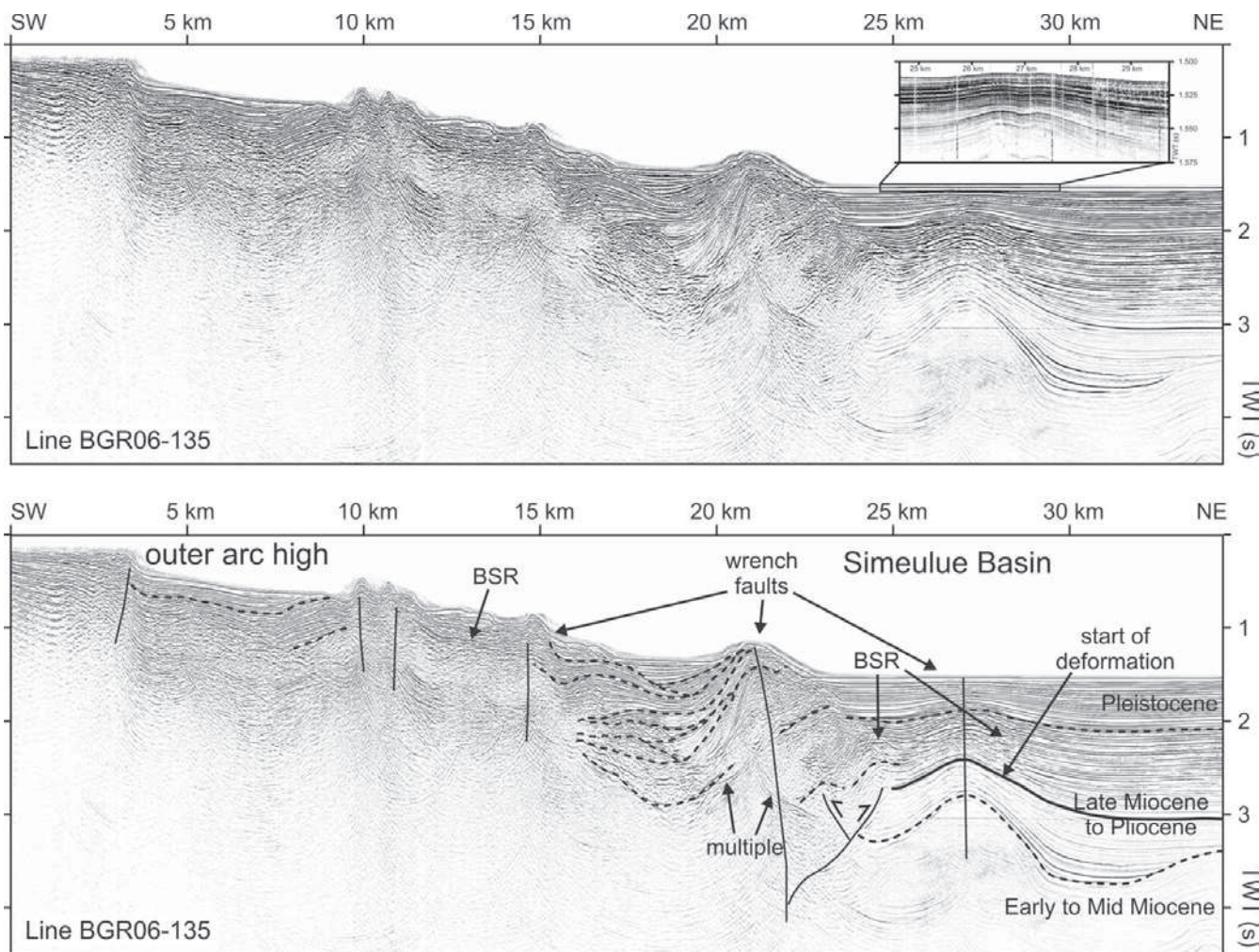
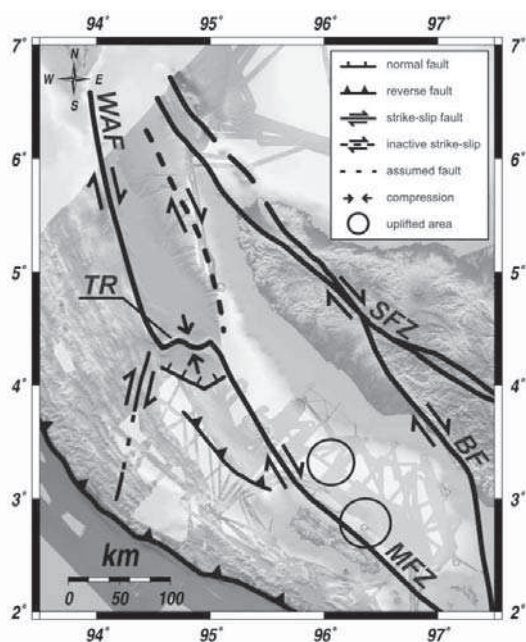


Figure 11:



Publikation

- * Lutz, R., Gaedicke, Chr., Berglar, K., Schlömer, S., Franke, D., Djajadihardja, Y. (eingereicht). Petroleum Systems of the Simeulue Forearc Basin off Sumatra, Indonesia: AAPG Bulletin (eingereicht 09.2008)

Petroleum Systems of the Simeulue Forearc Basin off Sumatra, Indonesia

AUTHORS

Rüdiger Lutz

Bundesanstalt für Geowissenschaften und Rohstoffe (BGR), Stilleweg 2, 30655 Hannover, Germany; ruediger.lutz@bgr.de

Christoph Gaedicke

Bundesanstalt für Geowissenschaften und Rohstoffe (BGR), Stilleweg 2, 30655 Hannover, Germany; christoph.gaedicke@bgr.de

Kai Berglar

Bundesanstalt für Geowissenschaften und Rohstoffe (BGR), Stilleweg 2, 30655 Hannover, Germany; kai.berglar@bgr.de

Stefan Schlömer

Bundesanstalt für Geowissenschaften und Rohstoffe (BGR), Stilleweg 2, 30655 Hannover, Germany; stefan.schloemer@bgr.de

Dieter Franke

Bundesanstalt für Geowissenschaften und Rohstoffe (BGR), Stilleweg 2, 30655 Hannover, Germany; dieter.franke@bgr.de

Yusuf S. Djajadihardja

Agency for the Assessment and Application of Technology (BPPT), Jl. M. H. Thamrin No. 8, Jakarta 10340, Indonesia; iyung@ceo.bppt.go.id

ACKNOWLEDGMENTS

The research projects were carried out with grants 03G0186A (SeaCause) and 03G0189A (SUMATRA) of the Federal Ministry of Education and Research (BMBF), Germany.

We thank all colleagues who made this work possible through organization data acquisition and processing. In particular we thank the ship's masters L. Mallon and O. Meyer and the crews of FS SONNE during the SeaCause and SUMATRA cruises.

ABSTRACT

Forearc basins develop as a result of plate subduction and are situated offshore between an outer-arc high and the main land. So far these regions are not

considered as important petroleum provinces because low heat flow does not necessarily support relevant petroleum generation.

The Simeulue forearc basin extends between Simeulue Island and northern Sumatra. Multichannel seismic data show bright spots above potential hydrocarbon reservoirs in carbonate platforms. AVO/AVA analyses indicate the presence of gas in sediments. Surface geochemical prospecting suggests thermal hydrocarbon generation within deep sediment strata. Heat flow in the Simeulue Basin ranges between 40 mW/m^2 and 60 mW/m^2 deduced from 1-D petroleum systems modeling and bottom-simulating reflector depths. Two source rocks (Eocene and Early-Middle Miocene) were assumed for 3-D petroleum systems modeling in the Simeulue Basin. Calculated heat flow scenarios (40 mW/m^2 and 60 mW/m^2 , respectively) reveal that hydrocarbon generation is possible in the main depocenters of the central and southern Simeulue Basin. In the model with the higher heat flow the carbonate buildups were charged with oil and gas.

This study shows that deep burial of source rocks can compensate for low heat flow and each forearc basin should be studied carefully to evaluate its hydrocarbon potential. Consequently, forearc basins may become areas of future oil and gas exploration and production.

INTRODUCTION

The discovery and exploration of new hydrocarbon reservoirs in classical rifted sedimentary basins becomes increasingly difficult which brings unconventional geologic settings into the focus of the hydrocarbon industry. Due to the generally low heat flow in forearc basins their hydrocarbon potential is believed to be low. Oceanic crust cools with age and increasing distance to the mid-oceanic ridge, where it was produced. The cold oceanic crust subducts at continental margins and reduces the

heat flow beneath the forearc basin. Heat flow is typically further reduced by high sediment input from the volcanic arc and the adjacent continent. Heat flow values of forearc basins range between 20 mW/m² and 45 mW/m² with a typical value of 40 mW/m² (Allen and Allen, 1990; Dickinson, 1995).

On the other hand forearc basins are located at almost all convergent continental margins between the deep sea trench and the magmatic arc. Active margins occupy some 44000 km (Von Huene and Scholl, 1991) mainly around the Pacific Ocean, but also along the Indonesian Island Arc, in the Caribbean, the Mediterranean, and the Arabian Sea. The widespread occurrence of this basin type makes it worth to study forearc basins in detail and decipher their hydrocarbon potential.

Forearc basins may overlay both continental crust and/or accreted rocks. Commonly they are bounded seawards by an outer-arc high that is part of the accretionary prism. The tectonic evolution of forearc basins is controlled by the subduction of an oceanic plate. Important factors controlling the basin dynamics are convergence rate, dip angle of the oceanic plate, obliquity of convergence, roughness and sedimentary cover of the oceanic crust, and the sedimentary input of the landward magmatic arc and continent. Forearc basins have an elongated shape extending parallel to the trench-arc system. Their width commonly ranges between 25 and 125 km, but their length may reach 500 km (Busby and Ingersoll, 1995). Typical forearc basins are the Southwest Java basin in the central part of the Indonesian Island arc that is up to 150 km wide and 325 km long containing about 6.5 km of sediments, and the 275 km long and 75 km wide Tofino Basin off British Columbia (Busby and Ingersoll, 1995). We present a study of the hydrocarbon potential of the Simeulue forearc basin off northern Sumatra. Based on multi-channel seismic data, originally acquired to study the area of the 26th December 2004 earthquake, well and gas-geochemical data, we

established a conceptual model of the basin evolution and we applied petroleum systems modeling to assess the hydrocarbon potential of that basin.

GEOLOGIC SETTING

The Sumatra-Java area is part of the Sunda Arc that stretches from the Andaman Sea in the northwest to the Banda Sea in the east. Along the Sunda Arc the Indo-Australian Plate subducts under the Eurasian Plate. The studied area (Figure 1) is a classical example of a subduction system, composed of the downgoing Indo-Australian slab along the Sumatra trench, an accretionary wedge, the outer-arc ridge emerging above sea level with the Simeulue Island (Pubellier et al., 1992; Samuel and Harbury, 1996), and the Simeulue forearc basin off Sumatra in front of the volcanic arc. Convergence along the Sunda Arc becomes increasingly oblique from south to north resulting in large-scale, dextral strike-slip fault systems within the forearc basins and on Sumatra (Malod and Kemal, 1996; Sieh and Natawidjaja, 2000).

The western Indonesian fore-arc basins extend for more than 1800 km from northwest of Aceh to southwest Java. The width of the basins varies from less than 70 km to the south of the Sunda Strait to about 120 km in the west off northern Sumatra. The basins form a strongly subsiding belt between the elevated Sumatra Paleozoic-Mesozoic arc massif cropping out along Sumatra and Java, and the rising outer-arc high (Karig et al., 1980; Schlueter et al., 2002; Susilohadi et al., 2005).

The Simeulue forearc basin is bounded to the west by Simeulue Island. The Banyak Islands separate the Simeulue Basin from the southerly located Nias forearc basin.

The northern end of the Simeulue Basin is formed by a ridge-like structure and a change in water depth of more than 1500 m (Izart et al., 1994) forming the transition to the Aceh Basin. The Simeulue Basin itself is trench-parallel elongated and extends

over 260 km in NW-SE direction and 100 km in SW-NE direction. It contains a Neogene sedimentary fill of up to 5 s two-way traveltime (TWT) and consists of a deep water area with a maximum water depth of about 1300 m (Figure 2) followed to the east by the basin slope and the shallow water inner shelf at the transition to the Sumatra mainland (Berglar et al., 2008). The Simeulue Basin is virtually unexplored in a petroleum geologic context. Few wells were drilled in the 1970ies along the northern shelf in water depths less than 100 m (Rose, 1983). Three wells encountered uncommercial quantities of gas. Isotopic data on gas composition is, to our knowledge not published, but the fact that only methane is reported suggests a biogenic origin of this gas.

The geologic evolution of the Simeulue Basin shows striking similarities to the evolution of the North Sumatra Basin (Figure 1) until the Early Miocene. North-south orientated horsts and grabens developed in the North Sumatra Basin during the Late Eocene rifting phase. A subsequent Late Oligocene-Early Miocene basin sag phase resulted in widespread carbonate deposition and reef growth (Clure, 2005). Initiation of wrench tectonic in the Mid-Miocene leads to uplift of the Barisan Range and separates the North Sumatra Basin from the forearc region including the Simeulue Basin. Ongoing compression since the Plio-Pleistocene formed the coastal fold belt of Sumatra (Clure, 2005).

In the present day back-arc area of Sumatra several prolific petroleum systems exist (e.g. Cole and Crittenden, 1997; Schiefelbein and Cameron, 1997). Oils in the North Sumatra Basin were generated from terrigenous or marine source rocks; biomarkers indicative for both environments were found in oil samples (Schiefelbein and Cameron, 1997). The Central Sumatra Basin (Figure 1) is the most prolific petroleum system with the lacustrine oil-prone Brown Shale Fm. as source rocks (Clure, 2005; Peters et al., 2005). The source rocks of both basins are of Eocene-Oligocene age.

Several coal seams of Oligocene, Miocene and Pliocene age are reported by Hadiyanto (1992). He studied eight offshore wells, 18 onshore wells (< 200 m depth) and several outcrop samples all of which are located west of the Barisan Range with some of them in the Simeulue Basin.

METHODS

During two marine surveys in 2006 carried out with the German RV SONNE a comprehensive dataset of some 9000 line km of multi-channel seismic (MCS) data was acquired coincident with high resolution sediment echo-sounding, bathymetry, gravity and magnetics data. The survey extends from the Mentawai forearc basin in the south to the northern tip of Sumatra. A total of 1500 line km were collected in the Simeulue Basin (Figure 2). MCS data were acquired with a 240 channel, 3 km streamer (towing depth: 6 m; offset to near group: 150 m; maximum offset: 3137.5 m), and a tuned airgun array comprising 16 airguns with a total capacity of 50.8 l (14.5 MPa). Record length was 14 s with a sample rate of 2 ms. A shot interval of 50 m resulted in a fold of 30. Detailed description of processing flow in Berglar et al. (2008).

Heat flow values derived from the depth of bottom simulating reflectors (BSRs) were calculated using the equation $Q = \lambda \cdot \text{grad}(t)$ with $\text{grad}(t) = (T_{\text{bsr}} - T_{\text{sf}}) / (D_{\text{bsr}} - D_{\text{sf}})$.

Interpreted BSRs were converted from TWT to depth (D_{bsr}) using a velocity profile derived from wide angle reflection seismic in the southern Simeulue Basin. Depth of the seafloor (D_{sf}) was calculated assuming a sound speed in water of 1500 m/s.

Temperature at BSR depth (T_{bsr}) was then determined with a water-methane phase diagram (Kvenvolden and Barnard, 1982). Water temperature at the seafloor (T_{sf}) was obtained from CTD-measurements for depths down to 1100 m, for greater depth

we assumed a temperature of 1 °C. For lambda we used a published value of 1.23 W/(m*K) from Delisle and Zeibig (2007).

Basin modeling or petroleum systems modeling is used to reconstruct the evolution of a sedimentary basin based on physical and chemical laws (e.g. Welte and Yücker, 1981; Tissot et al., 1987). The modeled geologic history of a basin delivers information on its thermal evolution, generation, migration and accumulation of hydrocarbons. Principles and limitations of the calculated models have been described by various authors (e.g. Ungerer et al., 1990; Hermanrud, 1993; Yalcin et al., 1997). The technique can be applied to sedimentary basins at all stages of exploration, from unexplored/frontier basins to very mature basins (e.g. Karlsen et al., 2004; Struss et al., 2008; Underdown and Redfern, 2008).

Surface geochemical exploration methods aim at surface alterations or indications related to past or active micro-seepage of subsurface hydrocarbons towards the surface. Thus positive indications of a hydrocarbon accumulation or, at least an active petroleum system, can support frontier basin evaluation or prospect ranking. Analysis of vertical migrated hydrocarbons (both oil and gas) reveals information about the type and maturity of potential source rocks. However, neither reservoir depth nor the amount of hydrocarbons present can be determined.

Sediment samples for hydrocarbon analysis were collected from cores taken with gravity (SL) and piston (KL) corers as well as samples from multicorers (MUC). Typically one sample for geochemical analysis was taken from the base of the core or core catcher and, if possible, at least one in the upper part of the core (typically 2 m above core catcher). At several sites additional sediment samples were taken from the lowermost part of a multicorer (typically 0.3-0.4 m depth). In total 26 samples from 15 sites in the Simeulue Basin were taken, furthermore 9 samples were taken from 5 sites located at two distal reference locations on the outer-arc high

(140KL, 142KL, 139MUC southeast of Simeulue Island and 115KL, 116KL northwest of Simeulue Island, Figure 2 & Table 1). Certainly the number of samples is not adequate for a detailed basin evaluation, but it can indicate whether an active petroleum system is present in this forearc basin or not.

Sediment samples were degassed aboard according to the technique described by (Faber and Stahl, 1983). This technique allows analysing composition and isotope ratios of hydrocarbons adsorbed in sediment samples. About 100 to 150 g of wet sediment are placed in a vacuum apparatus and treated with phosphoric acid. The carbon dioxide liberated is fixed in KOH or NaOH-solution. The composition of desorbed hydrocarbons (methane through pentane) were evaluated without delay by means of a standard GC analysis (Shimadzu GC 14b, packed Poropak Q column (2 m, 1/8"), isothermal at an oven temperature of 115 °C). The remaining hydrocarbon gases were compressed and displaced into evacuated glass sampling tubes for later analysis of isotope composition (GC-irMS with FinniganMAT Delta Plus).

Concentrations of hydrocarbons are given in nano (10^{-9}) gram hydrocarbons per gram of dry sediment (ppb), carbon isotope data of methane in the standard delta notation versus PDB.

STRATIGRAPHY

Published data of exploration wells (Karig et al., 1979; Rose, 1983; Beaudry and Moore, 1985) drilled on the Sumatra shelf in the 1970ies (Figures 2, 3) provide the chronostratigraphic framework for calibration of our seismic horizons. Berglar et al. (2008) reviewed existing data and established a detailed seismic stratigraphy of our MCS data. The conceptual model of this study bases on the stratigraphy and results of Berglar et al. (2008), therefore we briefly summarize their findings and present the 3-D model of the Simeulue forearc basin evolution (Figure 4).

Three major unconformities separate four main units that are found in the entire Simeulue forearc basin.

Pre-Neogene

The lowermost unconformity marks the top of the acoustic basement and separates the pre-Neogene from Miocene sediments. Some low-frequency, high-amplitude reflection bands are imaged below the unconformity. They either may be concordant to the unconformity or dip steeply. The acoustic basement is drilled in well Meulaboh-1 and consists of Eocene to Oligocene mudstone with minor interbeds of silt-sandstone (Rose, 1983; Beaudry and Moore, 1985).

Early and Middle Miocene

The Early to Middle Miocene succession shows parallel to sub-parallel continuous reflectors and concordantly overlies the basal Neogene unconformity with onlapping contacts. We attribute this seismic reflection pattern to clastic sediments. In well Meulaboh-1 this unit is described as nearshore marine and non-marine clastics. The thickness of the sediments reaches 3 s (TWT) in the deepest part of the forearc basin. On topographic highs of the acoustic basement several carbonate buildups developed on the paleo shelf (Figure 4, upper left). We distinguished three small basins developing along the western margin of the Simeulue Basin. They developed due to flexural subsidence caused by irregular load of the evolving accretionary prism (Matson and Moore, 1992; Berglar et al., 2008).

Late Miocene and Pliocene

A phase of rapid subsidence of the forearc basin center is marked by an unconformity that separates Middle Miocene from Late Miocene sediments (Figure 3). The onlapping contact of Late Miocene sediments is best imaged in the center of

the basin. The appearance of this sequence is similar to the one below the unconformity: high-amplitude low to moderate-frequency reflections are of high continuity. Along the former shelf break carbonate buildups developed again and are later buried by continuing sedimentation of clastic deposits. After consolidation and uplift of the outer-arc high the western part of the basin forms a subsiding elongated trough, while carbonate buildups develop on the shelf (Figure 4, lower left).

Pleistocene to Recent

The entire basin is draped with a cover of well stratified Pleistocene sediments reaching a thickness of 0.6 s (TWT). This sequence onlaps the Pliocene sediments at the basin fringe and reflects the present day depocenter (Figures 3, 4, lower right).

RESULTS

Our MCS data image several striking features in the Simeulue Basin which are highly relevant to our conceptual model.

Carbonate buildups

Miocene carbonate platforms are common in South-East Asia and form important petroleum reservoirs in the South China Sea e.g. Luconia Province, Malampaya and Pearl River Mouth Basin (Fournier and Borgomano, 2007). In the Simeulue Basin more than 30 carbonate buildups were identified. We recognize two phases of carbonate buildup evolution that are exemplarily imaged in Figure 5. The first phase took place after the formation of the pre-Neogene/Early Miocene unconformity. Only few buildups of this early phase are imaged in our seismic dataset. Commonly they have grown at highs of the pre-Neogene basement. The major phase of carbonate

buildup growth occurred after the development of the late Middle Miocene to early Late Miocene unconformity. Some carbonate buildups of the latter phase grew on top of the older buildups while others developed in shallow water areas between the paleo-shelf break and the shoreline. The top of the lower buildup (Figure 5) was eroded during the late Middle Miocene to early Late Miocene, whereas the basinward flank of the buildup is covered by Middle Miocene sediments. The buildups of the second phase are covered by Late Miocene to Recent sediments. We mapped 7 buildups of the first phase and 26 of the second phase.

Distinct high amplitude reflections are interpreted as the top and flanks of the carbonate buildups. In time-sections a distinct velocity pull-up at the base is well in accordance with the interpretation of high velocity carbonate rocks (Figure 5). Internal seismic reflectivity is generally weak but individual horizons are partially visible. The shape of the carbonate buildups varies. Some of them exhibit an asymmetrical geometry while others are developed as pinnacle reefs. The slopes are always steeper than the surrounding strata that onlap the flanks. Some buildups have a plateau-like top while others have an irregular uneven surface (Figures 5, 6). A chaotic seismic reflection pattern may occur at the shelfward side (Figure 5) which we interpret as consisting of reef debris, back reef and carbonatic shelf deposits. The reef debris sequence points at the carbonate platform interior.

The horizontal extent of the carbonate buildups along the 2-D seismic profiles varies between less than 1 km and more than 10 km. We crossed one carbonate buildup at different angles with lines BGR06-211 and BGR06-137 and measured an extension of 7.5 and 8.5 km, respectively. The thickness of the carbonate buildups is variably, too. Along line BGR06-135 (Figure 5) the maximum thickness of carbonate buildups was identified in our seismic data. That is 0.25 s (TWT) for the lower buildup and is 0.415 s (TWT) for the upper one.

The growth history of an individual buildup is shown in Figure 7. We adopt the evolutionary model for a carbonate buildup from Luconia to this buildup (Zampetti et al., 2004). The Late Miocene to Early Pliocene buildup has grown at the location of an Early to Middle Miocene buildup. Growth of the second buildup started in Late Miocene above the unconformity that separates the Middle Miocene from the Late Miocene. High amplitude, low frequency reflector bands are characteristic for the initial phase of platform growth (unit A on Figure 7). The aggradation phase is documented as the low reflectivity unit B. We interpret a wedge with low reflective, discontinuous reflection pattern as a lowstand wedge which implies a short relative sea level fall. High amplitude reflectors mark the change from aggradation to drowning (unit C), thus indicating a subsequent relative sea level rise. The growth of the buildup is accompanied by debris and platform deposits with chaotic reflection pattern in the vicinity of the buildup. The final phase of submergence and drowning is characterized by a chaotic, low reflective seismic pattern (unit D). Drowning of the buildup resulted in backstepping of units C and D. Progressive drowning is exhibited in onlapping of the surrounding strata. A transgressive cap terminates the drowning phase and the buildup is completely buried by sediments. At the steeper NNW flank of the buildup normal faults cut through the buildup. These faults may originate due to oversteepening and collapsing of the slope or by abundant earthquakes related to the subduction zone.

Bottom simulating reflectors

Bottom simulating reflectors (BSR) are common phenomena in multi-channel seismic profiles at continental margins. BSRs evolve at the base of the gas hydrate stability zone and mark the negative impedance contrast between pore space that is filled by hydrate and the underlying gas-charged sediments. The depths of BSRs are

controlled mainly by temperature, pressure and composition of the pore fluids (Pecher et al., 1998; Sloan, 1998). Another class of BSRs is caused by the diagenetic transition from opal A to opal CT (Berndt et al., 2004). Occurrences of BSRs are well constrained, where BSRs cut through dipping layers, but identification is difficult, where the layering of the sediments parallels the seafloor and therefore the BSRs.

The BSRs exhibit a clear negative polarity (negative acoustic impedance) compared to the seafloor reflection, indicating BSRs caused by free gas underneath the gas hydrate stability zone, and they cross-cut the sedimentary layering. We observe BSRs at several locations, especially in the southern part of the Simeulue Basin (Figure 9). Close to Simeulue Island we observe multiple BSRs, i.e. a succession of two (Figure 8) or up to five BSRs at different depths. The lower ones might be caused by mineralogical changes (Berndt et al., 2004). The upper BSR marks the current base of the gas hydrate stability zone (Popescu et al., 2006). This upper BSR occurs in the Simeulue Basin between 217 meters below seafloor (mbsf) and 642 mbsf at water depths between 831 m and 1157 m. The double BSRs on Figures 6 and 8 are separated by 70-80 ms (TWT). We derived heat flow values from BSR depths according to the method described above ranging from 37 mW/m² to 74 mW/m².

Bright spots

High reflective strong amplitude zones visible in reflection seismic profiles are often called bright spots. These zones are caused by changes of physical properties of the sediments. These changes indicate either a changing lithology (e.g. cementation) or changing fill of pore space (e.g. presence of gas or oil).

Exemplarily bright spots are shown in Figure 6, where they occur above carbonate buildups at depths between 1.8 and 2.1 s (TWT). The high-amplitude reflectors

extend over a distance of more than 40 km. Such reflectivity anomalies are recognized in particular above carbonate buildups in the study area. Above the northwestern carbonate buildup the bright spot is found in a gentle anticline. The other bright spots above the buildups occur in distinct layers which are probably constituted of coarser-grained sediments. At the north-western rim of the carbonate buildup on Figure 6 a bright spot is evident in sediments that onlap the toe of the carbonate buildup at a depth of 2.6 s (TWT). Above the south-eastern carbonate buildup a young fault system cuts from the buildup through the bright spot to the sea floor. No amplitude anomalies are observed along these faults indicating closed faults. Highest amplitudes of a bright spot are located above the carbonate buildup in Figure 8. The bright spot prolongs into south-westerly direction for about 8 km as a layer of parallel high amplitude reflectors and ascends within the inclined sediments from 1.9 s to 1.7 s (TWT) crossing the BSRs. Bright spots occur in the Simeulue Basin especially in the vicinity of the area with the highest sediment thickness. Carbonate buildups and bright spots are marked in Figure 9.

AVO-ANALYSIS

Amplitude versus Offset (or Angle) studies (AVO/AVA) are commonly used to detect gas- or oil-bearing sediments. Here, we performed a reconnaissance AVO/AVA analysis including analyses of the seismic data for amplitude variations, creating near- and far-offset stacks and picking and displaying the amplitudes of selected CDP gathers. We had no constraints from wells.

The quality of the input seismic data is crucial for any AVO result. We thus carefully selected the processing parameters and tried to apply as little processing steps as

possible. The excellent quality of the field data was very helpful with regard to this procedure. Processing was done with a commercial package of seismic data processing software (ProMax-2D). The raw data were smoothly bandpass filtered (zero-phase; 4-8-80-160 HZ) and a zero-phase spiking deconvolution was applied (40 ms operator length; white noise: 0.1; decon gates: water-bottom relative ~1.0 s). Extensive testing resulted in a time and offset variant gain function that mainly based on carefully selected stacking velocities. Applied was a combination of a spherical divergence correction to compensate for loss of amplitudes based on waveform spreading plus a receiver and source array correction to compensate filtering effects of both the source and the receiver array (offset amplitude correction). A NMO correction with zero-percent stretch mute using stacking velocities finalized the processing sequence. We skipped a DMO/Pre-stack migration, because the area under study is structurally uncomplex, as well as a multiple attenuation, because the water-bottom multiples appear much later in the data than the reflections of interest. In the following we describe the results of the AVO analysis procedure for the seismic section BGR06-139 (CDPs 20000-28000). The maximum offset in the data was 3137.5 m and the water depth about 1100 m (~1450 ms (TWT)). The target depth was about 1950 ms (TWT). Although the reflections are not perfectly flat, distinct higher amplitudes are observable at a depth of 1900-1950 ms (TWT) (Figure 6). This becomes more obvious in offset dependent stacks. Figure 10 shows range-limited stacks from a part of line BGR06-139 (CDPs 21000-22000). While the sea bottom at a depth of ~1500 ms (TWT) is merely unchanged the reflections at about 1900-2000 ms (TWT) depth show high amplitudes in the far-offset stack (Figure 10; bottom).

Figure 11 shows an example CDP from seismic line BGR06-139. The upper image shows the raw amplitudes in the depth range from 1880 to 2020 ms (TWT).

Particularly interesting is the reflection at ~1930 ms (TWT) depth that shows a pronounced increase in negative amplitudes with offset. The fact that the reflection is not flat, i.e. the average velocities are too high, may also suggest gas-bearing sediments at this location. The picked raw amplitudes increase from ~12 to ~25 as shown in the panel below the seismic section. The lower image in Figure 11 shows the same CDP but a wider depth area, ranging from 1300 to 2300 ms (TWT). Most reflections show decreasing amplitudes with increasing offset, indicating that the parameters for amplitude corrections during processing were not chosen too high. However, the interpreted gas sand reflection at ~1930 ms (TWT) shows increasing amplitudes and a phase reversal compared to the waterbottom reflection. The amplitudes normalized to those of the waterbottom reflection (Figure 11; below the lower seismic section) increase with offset from 0.4 to 1.5.

From these observations we conclude that the observed bright-spots have negative AVO intercept and gradient. We interpret the anomalies to be caused by gas sands that are classical class 3 anomalies (Rutherford and Williams, 1989; Ross and Kinman, 1995). These sands exhibit the amplitude increase versus offset which is commonly used as a gas indicator.

GEOCHEMISTRY

Methane concentrations of samples from the Simeulue Basin range from 27 ppb to 512 ppb, ethane and propane from 2 ppb to 14 ppb and 1 ppb to 7 ppb, respectively. A linear correlation between ethane and propane concentration can be observed (Tab. 1). $\delta^{13}\text{C}$ isotopic composition of methane ranges, with the exception of two samples, generally between -27.8‰ and -68‰ (Figure 12). Two samples reveal unusually heavy carbon isotopes, 112MUC -16.4‰ and 113SL -15.1 ‰.

Three samples from reference cores 140KL and 142KL show methane concentrations higher than 10000 ppb, the concentrations of the remaining samples from the reference sites (82 ppb to 277 ppb) are within the range for adsorbed methane in the Simeulue Basin. All cores of the reference sites exhibit similar ethane and propane concentrations (8 ppb-20 ppb and 4 ppb-12 ppb, respectively) and are comparable to the samples from the Simeulue Basin. The carbon isotopic composition of methane ranges between -91.1‰ and -28.4‰. Isotopic composition of ethane and propane could not be measured due to the low yields of these components.

CONCEPTUAL MODEL

We derive a conceptual model to integrate the results from seismic stratigraphy, bright spot and BSR occurrences as well as AVO-analysis and organic geochemistry. In our conceptual model we assume source rocks for oil and gas at two stratigraphic levels; namely an Eocene marine source rock within the acoustic basement and an Early to Middle Miocene terrigenous source rock. The upper part of the acoustic basement was drilled at wells Meulaboh-1 and Tuba-1A and consists of Eocene/Oligocene clastic sediments (Rose, 1983), indicating sediments in the upper portion of the acoustic basement.

During basin subsidence and burial of the source rocks hydrocarbon generation took place in the deep Neogene depocenter. Subsequent expulsion and migration of the hydrocarbons occurred and parts of these hydrocarbons accumulated in the Miocene carbonates which serve as reservoir rocks. Figure 13 depicts the main elements of the conceptual model. The bright spots within the Late Miocene to Early Pliocene sediments (NW of depocenter) might be caused by thermally generated hydrocarbon

gas. The bright spots above the carbonate buildups may be related to hydrocarbon gas that passed the carbonates or to leaking reservoirs in the buildups. The Pliocene clastic sediments form the seal above the Late Miocene carbonate buildups.

PETROLEUM SYSTEMS MODELING

1-D modeling

Close to the coast in water depth of mainly less than 200 m several exploration wells were drilled during an exploration phase from 1968-1978 (Rose, 1983). Published vitrinite reflectance values from six of these wells (Hadiyanto, 1992) were used in this study as calibration data (Figure 14). The sediment-water interface temperatures through time were calculated based on the present-day latitude (Wygrala, 1989) and corrected for water depth within the software (PetroMod). The wells are situated at the northern end of the Simeulue Basin. At wells Meulaboh-1 and Tuba the pre-Neogene sediments (mudstones, siltstones) were drilled. Therefore, the 1-D models at these locations start in the Eocene and include the Late Oligocene-Early Miocene unconformity. All other wells terminated in Neogene sediments (Tripa=Early Miocene; Keudepasi, Bubon, Teunom=Middle Miocene). Below the drilled Neogene sediments approximately 1000 m of sedimentary basement was assumed. A constant heat flow model was assigned to all 1-D models, because maximum burial for all wells is at present, but the heat flow values differ between the wells. Heat flow was adjusted to match the measured vitrinite reflectance values.

There is a general trend of increasing heat flow from the southeast to the northwest. At well Tripa a heat flow of 40 mW/m² is sufficient to match the measured vitrinite reflectance values. A heat flow of 50 mW/m² was used at Meulaboh-1, 55 mW/m² were used at Tuba and 60 mW/m² were used for the calculations at wells Keudepasi

and Bubon. The calibration of the model for well Teunom needed an exceptionally high heat flow of 100 mW/m².

3-D modeling

The 3-D model has an extension of around 240 km in NW-SE direction and around 100 km in NE-SW direction. The imported maps have a regular grid spacing of 500 m. The model was calculated with a 3x3 sampling resulting in cell sizes of 1.5x1.5 km.

The maps were calculated from interpreted 2-D seismic data and depth converted using velocity information from seismic processing, i.e. stacking velocities. Maps were imported for the recent sea floor, base Pleistocene, base Pliocene, base Late Miocene and base Early Miocene. Thicknesses for the sediment layers in the acoustic basement were assumed as 100 m Oligocene, 50 m Eocene source rock, 400 m Eocene sediments and 500 m Early Eocene sedimentary basement. The Late Oligocene-Early Miocene erosion removed 500 m of sediments in our models and the late Middle Miocene-Late Miocene erosion affected only the south-eastern part of the basin with an erosion of up to 500 m, whereas at the present-day shelf and in the central part of the basin erosion did not take place.

According to our conceptual model we assigned two source rocks in the Simeulue Basin. The Eocene source rock was classified as organofacies B and the Early to Middle Miocene source rock was classified as organofacies D/E (Pepper and Corvi, 1995). Based on the organofacies the respective reaction kinetic data sets were assigned (Pepper and Corvi, 1995).

The heat flow values derived from the 1-D models of the near-shore wells are in the range of 40-60 mW/m², with the exception of well Teunom. This range is supported by calculation of recent heat flow values from BSR depths. Therefore, we calculated

two different models/scenarios, one with a heat flow of 40 mW/m² and a second one with 60 mW/m² (Figure 15).

In the 40 mW/m² model large parts of the Simeulue Basin remain at an immature stage. Only deeper levels in the center and in the southern part of the basin reach the oil and wet gas zone. In the 60 mW/m² model the zones of hydrocarbon generation extend over a wider area. In the deepest part of the basin the sediments are already in the overmature zone at present.

The pseudo well is positioned at approximately the location of the thickest Neogene sedimentary succession (Figure 2). Burial history at this location and the calculated transformation ratios (TR) and temperatures are shown in Figure 16.

In the 40 mW/m² model hydrocarbon generation from the Eocene source rock began at 16 Ma. Expulsion (10 % TR) started at 15 Ma and peak expulsion (50 % TR) occurred at 10 Ma. Hydrocarbon generation at the base of the Early Miocene sediments started at 15 Ma and onset and peak expulsion occurred at 11 Ma and 5 Ma, respectively. The Eocene source rock reaches transformation ratios of 85 % at the base, whereas the Early Miocene sediments reach 65 % transformation ratio (Figure 16).

In the model with a higher heat flow (60 mW/m²) hydrocarbon generation from the Eocene source rock began at 19.5 Ma. Expulsion (10 % TR) started at 16 Ma and peak expulsion (50 % TR) occurred at 14 Ma. Hydrocarbon generation at the base of the Early Miocene sediments started at 17 Ma and onset and peak expulsion occurred slightly later than in the Eocene source rock at 15 Ma and 13 Ma, respectively. Oil expulsion ceased (95 % TR) at 10 Ma for the Eocene source rock and at 5 Ma for the base of the Miocene sediments. The Eocene source rock and the base Early Miocene sediments have lost their hydrocarbon generation potential at

this location, but large parts of the Early-Middle Miocene sediments are still capable of hydrocarbon generation and expulsion (Figure 16).

DISCUSSION

We are fully aware of the limitations of the numerical model, e.g. uncertainty in kinetics (Peters et al., 2006), lack of petrophysical data of the potential reservoirs and heat flow history.

In our conceptual model the identified carbonate buildups are regarded as the main reservoirs for hydrocarbons, because analog examples of the South China Sea are prolific hydrocarbon reservoirs (Zampetti et al., 2004; Fournier and Borgomano, 2007). The detailed architecture of the carbonate buildups of the Simeulue Basin is unknown. Therefore reservoir properties e.g. porosity, permeability can only be assumed. Additionally intra-carbonate seals could have been developed which limit migration.

Seals for the carbonate buildups are the Late Miocene and Pliocene clastic sediments deposited during basin subsidence. The presence of bright spots can be explained by migration of thermally generated hydrocarbon gas from the depocenter (location of pseudo well) into the Late Miocene/Pliocene sediments to the northwest and to the southeast. Leakage of hydrocarbon gas out of the carbonate buildups may also contribute to the formation of bright spots, but gas chimneys were not observed in our seismic data.

Multiple BSRs occur close to the island of Simeulue in the south-western part of the basin. Multiple BSRs are explained by either compositional change of gas hydrates that effects their stability fields, a transitional zone between gas hydrates and free gas or they represent past (relict) positions of the hydrate stability zone (Foucher,

2002; Popescu et al., 2006). Multiple BSRs are located at the slope of the uplifted Simeulue Island which supports the interpretation that the lower BSRs in a multiple BSR-sequence were formed by rapid uplift due to tectonic activity and therefore represent paleo-BSRs. The Simeulue Basin is subject of recent strong tectonic activity and basin inversion (Berglar et al., 2008).

With a few exceptions, the wetness ratio methane/ Σ (ethane + propane) of the adsorbed gases indicates a thermal generation of the hydrocarbons (Figure 12). One sample from the Simeulue Basin (97MUC, $\delta^{13}\text{C}$ -68‰) shows a large contribution of isotopically light biogenic methane and can be interpreted as a mixed gas. However, the absolute ethane concentrations are very low (mostly less than 10 ppb). These are comparable to data from the southern Mentawai Basin obtained during a previous cruise (SO139), where this concentration was interpreted as the prevailing geogene background (Faber et al., 2001). Wetness data combined with the $\delta^{13}\text{C}$ isotopic composition of methane indicates a marine source rock of the adsorbed gases (Figure 12), whereas the data from the Mentawai Basin point towards an almost exclusively biogenic gas (Figure 12). Two samples exhibit unusually heavy $\delta^{13}\text{C}$ values (112MUC -16.4‰, 113SL -15.1‰) which are most likely a result of methane oxidation during sample storage. Data from the reference sites at the outer-arc high do not show a distinctive difference from the results of the Simeulue Basin. The above mentioned samples 140KL and 142KL with exceptionally high methane concentrations are evidently representing a biogenic gas. This is supported by the $\delta^{13}\text{C}$ values of these samples, which are generally lighter than -80‰.

An important parameter for hydrocarbon generation is the temperature history of the sedimentary basin. This is controlled by the basal heat flow and has to be defined as an input parameter in the numerical model. Several sources for heat flow determination were available. Measurements of recent heat flow at several locations

in the Simeulue Basin provided values between 47-107 mW/m² (Delisle and Zeibig, 2007). In particular, the higher values were measured at active faults where fluid expulsion occurs, thus documenting values which are not representative for the entire basin. Calculations of heat flow based on the depth of BSRs is useful, where wells are absent (Grauls, 2001) and deliver information on a larger area of the basin. The calculated heat flow ranges between 37 mW/m² and 74 mW/m². The third source of heat flow values are the calculated 1-D models for the six wells with published vitrinite reflectance values. These models required heat flow values between 40 mW/m² and 100 mW/m² to match the measured vitrinite data. The very high heat flow of 100 mW/m² at well Teunom might be explained by its location at the transition to the Aceh Basin. The Simeulue Basin is separated from the Aceh Basin today by a compressional ridge (Izart et al., 1994; Mosher et al., 2008) and strike-slip faults might act as fluid conduits and hence warm fluids could have heated up the sediments locally. The other heat flow values used in the 1-D models (40, 50, 55, 60 mW/m²) lie all in the range of the BSR derived heat flows. Based on these results we calculated two heat flow scenarios for the 3-D model, with 40 mW/m² and 60 mW/m², respectively.

Petroleum systems modeling offers the ability to study a basin before drilling and assessing the important factors for hydrocarbon generation, migration and accumulation. Based on the same geologic evolution of the present day forearc basin and the North Sumatra backarc basin until the Late Oligocene-Early Miocene (Barber et al., 2005), we assume an Eocene marine source rock, which is typical for the North Sumatra Basin (Schiefelbein and Cameron, 1997; Clure, 2005) and an Early-Middle Miocene terrestrial source rock (Figure 17) in our model. According to their kinetics they are both capable of oil generation.

The Eocene source rock has lost its hydrocarbon generation potential in the deepest part of the basin (Figs. 15 & 16) in the 60 mW/m² model but at shallower depth hydrocarbon generation is still possible. In the 60 mW/m² model hydrocarbon generation started in late Early Miocene and expulsion peaked at the deepest parts of the depocenter in the late Middle Miocene when the first phase of carbonate buildup growth occurred. These buildups were partially eroded at their tops (Figs. 5 & 8) by the Middle-Late Miocene erosional event which formed the unconformity and resulted in the loss of significant amounts of hydrocarbons. Subsequent generation of oil and gas from medium depths of the depocenter and migration of hydrocarbons from deeper parts resulted in the filling of the carbonate buildups during the Pliocene and Pleistocene (Figure 17).

In the 40 mW/m² model the Eocene source rock and the Early-Middle Miocene sediments maintain hydrocarbon generation potential and the Early-Middle Miocene sediments which fill most of the basin are still in the range of hydrocarbon generation or are still immature. Hydrocarbon generation started during the early Middle Miocene and peaked in the Late Miocene for the deeply buried Eocene source rock and in the Early Pliocene for the base of the Early Miocene sediments. In this model the amount of generated hydrocarbons is too low for a significant charge of the carbonate buildups, but it is enough to explain the bright spots. The majority of the hydrocarbons remain in their source rocks, and significant expulsion and migration from the Early-Middle Miocene sediments did not occur.

The calculated vitrinite reflectance and the zones of hydrocarbon generation (Figure 15) show that in both models hydrocarbons could have been generated and may still be generated in the Simeulue Basin at present. From these results it is obvious that the location of the source rocks in the sedimentary column is crucial for the timing of hydrocarbon generation. Expulsion and migration are furthermore strongly dependent

on the petrophysical properties of the overburden rock. Identification of reservoir zones and petrophysical properties in carbonate rocks is difficult due to the strong heterogeneities of carbonate rock properties (Borgomano et al., 2008).

Without well control in the deep central part of the Simeulue Basin this model depends on geological, geochemical and geophysical data. The petroleum systems modeling integrates all the available data and adds additional information to the timing of hydrocarbon generation and migration and shows that hydrocarbon generation is possible in forearc basins.

CONCLUSION

- Bright spots occur widespread in the central Simeulue Basin in Late Miocene/Pliocene sediments and are most likely caused by gas bearing sediments as supported by AVO/AVA analysis.
- Heat flow in the basin ranges between 40 mW/m² and 60 mW/m², according to 1-D modeling of six wells and BSR depths. Higher heat flows were measured at active fault zones.
- According to our models hydrocarbons migrated from the depocenter into potential reservoir rocks.
- Surface geochemical data suggest a thermal origin of hydrocarbon gas from marine source rocks.
- Carbonate buildups can serve as reservoirs and were charged with oil and gas in the 60 mW/m² model; additionally Late Miocene/Pliocene sediments might act as reservoirs.
- The 40 mW/m² model predicts significantly less hydrocarbon generation. The amount of generated hydrocarbons is enough to explain the bright spots but

the carbonate reservoirs are not charged with significant amounts of hydrocarbons.

- Exploration failures in the seventies can be explained by large distance from potential source area to the drilled wells.

REFERENCES CITED

- Allen, P. A., and J. R. Allen, 1990, *Basin Analysis - Principles & Applications*, Blackwell, 451 p.
- Barber, A. J., M. J. Crow, and M. E. M. de Smet, 2005, Tectonic evolution, *in* A. J. Barber, M. J. Crow, and J. S. Milsom, eds., *Sumatra: Geology, Resources and Tectonic Evolution: Memoirs*, v. 31, Geological Society, London, p. 234-259.
- Beaudry, D., and G. F. Moore, 1985, Seismic stratigraphy and Cenozoic evolution of West Sumatra forearc basin: *AAPG Bulletin*, v. 69, p. 742-759.
- Berglar, K., C. Gaedicke, R. Lutz, D. Franke, and Y. S. Djajadihardja, 2008, Neogene subsidence and stratigraphy of the Simeulue forearc basin, Northwest Sumatra: *Marine Geology*, v. 253, p. 1-13.
- Berndt, C., S. Bunz, T. Clayton, J. Mienert, and M. Saunders, 2004, Seismic character of bottom simulating reflectors: examples from the mid-Norwegian margin: *Marine and Petroleum Geology*, v. 21, p. 723-733.
- Borgomano, J., F. Fournier, S. Viseur, and L. Rijkels, 2008, Stratigraphic well correlations for 3-D static modeling of carbonate reservoirs: *AAPG Bulletin*, v. 92, p. 789-824.
- Busby, C. J., and R. V. Ingersoll, 1995, *Tectonics of sedimentary basins: United Kingdom*, Blackwell Science : Oxford, United Kingdom, 579 p.
- Clure, J., 2005, Fuel resources: oil and gas, *in* A. J. Barber, M. J. Crow, and J. S. Milsom, eds., *Sumatra: Geology, Resources and Tectonic Evolution: Geological Society Memoirs*, v. 31, Geological Society, London, p. 131-141.
- Cole, J. M., and S. Crittenden, 1997, Early Tertiary basin formation and the development of lacustrine and quasi-lacustrine/marine source rocks on the Sunda Shelf of SE Asia, *in* A. J. Fraser, S. J. Matthews, and R. W. Murphy, eds., *Geological Society Special Publications*, v. 126: United Kingdom, Geological Society of London : London, United Kingdom, p. 147-183.
- Delisle, G., and M. Zeibig, 2007, Marine Heat Flow Measurements in Hard Ground Offshore Sumatra: *EOS Transactions AGU*, v. 88, p. 38-39.
- Deplus, C., M. Diament, H. Hebert, G. Bertrand, S. Dominguez, J. Dubois, J. Malod, P. Patriat, B. Pontoise, and J.-J. Sibilla, 1998, Direct evidence of active deformation in the eastern Indian oceanic plate: *Geology*, v. 26, p. 131-134.
- Dickinson, W. R., 1995, Forearc basins, *in* C. J. Busby, and R. V. Ingersoll, eds., *Tectonics of sedimentary basins: United Kingdom*, Blackwell Science : Oxford, United Kingdom, p. 221-261.
- Faber, E., J. Poggenburg, and W. Stahl, 2001, Methane in Seawater, *in* H. Beiersdorf, ed., *Geoscientific Investigations at the active convergence zone between the Eastern Eurasian and Indo-Australian Plates off Indonesia. Summary and Synthesis of Cruises SO137 - 139, and Final Report of Cruise SO139*, Hannover, BGR.
- Faber, E., and W. Stahl, 1983, Analytical procedure and results of an isotope geochemical surface survey in an area of the British North Sea, *in* J. Brooks, ed., *Petroleum geochemistry and exploration of Europe; International congress.: Special Publication - Geological Society of London*, v. 12: London, United Kingdom, Geological Society of London, p. 51-63.
- Foucher, J.-P., 2002, Observation and tentative interpretation of a double BSR on the Nankai Slope, *in* H. Nouze, and P. Henry, eds., *Marine Geology*, Netherlands, Elsevier : Amsterdam, Netherlands, p. 161-175.

- Fournier, F., and J. Borgomano, 2007, Geological significance of seismic reflections and imaging of the reservoir architecture in the Malampaya gas field (Philippines): AAPG Bulletin, v. 91, p. 235-258.
- Grauls, D., 2001, Gas hydrates: importance and applications in petroleum exploration: Marine and Petroleum Geology, v. 18, p. 519-523.
- Hadiyanto, 1992, Organic petrology and geochemistry of the tertiary formations at Meulaboh area, West Aceh Basin, Sumatra, Indonesia, PhD thesis, University of Wollongong, Wollongong, 219 p.
- Hermanrud, C., 1993, Basin modelling techniques - an overview, *in* A. G. Doré, ed., Basin Modelling: Advances and Applications, Norwegian Petroleum Society, Special Publication No. 3, p. 1-34.
- Izart, A., B. Mustafa Kemal, and J. A. Malod, 1994, Seismic stratigraphy and subsidence evolution of the Northwest Sumatra fore-arc basin: Marine Geology, v. 122, p. 109-124.
- Karig, D. E., M. B. Lawrence, G. F. Moore, and J. R. Curray, 1980, Structural framework of the fore-arc basin, NW Sumatra: Journal of the Geological Society of London, v. 137, Part 1, p. 77-91.
- Karig, D. E., S. Suparka, G. F. Moore, and P. E. Hehanussa, 1979, Structure and Cenozoic evolution of the Sunda Arc in the central Sumatra region, *in* J. S. Watkins, L. Montadert, and P. W. Dickerson, eds., Geological and geophysical investigations of continental margins.: Memoir - American Association of Petroleum Geologists, v. 29: Tulsa, OK, United States, American Association of Petroleum Geologists, p. 223-237.
- Karlsen, D. A., J. E. Skeie, K. Backer-Owe, K. Bjorlykke, R. Olstad, K. Berge, M. Cecchi, E. Vik, and R. G. Schaefer, 2004, Petroleum migration, faults and overpressure; Part II, Case history; the Haltenbanken petroleum province, offshore Norway, *in* J. M. Cubitt, W. A. England, and S. R. Larter, eds., Understanding petroleum reservoirs; towards an integrated reservoir engineering and geochemical approach, v. 237: United Kingdom, Geological Society of London : London, United Kingdom, p. 305-372.
- Kvenvolden, K. A., and L. A. Barnard, 1982, Hydrates of natural gas in continental margins, *in* J. S. WATKINS, and C. L. DRAKE, eds., Studies in continental margin geology: AAPG Memoir, v. 34: United States, American Association of Petroleum Geologists: Tulsa, OK, United States, p. 631-640.
- Malod, J. A., and B. M. Kemal, 1996, The Sumatra Margin; oblique subduction and lateral displacement of the accretionary prism: Geological Society Special Publications, v. 106, p. 19-28.
- Matson, R. G., and G. F. Moore, 1992, Structural influences on Neogene subsidence in the central Sumatra fore-arc basin: AAPG Memoir, v. 53, p. 157-181.
- Mosher, D. C., J. A. Austin Jr, D. Fisher, and S. P. S. Gulick, 2008, Deformation of the northern Sumatra accretionary prism from high-resolution seismic reflection profiles and ROV observations: Marine Geology, v. 252, p. 89-99.
- Mueller, R. D., W. R. Roest, J.-Y. Royer, L. M. Gahagan, and J. G. Sclater, 1997, Digital isochrons of the world's ocean floor: Journal of Geophysical Research, v. 102, p. 3211-3214.
- Pecher, I., C. R. Ranero, R. v. Huene, T. A. Minshull, and S. C. Singh, 1998, The nature and distribution of bottom simulating reflectors at the Costa Rican convergent margin: Geophysical Journal International, v. 133, p. 219-229.
- Pepper, A. S., and P. J. Corvi, 1995, Simple kinetic models of petroleum formation. Part I: oil and gas generation from kerogen: Marine and Petroleum Geology, v. 12, p. 291-319.

- Peters, K. E., J. M. Moldowan, and C. C. Walters, 2005, *The biomarker guide; II, Biomarkers and isotopes in petroleum systems and Earth history*, Cambridge University Press, p. 475-1155.
- Peters, K. E., C. C. Walters, and P. J. Mankiewicz, 2006, Evaluation of kinetic uncertainty in numerical models of petroleum generation: *AAPG Bulletin*, v. 90, p. 387-403.
- Popescu, I., M. De Batist, G. Lericolais, H. Nouze, J. Poort, N. Panin, W. Versteeg, and H. Gillet, 2006, Multiple bottom-simulating reflections in the Black Sea; potential proxies of past climate conditions: *Marine Geology*, v. 227, p. 163-176.
- Prawirodirdjo, L., and Y. Bock, 2004, Instantaneous global plate motion model for 12 years of continuous GPS observations: *Journal of Geophysical Research*, v. 109, p. B08405.
- Pubellier, M., C. Rangin, J. P. Cadet, I. Tjashuri, J. Butterlin, and C. M. Mueller, 1992, L'île de Nias, un édifice polyphase sur la bordure interne de la fosse de la Sonde (archipel de Mentawai, Indonésie): *Comptes Rendus de l'Académie des Sciences, Série 2, Mécanique, Physique, Chimie, Sciences de l'Univers, Sciences de la Terre*, v. 315, p. 1019-1026.
- Rose, R. R., 1983, Miocene carbonate rocks of Sibolga Basin, Northwest Sumatra: *Proceedings Indonesian Petroleum Association*, v. Twelfth Annual Convention, June, 1983, p. 107-125.
- Ross, C. P., and D. L. Kinman, 1995, Nonbright-spot AVO; two examples: *Geophysics*, v. 60, p. 1398-1408.
- Rutherford, S. R., and R. H. Williams, 1989, Amplitude-versus-offset variations in gas sands: *Geophysics*, v. 54, p. 680-688.
- Samuel, M. A., and N. A. Harbury, 1996, The Mentawai fault zone and deformation of the Sumatran Forearc in the Nias area: *Geological Society Special Publications*, v. 106, p. 337-351.
- Schiefelbein, C., and N. Cameron, 1997, Sumatra/Java oil families, *in* A. J. Fraser, S. J. Matthews, and R. W. Murphy, eds., *Geological Society Special Publications*, v. 126: London, Geological Society of London, p. 143-146.
- Schlueter, H. U., C. Gaedicke, H. A. Roeser, B. Schreckenberger, H. Meyer, C. Reichert, Y. Djajadihardja, and A. Prexli, 2002, Tectonic features of the southern Sumatra-western Java forearc of Indonesia: *Tectonics*, v. 21, p. 1047.
- Sieh, K., and D. Natawidjaja, 2000, Neotectonics of the Sumatran Fault, Indonesia: *Journal of Geophysical Research*, v. 105, p. 28,295-28,326.
- Sloan, E. D., 1998, *Clathrate hydrates of natural gases*, Marcel Dekker, 705 p.
- Smith, W. H. F., and D. T. Sandwell, 1997, Global sea floor topography from satellite altimetry and ship depth soundings: *Science*, v. 277, p. 1956-1962.
- Struss, I., V. Artiles, B. Cramer, and J. Winsemann, 2008, The petroleum system in the Sandino forearc basin, offshore western Nicaragua: *Journal of Petroleum Geology*, v. 31, p. 221-244.
- Susilohadi, S., C. Gaedicke, and A. Erhard, 2005, Neogene structures and sedimentation history along the Sunda forearc basins off southwest Sumatra and southwest Java: *Marine Geology*, v. 219, p. 133-154.
- Tissot, B. P., R. Pelet, and P. Ungerer, 1987, Thermal history of sedimentary basins, maturation indices, and kinetics of oil and gas generation: *AAPG Bulletin*, v. 71, p. 1445-1466.

- Underdown, R., and J. Redfern, 2008, Petroleum generation and migration in the Ghadames Basin, north Africa: A two-dimensional basin-modeling study: AAPG Bulletin, v. 92, p. 53-76.
- Ungerer, P., J. Burrus, B. Doligez, P. Y. Chenet, and F. Bessis, 1990, Basin evaluation by integrated two-dimensional modeling of heat transfer, fluid flow, hydrocarbon generation, and migration: AAPG Bulletin, v. 74, p. 309-335.
- Von Huene, R., and D. W. Scholl, 1991, Observations at Convergent Margins Concerning Sediment Subduction, Subduction Erosion, and the Growth of Continental Crust: Reviews of Geophysics, v. 29, p. 279-316.
- Welte, D. H., and M. A. Yüklér, 1981, Petroleum origin and accumulation in basin evolution - a quantitative model: AAPG Bulletin, v. 65, p. 1387-1396.
- Wygrala, B., 1989, Integrated study of an oil field in the southern Po Basin, northern Italy, PhD thesis, University of Cologne, Köln, 217 p.
- Yalcin, M. N., R. Littke, and R. F. Sachsenhofer, 1997, Thermal History of Sedimentary Basins, *in* D. H. Welte, B. Horsfield, and D. R. Baker, eds., Petroleum and Basin Evolution, Springer, p. 71-167.
- Zampetti, V., W. Schlager, J.-H. van Konijnenburg, and A.-J. Everts, 2004, 3-D seismic characterization of submarine landslides on a Miocene carbonate platform; Luconia Province, Malaysia: Journal of Sedimentary Research, v. 74, p. 817-830.

Figure captions

Figure 1. Regional tectonic setting of the Sunda subduction zone. The forearc basins off Sumatra lie between Sumatra mainland and the outer-arc high that occasionally emerges above sea level forming the island chain west of Sumatra. Abbreviations: SFZ: Sumatran Fault Zone, MFZ: Mentawai Fault Zone, BF: Batee Fault, WAF: West Andaman Fault. Deformation front in the Sunda Trench is based on Sieh and Natawidjaja (2000). Ages of the oceanic crust after Mueller et al. (1997) and Deplus et al. (1998). Black arrows indicate relative plate motion based on CGPS data (Prawirodirdjo and Bock, 2004).

Figure 2. Location of multi-channel seismic profiles covering the Simeulue Basin between Simeulue Island and Sumatra. Isolines depict bathymetric contours (Smith and Sandwell, 1997) and circles show locations of wells (Rose, 1983; Beaudry and Moore, 1985). Filled diamonds mark the locations of organic geochemical gas samples. Hollow diamonds mark sections of seismic lines used for AVO/AVA analysis. Bold lines highlight seismic profiles shown in this study.

Figure 3. Location of exploration wells Tuba (A), Meulaboh-1 (B) and Tripa-1 (C) on multi-channel seismic lines BGR06-210 and BGR06-211. The stratigraphy of well Meulaboh-1 (A) is used in this study for chrono-stratigraphic correlation of seismic horizons (Berglar et al., 2008). Two phases of carbonate buildup growth occurred in the early to middle Miocene and in the late Miocene to early Pliocene, respectively. Line-tie with profile BGR06-137 is indicated at the top. See Figure 2 for location of profile.

Figure 4. 3-D model for the spatial and temporal evolution of the Simeulue Basin. Time steps are 20 Ma, 11 Ma, 5.3 Ma and Recent. Dimension of the cube is ca. 205x205 km and depth from sea level down to approx. 11300 m.

Figure 5. Part of multi-channel seismic profile BGR06-135 (upper panel) and interpretation (lower panel). Two carbonate buildups have grown at the same location on a pre-Neogene basement high. The growth phases are interrupted by a drowning phase and the lower buildup is truncated by an unconformity. The carbonate buildups mark the paleo-shelf edge. The late Miocene to early Pliocene paleo-shelf is occupied by carbonate platform sediments with typical chaotic reflection pattern. Half arrows indicate onlapping strata at the flank of the buildups. See Figure 2 for location of profile.

Figure 6. Part of multi-channel seismic profile BGR06-139 (upper panel) and interpretation (lower panel). Carbonate buildups have grown above a regional unconformity at the paleo-shelf edge. Faults cut through the upper sedimentary succession and occasionally reach the seafloor. Ellipsoids mark areas with bright spots. BSR: bottom simulating reflector; a half arrow indicates onlapping strata above an unconformity at the slope of the basin. The locations for amplitude versus offset analysis (Figures 10, 11) are marked at the top. See Figure 2 for location of profile.

Figure 7. Part of multi-channel seismic profile BGR06-138 (upper panel) the black box marks the section of the interpretation (lower panel). We distinguish in the upper buildup the buildup stages A and B and build-in and drowning stage C and D, respectively. The surrounding area is covered by debris and platform deposits; a

lowstand wedge is interpreted at the NNW flank. Half arrows indicate onlapping strata at the flank of the buildups. See Figure 2 for location of profile.

Figure 8. Part of multi-channel seismic profile BGR06-137 (upper panel) and interpretation (lower panel). A bright spot (ellipsoids) occupies sediments above carbonate buildups. It prolongs parallel to the layering above two distinct bottom-simulating reflectors. Arrow (bottom right) marks cut-off layers at an erosional truncation. Line-tie with profile BGR06-211 is indicated at the top. See Figure 2 for location of profile.

Figure 9. Map shows the location of carbonate buildups (green), bright spots (blue) and BSRs (red) interpreted on multi-channel seismic profiles.

Figure 10. 6250 m long part of seismic line BGR06-139 (CDPs 2100-2200). Top: Near offset stack with the seabottom at 1500 ms (TWT). Bottom: Same part of line as on top, but displayed as far offset stack. High amplitudes at 1900-2000 ms (TWT) indicate gas-bearing sediments.

Figure 11. Supergather formed from CDPs 26000-26010 of line BGR06-139. Top: Raw amplitudes in the depth range from 1880 to 2020 ms (TWT) and extracted raw amplitudes along the prominent negative reflection at 1920 to 1930 ms (TWT). Bottom: Raw amplitudes in the depth range from 1300 to 2300 ms (TWT) and extracted normalized amplitudes along the waterbottom and the prominent negative reflection at 1920 to 1930 ms (TWT).

Figure 12. Chemical composition and carbon isotopes of adsorbed methane in the Bernard-Diagram. Crossed line indicates hypothetical composition of a mixed bacterial and thermogenic gas.

Figure 13. Conceptual model depicted on seismic profile BGR06-139. See Figure 2 for location of profile.

Figure 14. 1-D models of near-shore wells (a-f) with published vitrinite reflectance values (Hadiyanto, 1992) used for calibration of the models. Left part of panels shows measured (dots) and calculated (solid line) vitrinite reflectance values. Right part of panels shows burial history of the respective well. Wells Meulaboh (b) and Tuba (c) reached pre-Neogene sediments, all other wells terminated in Neogene sediments. All wells were calculated using a constant heat flow model, but heat flows are different for each well. See Figure 2 for location of wells.

Figure 15. 3-D model with cut plane trending NW-SE showing the Neogene depocenter with highest sediment thickness. Top: Calculated vitrinite reflectance values and zones of hydrocarbon formation for the 40 mW/m² model; present day. Bottom: Calculated vitrinite reflectance values and zones of hydrocarbon formation for the 60 mW/m² model; present day.

Figure 16. Calculated transformation ratio (TR) for two source rocks (thin Eocene source rock at the bottom; Early-Middle Miocene source rock) at the pseudo well (for location see Figure 2). Isolines show temperature evolution. Left: Calculated transformation ratio for the 40 mW/m² model. Right: Calculated transformation ratio for the 60 mW/m² model.

Figure 17. Petroleum system events chart for the Simeulue Basin. Eocene source rock=grey, Early-Middle Miocene source rock=black, Early-Middle Miocene carbonate buildups=hatched area, Pli.=Pliocene, Pl.=Pleistocene. Petroleum generation and expulsion are shown separately for the 40 mW/m² and 60 mW/m² models.

Table 1: Geochemical results from gas samples of the Simeulue Basin and two reference locations

Station	Latitude (North)	Longitude (East)	Sample ID	Depth (m)	CH4 (ppb)	C2H6 (ppb)	C2H4 (ppb)	C3H8 (ppb)	C3H6 (ppb)	delta13C Methane
70SL	2°33.830	96°45.410	70SL1	1.3	92	9	1	5	1	-42.7
			70SL2	1.5	108	9	2	6	1	-45.6
73KL	2°49.803	96°23.103	73SL1	2.7	60	5	1	2	0	-31.6
			73SL2	4.7	100	7	1	3	0	-28.9
77SL	2°49.015	96°36.830	77SL1	2.7	68	6	1	3	1	-34.6
			77SL2	4.7	66	6	1	3	0	-37.6
79SL	2°57.082	96°29.985	79SL1	2.7	52	4	1	2	0	-33.2
			79SL2	4.7	61	5	1	2	0	-33.7
85SL	2°59.390	96°13.208	85SL1	2.7	125	9	1	5	0	-38.7
			85SL2	4.7	41	2	0	1	0	-37.8
90SL	2°46.985	96°24.941	90SL1	2.7	75	6	1	2	0	-37.2
			90SL2	4.7	98	8	1	3	0	-41.2
97MUC	2°33.804	96°45.400	97MUC1	0.3	512	8	1	4	1	-68.0
102SL	2°29.218	97°07.281	102SL1	2.7	60	6	1	1	0	-41.6
			102SL2	4.7	51	4	1	2	0	-33.6
105SL	3°11.704	96°46.694	105SL1	5.4	42	2	1	1	0	-33.9
			105SL2	6.4	53	4	1	2	0	-41.0
106SL	3°10.241	96°46.808	106SL1	2.7	101	14	1	7	1	-36.0
			106SL2	4.7	48	4	1	2	1	-33.6
112MUC	3°52.471	96°00.444	112MUC1	0.4	37	2	1	2	0	-16.4
113SL	3°52.440	96°00.451	113SL1	1.2	27	2	1	1	0	-15.1
119KL	3°31.054	96°18.872	119KL1	7.7	92	6	1	3	0	-34.0
122SL	3°16.488	96°09.245	122SL1	3.7	75	5	1	2	0	-27.8
			122SL2	4.7	104	6	1	4	0	-31.9
131SL	3°33.781	96°45.429	131SL1	0.2	76	7	1	3	0	-39.6
			131SL2	3.7	113	7	1	4	0	-43.6
115KL	3°29.494	95°19.878	115KL1	5.6	82	9	1	5	0	-29.5
			115KL2	7.7	73	9	1	5	0	-30.8
			115KL3	9.7	78	8	1	4	1	-34.2
116KL	3°29.569	95°19.885	116KL1	8.7	71	9	1	4	0	-28.4
139MUC	1°45.573	96°46.433	139MUC1	0.4	124	9	2	5	1	-49.8
140KL	1°45.571	96°46.438	140KL1	6.8	11748	15	1	7	0	-91.1
			140KL2	6.8	277	10	1	8	1	-79.7
			140KL3	7.8	20823	19	1	11	1	-90.4
142KL	1°45.570	96°46.440	142KL1	8.6	10281	20	2	12	1	-85.1

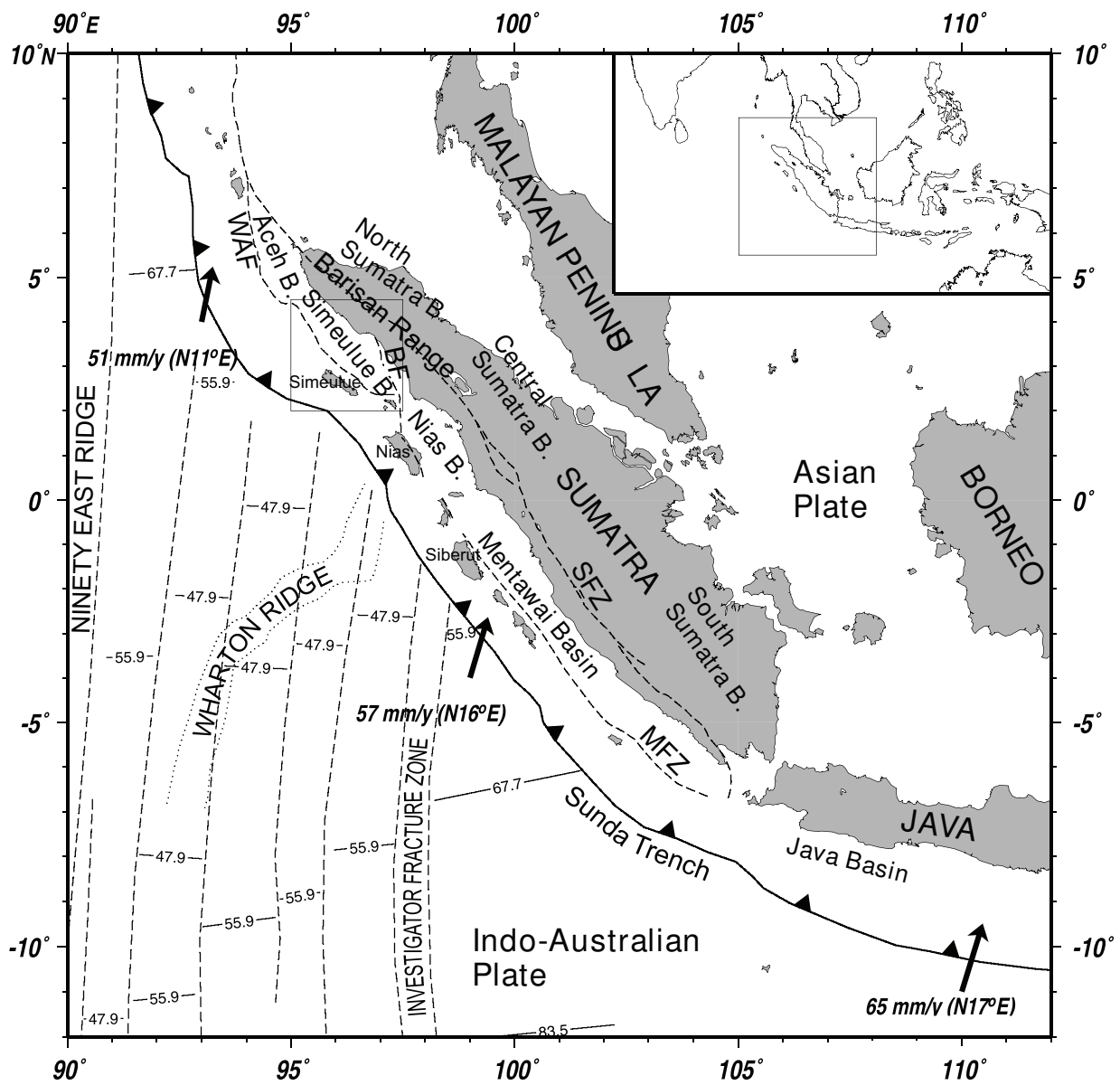


Figure 1

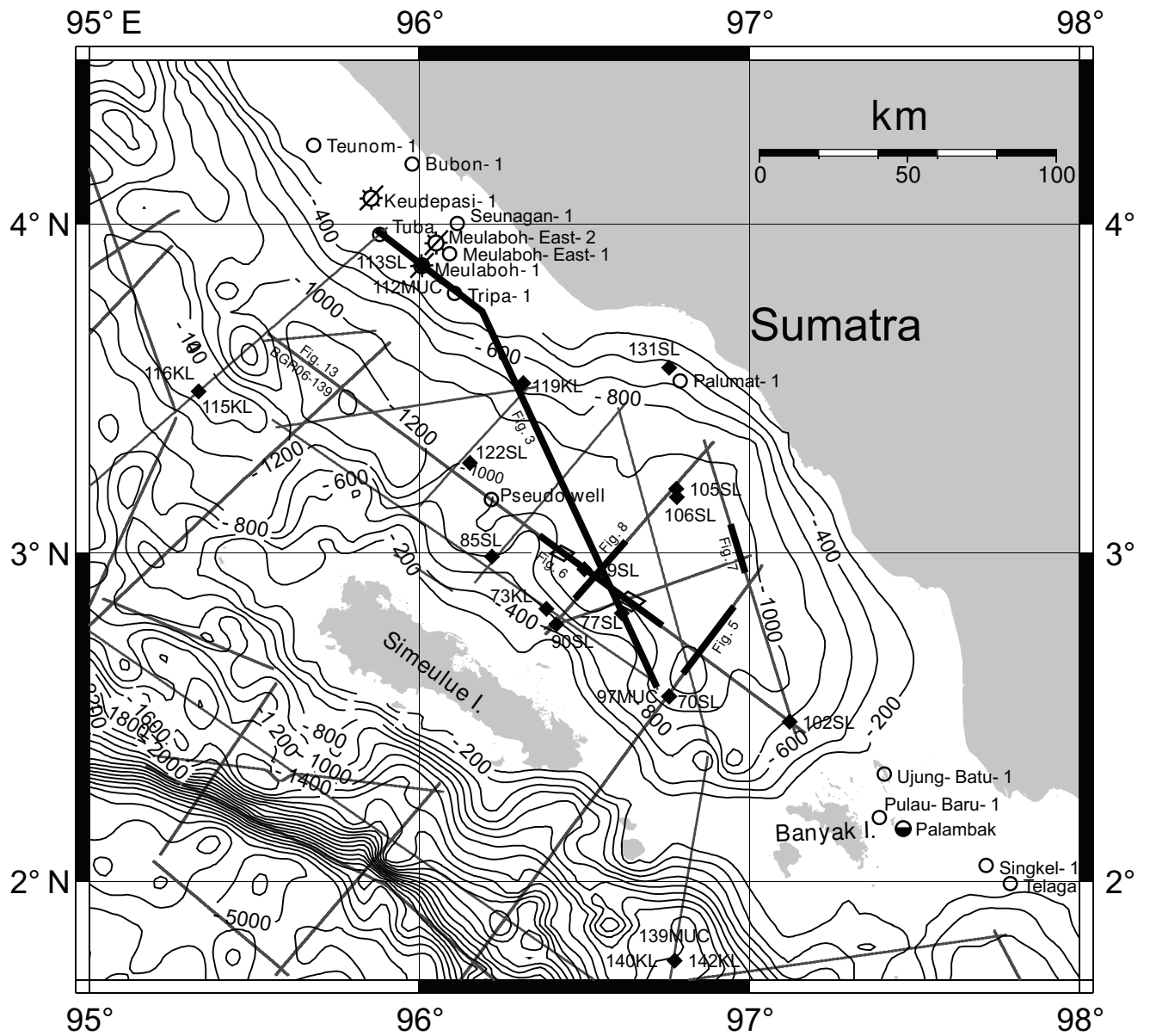


Figure 2

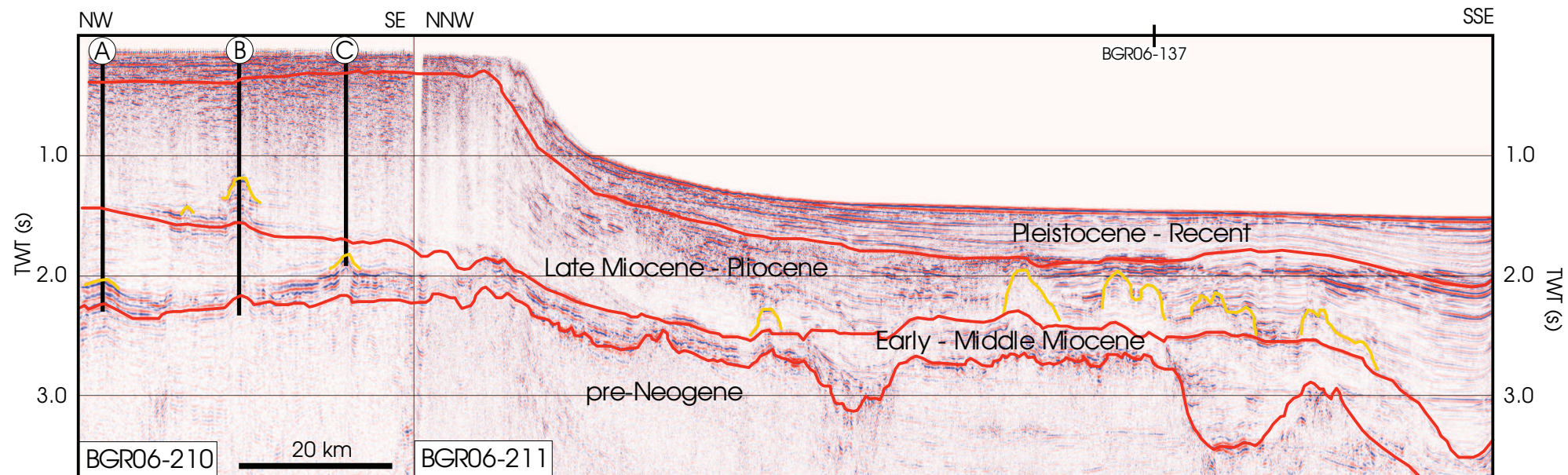


Figure 3

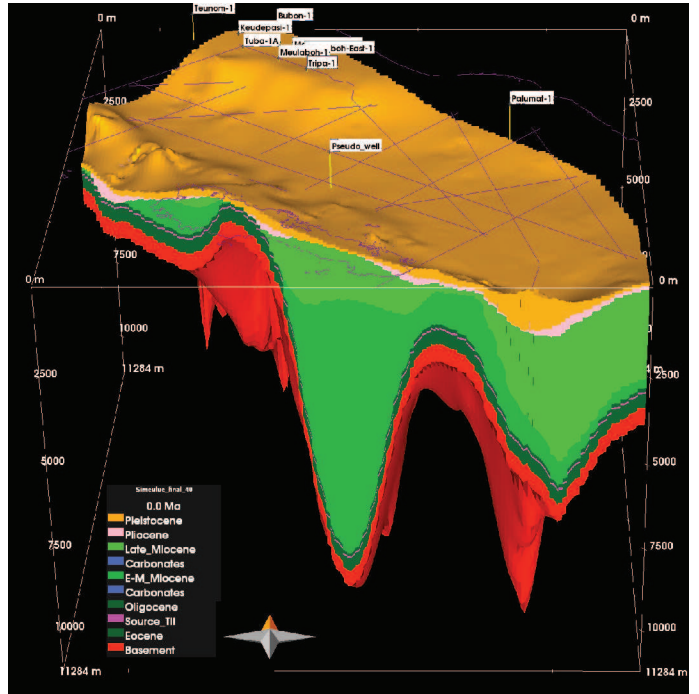
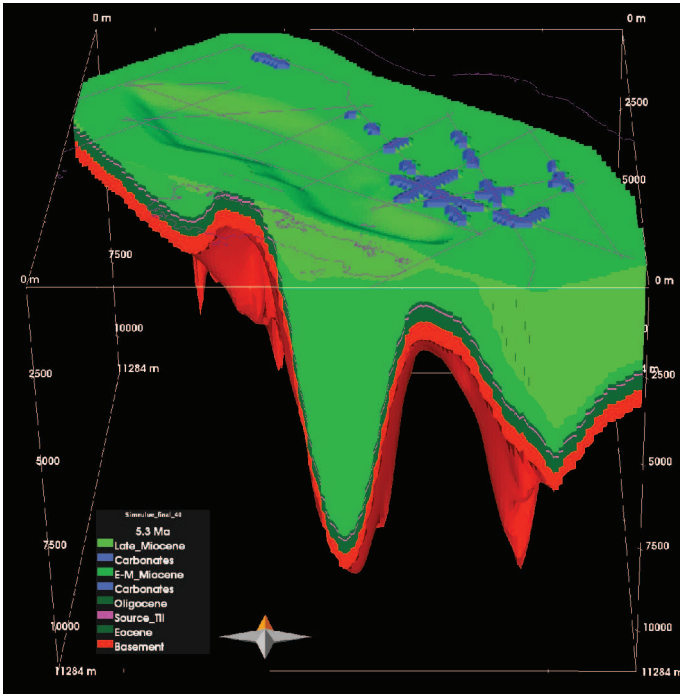
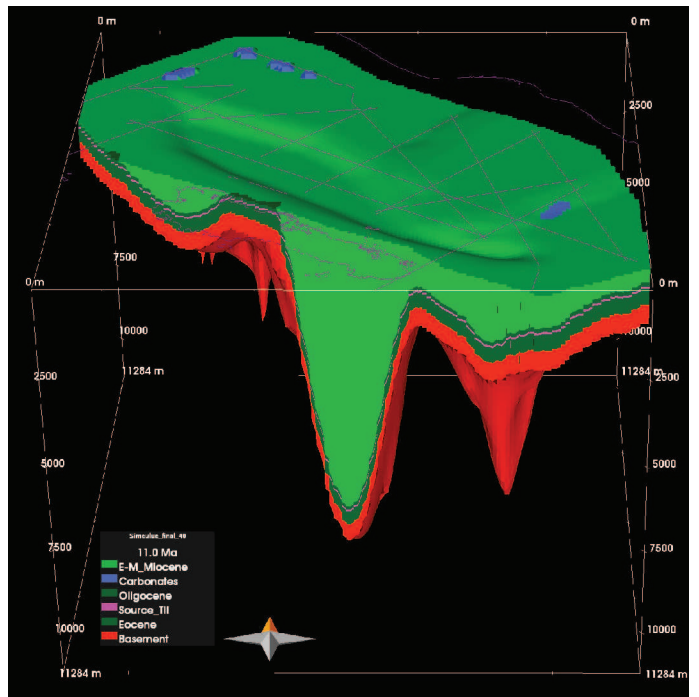
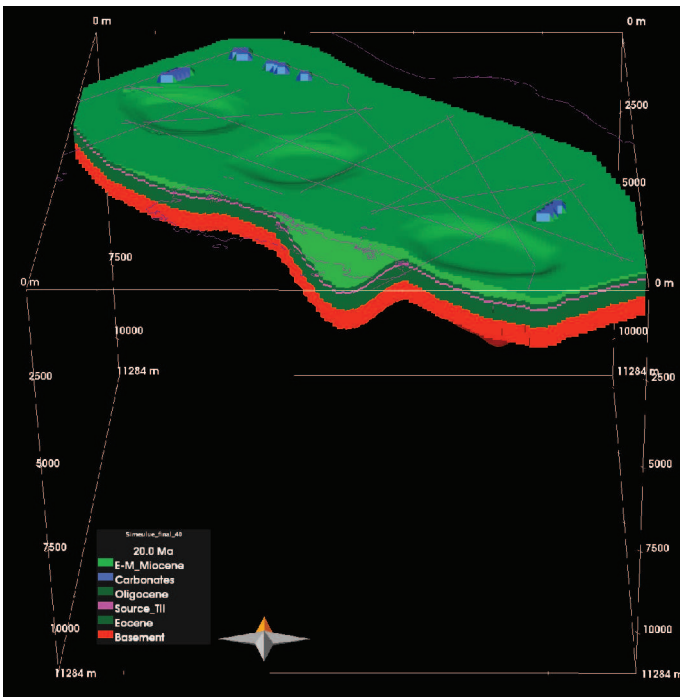


Figure 4

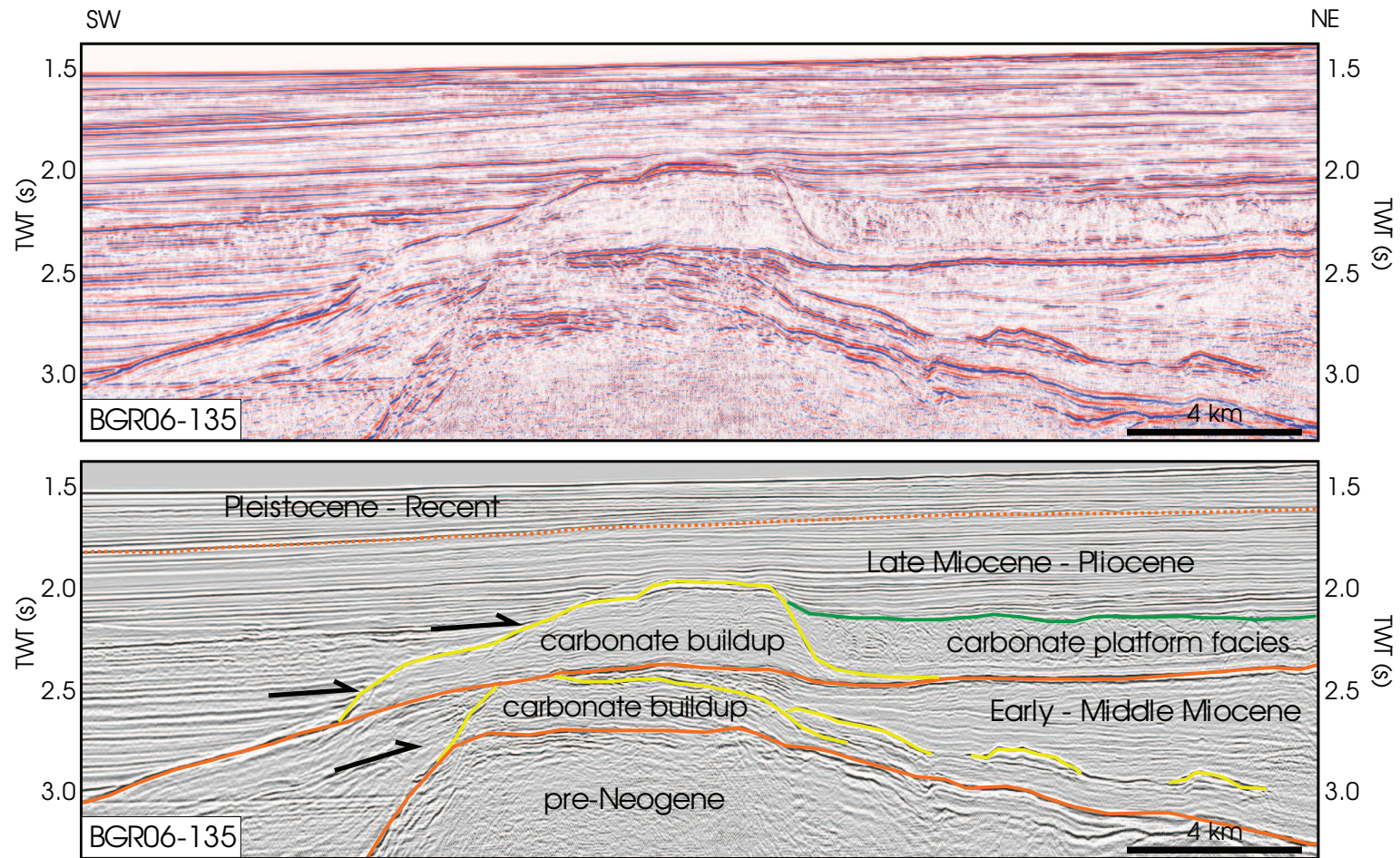


Figure 5

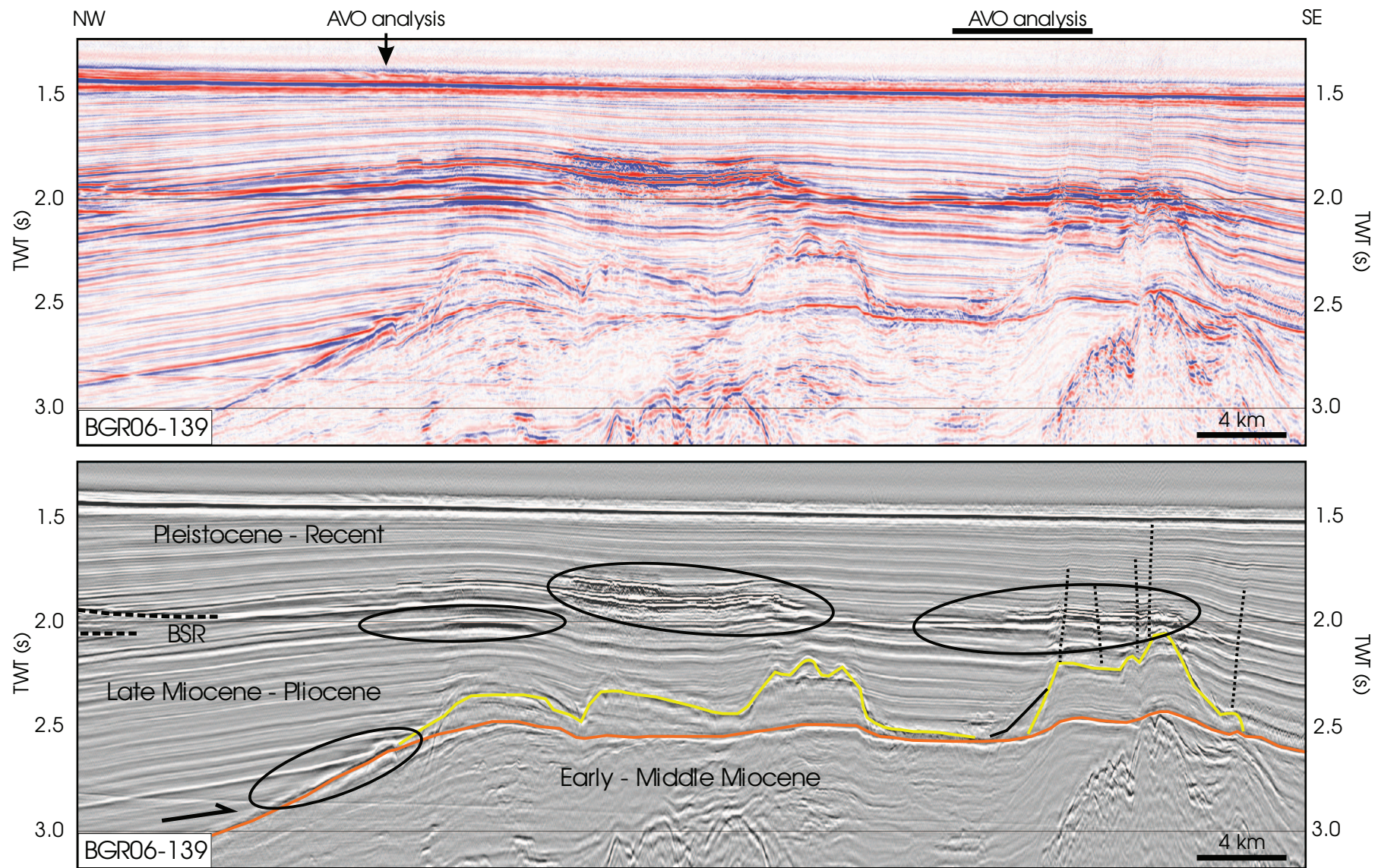


Figure 6

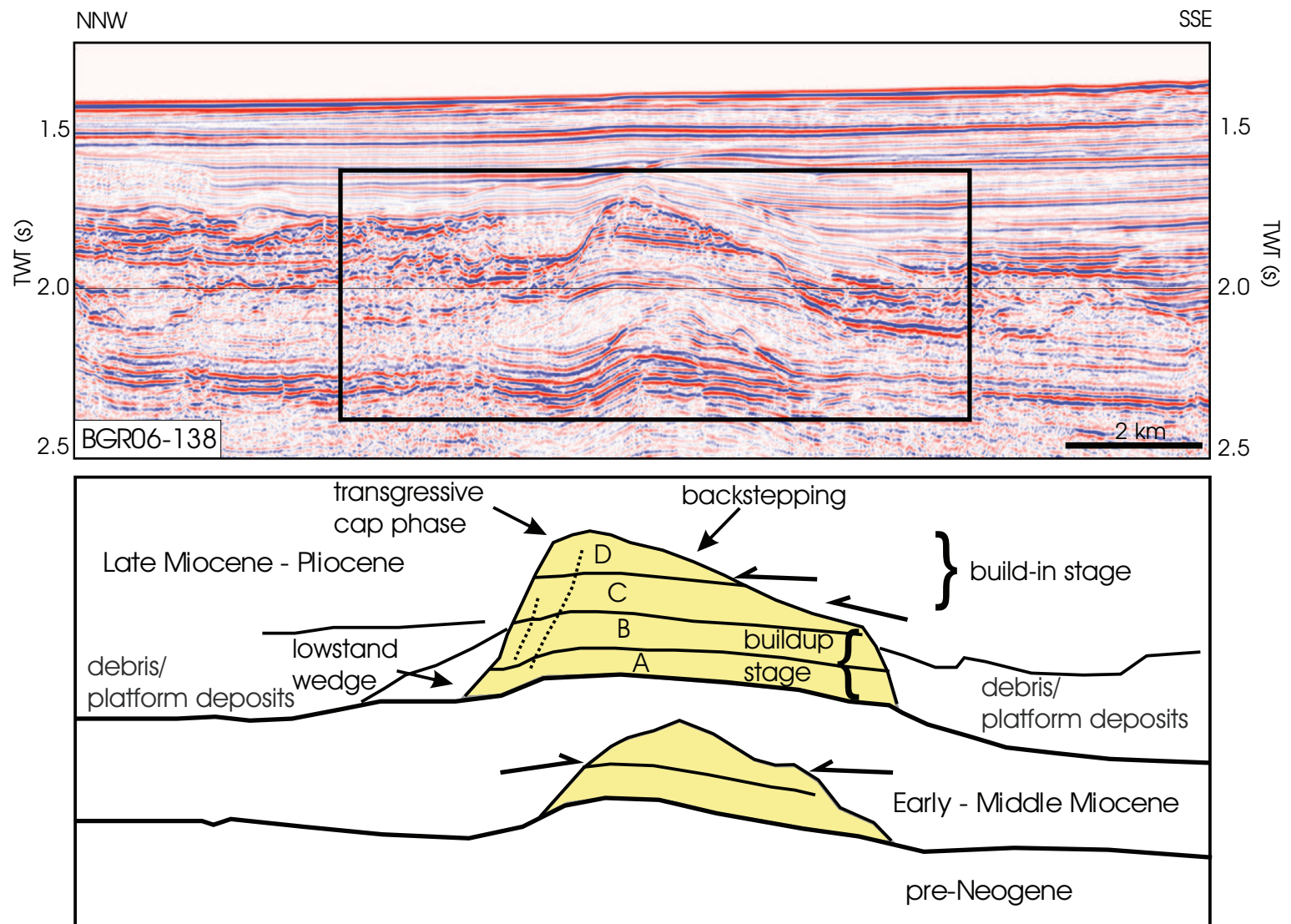


Figure 7

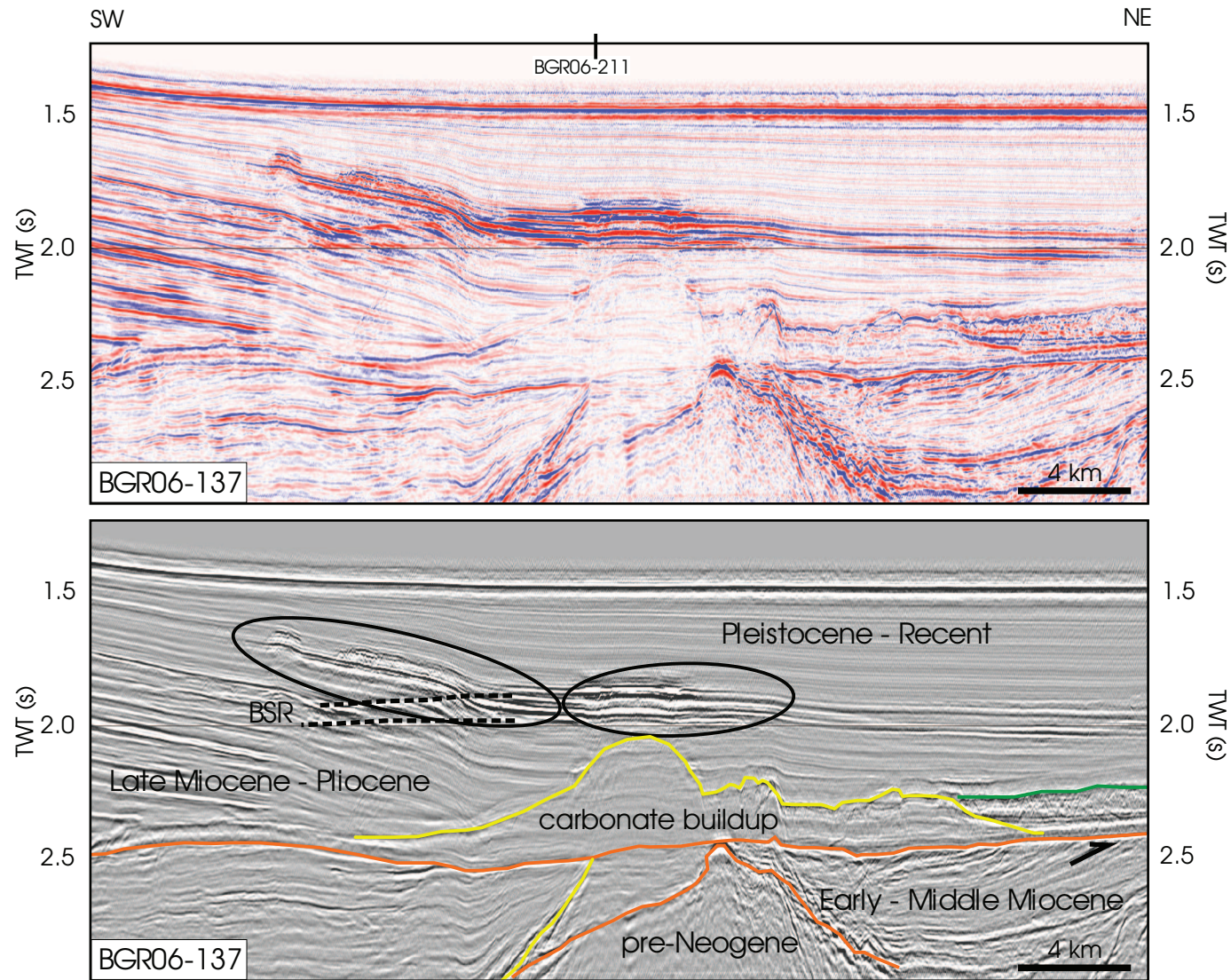


Figure 8

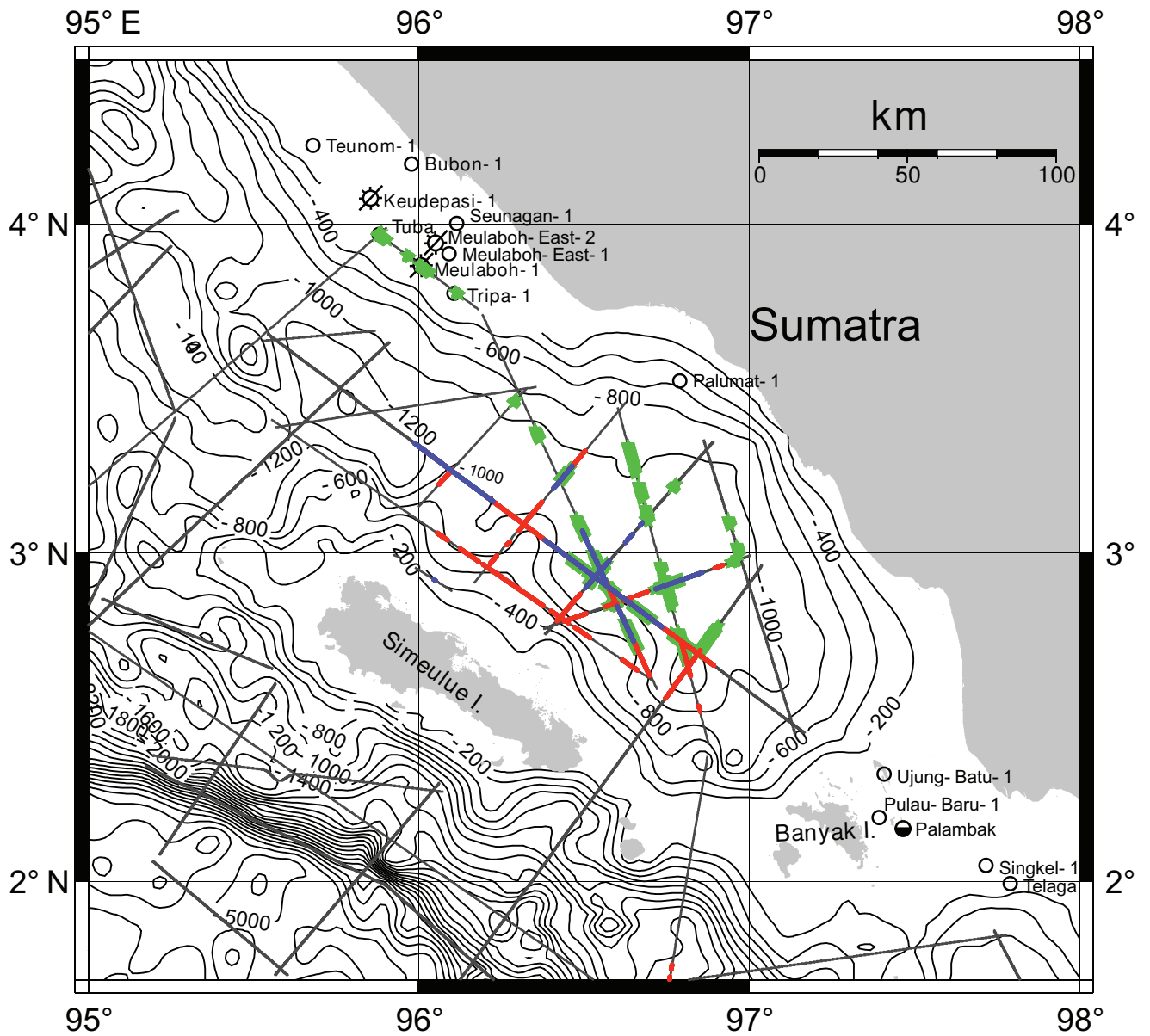


Figure 9

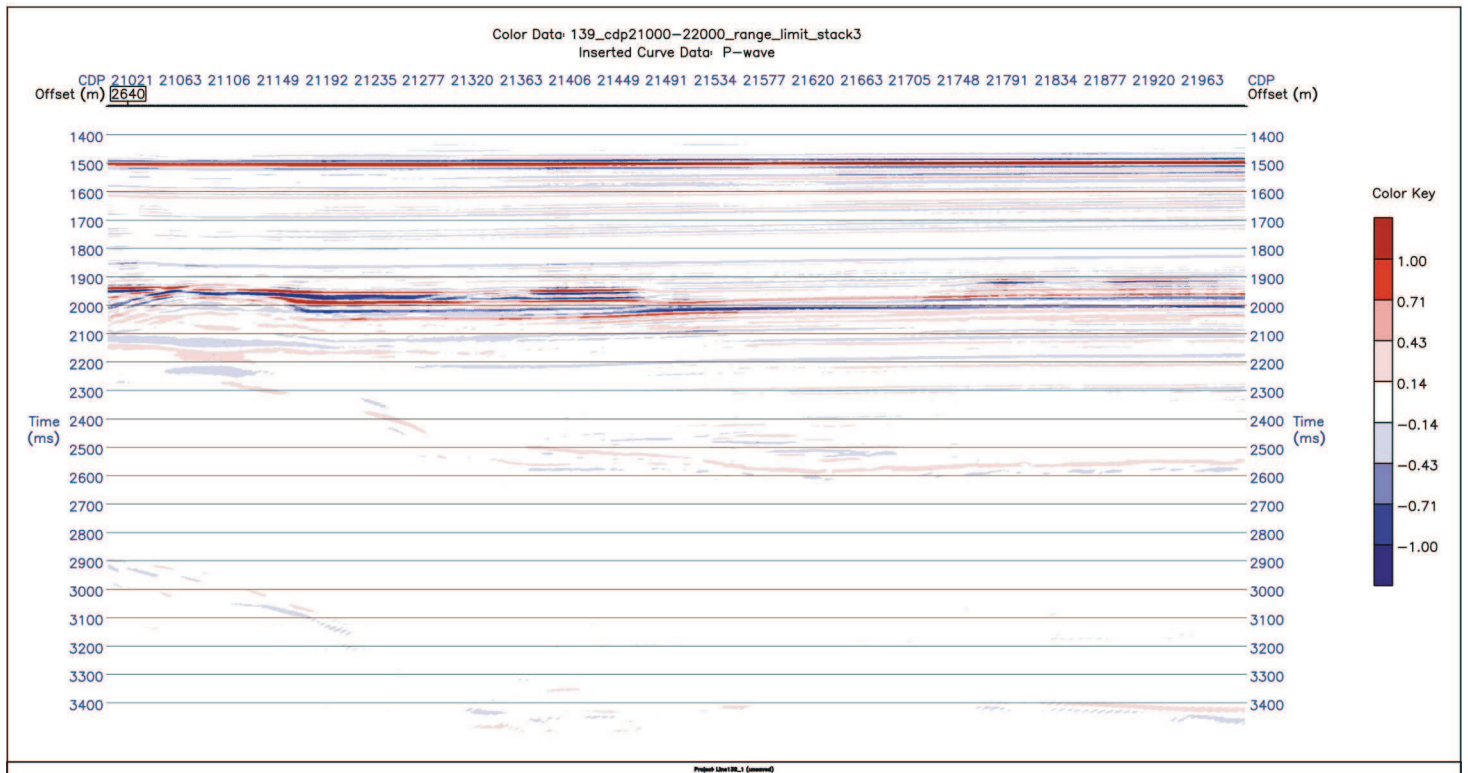
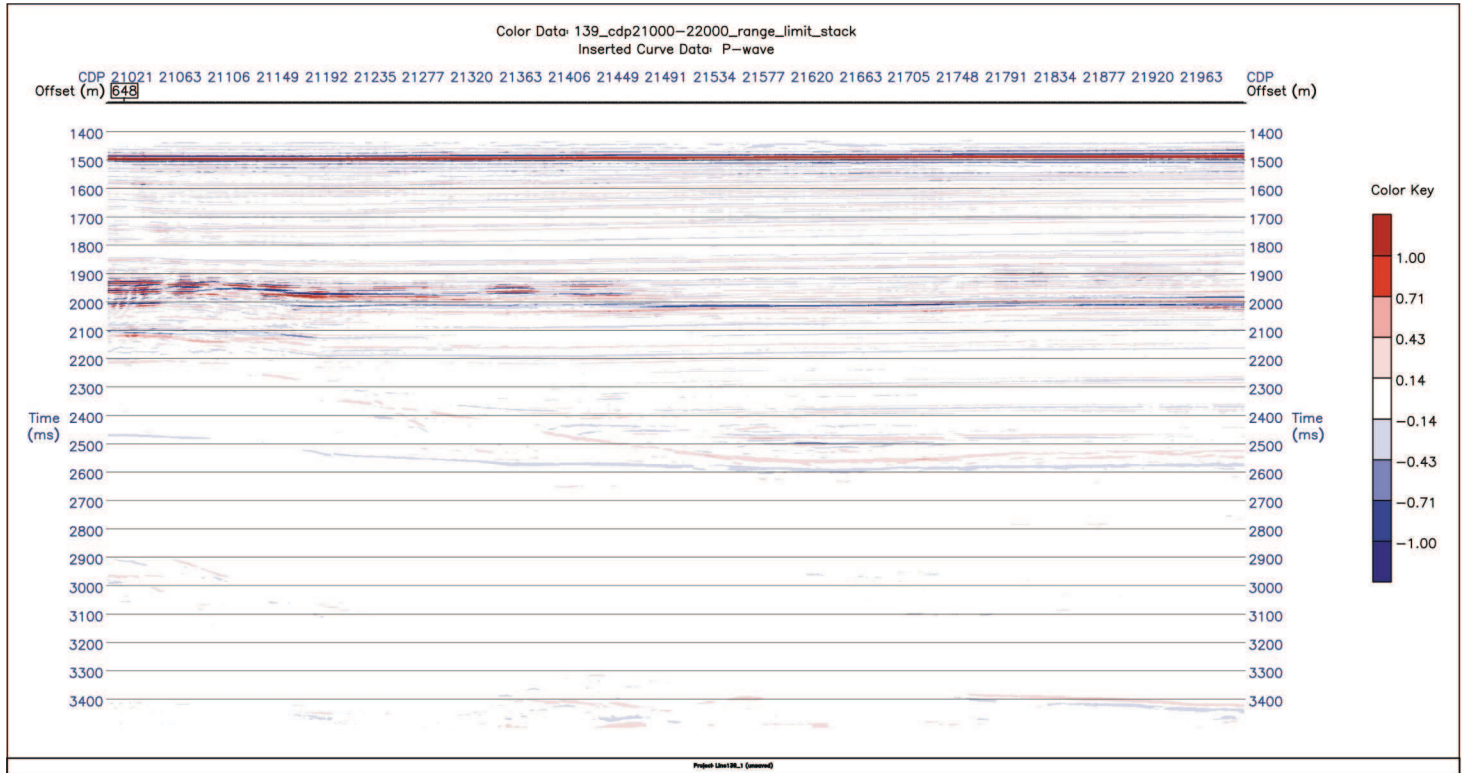


Figure 10

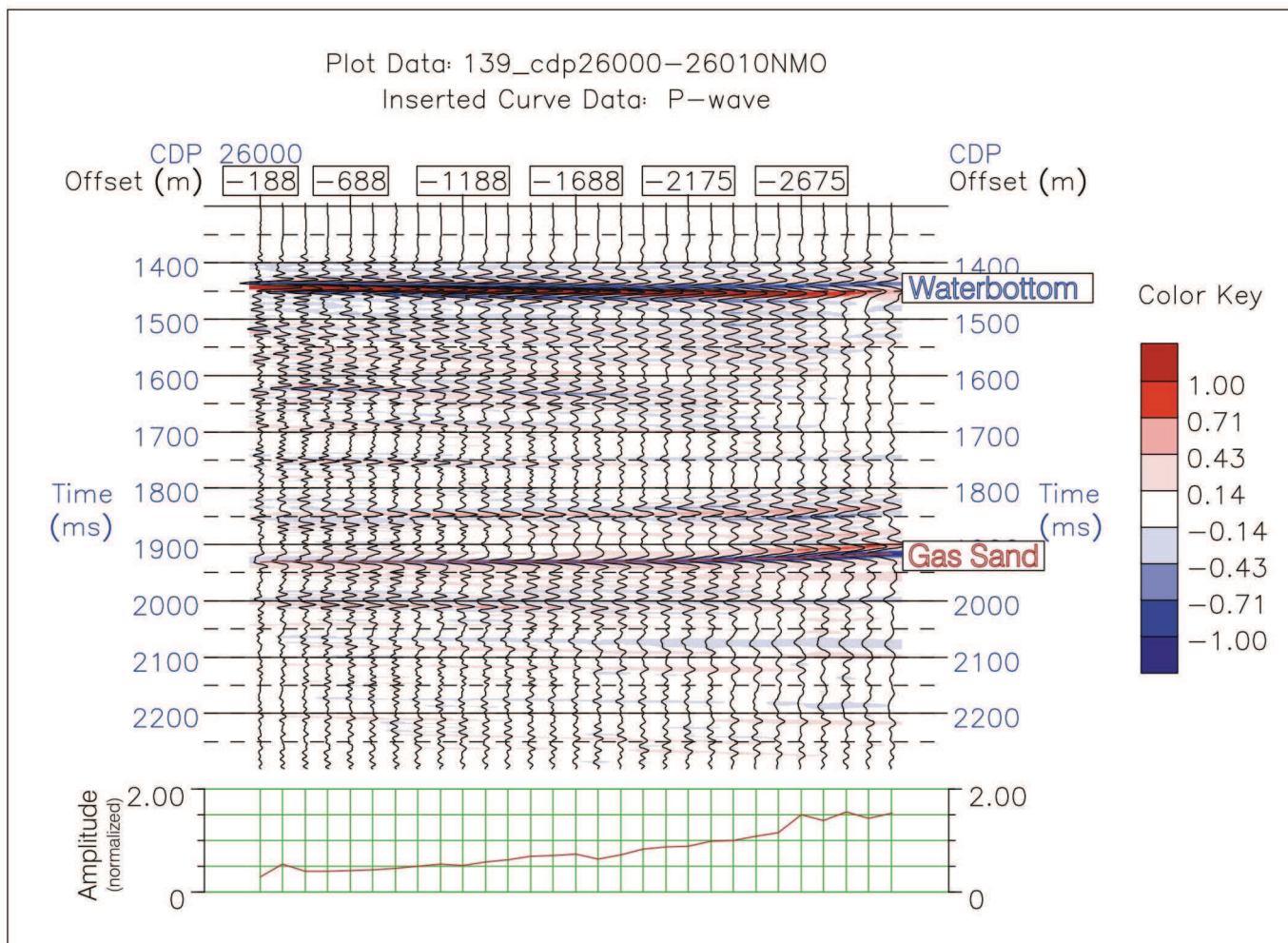
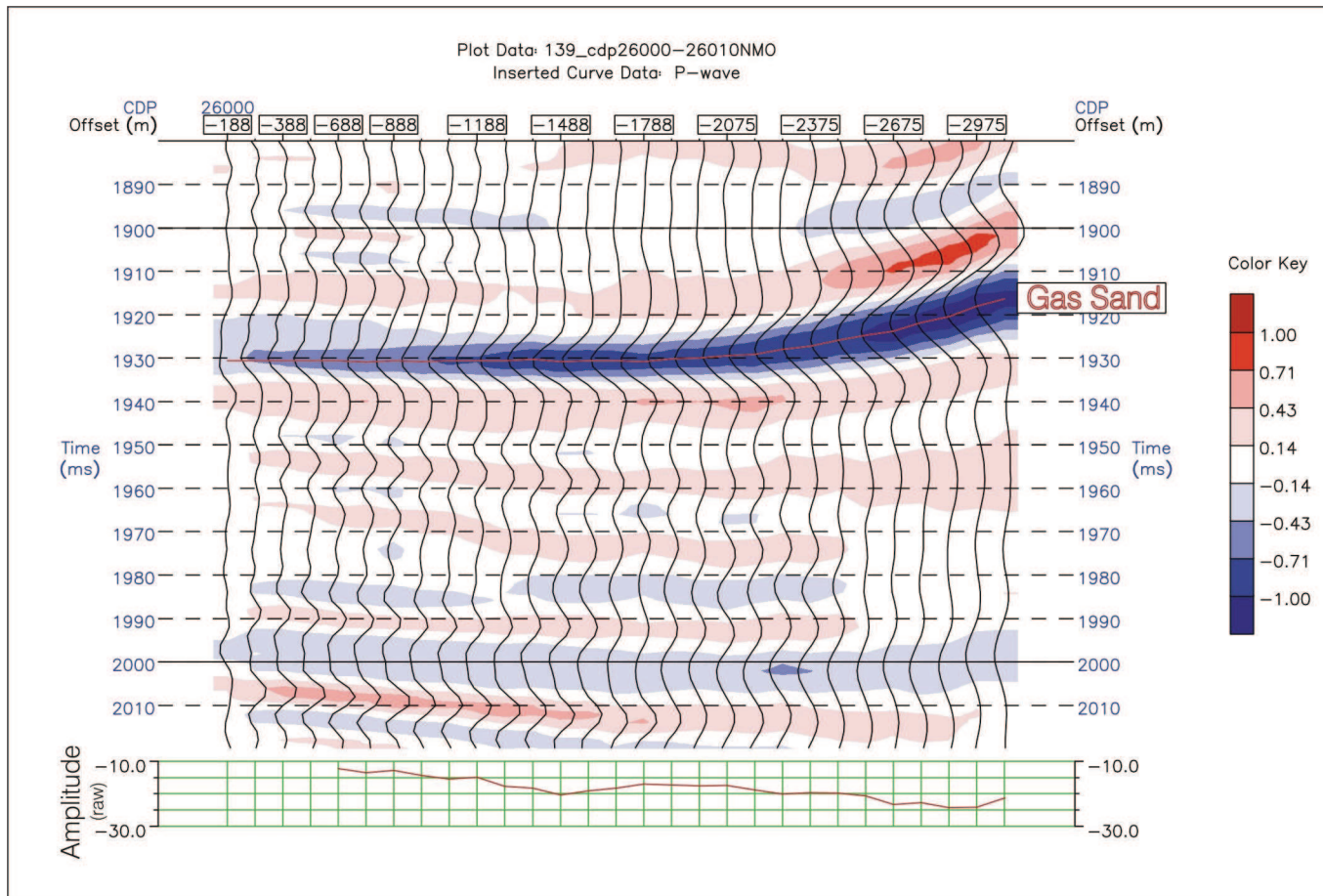


Figure 11

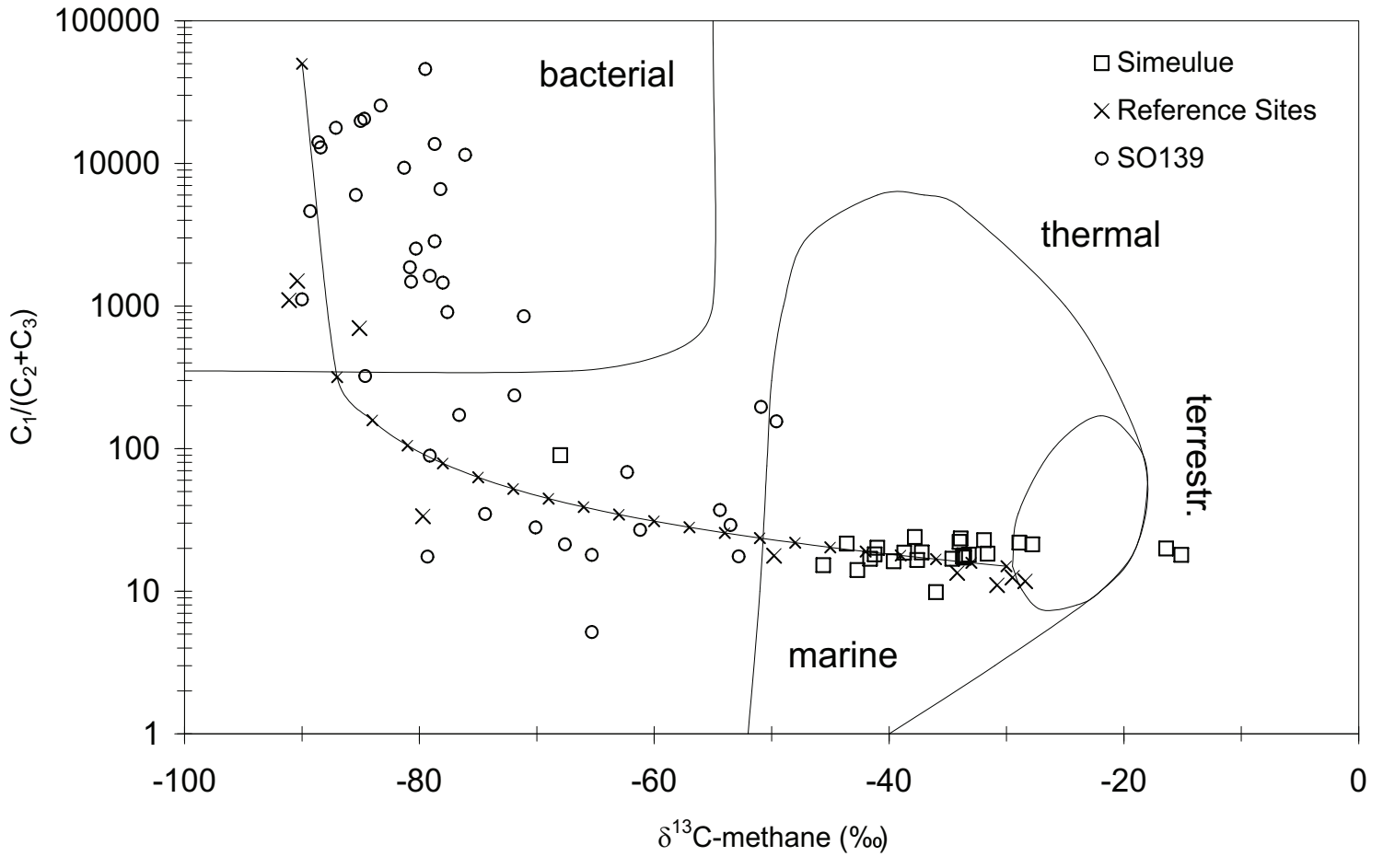


Figure 12

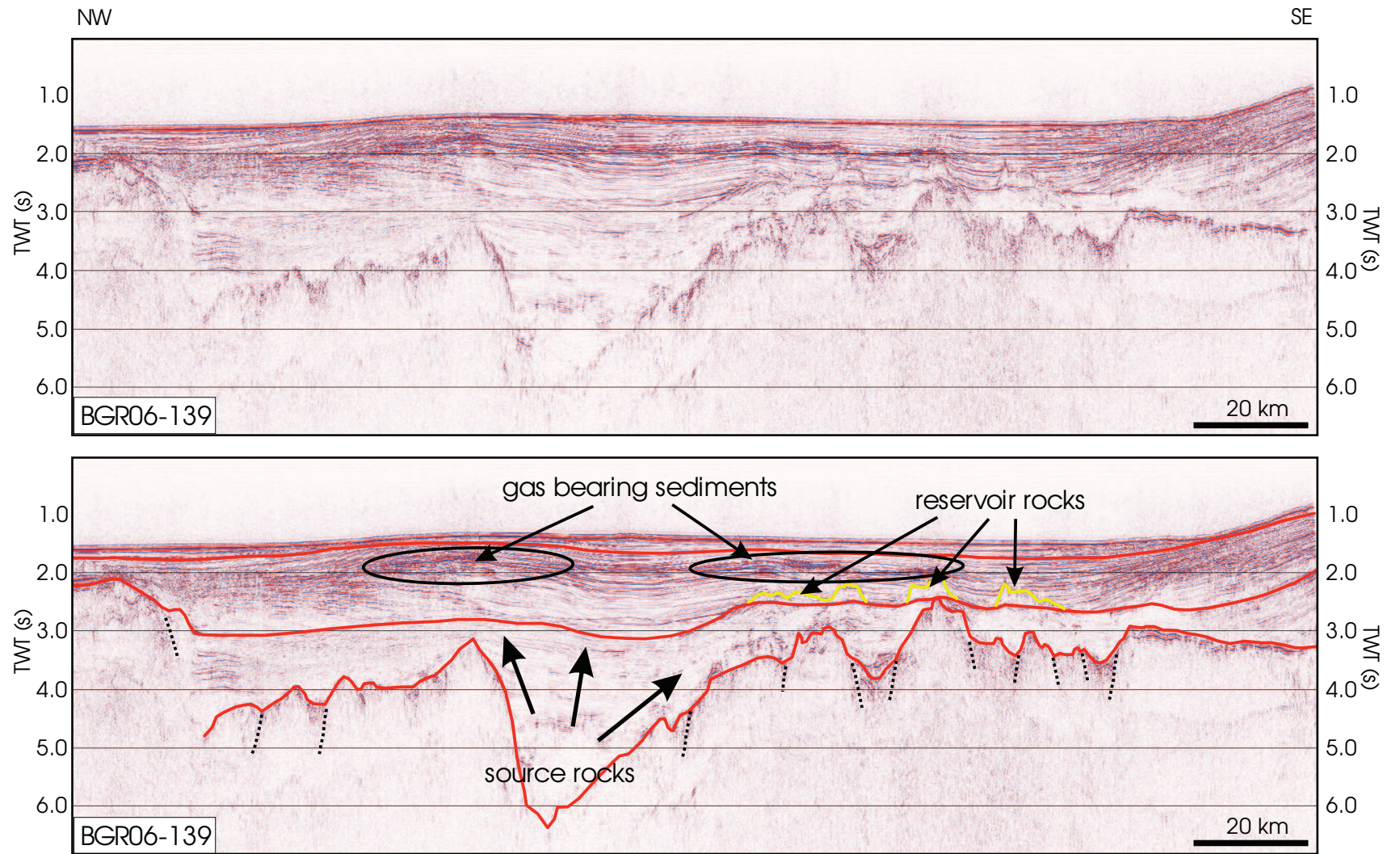


Figure 13

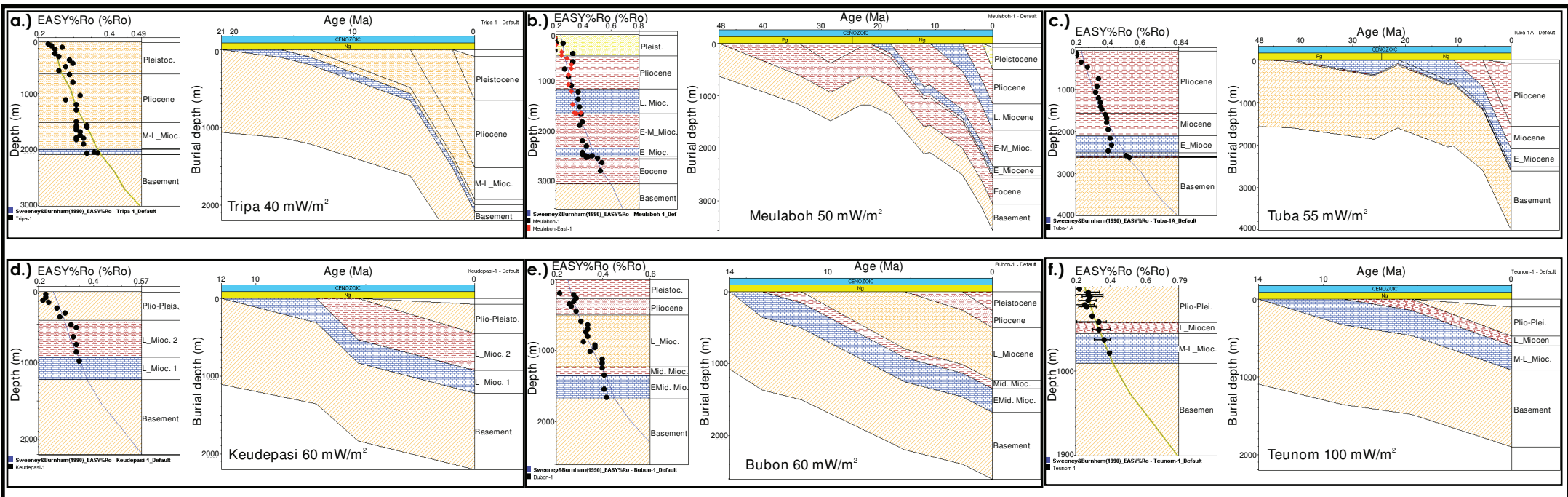


Figure 14

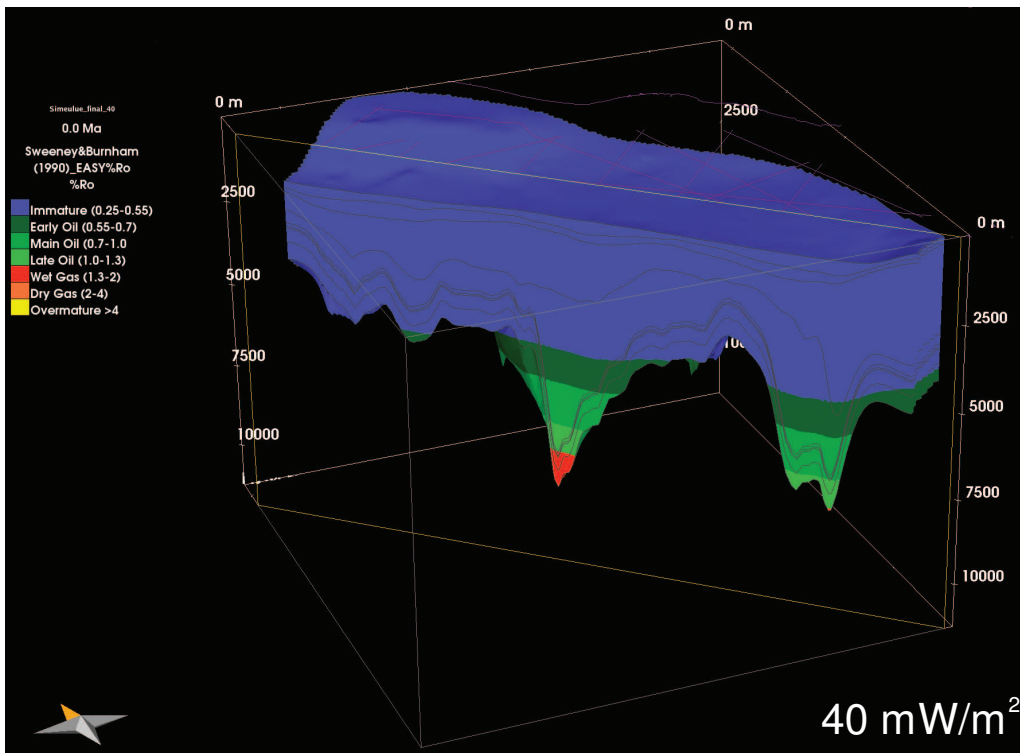
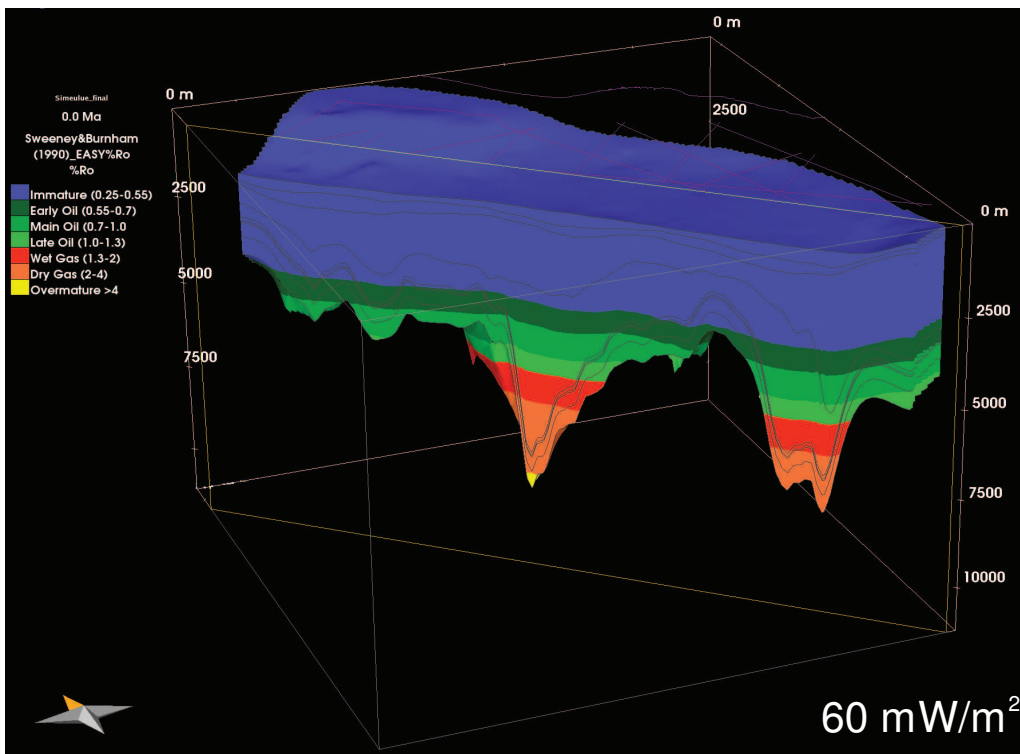


Figure 15



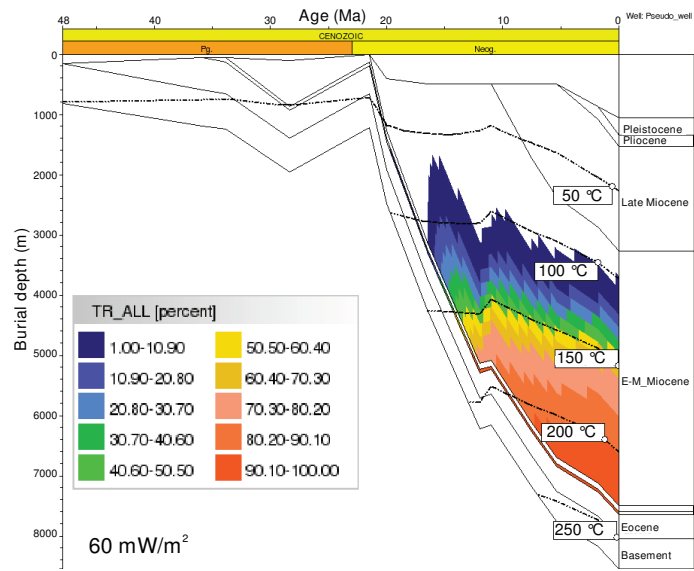
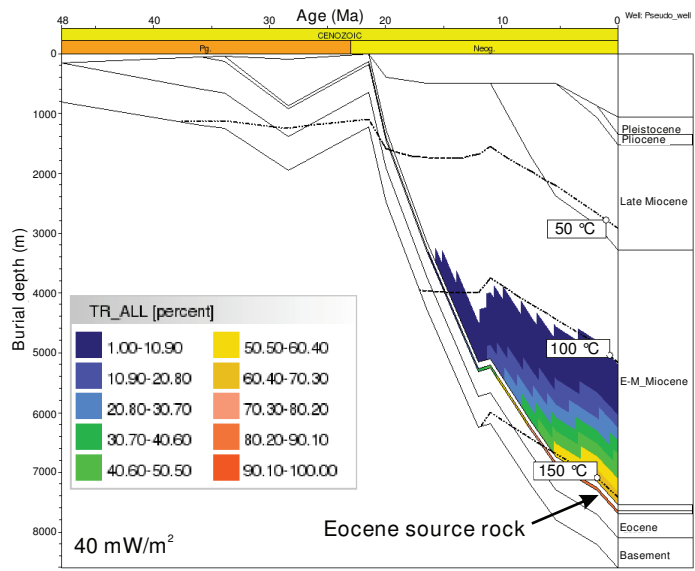


Figure 16

Ausgewählte Posterbeiträge

- K. Berglar, C. Gaedicke, D. Franke, S. Ladage, F. Klingelhoefter, Y.S. Djajadihardja: Strukturelle Entwicklung und Blattverschiebungstektonik vor Nordwestsumatra - SO186/SO189. Sonnestatusseminar, Bremerhaven, 12.-13.02.2009
- C. Gaedicke, S. Ladage, W. Soh, W. Weinrebe, D.R. Tappin, T. Henstock, L. McNeill, J.-C. Sibuet, F. Klingelhoefter, S. Singh, E. Flueh, Y.S. Djajadihardja: Bathymetry Offshore Sumatra – First Comprehensive map of International Data Sets. American Geophysical Union - Fall Meeting, San Francisco, 11.-15.12.2006
- H. Kopp, W. Weinrebe, S. Ladage, C. Gaedicke, E. Flueh, U. Barckhausen, I. Grevermeyer, A. Krabbenhoeft, C. Papenberg, & M. Zillmer: Geomorphic and seismotectonic segmentation of the Sumatra margin. American Geophysical Union - Fall Meeting, San Francisco, 11.-15.12.2006
- R. Lutz, K. Berglar, C. Gaedicke, D. Franke: Petroleum Systems Modelling in the Simeulue Forearc Basin. AAPG Hedberg Conference, Den Haag, 06.-09.05.2007
- M Zillmer, D. Klaeschen, H. Kopp, E. Flueh, A. Krabbenhoeft, C. Papenberg, L. Planert, W. Weinrebe, D. Franke, C. Gaedicke, Y.S. Djajadihardja: Firstarrival Tomography of Seismic OBS Data and Prestack Depth Migration of MCS Data from the Sumatra Continental Margin. American Geophysical Union - Fall Meeting, San Francisco, 10.-14.12.2007.

Strukturelle Entwicklung und Blattverschiebungstektonik vor Nordwestsumatra - SO186/SO189

Kontakt: kai.berglar@bgr.de

Kai Berglar^a, Christoph Gaedicke^a, Dieter Franke^a, Stefan Ladage^a,
Frauke Klingelhofer^b, Yusuf S. Djajadihardja^c

^aBundesanstalt für Geowissenschaften und Rohstoffe, Stilleweg 2, 30655 Hannover

^bIfremer Centre de Brest, B.P. 70, 29280 Plouzané cedex, France

^cAgency for the Assessment & Application of Technology, Jl. M.H. Thamrin No.8, Jakarta 10340, Indonesia

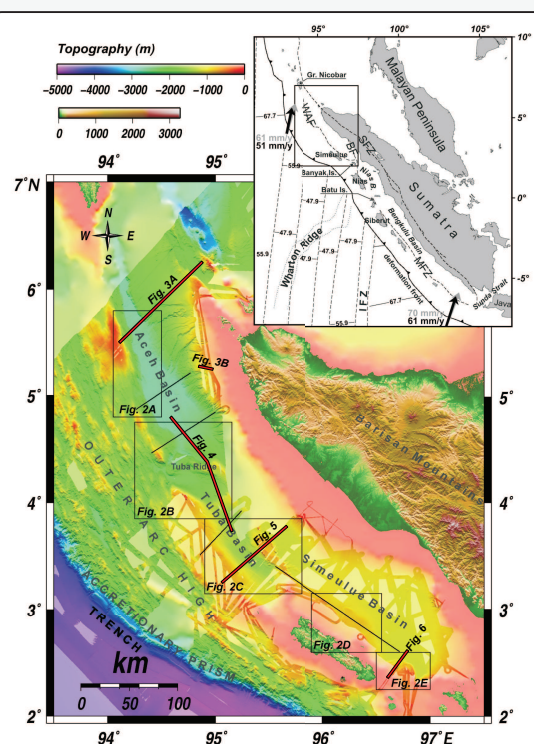
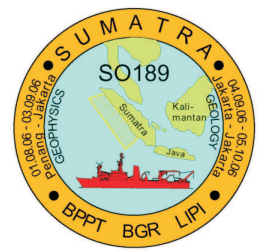


Abb. 1: Wichtige tektonische Strukturen und Lage der Profile und Detailschnitte. IFZ= Investigator-Bruchzone, SFZ=Sumatra-Störung, MFZ=Mentawai-Störung, BF=Batee-Störung, WAF=West-Andaman-Störung.

Überblick

Das Untersuchungsgebiet vor Nordwestsumatra umfasst das Seegebiet von 2°N bis 7°N zwischen Tiefseeegraben und Festland (Abb.1). In diesem Bereich liegen die nördlichsten Vorderbogenbecken Sumatras, die durch eine Antiklinalstruktur voneinander getrennt sind und einen Sprung in der Wassertiefe von 1300 m im Simeulue-Becken zu 2800 m im Aceh-Becken zeigen. Die dextralen Mentawai- und West-Andaman-Störungssysteme am Westrand der Vorderbogenbecken und die an Land gelegene Sumatra-Störung nehmen die parallel zur Deformationsfront orientierte Komponente der schiefen Konvergenz zwischen der Indo-Australischen und Eurasischen Platte auf.

Ziel

Entwicklung eines Modells für die Interaktion von Blattverschiebungssystemen und Vorderbogenbeckenentwicklung vor Nordwestsumatra.

Fragen

- ▶ Wann setzten Bewegungen an Blattverschiebungen ein?
- ▶ Lässt sich eine zeitliche Abfolge erkennen?
- ▶ Wie interagieren Mentawai-Störung und West-Andaman-Störung?
- ▶ Wie ist ihr Einfluss auf die Entwicklung der Vorderbogenbecken?

Daten

- ▶ 2800 km Mehrkanalseismik
- ▶ Parallel aufgezeichnetes parametrisches Sedimentecholot
- ▶ 4800 km Einkanalseismik (SCS) der SUMENTA-Fahrten
- ▶ Fächerecholot-Bathymetrie: Kompilation von japanischen, britischen, französischen, US-amerikanischen und deutschen Datensätzen

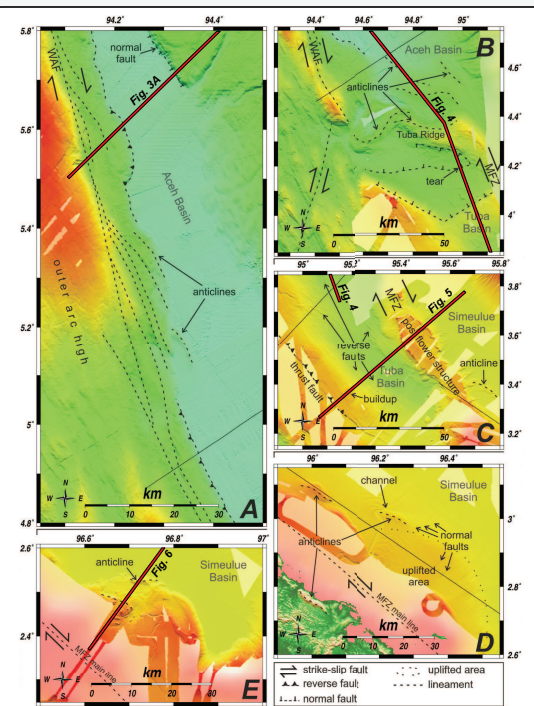
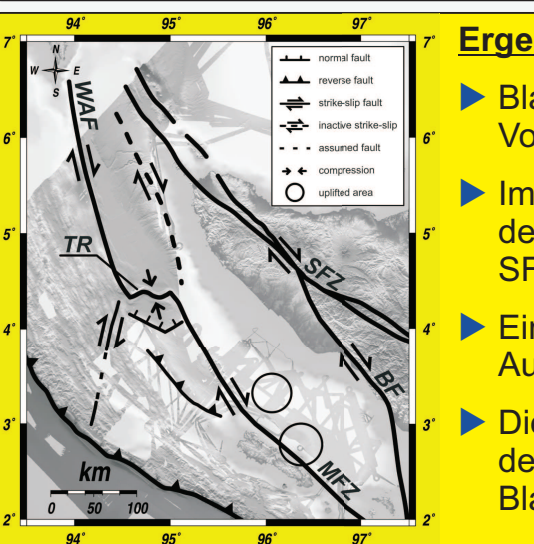


Abb. 2: Detaillierte Bathymetrie und Interpretation der Vorderbogenbecken vor Nordwestsumatra.

Ergebnisse

- ▶ Blattverschiebungen durch schiefe Subduktion setzten in den Vorderbogenbecken im oberen Miozän ein.
- ▶ Im Bereich des Aceh-Beckens findet eine westwärtige Verlagerung der Blattverschiebungsbewegungen statt, das nördliche Segment der SFZ wird im Pliozän durch die WAF abgelöst.
- ▶ Ein lateraler Versatz verbindet MFZ und WAF und führt zur Ausbildung des kompressiven Tuba-Rückens.
- ▶ Die Vorderbogenbecken zeigen unterschiedliche Entwicklung seit dem oberen Miozän, insbesondere das Aceh-Becken ist stark von Blattverschiebungen geprägt.



Quellen

Abb. 1 - Regionale Tektonik, relative Plattenbewegungen, Krustenalter:
DeMets, C., Gordon, R.G., Argus, D.F., Stein, S., 1994. Effect of recent revisions to the geomagnetic reversal time scale on estimates of current plate motions. *Geophysical Research Letters* 21(20), 2191-2194.
Deplus, C., Diament, M., Hebert, H., Bertrand, G., Dominguez, S., Dubois, J., Malod, J., Patriat, P., Pontolise, B., Sibilla, J.J., 1998. Direct evidence of active deformation in the eastern Indian oceanic plate. *Geology* 26(2), 131-134.
Prawirodirdjo, L., Bock, Y., 2004. Instantaneous global plate motion model for 12 years of continuous GPS observations. *Journal of Geophysical Research* 109, B08405.
Siah, K., Natawidjaja, D., 2000. Neotectonics of the Sumatran Fault, Indonesia. *Journal of Geophysical Research* 105(B12), 28,295-28,326.
Abb. 2 - Bathymetrische Datensätze:
Henstock, T.J., McNeill, L.C., Tappin, D.R., 2006. Seafloor morphology of the Sumatran subduction zone: Surface rupture during megathrust earthquakes? *Geology*, 34(6), 485-488.
Ladage, S., Weinrebe, W., Gaedicke, C., Barckhausen, U., Flueh, E.R., Heyde, I., Krabbenhoft, A., Kopp, H., Fajar, S., Djajadihardja, Y., 2006. Bathymetric Survey Images Structure off Sumatra. *Eos, Transactions American Geophysical Union*, 87(17), 165-172.
Cruise report RR0705, 2007. Paleoseismic Studies of the Sunda Subduction Zone. Oregon State University Active Tectonics Laboratory, Agency for the Assessment and Application of Technology, Indonesia. <http://www.activetectonics.coas.oregonstate.edu/sumatra/report/index.html>.
Sibuet, J.C., Rangin, C., Le Pichon, X., Singh, S., Cattaneo, A., Craindorge, D., Klingelhofer, F., Lin, J.Y., Malod, J., Maury, T., Schneider, J.L., Sultan, N., Umler, M., Yamaguchi, H., 2007. 26th December 2004 great Sumatra-Andaman earthquake: Co-seismic and post-seismic motions in northern Sumatra. *Earth and Planetary Science Letters*, 263(1-2), 88-103.
Soh, W., 2006. Seismic and Tsunami Sciences of 26th Dec. 2004 Sumatra-Andaman Clarified in the Urgent Study. *Blue Earth, Special Issue* 1, 14-17.
Abb. 3B - SCS Daten:
Malod, J.A., Mustafa Kemal, B., Beslier, M.O., Deplus, C., Diament, M., Karta, K., Mauffret, A., Patriat, P., Pubellier, M., Regnaud, H., Artonang, P., Zen, M. T., J., 1993. Deformations du bassin d'avant-arc au nord-ouest de Sumatra: une réponse à la subduction oblique. *Comptes Rendus de l'Académie des Sciences de Paris, Série 2*, 316(6), 791-797.

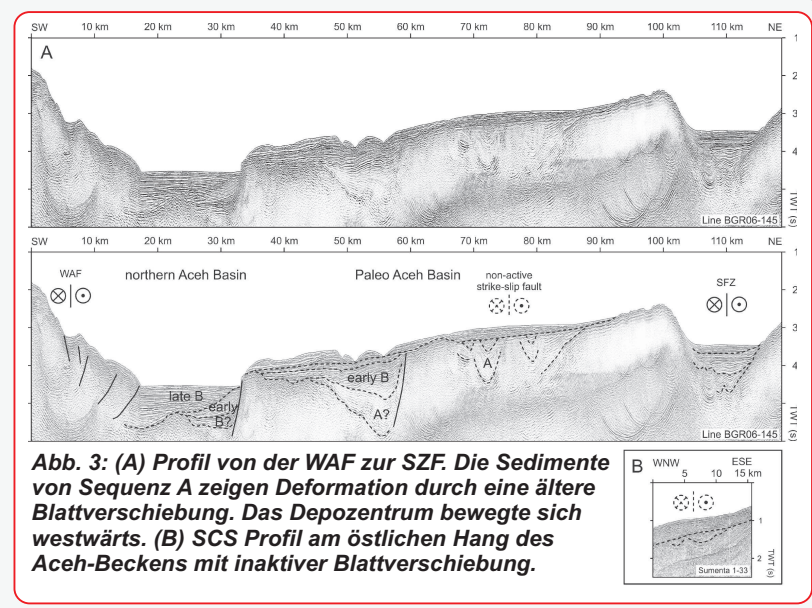


Abb. 3: (A) Profil von der WAF zur SFZ. Die Sedimente von Sequenz A zeigen Deformation durch eine ältere Blattverschiebung. Das Depozentrum bewegte sich westwärts. (B) SCS Profil am östlichen Hang des Aceh-Beckens mit inaktiver Blattverschiebung.

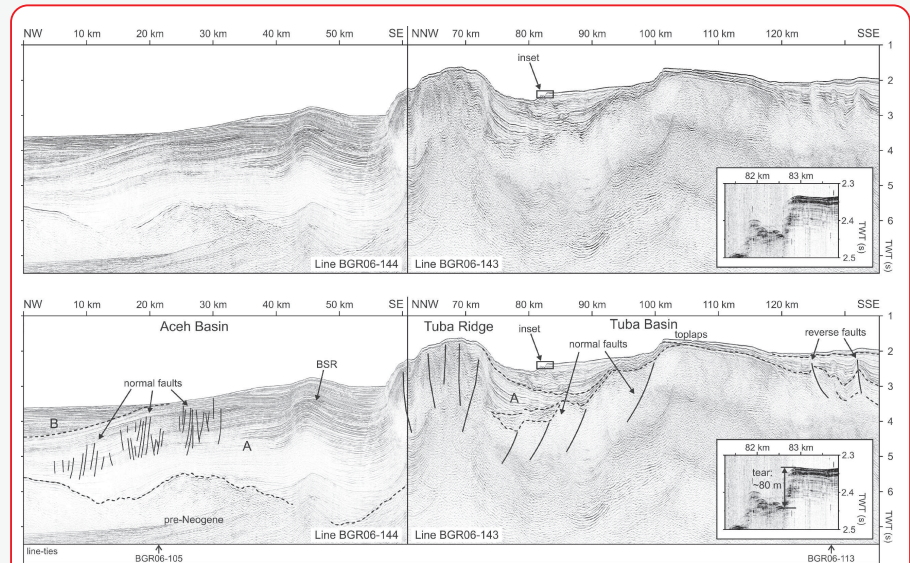


Abb. 4: Ältere Sedimente des nördlichen Tuba-Beckens sind durch die Bildung des Tuba-Rückens vom Aceh-Becken abgeschnitten (Sequenz A). Das Sedimentecholot (Ausschnitt) zeigt einen Abriss der jüngsten Sedimente durch Extrusion. Überschiebungen im Beckenzentrum weisen auf aktive Kompression hin.

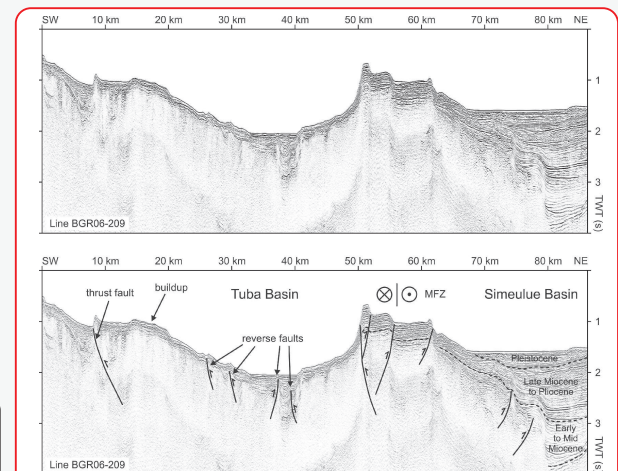


Abb. 5: Die MFZ ist als positive Blumenstruktur entwickelt und schneidet das Tuba-Becken von kontinentaler Sedimentation ab. Es ist an einer Aufschiebung ostwärts verkippt, was zu Kompression im Beckenzentrum führte.

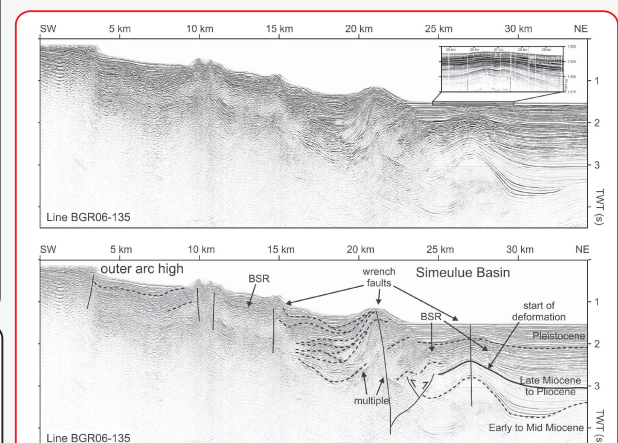


Abb. 6: Wechselnde Intensität von Blattverschiebungen zeigt sich in verzahnten Sedimentpaketen. Die durchgezogene Linie markiert den Einsatz der Deformation durch die östlichste Störung.



Bundesanstalt für Geowissenschaften und Rohstoffe

GEOZENTRUM HANNOVER

Bathymetry Offshore Sumatra – First Comprehensive Map of International Data Sets

C. Gaedicke¹, S. Ladage¹, W. Soh², W. Weinrebe³, D. Tappin⁴, T. Henstock⁵, L. McNeill⁵, J.-C. Sibuet⁶, F. Klingelhoefer⁶, S. Singh⁷, E. Flueh³, Y. Djajadihardja⁸

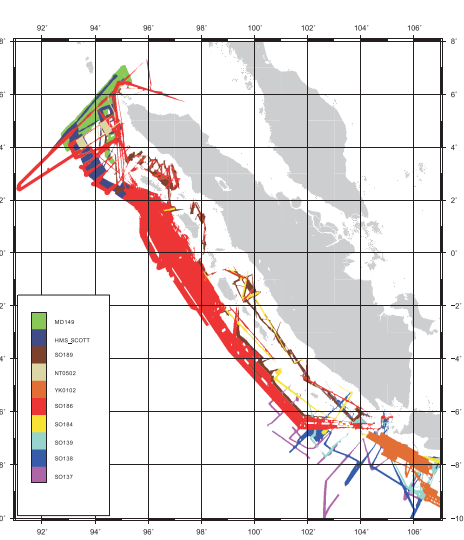
U53A-0018
AGU Fall Meeting 2006

CONTACT
Christoph.Gaedicke@bgr.de
Stefan.Ladage@bgr.de



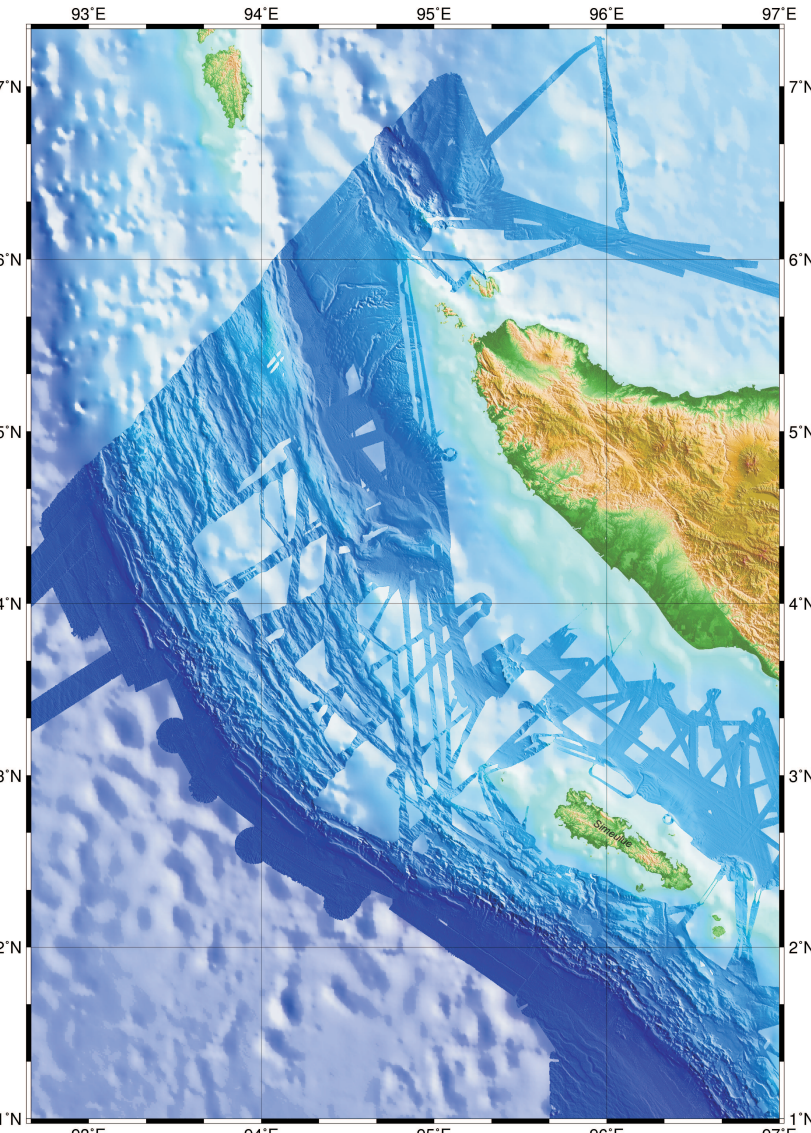
INTRODUCTION

Knowledge of the bathymetry offshore Sumatra is of great importance for geohazard risk assessment, modelling of tsunami runup heights and development of tsunami early warning systems as well as for the general understanding of plate boundary processes and morphotectonic features. Since the devastating December 26, 2004 Sumatra-Andaman Islands earthquake and tsunami a number of marine expeditions, funded by Canada, France, Germany, India, Indonesia, Japan, United Kingdom and the United States have acquired bathymetric data over the southern part of the earthquake rupture zone but also along strike the whole Sunda trench. Here we present the first compilation of these bathymetric data sets as one bathymetric map.



VESSEL AND CRUISE INFORMATION

- R/V Marion Dufresne **MD149**
Thomson MARCONI TSM 5265
dual frequency 12 / 3.5 kHz
- R/V NATSUSHIMA **NT0502**
SeaBat 8160 by RESON Inc.
50kHz, 126 beams,
max. 130° swath width,
~ 1m resolution
- HMS-SCOTT **HMS-Scott**
SASS-IV by U.S. Navy &
SeaBeam Instruments Inc.
12 kHz, 326 beams
max. 120° swath width
~ 25 - 100m resolution
- R/V SONNE **SO137 - SO139**
HydroSweep DS2
by Atlas Elektronik GmbH
15.5kHz, 59 beams
- SO184, SO186 & SO189**
Simrad EM121
by Kongsberg Maritime GmbH
12kHz, 159 beams
max. 2° beam width
resolution ~ 1% water depth
- R/V YOKUSUKA **YK0102**
Seabeam 2000
by SeaBeam Instruments Inc.



Detail of the compiled map off northern Sumatra
0 100 200 km

DATA PROVIDED

The bathymetric data acquired up to date covers a vast part of the trench, continental slope and in part also of the fore arc basins. The map incorporates the newest data sets from 2005 of the British high-resolution HMS SCOTT survey, the French Marion-Dufresne "Aftershocks" and the Japanese Natsushima cruises. While these surveys concentrated on the southern rupture zone of the Dec. 26th, 2004 earthquake, the German R/V SONNE SeaCause and Sumatra cruises in 2005 and 2006 mapped the March 28th 2005 rupture area as well as large parts of the central Sunda trench and slope and in part the fore arc basins. Surveys reaching back to 1997 covering parts of the Sunda Strait and offshore southern Sumatra are also incorporated. A nearly complete coverage of the Sunda trench and slope area in the north is achieved. In the south data gaps on the slope still exist.

COMPILATION PROCEDURE

The bathymetric datasets were provided either in different native multibeam-system formats or as dumped grid data in xyz-ascii format. The data were used as delivered, i.e. no further editing has been performed. The total volume of the data amounts to 90GB. The data has been merged using the command line utility "mgrid" from MB-System software package (Version 5.0.7) since it is capable of simultaneously handling data in native binary and xyz-ascii formats. Gridding was performed in geographical coordinate system with grid spacing of 0.002° corresponding ~ 220 m. The different surveys have been given priorities by a weighting scheme during gridding to minimize artefacts and inconsistencies in regions of overlap. The HMS Scott data set with its exceptional resolution has been given the highest priority of all surveys. Data gaps smaller 500 m in the resulting grid either along track or due to missing overlap were filled using spline interpolation with the GMT "surface" tool. The resulting grid was then plotted with the GMT software package.

ACKNOWLEDGMENTS

This map compilation is a collaborative international effort initiated and partly funded by InterMARGINS. It is a major contribution to the Indonesian and international science community. The bathymetry data acquired with R/V Sonne have been funded by The German Ministry of Education and Research (BMBF) in following projects: SeaCause (SO186) - grant number 03G0186A, Sumatra (SO189) - grant number 03G0189A and GITEWS (German Indonesian Tsunami Warning System) - grant number 03TSU01. Thanks to Kai Berglar, Stephan Feller and Michael Schauer for assistance in compiling the data.

INSTITUTIONS

- ¹Federal Institute for Geosciences and Natural Resources, Stilleweg 2, 30655 Hannover, Germany
- ²JAMSTEC – Japan Agency for Marine-Earth Science and Technology, 200, Monobe Nankoku, Kochi, 783-8502, Japan
- ³IFM-GEOMAR Leibniz-Institute of Marine Sciences, Wischhofstr. 1-3, 24148 Kiel, Germany
- ⁴BGS - British Geological Survey, Kingsley Dunham Centre Keyworth, Ng12 5 GG Nottingham, United Kingdom
- ⁵NOC - National Oceanography Centre Southampton, University of Southampton, European Way, SO 14 3ZH Southampton, United Kingdom
- ⁶IFREMER, Geosciences Marine/Centre de Brest, BP 70, Plouzane, 29280 France
- ⁷IPGP, Laboratoire de Geosciences Marines, Institut de Physique du Globe de Paris, 4, Place Jussieu, 75252 Paris, France
- ⁸Agency for the Assessment and Application of Technology (BPPT), Jl. Thamrin 8, 10340 Jakarta, Indonesia

REFERENCES

- Berglar, K., Ladage, S., Schauer, M., Weinrebe, W. and Soh W., 2006. Bathymetry offshore Westem Sumatra: Compilation of German and Japanese Datasets, in *Workshop: Offshore Studies of the Andaman-Sumatran Earthquakes*, BGR, p.37.
- Henstock, T.J., McNeill, L.C. and Tappin, D.R., 2006. Seafloor morphology of the Sumatran subduction zone: Surface rupture during megathrust earthquakes? *Geology*, 34(6), p.485-488.
- Ladage, S. et al., 2006. Bathymetric Survey Images Structure off Sumatra. *Eos, Transactions, American Geophysical Union*, 87(17), p.165-172.
- Singh, S.C., 2005. Sumatra Earthquake Research Indicates Why Rupture Propagated Northward. *Eos, Transactions, American Geophysical Union*, 86(48).
- Soh, W., 2006. Seismic and tsunamii tectonics of 26th Dec, 2004 Sumatran-Andaman clarified in the urgent study, *Blue Earth, Jamstec, Special Issue No. 1:14-17*.
- HMS Scott survey of Sumatra subduction, 2005. http://www.noc.soton.ac.uk/gg/sumatra/hms_scott.html
- Cruise Report on NT05-02 "Survey off northwest Sumatra Island", 2005. <http://www.jamstec.go.jp/jamstec-e/sumatra/natsushima/bm/contents.html>
- Smith, W. H. F., and D. T. Sandwell, Global seafloor topography from satellite altimetry and ship depth soundings, *Science*, v. 277, p. 1957-1962, 26 Sept., 1997.
- SRTM V2 3s - data courtesy of NASA/NGA/USGS, <http://www2.jpl.nasa.gov/srtm/>
- GMT - Generic Mapping Tool, School of Ocean and Earth Sciences and Technology, Hawaii. <http://gmt.soest.hawaii.edu/>

Bathymetric grid : 220m x 220m resolution, illuminated from 60°N
Mercator Projection - Map Datum: WGS84

Land Topography: Shuttle Radar Topography Mission - SRTM V2 3s
Background Bathymetry: Satellite Altimetry 2min resolution (Smith & Sandwell 1997)



GEOMORPHIC AND SEISMOTECTONIC SEGMENTATION OF THE SUMATRA MARGIN

¹H. KOPP, ¹W. WEINREBE, ²S. LADAGE, ²C. GAEDICKE, ¹E. R. FLUEH, ²U. BARCKHAUSEN, ¹D. KLAESCHEN, ¹I. GREVEMEYER, ¹A. KRABBENHOEFT, ¹C. PAPERBERG, ¹M. ZILLMER
(¹IFM-GEOMAR, KIEL, GERMANY; ²BGR, HANNOVER, GERMANY)

CONTACT: hkopp@ifm-geomar.de

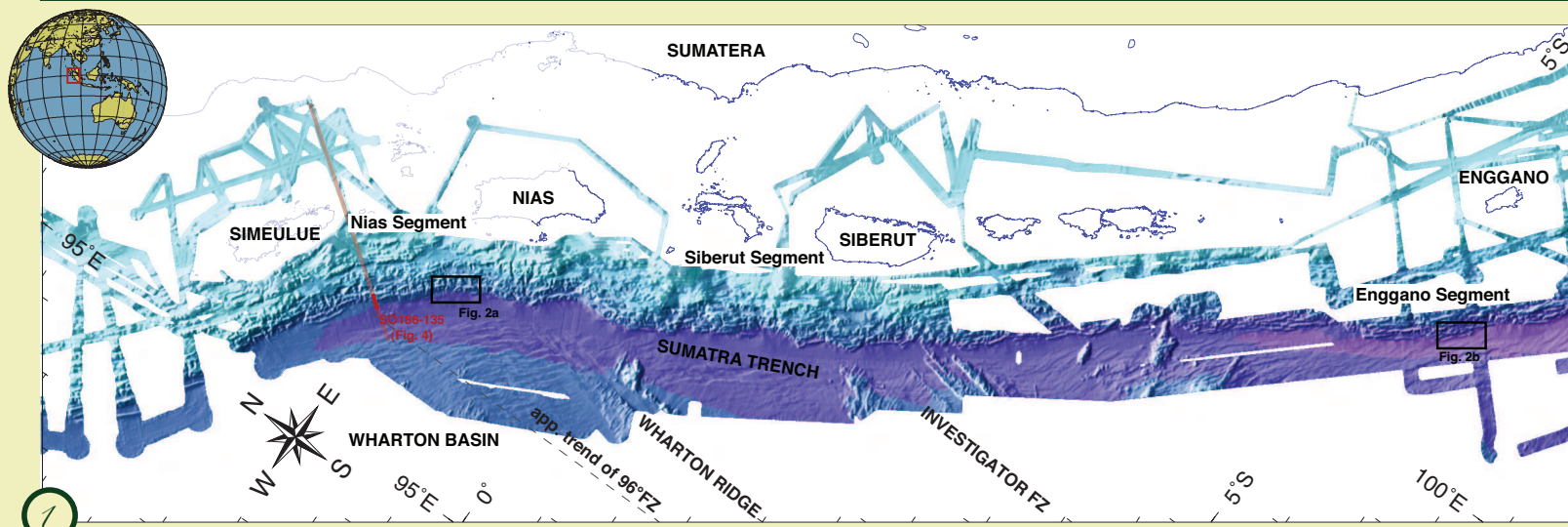


Fig. 1 From October 2005 to March 2006 high-resolution swath mapping of the Sumatra margin was performed concurrent to seismic (Fig. 4) gravimetric and magnetic profiling using RV Sonne (Ladage et al. 2006). Seafloor mapping was concentrated on the lower slope south of the Sumatran forearc islands of Simeulue, Nias, Siberut, and Enggano (Kopp and Flueh, 2006) to complement bathymetric mapping to the northwest conducted by HMS Scott along the southern part of the rupture zone of the 2004 earthquake (Henstock et al. 2006). Swath bathymetry data were acquired using Sonar's 12 kHz Simrad EM120 echosounder system with 90 beams with widths of 2' across track and 20' along track. The emission beam is 150' wide across track and 2' wide along track direction. Seafloor of the Wharton Basin was generated between 85 m and 45 m at the Wharton Ridge that consists of an echelon east-west trending segments of a now fossil spreading axis. Bathymetric features are prominent in the Wharton Basin and trend in a N-S direction following fossil transform faults that are currently being reactivated as left-lateral strike-slip faults. The 96°E Fracture Zone (indicated by stippled line) shows considerable basement relief as evidenced in seismic data (Gaedicke et al. 2006). The Investigator Fracture Zone at 98.25°E outcrops at the seafloor and comprises four individual ridges of parallel trend of up to 1400 m height above the trench and approximately 120 km width.

INTRODUCTION: Lower slope morphology

Merging of various bathymetric data sets acquired by the German RV SONNE in 2005 and 2006 yields a continuous seafloor swath map of the trench and deformation front from Simeulue Island off northern Sumatra, where the termination of the 2004 and 2005 ruptures is located, to southern Sumatra at around 7°S, covering an extent of more than 1300 km (Fig. 1). These new data reveal a highly segmented regional morphology of the lower slope. Off southern Sumatra along an app. 600 km long sector (termed Enggano segment), the deformation front is characterized by frontal accretion and recent growth of a smooth fold-and-thrust-belt that lacks any indication of major current erosional processes, except where an isolated seamount impinges on the margin at 99°6'E/3'8'S, locally scarring the margin toe (Fig. 1). Away from the seamount collision zone, trench material is frontally accreted and sub-parallel nascent thrust folds develop at the slope base with a singular fold length of 20-70 km (Fig. 2b). Analysis of the bathymetric data across the lower slope yields a mean surface slope α of 1.8° (Fig. 2f). Lower slope morphology changes abruptly where the ridges composing the Investigator Fracture Zone (IFZ) dissect the trench sediments (Fig. 3). Between the entry point of the IFZ at 98.25°E/2°S and the current collision of the Wharton Ridge at 97°E/0.2°N (labelled Siberut segment) (Fig. 1), the lower slope has extensively been re-worked and the frontal accretionary prism eroded as the Wharton Ridge migrated along the trench. Geometric calculations yield a current lateral migration velocity for the IFZ of 4.0-4.5 cm/y. Due to the variable angle of the en-echelon segmented Wharton Ridge with the trench, the lateral migration velocity of the abandoned spreading center is highly erratic. Slope morphology changes again to the northwest of the Wharton Ridge in the Nias segment (Fig. 2a): here, the lower slope consists of steeply rising thrust folds ($\alpha = 3.1^\circ$) that show extensive geomorphic evidence of surface erosion. Though the frontal accretionary prism here is still intact, collapse structures are ubiquitous. Ladage et al. (2006) concluded that the frontal folds along the Nias segment are older compared to the nascent frontal thrust folds in the Enggano segment and have not been tectonically reactivated recently. An extensive transverse pattern of downslope gullies and rills dissects the prism and can be traced into the trench, supplying material by downslope mass wasting (Fig. 2a). Evidence for erosion also comes from seismic reflection data (see Fig. 4).

Fig. 3 Perspective view of the entrant point of the Investigator Fracture Zone (IFZ) into the Sumatra trench. The geomorphology of the upper plate is profoundly modulated by the subducted bathymetric elevations. Several mid-slope basins alternate with local elevated highs in the Siberut segment that recently experienced the passage of the Wharton Ridge. These features represent remnant tectonic imprints of oceanic relief subduction. Immediate restoration of the margin toe in the south after the passage of the IFZ is facilitated by ample sediment supply and low basal friction (Kopp and Kukowski, 2003).

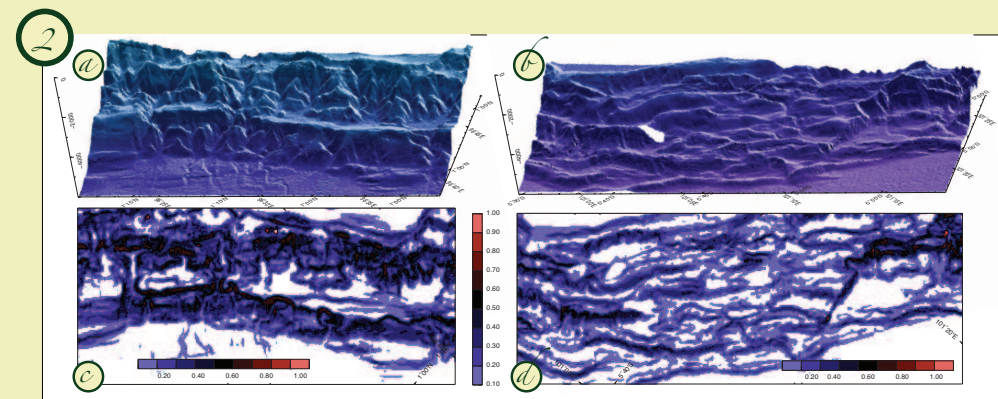


Fig. 2 High resolution bathymetry (a & b) in the Nias and Enggano segments (compare black boxes in Fig. 1 for location) and corresponding gradients (c & d). The surface angle α was averaged from the bathymetric slope measured along five tracks perpendicular to the trench axis over a distance of 15 km from the deformation front (e&f). It was not possible to use a longer distance due to the limited data coverage. A large-scale variation in slab dip offshore Sumatra does not occur, so that the larger taper in the north primarily results from the increase in surface slope. The locus of the taper stability field with regards to surface slope α and slab dip β is largely insensitive to fluctuations of friction, but is highly sensitive to variation of pore fluid pressure (Lallemand et al. 1994; Wang and Hu, 2006). Overpressuring is negligible off southern Sumatra (Kopp and Kukowski, 2003). Sediment accretion at the toe of the wedge leads to the growth of a fold-and-thrust-belt as imaged in the bathymetric data (Fig. 2b). Conversely offshore northern Sumatra, elevated fluid pore pressures have been proposed by several authors (Prawirodirdjo et al. 1997; Briggs et al. 2006). Excess water is supplied by the thicker trench sediment fill in the Nias segment. Elevated pore pressure will shift the locus of the taper stability field and allow for a steeper slope angle while maintaining the slab dip. The opening of the frontal taper leads to an oversteepening of the lower slope and thus facilitates surface erosion as witnessed in the bathymetry data.

Fig. 4 MCS Line SO186-135 was collected by the BGR, Hannover, Germany (see Fig. 1 for location). Truncated reflectors in this time migrated section of the lower slope are indicative of surface erosion and mass wasting processes resulting in slumps.

DISCUSSION: Seismotectonic segmentation

The distinction in modes of mass transfer from frontal accretion in the south (Fig. 2a) to surface erosion in the north (Fig. 2b) correlates with the increase in gradient (Fig. 2 c&d) and in frontal slope angle (Fig. 2 e&f) and is proposed to result from differences in pore fluid pressure. The different sectors along the Sumatra trench show a strong variability in pore pressure (this study), plate coupling (Prawirodirdjo et al., 1997; Ammon et al., 2005) and state of stress (Nalbant et al., 2005).

The segmentation of the Sumatra margin is furthermore linked to discontinuities in the geometry of the subduction zone resulting from topographic relief on the lower plate (Fig. 1), which modulate upper plate structure (Fig. 3) and from changes in the trend of interplate motion due to the curvature of the trench off northern Sumatra. The variation in age of the oceanic lithosphere entering the trench offshore Sumatra reaches 40 m.y. and age jumps across the fracture zones of more than 10 m.y. characterize the oceanic plate (Liu et al., 1983), implying a contrast in lithosphere thickness and buoyancy as well as density and thermal state between different slab segments. The fracture zones and the Wharton Ridge represent tectonic segment boundaries and zones of anomalous crust with regards to density, crustal composition and thickness. The segmentation of the downthrusting plate is mirrored in the seismotectonics of the upper plate. The extent of the 1861, 2004 and 2005 rupture zones shows an intriguing correlation to the segment boundaries (Fig. 5). This remarkable correspondence suggests that earthquake rupture propagation may be inhibited across segment boundaries due to the variation in thrust geometry, material strength, fluid content and pre-stresses. The aftershock distribution of the 2004 event shows a very sharp southern boundary at the prolongation of the 96°E Fracture Zone, implying that rupture did not jump across the anomaly to the stress-reduced adjacent segment. In the wake of the 2004 earthquake, however, the state of stress along the margin was appreciably altered: strain was released along the Andaman trench (Stein and Okal, 2005) while the adjacent southern segment was brought closer to failure (McCloskey et al., 2005). Failure occurred on March 28, 2005, but the rupture was terminated by the 96°E Fracture Zone and the Investigator Fracture Zone, respectively.

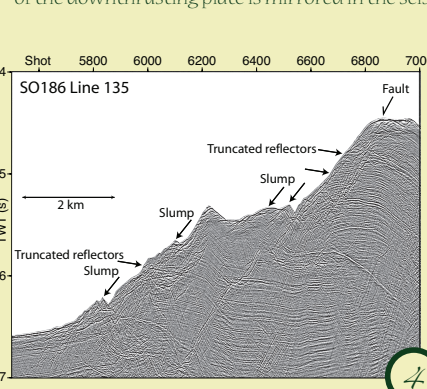
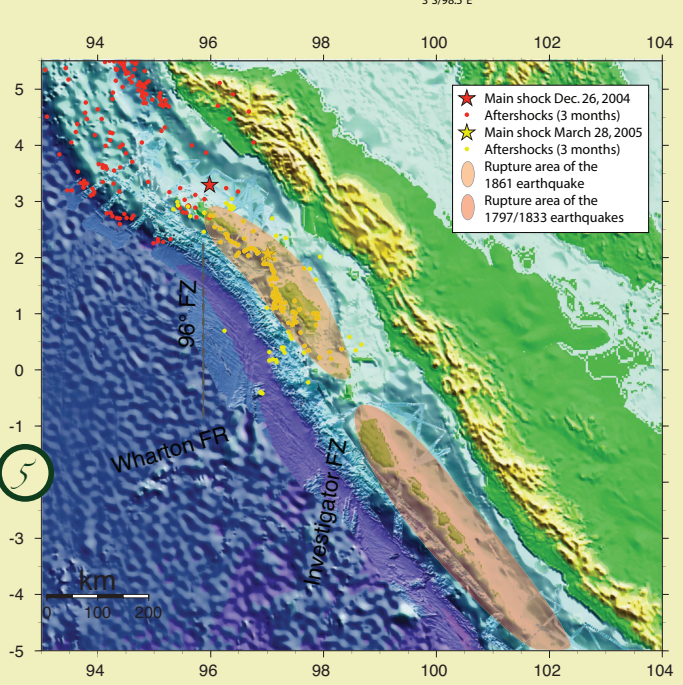
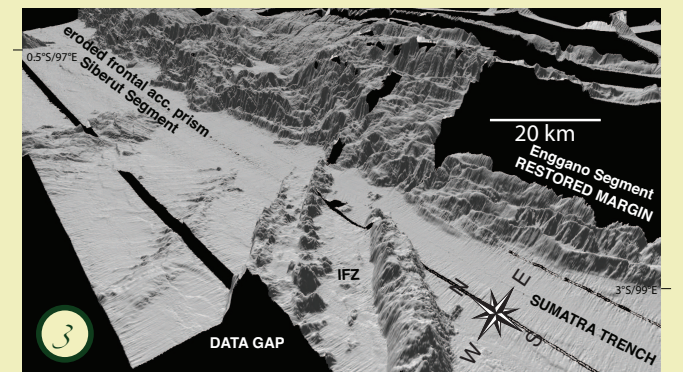


Fig. 5 Regional map of the 2004 and 2005 events and their aftershock sequence in a three-month period (red and yellow dots, respectively). The two earthquake ruptures show little overlap but have very distinct rupture terminations. The 2005 rupture area largely coincides with the rupture zone of the 1861 earthquake. Both ruptures terminated in the south where the IFZ and the Wharton Fossil Spreading Center enter the subduction zone. The northern limit of this rupture correlates to the southern extent of the 2004 rupture and coincides with the prolongation of the 96°E Fracture Zone. This fracture zone shows considerable basement relief, as evidenced in seismic data (Gaedicke, 2006). The distinct rupture zones of the 2004/2005 earthquake couplet as well as of previous earthquakes on this margin (e.g. in 1797/1833, 1907) suggest that tectonic segment boundaries formed by subducting lithosphere anomalies strongly influence the seismotectonic behaviour of the margin.



We would like to thank our Indonesian partners, namely the BPPT (Agency for the Assessment and Application of Technology) of Jakarta and Dr. Y. Djajadhardja for their continuous assistance. The SeaCause and GITEWS projects, on which this study is based, are supported by the German Ministry of Education and Research (BMBWF) grants 03G086 and 03T5U01. The offshore data were acquired from the RV SONNE. The support of the vessel's crew and their crew is warmly acknowledged. We would further like to thank all participants of the related cruises for their professional help at sea.

Ammon, C.J. et al., 2005. Rupture Process of the 2004 Sumatra-Andaman Earthquake. *Science*, 308, p. 1133-1139.
Briggs, R. W. et al., 2006. Deformation and slip along the Sunda megathrust in the great 2005 Nias-Simeulue earthquake. *Science*, 311, p. 1897-1901.
Gaedicke, C., ed., 2006. Cruise Report SO186 Leg. 2 SeaCause II. BGR Report, 025999, 444 pp.
Henstock, T. J. et al., 2006. Seafloor morphology of the Sumatran subduction zone: Surface rupture during megathrust earthquakes?. *Geology*, 34, 485-488.
Kopp, H. and Kukowski, N., 2003. Backstop geometry and accretionary mechanics of the Sunda margin. *Tectonics*, 22, 6, 1072, doi:10.1029/2002TC001420.
Kopp, H. and Flueh, E. R., eds., 2006. Cruise Report SO186 Leg. 3 SeaCause II. IFM-GEOMAR Report, 4, 205 pp.
Ladage, S. et al., 2006. Bathymetric survey images structure of the Sumatra. *EOS*, vol. 87, no. 17, p. 165-172.
Lallemand, S. et al., 1994. Coulomb theory applied to tectonic erosion and/or frontal accretion. *Journal of Geophysical Research*, 99, p. 12033-12055.
Liu, C. et al., 1983. New constraints on the evolution of the eastern Indian Ocean. *Earth and Planetary Science Letters*, 65, p. 331-342.
McCloskey, E. et al., 2005. Earthquake risk on the Sunda megathrust. *Nature*, 435, p. 756-757.
Nalbant, S. et al., 2005. Earthquake risk on the Sunda trench. *Nature*, 435, p. 756-757.
Prawirodirdjo, L. et al., 1997. Geologic observations of interseismic strain segmentation at the Sumatra subduction zone. *Geophysical Research Letters*, vol. 24, 21, p. 2601-2604.
Stein, S. and Okal, E. A., 2005. Speed and size of the Sumatra earthquake. *Nature*, 434, 581-582.
Wang, K. and Hu, Y., 2006. Accretionary prisms in subduction earthquake cycles: The theory of dynamic Coulomb wedge. *Journal of Geophysical Research*, 111, B06410, doi:10.1029/2005JB004094.

Petroleum Systems Modelling in the Simeulue Forearc Basin off Sumatra

R. Lutz, K. Berglar, Chr. Gaedicke, D. Franke

Federal Institute for Geosciences and Natural Resources (BGR), Germany

Introduction

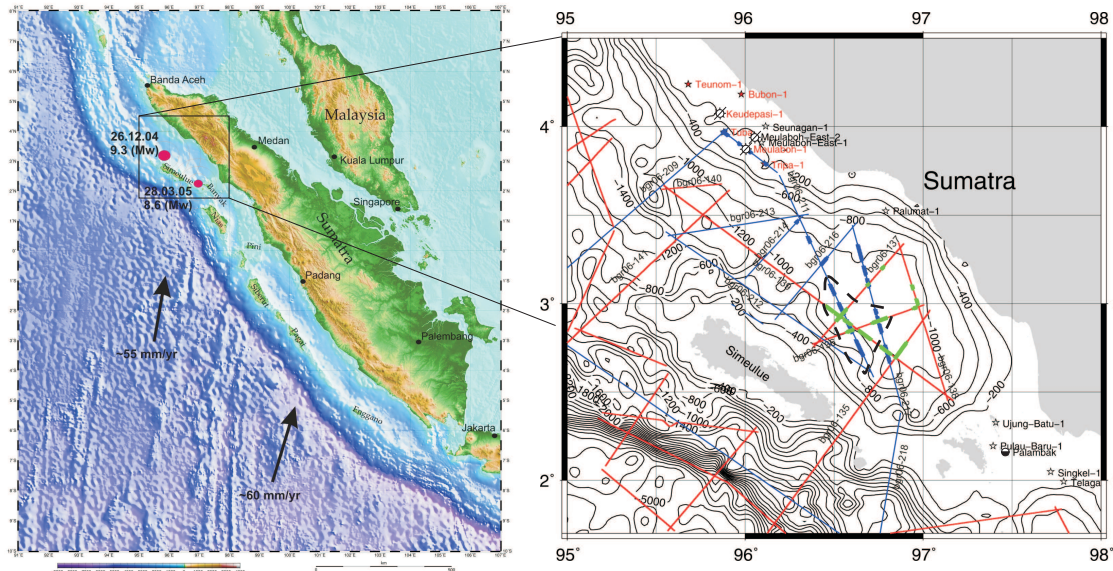


Figure 1.1: Location of study area in SE Asia. Red dots designate the epicenters of the largest earthquakes in the area (left). Right map shows the location of the seismic profiles acquired during SeaCause and SUMATRA expeditions and identified carbonate buildups (green and blue marks; wells in red are shown in Figure 2.1, dashed line shows area of bright spots above carbonates).

After the devastating earthquakes and the subsequent tsunamis from 26th Dec. 2004 and 25th March 2005 the area of northern Sumatra attracted much interest. The Federal Institute for Geosciences and Natural Resources (BGR) conducted several scientific cruises with RV SONNE off the western coast of Sumatra. The project SeaCause aimed at the investigation of the whole subduction system from the deep sea to the coast offshore Sumatra. The goal of the project SUMATRA is to study the hydrocarbon potential of forearc basins along western Sumatra. In the Simeulue forearc basin app. 1500 km of 2D seismic data together with potential field (gravity, magnetics) and swath bathymetry data was collected during two cruises.

The Simeulue Basin was the target of petroleum exploration from 1968-1978 and several wells were drilled on the shelf during this exploration phase (Figure 1.1). Three wells encountered uncommercial quantities of gas (methane) in carbonate units.

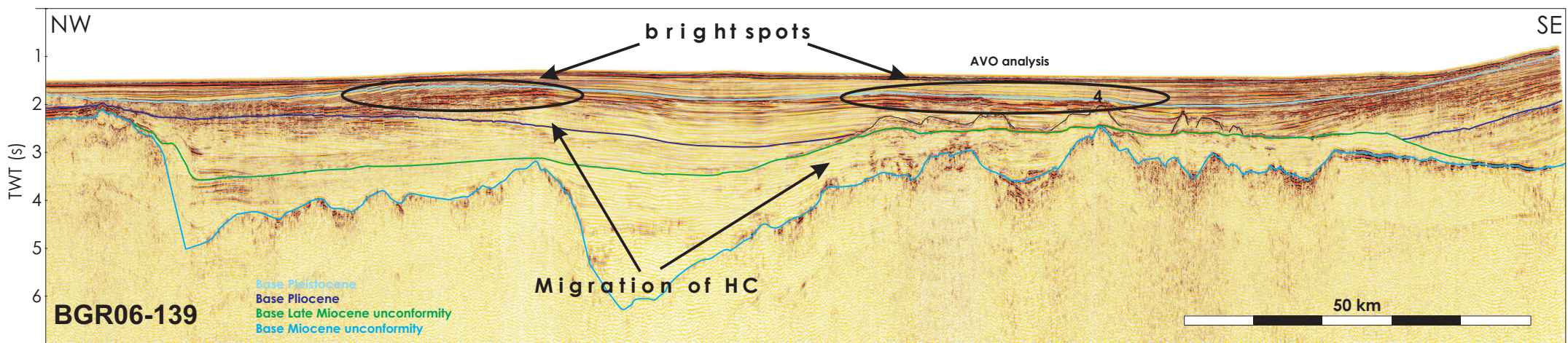


Figure 1.2: Seismic profile along the center of the basin showing depocenter, major unconformities, carbonate buildups and bright spots. AVO analysis (Figure 1.5) indicate gas in the sediments above the buildups.

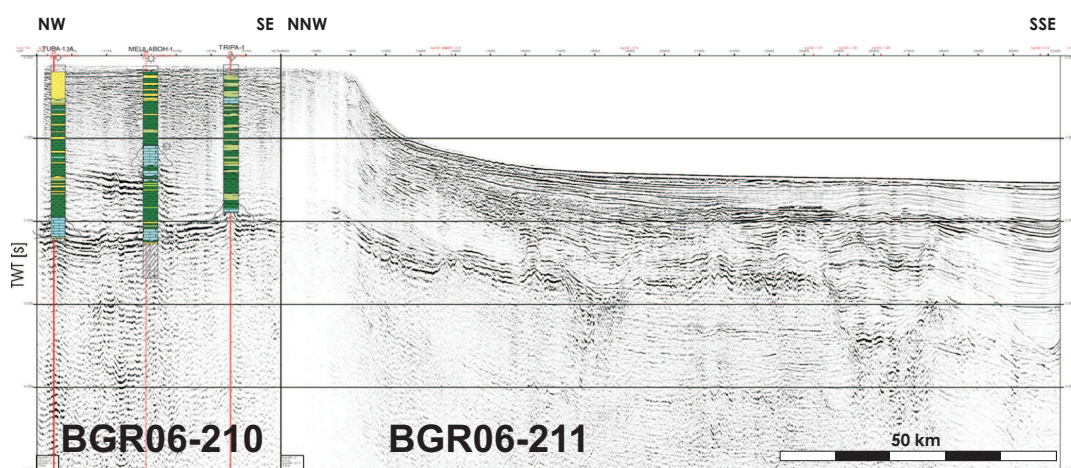


Figure 1.3: Composite display of two seismic profiles connecting three near-shore wells with the deep water area.

The geophysical data shows more than 4.5 s (TWT) of sediments in the deepest parts of the basin which suggests hydrocarbon generation in this half-graben or below and upward migration at the flanks. In our model source rocks were assumed in the Miocene (terrestrial sediments, type III) and in the Eocene (lacustrine source rocks, type I) buried beneath the acoustic basement in Figure 1.2. Eocene and Oligocene sediments were drilled in well Meulaboh-1, Figure 1.3.

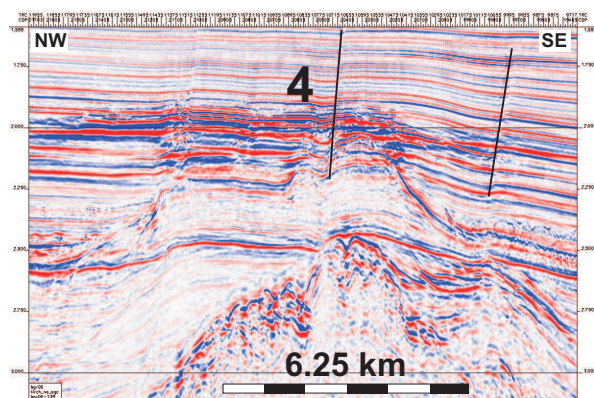


Figure 1.4: High amplitudes above carbonate platform which developed above a major unconformity.

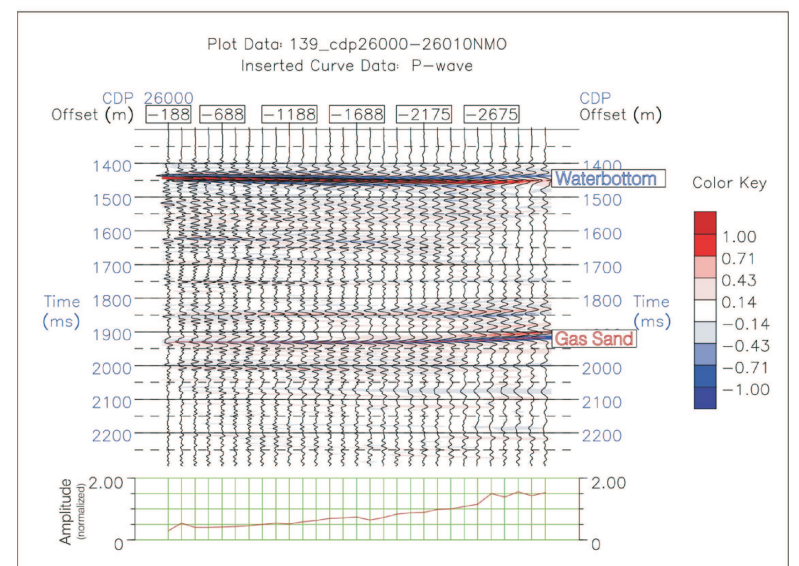


Figure 1.5: AVO analysis show a clear increase in amplitude with offset thus indicating the presence of gas in the sediments above the carbonate buildups.

Petroleum Systems Modelling in the Simeulue Forearc Basin off Sumatra

R. Lutz, K. Berglar, Chr. Gaedicke, D. Franke

Federal Institute for Geosciences and Natural Resources (BGR), Germany

Near-shore wells

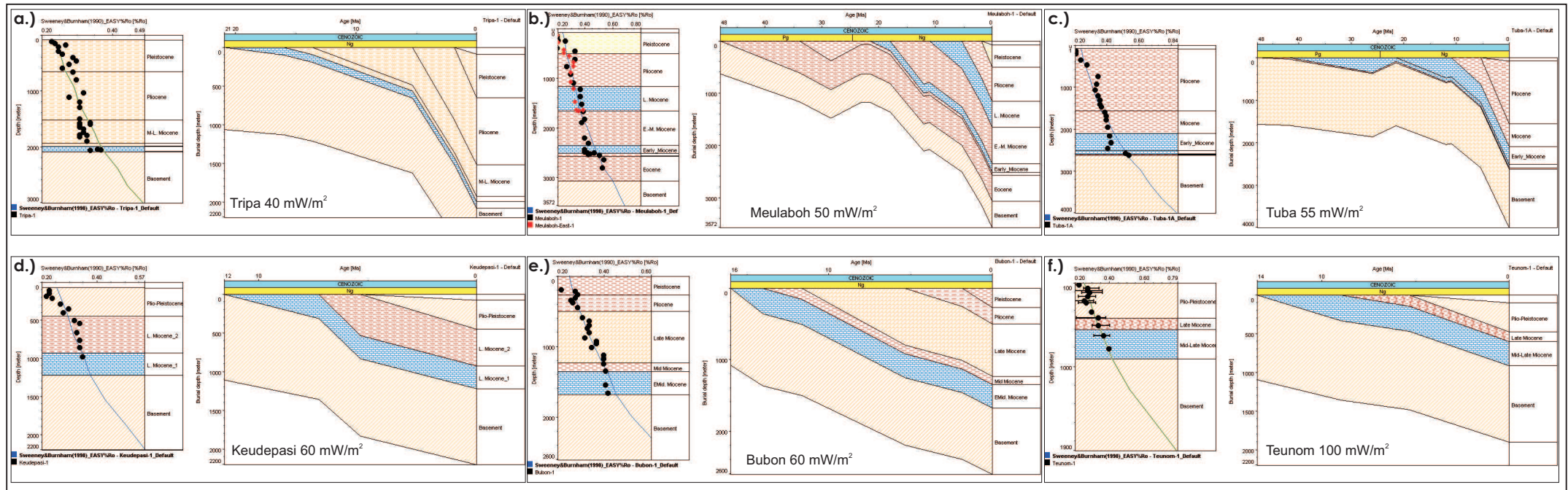


Figure 2.1: 1D models of near-shore wells (a-f) with published vitrinite reflectance values (Hadiyanto, 1992) used for calibration of the models. Left part of figure shows measured (dots) and calculated (solid line) vitrinite reflectance values. Right part of figure shows burial history of the respective well. Wells Meulaboh and Tuba reached pre-Neogen sediments; all other wells terminated in Neogen sediments. All wells were calculated using a constant heat flow model but heat flows are different for each well (see figures).

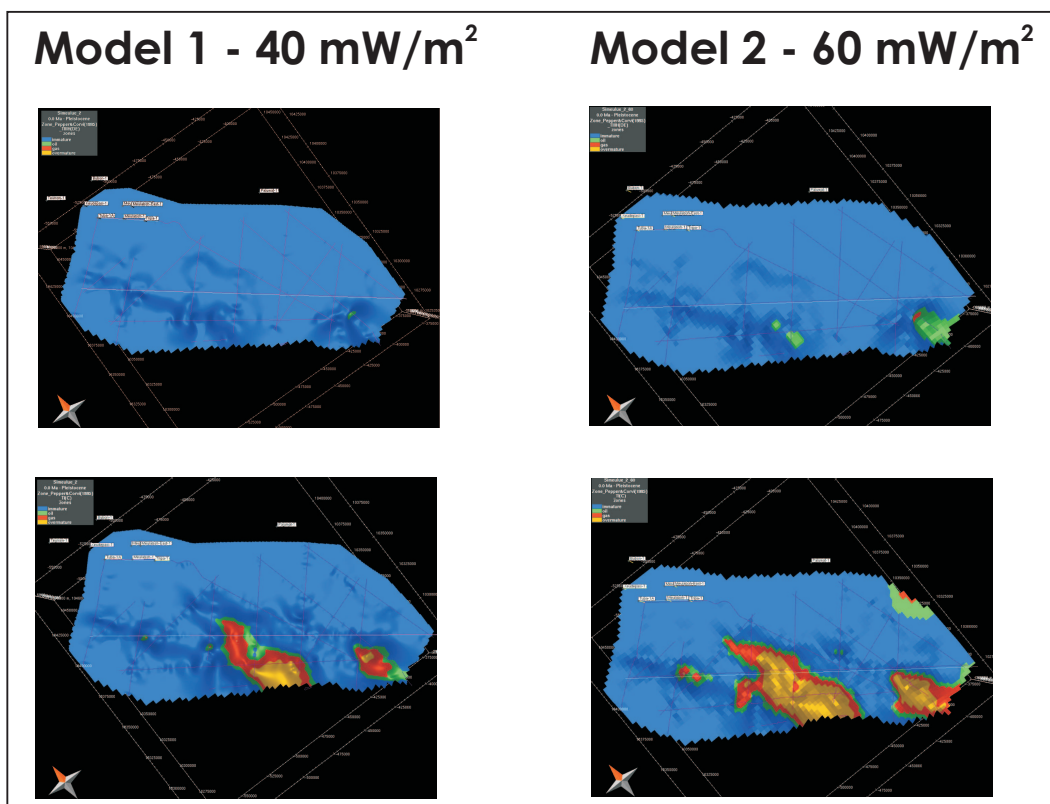


Figure 2.3: Calculated present day HC zones for the top of the Mid Miocene (top) and the top of the Eocene source rock (bottom) for both heat flow scenarios (left and right).

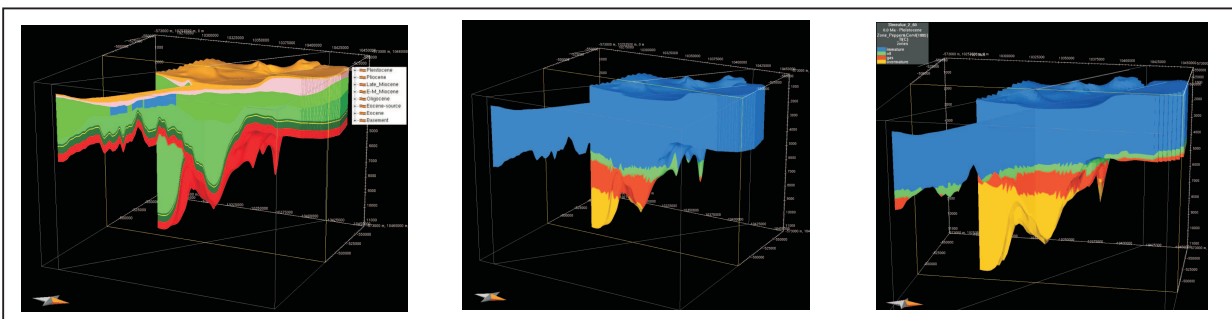


Figure 2.4: 3D model of Simeulue Basin, left. Calculated HC zones for model 1, center and model 2, right. HC zones calculated for type I kerogen.

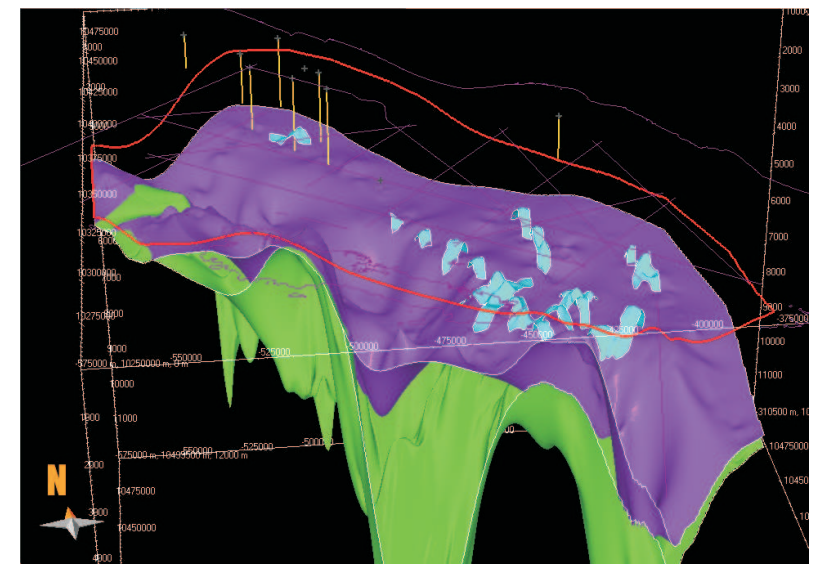


Figure 2.2: 3D model of the Simeulue Basin, constructed from 2D seismic profiles. Yellow: wells, blue: carbonates, purple: base Late Miocene, green: base Miocene, red line: seafloor. Length 235 km, width 105 km, cell size 500 m x 500 m (calculated 3 x 3 km).

Heat flow values derived from 1D models (Fig. 2.1) of six near-shore wells range between 40 and 100 mW/m². BSR-derived heat flow values range between 30 and 60 mW/m². As a first approach two scenarios were calculated with 40 mW/m² and 60 mW/m², respectively.

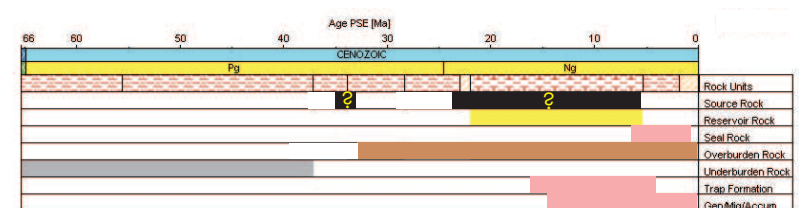


Figure 2.5: Petroleum system elements for the Simeulue Basin.

Conclusion

- Exploration failures in the 70s explained by long distance to possible source area
- Large isolated carbonate platforms could act as petroleum reservoirs
- Bright spots above carbonate platforms indicate hydrocarbons in the system
- Both models generate hydrocarbons and explain the bright spots
- Model 2 produces significant amounts of oil and gas and carbonates could be charged
- Despite the low heat flow values in forearc basins hydrocarbon generation at these locations is possible and these areas should be studied in greater detail

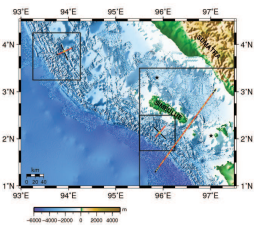
First-arrival Tomography of seismic OBS data and pre-stack depth migration of MCS data from the Sumatra continental margin

M. Zillmer, D. Klaeschen, H. Kopp, E. Flueh, A. Krabbenhoef, C. Papenberg, L. Planert, W. Weinrebe (IFM-GEOMAR: Kiel, Germany)

D. Franke, C. Gaedicke (BGR: Hannover, Germany) Y. Djajadihardja (BPPT: Djakarta, Indonesia)



The SEACAUSE project is sponsored by the German Ministry for Education and Research (BMBF)



The cruise SO186-3 with the German research vessel RV Sonne started on February 26, 2006, in Penang, Malaysia, and ended in Singapore on March 15, 2006 (Kopp and Flueh, 2006). The cruise was a continuation of previous surveys in the same area, which were related to the German-Indonesian Tsunami Early Warning System (GITEWS). The cruise was a part of the SEACAUSE project, which uses seismic methods to investigate the geotectonic potential along the active convergence zone between the Indo-Australian and Eurasian plates offshore Sumatra. Three active seismic wide-angle experiments were performed with IFM-GEOMAR Ocean Bottom Hydrophones (OBH) and Seismometers (OBS) (Bialas and Flueh, 1999) and a BGR (Bundesamt fuer Geowissenschaften und Rohstoffe) airgun source (FIG. 1).

The first experiment was a 240 km long profile south-east of Simeulue Island. The line was directed from the trench in the south-west to the coast of Sumatra in the north-east (FIG. 2). A coincident seismic multi-channel streamer profile was acquired by BGR during the previous RV Sonne cruise SO186-2 (Gaedicke, 2006). The depth-migrated section shows a classical accretionary subduction zone (FIGS. 4, 4a, 4b) (Kopp et al., 2001). The water depth varies between 5120 m in the trench and 40 m near Simeulue Island. The oceanic basement can be observed and correlated along a distance of 90 km landwards from the trench. The oceanic plate is subducting on average at an angle of 5-6 degrees. The wide-angle experiment comprises 30 OBH/OBS stations and 1948 airgun shots at a distance of 125 m. 25 hydrophones and seismometers recorded the seismic wavefield with very good data quality (FIG. 3). We apply first-arrival traveltomography to compute a 2D P-wave velocity model of the subduction zone (FIG. 5). The velocity is defined on a 974x100 irregular grid and the data consist of 9357 traveltimes. Jun Korenaga's software is used (Korenaga et al., 2000) and a solution is obtained after 20 iterations of the linearized inverse problem. The regularization parameter is reduced during the iterations and the final RMS traveltim misfit is 0.060 s.

FIG. 1 3 seismic experiments offshore Sumatra: OBS profiles (black), MCS profiles (red)

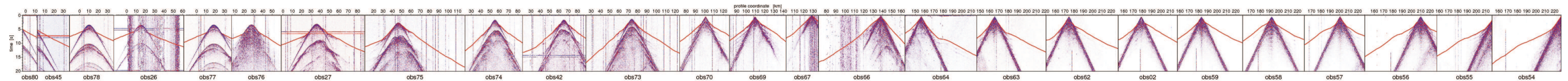


FIG. 3 Seismic wide-angle data recorded at 25 OBS stations of profile 1 used for traveltomography. The first arrival traveltimes are marked by a red line.

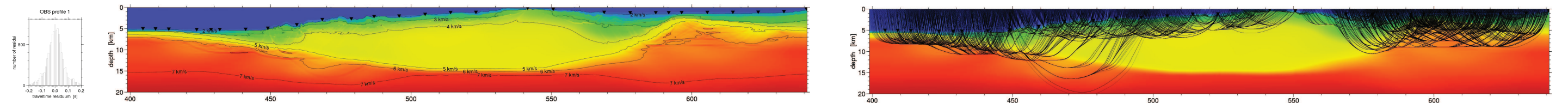


FIG. 5 2D P-wave velocity model and seismic rays obtained by first arrival traveltomography of OBS wide-angle data.

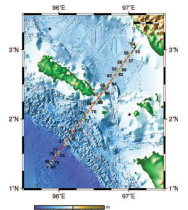


FIG. 2 240 km OBS profile (black) and MCS profile (red)

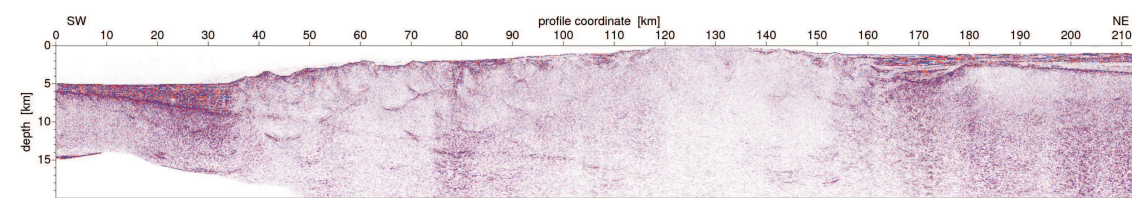


FIG. 4 Pre-stack depth migration of MCS data BGR 06-135. The profile coincides with OBS profile 1 (see FIG. 2).

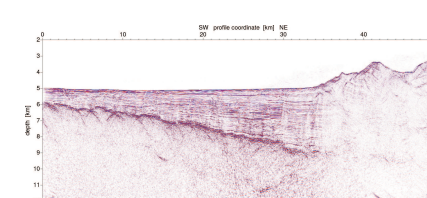


FIG. 4a Detail of FIG. 4: Trench, subducting plate.

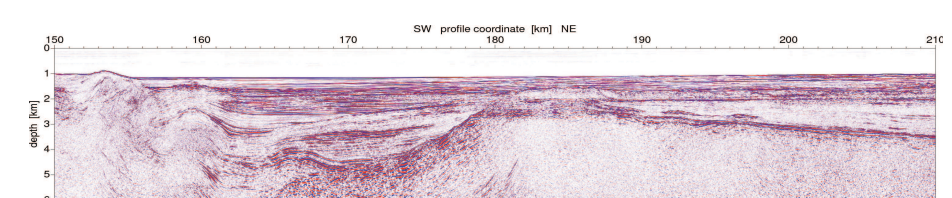


FIG. 4b Detail of FIG. 4: Fore-arc with continental crust.

The second experiment was a 40 km long wide-angle profile south of Simeulue Island (FIGS. 1, 6-8) and the third experiment consists of two cross-lines northwest of Simeulue Island (FIGS. 1, 9-11). The traveltomography leads to 2D velocity models with an increase of about 0.7 km/s per 1 km depth interval for the first 10 km depth below the sea floor.

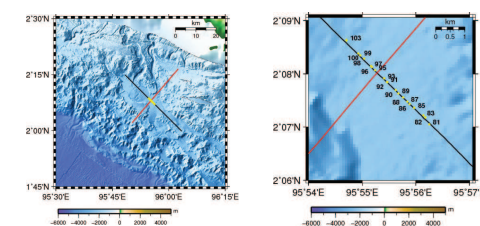


FIG. 6 OBS profile 2 (black) and crossing MCS line BGR 06-119

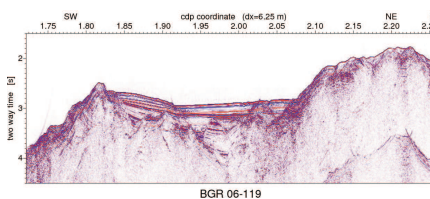


FIG. 7 Post-stack time migration of line BGR 06-119.

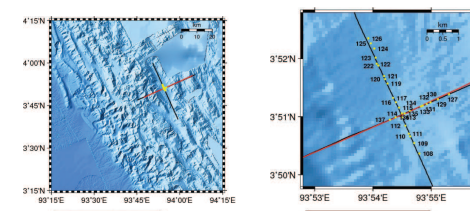


FIG. 9 OBS profiles 7 and 14 (black) and MCS line BGR 06-119 (red)

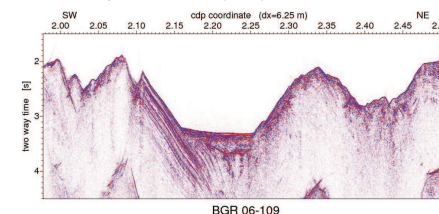


FIG. 10 Post-stack time migration of line BGR 06-109.

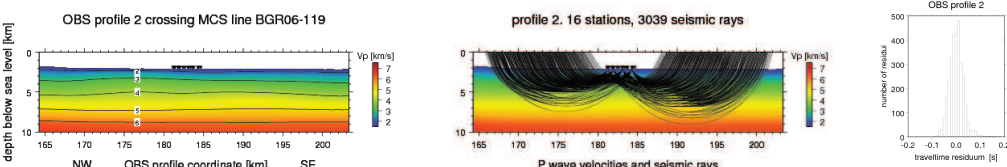


FIG. 8 2D P-wave velocity model, seismic rays and traveltim residui of OBS profile 2 (see FIG. 6).

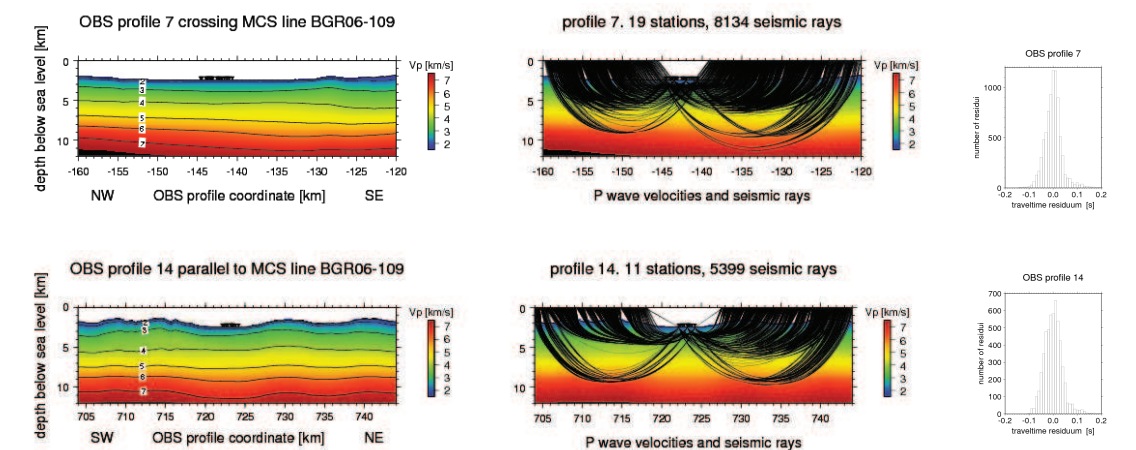


FIG. 11 2D P-wave velocity models, seismic rays and traveltim residui of OBS profiles 7 and 14 (see FIG. 10).